Title
T Cell Receptor Gene Engineered Cell Therapy for Cancer

Author
Yu, Jiaji

Publication Date
2021

Peer reviewed|Thesis/dissertation

UNIVERSITY OF CALIFORNIA

Los Angeles

T Cell Receptor Gene Engineered Cell Therapy for Cancer

A dissertation submitted in partial satisfaction of the

requirements for the degree Doctor of Philosophy

in Molecular Biology

by

Jiaji Yu

2021

ABSTRACT OF THE DISSERTATION

T Cell Receptor Gene Engineered Cell Therapy for Cancer

by

Jiaji Yu

Doctor of Philosophy in Molecular Biology

University of California, Los Angeles, 2021

Associate Professor Lili Yang, Chair

Cancer immunotherapy has become the new medicine for cancer patients providing curative hopes. The adoptive cell transfer of engineered T cells has demonstrated promising clinical response rates, especially for chimeric antigen receptor (CAR) therapies and T cell receptor (TCR) engineered therapies. This dissertation aims to extend the findings of previous engineered T cell therapies focusing on TCR-engineered T cells. Two TCRs are studied here: NY-ESO-1-specific TCR (esoTCR) and invariant natural killer T (iNKT) cell TCR. Towards the "off-the-shelf" T cell immunotherapy, we demonstrated the efforts in developing the TCR toolbox, the

ex vivo allogeneic T cell generation platform, combination engineering methods for next-generation allogeneic T cell product, and nanomaterials for T cell activation and expansion.

NY-ESO-1 attracts wide attention for developing targeted cancer therapies for its broad aberrant expression across tumor types and strong ability to elicit immune responses. Due to the MHC restriction nature of TCR, a toolbox of esoTCRs with various NY-ESO-1 epitope specificity and MHC restriction is in great need to expand the patient pool and prevent tumor evasion through the loss of MHC heterozygosity. Chapter 2 of this dissertation will present the work on isolation and characterization of NY-ESO-1-specific TCRs restricted on various MHCs.

Most current engineered T cell therapies, including CAR and TCR therapies, fall under autologous cell therapy. The autologous approach has demonstrated its feasibility and effectiveness. The personalized nature of autologous therapies has also greatly limited the further extended use of engineered T cells in the clinic. In Chapters 3 and 4, we established a novel ex vivo HSC-based TCR-engineered T cell generation platform for allogeneic "off-the-shelf" T cell therapies for cancer. In two separate works, we demonstrated the use of esoTCR and iNKT TCR in this platform. The combinational uses of CAR, CRISPR-Cas9 gene editing, and other enhancement genes were also explored in these two chapters.

T cell activation and expansion is an essential step required for all T cell-based immunotherapies. The developmental path of T cell activating methods starts from the simple addition of anti-CD3 antibodies to magnetic antibody-conjugated beads that are commercially available nowadays. Striving to mimic the natural cell-cell interaction and immunological synapse

relating to T cell activation, in Chapter 5, we present a novel nanomaterial-based method for ultrahigh T cell activation and expansion.

Collectively, the work described here advances the field of T cell therapies by enriching the toolbox of TCRs restricted on various MHC, establishing an ex vivo HSC-based TCR-engineered T cell generation platform which provides new allogeneic T cell sources towards the "off-the-shelf" T cell therapies for cancer patients, and providing a new nanomaterial-based method for ultrahigh T cell activation and expansion.

The dissertation of Jiaji Yu is approved.

Arnold I. Chin

Andrew Goldstein

Yu Huang

Donald B. Kohn

Lili Yang, Committee Chair

University of California, Los Angeles

2021

DEDICATION

This dissertation is dedicated to my mom and dad:

Bo Dai

and

Hong Yu

who created, loved, and shaped me.

TABLE OF CONTENTS

LIST OF FIGURES AND TABLES

Chapter 1:

No figures.

Chapter 2:

Chapter 3:

Chapter 4:

Chapter 5:

ACKNOWLEDGEMENTS

First, I would like to acknowledge my mentor, Lili Yang. I will never forget the Christmas day of 2015, Lili interviewed me at a hotel in suburban Shanghai. She granted me the chance to come to UCLA and pursuit the study of immunology in a foreign land. My life course would have been changed drastically without her taking the chance on me. I would always be thankful for that. During my study at UCLA, Lili's patience in mentoring and teaching, constant support to my research, and her extraordinary enthusiasm towards sciences propelled me well through the turbulent course of my Ph.D. study. She is not only a mentor of scientific research but also a mentor of my professional career. Being lucky enough to join the lab at the exciting time when cancer immunotherapy is undergoing dynamic development, it is my great hope that the technologies we studied and worked on would bring new hope to patients who suffer from cancer.

I want to acknowledge all the members of the Yang lab who mentored, helped, supported, and collaborated with me over the past five years of my Ph.D. study. They generously shared their scientific knowledge, laboratory skills, and their wisdom in life. The supportive and collaborative lab environment nurtured me to become a better researcher. I want to thank Drake Smith and Stefano Di Biase, who mentored me, and I really enjoyed sharing the bay with them. Thank you, Xi Wang, for being the most reliable senior member to go to whenever I am in doubt at work and for being such a caring person in life. Thank Yucheng Wang for all the laughter we shared and for being my loyal friend inside and outside the lab. I want to acknowledge Yujeong Kim for her consistent support, for being my most important collaborator in the lab, and taking me to SoulCycle. I want to thank Zhe Li for all the insightful discussions and skills she taught me, and for sharing all the hotpot nights. I would like to thank my fellow graduate student lab mates Yanruide Li, Yang

Zhou, and Derek Lee for supporting each other and sharing the journey of Ph.D. study. I need to especially thank Li and Zhou, who enabled my research and assisted me tons on experiments. My progress wouldn't be possible without them. I also need thank our lab manager Jie Huang for her wonderful support to our daily activities. The lab won't run in such a smooth way without her. I truly appreciate all the mentorship and friendship that I gained in the lab. I will miss you all.

I would like to thank all my wonderful collaborators with whom I have had the luck to work for the past five years. I would like to thank Michael Bethune and Xiaohua Li, who are my first two collaborators on the NY-ESO-1 TCR project. The work we shared laid the foundation of my entire Ph.D. study and granted me my first ever publication. All the techniques and skills I acquired through this project benefitted me throughout my five years of Ph.D. study. I would like to thank Yujeong Kim, who I collaborated with on two major "off-the-shelf" projects presented here in this dissertation. She is such a wonderful human being and a sincere friend. I wish to thank her for all those 12-hour lab days we shared and all the support and care she gave. I would like to thank Enbo Zhu. With his dedication and hard work, we were able to make a sideline collaboration into a major project which is also presented in this thesis. His earnestness to work, generous personality, and great sense of humor made him an amazing collaborator and a wonderful friend.

I would like to acknowledge all the members of my thesis committee for their insightful advice on my thesis work and constant support for my study at UCLA. I received tremendous amounts of support from my committees on all kinds of applications for scholarships, fellowships, and training grants. Special thanks go to Dr. Donald Kohn, who taught me a great lesson in my first application to a training grant and continuously supported me.

I had the pleasure to TA the class immunology with Lili and Dr. Zoran Galić for two quarters. Zoran taught me the definition of enthusiasm for teaching, responsibility, and caring for students. His sense of humor lighted up the entire experience. I genuinely appreciate his mentorship and him being the exemplary teacher. I would also like to thank all the students that I have taught. They made my experience, and I genuinely enjoyed teaching them.

I would like to thank all the undergraduate students who have assisted me in the lab. A lot of my research work would not be possible without their hardworking. I need to specially acknowledge Zoe Hann and Yuchong Zhang, who I directly supervised. They were my keys to survival in those days of intense lab work. They worked hard and never complained. I am delighted to see both of them graduate with honors and well off on their journey to become successful future physicians.

I would like to thank all the core services that supported our research on campus: the FACS Core, Virology Core, Pathology Core, and Technology Center for Genomics & Bioinformatics. I need especially thank Jeff Calimlim from FACS Core, who always agrees to my last-minute late-time sorting request.

I need to acknowledge the Ph.D. program of molecular biology by the Molecular Biology Institute (MBIDP). The offer I got from MBIDP at UCLA changed my life course. My special thanks go to Peter Bradley, who was my home area director. His warm caring for students made me feel at home in a foreign land.

I would like to acknowledge my funding source for the last three years of my Ph.D. study. The UCLA Eli and Edythe Broad Center of Regenerative Medicine and Stem Cell Research (BSCRC) generously supported me in three consecutive years, enabling my research towards better stem-cell-based cell therapies for cancer.

My fellow Ph.D. classmates – Jiaying Han, Feiyang Ma, Zhiyuan Mao, Lingyu Zhan, Weixian Deng, Jiajing Li, and Xinyuan Chen -- thank you for being my friends. I enjoyed all the meals, drinks, basketball, and tennis sessions you shared with me. I need to especially thank Feiyang Ma for his tremendous support on all the sequencing data analysis, which significantly improved my research quality.

My friends outside my Ph.D. study – Yuhuai Lin, Cong Jin, Sixuan Lu, Yuxi Lin, Xiaorui Ge, Yao Meng, Ruifan Deng, and Changling Dai – your accompany and friendship granted me joy and confidence, which strongly backed me up when I am exhausted by the lab work.

Lastly, my eternal gratefulness goes to my mom, dad, and family, who loved and supported me as always. Dr. Bo Dai and Dr. Hong Yu, I can finally be one of you PhDs (haha). It was not easy to move across the world from you, and I really regret that I wasn't able to be home for the past four years. All the phone calls and video chats with you brought me great comfort and tranquility. You can always replenish me with courage and determination to become a better version of myself. You will always be my biggest motivation in life.

VITA

EDUCATION

University of California, Los Angeles, Los Angeles, USA *2016 – 2021*
Ph.D. candidate, expected date of completion: Aug 2021
Home area: Immunity, Microbes, and Molecular Pathogenesis, UCLA Molecular Biology Institute
- MBIDP Dissertation Year Award
- UCLA BSCRC Stem Cell Predoctoral Fellowship (2018-2021)

The Hong Kong Polytechnic University, Hung Hom, Hong Kong *2012 – 2016*
BSc in Applied Biology and Biotechnology
-First-Class Honors | GPA: 3.99/4.0

Georgia Institute of Technology, Atlanta, USA *2015*
Exchange

RESEARCH & TEACHING

- **Stem cell-based cell therapy for cancer / T cell-based immunotherapy for cancer**
- **Nanomaterial-based biomimetics for T cell activation**
- **Tumor immunology**

(Graduate Student Researcher, Ph.D. Candidate, Lili Yang Lab, UCLA) *2016 – 2021*
- HSC engineered iNKT cell therapy for cancer
- NYESO-specific-TCR engineered T cell therapy
- Off-the-shelf iNKT/CART cell immunotherapy for
- Nanomaterial-based biomimetics of immune synapses for ultrahigh lymphocyte activations
- Immune regulatory roles of creatine transporter and monoamine oxidase in tumor environment

- **Comparative proteomics for chronic MeHg intoxication in brain** 2015 – 2016

(Research Assistant, Samuel Chun-lap Lo Lab, Hong Kong Polytechnic University)

Teaching Assistant
(**Immunology,** MIMG185A, Department of MIMG, UCLA) *Winter 2018 / Spring 2019*

PUBLICATIONS

1. Michael T. Bethune*, Xiao-Hua Li*, **Jiaji Yu***, Jami Witte, ..., Antoni Ribas, Lili Yang§, Owen Witte§, and David Baltimore§. **(*Contributed equally)** (2018). "Isolation and characterization of NY-ESO-1–specific T cell receptors restricted on various MHC molecules." *Proceedings of the National Academy of Sciences* 115.45 (2018): E10702-E10711.
2. Yanni Zhu*, Drake J. Smith*, Yang Zhou, Yan-Ruide Li, **Jiaji Yu**, Derek Lee, ..., Stephen Forman, James Heath, David Baltimore, James Economou, Jerome A. Zack, Gay M. Crooks, Caius Radu, Antoni Ribas, Donald B. Kohn, Owen N.Witte, and Lili Yang§ (2019) "Development of Hematopoietic Stem Cell-Engineered Invariant Natural Killer T Cell Therapy for Cancer." *Cell stem cell*, 25(4), 542-557.
3. Stefano Di Biase*, Xiaoya Ma*, Xi Wang, **Jiaji Yu**, Yu-Chen Wang, ..., Lili Yang§. (*Contributed equally). (2019). "Creatine uptake regulates CD8 T cell antitumor immunity." *Journal of Experimental Medicine*, jem-20182044.
4. Yu-Chen Wang, Xi Wang, **Jiaji Yu**, Feiyang Ma, ..., Sanaz Memarzedeh, Matteo Pellegrini and Lili Yang. (2021). "Targeting Monoamine Oxidase A-Regulated TAM Polarization for Cancer

Immunotherapy" *Nature communications*, *12*(1), 1-17.

5. Xi Wang, Bo Li, Yu Jeong Kim, Yu-Chen Wang, Zhe Li, **Jiaji Yu**, Samuel Zeng, ..., Matteo Pellegrini, and Lili Yang§. (2021). "Targeting monoamine oxidase A for cancer immunotherapy" *Science Immunology*, 6.
6. Yan-Ruide Li*, Yang Zhou*, Yu Jeong Kim, Yanni Zhu, Feiyang Ma, Xianhui Chen, **Jiaji Yu**, Yu-Chen Wang, ..., Gay M.Crooks, Donald B.Kohn, Owen Witte, Ping Wang and Lili Yang§. (*Contributed equally). "Generation of Allogeneic Hematopoietic Stem Cell-Engineered Invariant Natural Killer T cells for Off-the-Shelf Immunotherapy." In revision at *Cell Stem Cell.*
7. **Jiaji Yu***, Yu Jeong Kim*, Yang Zhou, Yan-ruide Li, ... and Lili Yang§. "An *Ex Vivo* Feeder-Free Culture Method to Generate Hematopoietic Stem Cell-Engineered Off-The-Shelf CAR-iNKT Cells for Cancer Immunotheraoy." **(*Contributed equally)**. In Preparation for submission.
8. **Jiaji Yu***, Yu Jeong Kim*, Yan-ruide Li, Yang Zhou, ... and Lili Yang§. "Off-the-shelf Hematopoietic Stem Cell-based NY-ESO-1-specific T cells for Immunotherapy." **(*Contributed equally)**. In preparation for submission.
9. **Jiaji Yu***, Enbo Zhu*, Feiyang Ma, Chengzhang Wan, ..., Lili Yang§ and Yu Huang§ "Ultrahigh T cell Activation through Biomimetic Graphene Oxide Antigen Presenting Platform" **(*Contributed equally)**. In preparation for submission.

PATENTS

- Lili Yang, **Jiaji Yu**, Yu Jeong Kim, Pin Wang, Yan-Ruide Li. 2019. "A feeder-free ex vivo differentiation culture method to generate off-the-shelf monoclonal TCR-Armed Gene-Engineered T (TARGET) cells", 2019. U.S. Provisional Patent Application No. 62/946,747
- Lili Yang, **Jiaji Yu**, Yu Jeong Kim, Pin Wang, Yan-Ruide Li.2019. "A feeder-free ex vivo differentiation culture method to generate off-the-shelf monoclonal TCR-Armed Natural Killer (TANK) cells", 2019 U.S. Provisional Patent Application No. 62/946,788
- Lili Yang, Yu Huang, **Jiaji Yu**, Enbo Zhu. 2020. "IL-2 independent ultrahigh human T cell activations through biomimetics of immune synapses by graphene oxides" UCLA Case No. 2021-068-1.

HONORS & AWARDS

- UCLA Molecular Biology Interdepartmental Doctoral Program Dissertation Award — Sep 2020
- UCLA BSCRC Predoctoral Fellowship — Jun 2020
- UCLA BSCRC Predoctoral Fellowship — Jun 2019
- UCLA Broad Center of Regenerative Medicine and Stem Cell Research (BSCRC) Predoctoral Fellowship — Jun 2018
- Outstanding Poster Presentation Award, MBI annual retreat, UCLA — Mar 2018
- Bachelor of Science with First-Class Honours, GPA of Award: 3.99 — Jun 2016
- Hong Kong Special Administrated Region Government Scholarship — *Nov 2015*
- Hong Kong Polytechnic University Scholarship — *Apr 2014*
- Hong Kong Special Administrated Region Government Reaching Out Award — *Jun 2014*
- Dean's Honours List 15/16, Hong Kong Polytechnic University — *Nov 2016*
- Dean's Honours List 14/15, Hong Kong Polytechnic University — *Nov 2015*
- Dean's Honours List 13/14, Hong Kong Polytechnic University — *Nov 2014*
- Subject Prize for Outstanding Performance 15/16, Hong Kong Polytechnic University — *Nov 2016*
- Prize of Academic Excellence 14/15, Hong Kong Polytechnic University — *Nov 2015*
- Subject Prize for Outstanding Performance 13/14, Hong Kong Polytechnic University — *Oct 2014*
- Second Prize for China National Biology Olympiad — *Mar 2011*
- Second Prize in 23th Yunnan Youth Science & Technology Innovation Contest — *Apr 2008*

CHAPTER 1:

TCR Gene Engineered Cell Therapy for Cancer

A brief introduction to therapeutic T cell engineering

T cell is a type of lymphocyte that develops in thymus[1], and is distinguished by its expression of T cell receptor (TCR), which delivers the specificity[2]. T cell plays a central role in the adaptive immunity fighting against cancerous cells and infectious pathogen[3]. There was a long history of adoptive T cell transfer (ACT) in the laboratory for research and continued exploration in the clinic because of T cell's pivotal role in tumor rejection[4]. Early clinical exploration of ACT included the use of autologous lymphokine-activated killer cells and tumor-infiltrating lymphocytes (TIL) to treat human solid tumors[5, 6]. At the same time, the idea of adopting T cells in cancer treatment was also inspired by bone marrow transplantation, wherein allogeneic T cells were sometimes found to eradicate blood cancer through graft-versus-leukemia (GvL) effect[7]. And now, with the development of gene transfer technology, transgenic T cell immunotherapy has already become a powerful new generation of cancer medicines, offering promising even curative responses to patients with cancer[4, 8]. In particular, chimeric antigen receptor (CAR) T cell therapy has shown great clinical success because of the durable clinical responses of otherwise treatment-refractory cancers[8-10]. In 2017, the first CAR T therapy targeting CD19 B lymphocyte molecule was approved by the U.S. Food and Drug Administration (FDA) to treat refractory pre-B cell acute lymphoblastic leukemia (ALL) and diffuse large B cell lymphoma. Recently, in April 2021, B-cell maturation antigen (BMCA)-targeted CAR T therapy was also approved by the FDA to treat multiple myeloma. With these successful precedent cases, the scientific field of T cell therapy is advancing fast, and the runway of commercializing various forms of ACT by pharmaceutical and biotechnology companies is getting more and more crowded.

There are two major types of ACT based on gene engineering that are being developed for cancer immunotherapies. They are TCR T cell therapies and CAR T cell therapies. Both TCR and CAR engineering aim to redirect T lymphocytes' natural specificity to targeting tumors[4, 8, 11]. In most current T cell cancer immunotherapies, including the FDA-approved ones, peripheral blood is drawn from the patient and peripheral blood mononuclear cells (PBMCs), containing T and other lymphocytes. PBMCs are stimulated and then transduced with a viral vector encoding a TCR or CAR gene. Transduced cells are further expanded to reach therapeutic numbers before the final transfusion back to the patient[12-17]. This approach is described as autologous for cells derived from one will only be used to treat that particular patient. There are many variations and modifications to the brief protocol described, but they share this core autologous approach.

TCRs are comprised of an α- and β-chain, upon noncovalent assembly with CD3 molecules, TCR/CD3 complex present on the T cell surface[18]. TCR surveils peptide ligand presented by to major histocompatibility complex (MHC) on all nucleated cells. T cell will get activated upon sufficient binding with correct recognition of TCR to peptide/MHC complex. The specificity of the TCR is determined by both the peptide ligand and the presenting MHC molecule. The MHC, also known as human leukocyte antigen (HLA) in humans, is the most multiallelic gene in the human genome, encompassing more than 18,000 MHC class I and II alleles that vary widely in frequency ethnic groups[19, 20]. Normally, endogenously generated antigens get to be presented on MHC class I (MHC-I) molecules and after proteasomal processing. Tumor and infected cells present aberrant or foreign peptides that can be recognized by $CD8^+$ T cells, leading to T-cell mediated killing of the presenting cells. With the transfer of tumor-specific TCR genes, T cells can be engineered to target and kill the tumor, so that TCR-engineered ACT for cancer was developed.

Considering the antigen peptide specificity and MHC restriction of TCR, for TCR gene therapy to work, patients need to express both the MHC allele that the transgenic TCR is restricted to and the tumor-specific antigen. Therefore, numerous research efforts were paid to public tumor-specific antigen discovery. For each of these tumor antigens, multiple TCRs need to be identified to ensure patients' eligibility with different HLA haplotypes[21]. TCR-engineered ACT is compelling because it utilizes the physiological antigen recognition and activation of T cells. It has generated very promising clinical responses in patients with metastatic melanoma and synovial sarcoma[14, 22].

An alternative approach to redirect the specificity of T cells lies in the design of CAR, which contains an antigen-binding domain--usually a single-chain variable domain of antibodies (scFv), a transmembrane linker, a singling domain from CD3 ζ chain, and a costimulatory domain from receptors like CD28, OX40, and 41BB[8]. CARs overcome some of the limitations of TCRs, including the MHC restriction and the need for co-stimulation. One major tumor evasion mechanism is through the loss of MHC expression[23], and the MHC independent targeting of CAR renders its great advantage in cancer immunotherapy. Nevertheless, limitations for CARs also exist, such as the tonic signaling resulting in T cell exhaustion and the target requirement of an extracellular surface antigen.

TCR-engineered T cell therapy and NY-ESO-1-based T cell therapy for cancer

To enable TCR-engineered T cell immunotherapy against cancer, tumor-associated or tumor-specific antigen targeting is the key. Neoantigens resulting from tumor-specific mutations are a potential source of such targets; however, these neoantigens are usually patient-specific or

also described as private[24]. Therefore, the implementation of TCR-engineered T cell therapy will have to be personalized to each patient. The steps of personalized TCR therapy can be very hard to implement for its complex procedures and the prolonged time. First, tumor mutations need to be identified via sequencing. Then TCRs specific to the mutation and the patient need to be isolated, and last patient T cells need to be engineered by the isolated TCR for the ACT uses. This process will be more challenging or even impossible for tumors inaccessible for sequencing and tumors with low mutational burden[25]. As a result, the identification and targeting of public antigens commonly expressed across patients become compelling to researchers and clinicians.

MART1 (melanoma antigen recognized by T cells 1) is the first public antigen tested under a TCR-engineered ACT context. The first clinical trial came with the objective responses in 2/15 patients with metastatic melanoma[26]. The subsequent use of a high-avidity MART1-specific TCR (clone F5) boosted the response rate to 30%. Yet, it came with the cost of targeting normal healthy melanocytes in the skin, eye, and cochlea engendering vitiligo, uveitis, and transient hearing loss[27]. TCR-engineered T cell therapies targeting other public antigens have caused serious adverse effects or even morbidity because of this on-tumor/off-target reactivity. T cell therapy targeting carcinoembryonic antigen endangered severe colitis in patients with metastatic colorectal for causing cross-reactivity with normal colorectal tissues[28]. Unfortunately, morbidity was caused in T cell therapies targeting ERBB2 and MAGE-A3 due to the under-appreciated expression of target antigens on vital organs[29, 30]. All these make the field recognized the thin line between efficacy and toxicity in targeting public tumor-associated antigens, underscoring the necessity to identify more stringently tumor-specific public antigen[31].

New York esophageal squamous cell carcinoma 1 (NY-ESO-1) is a prototypical caner-testis antigen (CTA) encoded by the gene *CTAG1B*[32]. CTAs are considered great candidates for immunotherapy due to their unique set of features, including restricted expression in immune-privileged organs, the stable expression on cancer cells, and their ability to elicit immune responses[33]. Of the group of CTAs, which to date comprise more than 250 proteins[34], NY-ESO-1 is a particularly attractive target for TCR-engineered T cell therapy. The aberrant expression of NY-ESO-1 was reported in a wide range of tumor types. The aberrant expression frequency ranges from 10-50% among solid tumors, 26% of prostate cancer, 46% of melanoma, 43% of ovarian cancer, and up to 80% in synovial sarcoma neuroblastoma[21, 35, 36], with increased expression higher-grade metastatic tumor tissue[22, 37, 38]. More importantly, NY-ESO-1 is highly immunogenic and can elicit a potent cellular immune response against multiple epitopes presented by various MHC alleles, including both $CD4^+$ and $CD8^+$ T cell responses[39-41]. Retroviral-mediated clinical trials on the ACT of NY-ESO-1-specific TCR (esoTCR) engineered T cells have been performed successfully to treat melanoma and synovial sarcoma with 45% and 67% response rates respectively[14]. Another lentiviral-mediated esoTCR engineered T cell therapy in patients with multiple myeloma resulted in 70% complete or near-complete responses without significant safety concerns[42]. The majority of these ACT clinical trials focused on esoTCRs specific to the NY-ESO-$1_{157-165}$ (SLLMWITQC) presented by HLA-A*02:01 (HLA-A2) and again falls into the category of autologous therapies[35]. To broaden the clinical utility of NY-ESO-1 as a TCR target, we previously have successfully isolated and characterized multiple esoTCRs targeting NY-ESO-1 epitopes presented by other common MHC alleles different than HLA-A2[21]. This part of the research will be discussed in detail in Chapter 1 of this dissertation.

Invariant natural killer (iNKT) cells and iNKT immunotherapy for cancer

Invariant natural killer T (iNKT) cells, or type I NKT cells, are a unique subset of αβ T lymphocytes characterized by their expression of NK lineage markers (CD161 in humans and NK1.1 in mouse) and a semi-invariant T cell receptor comprised of a semi-invariant TCR α chain (Vα24-Jα18 in human and Vα14-Jα18 in the mouse) paired to a limited repertoire of Vβ chains (Vβ 11 in human and Vβ 2, 7, or 8.2 in mouse)[43, 44]. They derive from the same lymphoid precursor pool as conventional αβ T cells and mature in the thymus. Nevertheless, unlike conventional αβ T cells that recognize peptide antigens, iNKT cells recognize lipid antigens presented by non-polymorphic MHC-I like molecule CD1d[45]. iNKT cells are also characterized by their small numbers *in vivo*: ~0.1%–1% in mouse blood and ~0.01%–1% in human blood[43]. iNKT cells belong to the first batch of activated cells during an immune response. They can rapidly produce copious amounts of cytokines and chemokines, thus serving as a "bridge" between innate and adaptive immune responses[43].

There are three major mechanisms to activate iNKT cells: 1) through TCR stimulation; 2) through cytokine stimulation; 3) through NK activating receptor stimulation. Potent non-physiological lipid antigen (e.g., α-GalCer) presented on CD1d directly activates iNKT cells independent of co-stimulation and cytokine engagement. Nevertheless, under physiological context, microbial or self-derived lipid antigens are usually poorly immunogenic, so that proinflammatory cytokine stimulation is required for the proper activation of iNKT cells. Of note, in some situations, cytokine alone (e.g., IL-12, IL-18, IL-23, and IL-25) are sufficient enough to induce iNKT activation independent of TCR engagement. The third way to activate iNKT cells is

through the NK path, wherein activation gets granted when total signals from NK activating receptors surpass those from NK inhibitory receptors. Upon the activation, iNKT cells display a significant effector function through secreting a variety of and copious amounts of cytokines, including T helper (Th)1-like (IFN-γ), Th2-like (IL-4, IL-13), Th17-like (IL-17, IL-22), and regulatory (IL-10) cytokines. The mechanisms of cell activation, the localization, and the iNKT cell subsets all together decide which cytokines are to produce. More importantly, compared to conventional T cells, the activation and cytokine release of iNKT cells respond much faster and at a much high magnitude (up to 100 times more cytokine than conventional T cells). By secreting a panel of cytokines, iNKT cells exert their function as master regulators modulating the immune responses bridging innate and adaptive immune systems.

Recent progress on understanding the activation and effector function of iNKT cells has accelerated related clinical research and particularly boosted the development of iNKT-based cancer immunotherapies. There are three major categories of functions iNKT cells exert under a cancer immunotherapy context: 1) direct cytotoxicity against tumor cells; 2) regulation of antitumor effector cells; 3) modulation of the immunosuppressive tumor microenvironment (TME)[46, 47]. iNKT cells directly kill $CD1d^+$ tumor cells via the production of cytolytic molecules like granzyme B and perforin and engaging death-inducing receptors like Fas and TRAIL receptors[48, 49]. In addition, with the expression of NK activating receptors like NKG2D and DNAM-1, direct cytotoxicity against tumors can also be induced through NK pathways[50]. Apart from the direct killing, iNKT cells are known to potentiate antitumor activities of various immune cells like NK cells, dendritic cells (DCs), and cytotoxic T lymphocytes (CTL)[47]. Most of these regulation functions link to DCs. Activated iNKT cells induce DC maturation through IL-12

upregulation and CD40L/CD40 interaction[51, 52]. Matured DCs in term will transactivate NK cells and prime cytotoxic T cells, mounting up both innate and adaptive immune responses against tumor[51, 52]. Last but not least, iNKT cells augment antitumor activities through counteracting immunosuppressive tumor-associated macrophages (TAMs)[47]. iNKT cells were found to kill $CD1d^+$ TAMs, alleviating the immunosuppressive TME and metastasis[53].

Currently, there are four approaches for utilizing iNKT cells for cancer immunotherapy: 1) autologous transfer approach, 2) allogeneic transfer approach, 3) CAR-iNKT approach, and 4) iPSC-iNKT approach[47]. The autologous transfer approach aims to increase iNKT cell numbers in cancer patients by expanding iNKT cells derived from patients' own PBMCs. The expansion of iNKT cells was achieved with α-GalCer and/or cytokines[54-56]. Autologous iNKT transfer showed no adverse effects in clinical trials[54, 57]; however, further improvement in clinical outcomes is needed. Our lab developed a variation of this approach, wherein autologous HSCs were engineered with iNKT TCR to enable long-term *in vivo* provision of iNKT cells[58, 59]. A preclinical model of this HSC-iNKT approach was developed by Zhu et al.. Effectively tumor suppression in multiple human tumor xenograft mouse models was demonstrated with no toxicity or tumorigenicity from the HSC-iNKT therapy[59]. Allogeneic hematopoietic cell transplant (Allo-HCT) is another powerful approach to fight against blood cancer. Allogeneic iNKT cells were shown to promoting graft-versus-leukemia (GvL) effect while preventing the development of graft-versus-host diseases (GvHD) in preclinical models[60-62]. The protective role of iNKT cells against GvHD has been highlighted by several clinical trials[63, 64], indicating the potential use of allogeneic iNKT cells in future Allo-HCT therapies to promote safety. Adding CARs to iNKT cells represents another approach for improving tumor specificity of iNKT immunotherapies for cancer. Two car

constructs (i.e., CD19-CAR and GD2-CAR) have been tested using iNKT cells as carriers against neuroblastoma and CD19+ lymphoma preclinically[65-67]. The GD2-CAR approach was rather promising, especially with the coexpression of IL-15[68], leading to clinical trials that are currently ongoing. No dose-limiting toxicities were found to observe expansion and tumor localization of GD2CAR-iNKT cells in the interim report of three patient[69]. Induced pluripotent stem cells (iPSCs) provide another allogeneic cell source for developing new iNKT therapies. The differentiation of NK and T cells from iPSCs was successfully demonstrated *in vitro*[70]. Recently, the generation of iNKT cells from iPSCs was also reported by two separated groups from Japan[71, 72]. The antitumor efficacy of iPSC-iNKT was well demonstrated with blood cancer models in preclinical studies. The first clinical trial of iPSC-iNKT was already planned for treating patients with head-and-neck cancer and expected to last for 2years involving 4-18 patients[47].

References

1. Koch, U. & Radtke, F. Mechanisms of T cell development and transformation. *Annual review of cell and developmental biology* **27**, 539-562 (2011).
2. Jorgensen, J.L., Reay, P.A., Ehrich, E.W. & Davis, M.M. Molecular components of T-cell recognition. *Annual review of immunology* **10**, 835-873 (1992).
3. Smith-Garvin, J.E., Koretzky, G.A. & Jordan, M.S. T cell activation. *Annual review of immunology* **27**, 591-619 (2009).
4. Sadelain, M., Rivière, I. & Riddell, S. Therapeutic T cell engineering. *Nature* **545**, 423-431 (2017).
5. Rosenberg, S.A., Spiess, P. & Lafreniere, R. A new approach to the adoptive immunotherapy of cancer with tumor-infiltrating lymphocytes. *Science* **233**, 1318-1321 (1986).
6. Rosenberg, S.A. & Lotze, M.T. Cancer immunotherapy using interleukin-2 and interleukin-2-activated lymphocytes. *Annual review of immunology* **4**, 681-709 (1986).
7. Weiden, P.L. et al. Antileukemic effect of graft-versus-host disease in human recipients of allogeneic-marrow grafts. *New England Journal of Medicine* **300**, 1068-1073 (1979).
8. June, C.H. & Sadelain, M. Chimeric antigen receptor therapy. *New England Journal of Medicine* **379**, 64-73 (2018).
9. Labanieh, L., Majzner, R.G. & Mackall, C.L. Programming CAR-T cells to kill cancer. *Nature biomedical engineering* **2**, 377-391 (2018).
10. Hong, M., Clubb, J.D. & Chen, Y.Y. Engineering CAR-T cells for next-generation cancer therapy. *Cancer cell* (2020).
11. Schmitt, T.M., Ragnarsson, G.B. & Greenberg, P.D. T cell receptor gene therapy for cancer. *Human gene therapy* **20**, 1240-1248 (2009).
12. Eshhar, Z., Waks, T., Gross, G. & Schindler, D.G. Specific activation and targeting of cytotoxic lymphocytes through chimeric single chains consisting of antibody-binding domains and the gamma or zeta subunits of the immunoglobulin and T-cell receptors. *Proceedings of the National Academy of Sciences* **90**, 720-724 (1993).
13. Porter, D.L., Levine, B.L., Kalos, M., Bagg, A. & June, C.H. Chimeric antigen receptor-modified T cells in chronic lymphoid leukemia. *N engl j Med* **365**, 725-733 (2011).
14. Robbins, P.F. et al. Tumor regression in patients with metastatic synovial cell sarcoma and melanoma using genetically engineered lymphocytes reactive with NY-ESO-1. *Journal of Clinical Oncology* **29**, 917 (2011).
15. Brentjens, R.J. et al. Safety and persistence of adoptively transferred autologous CD19-targeted T cells in patients with relapsed or chemotherapy refractory B-cell leukemias. *Blood, The Journal of the American Society of Hematology* **118**, 4817-4828 (2011).
16. Pule, M.A. et al. Virus-specific T cells engineered to coexpress tumor-specific receptors: persistence and antitumor activity in individuals with neuroblastoma. *Nature medicine* **14**, 1264-1270 (2008).
17. Liu, Y. et al. Durable remission achieved from Bcma-directed CAR-T therapy against relapsed or refractory multiple myeloma. *Blood* **132**, 956-956 (2018).
18. Murphy, K. & Weaver, C. Janeway's immunobiology. (Garland science, 2016).
19. González-Galarza, F.F. et al. Allele frequency net 2015 update: new features for HLA epitopes, KIR and disease and HLA adverse drug reaction associations. *Nucleic acids research* **43**, D784-D788 (2015).

20. Robinson, J. et al. The IPD and IMGT/HLA database: allele variant databases. *Nucleic acids research* **43**, D423-D431 (2015).
21. Bethune, M.T. et al. Isolation and characterization of NY-ESO-1–specific T cell receptors restricted on various MHC molecules. *Proceedings of the National Academy of Sciences* **115**, E10702-E10711 (2018).
22. Aung, P.P. et al. Expression of New York esophageal squamous cell carcinoma-1 in primary and metastatic melanoma. *Human pathology* **45**, 259-267 (2014).
23. Garrido, F., Aptsiauri, N., Doorduijn, E.M., Lora, A.M.G. & van Hall, T. The urgent need to recover MHC class I in cancers for effective immunotherapy. *Current opinion in immunology* **39**, 44-51 (2016).
24. Schumacher, T.N. & Schreiber, R.D. Neoantigens in cancer immunotherapy. *Science* **348**, 69-74 (2015).
25. Bethune, M.T. & Joglekar, A.V. Personalized T cell-mediated cancer immunotherapy: progress and challenges. *Current opinion in biotechnology* **48**, 142-152 (2017).
26. Morgan, R.A. et al. Cancer regression in patients after transfer of genetically engineered lymphocytes. *Science* **314**, 126-129 (2006).
27. Johnson, L.A. et al. Gene therapy with human and mouse T-cell receptors mediates cancer regression and targets normal tissues expressing cognate antigen. *Blood, The Journal of the American Society of Hematology* **114**, 535-546 (2009).
28. Parkhurst, M.R. et al. T cells targeting carcinoembryonic antigen can mediate regression of metastatic colorectal cancer but induce severe transient colitis. *Molecular Therapy* **19**, 620-626 (2011).
29. Morgan, R.A. et al. Case report of a serious adverse event following the administration of T cells transduced with a chimeric antigen receptor recognizing ERBB2. *Molecular Therapy* **18**, 843-851 (2010).
30. Morgan, R.A. et al. Cancer regression and neurologic toxicity following anti-MAGE-A3 TCR gene therapy. *Journal of immunotherapy (Hagerstown, Md.: 1997)* **36**, 133 (2013).
31. Jorritsma, A. et al. Selecting highly affine and well-expressed TCRs for gene therapy of melanoma. *Blood, The Journal of the American Society of Hematology* **110**, 3564-3572 (2007).
32. Chen, Y.-T. et al. A testicular antigen aberrantly expressed in human cancers detected by autologous antibody screening. *Proceedings of the National Academy of Sciences* **94**, 1914-1918 (1997).
33. Gjerstorff, M.F., Andersen, M.H. & Ditzel, H.J. Oncogenic cancer/testis antigens: prime candidates for immunotherapy. *Oncotarget* **6**, 15772 (2015).
34. Almeida, L.G. et al. CTdatabase: a knowledge-base of high-throughput and curated data on cancer-testis antigens. *Nucleic acids research* **37**, D816-D819 (2009).
35. Thomas, R. et al. NY-ESO-1 based immunotherapy of cancer: current perspectives. *Frontiers in immunology* **9**, 947 (2018).
36. Jain, R.K. et al. (American Society of Clinical Oncology, 2017).
37. Goydos, J.S., Patel, M. & Shih, W. NY-ESO-1 and CTp11 expression may correlate with stage of progression in melanoma. *Journal of Surgical Research* **98**, 76-80 (2001).
38. Sharma, P. et al. Frequency of NY-ESO-1 and LAGE-1 expression in bladder cancer and evidence of a new NY-ESO-1 T-cell epitope in a patient with bladder cancer. *Cancer Immunity Archive* **3** (2003).

39. Raza, A. et al. Unleashing the immune response to NY-ESO-1 cancer testis antigen as a potential target for cancer immunotherapy. *Journal of translational medicine* **18**, 1-11 (2020).
40. Ademuyiwa, F.O. et al. NY-ESO-1 cancer testis antigen demonstrates high immunogenicity in triple negative breast cancer. *PloS one* **7**, e38783 (2012).
41. Zhao, R.Y. et al. A novel HLA-B18 restricted CD8+ T cell epitope is efficiently cross-presented by dendritic cells from soluble tumor antigen. (2012).
42. Rapoport, A.P. et al. NY-ESO-1–specific TCR–engineered T cells mediate sustained antigen-specific antitumor effects in myeloma. *Nature medicine* **21**, 914-921 (2015).
43. Bendelac, A., Savage, P.B. & Teyton, L. The biology of NKT cells. *Annu. Rev. Immunol.* **25**, 297-336 (2007).
44. Lee, P.T., Benlagha, K., Teyton, L. & Bendelac, A. Distinct functional lineages of human Vα24 natural killer T cells. *The Journal of experimental medicine* **195**, 637-641 (2002).
45. Brigl, M. & Brenner, M.B. CD1: antigen presentation and T cell function. *Annu. Rev. Immunol.* **22**, 817-890 (2004).
46. Bae, E.-A., Seo, H., Kim, I.-K., Jeon, I. & Kang, C.-Y. Roles of NKT cells in cancer immunotherapy. *Archives of pharmacal research* **42**, 543-548 (2019).
47. Li, Z., Lee, D., Zeng, S. & Yang, L. in Successes and Challenges of NK Immunotherapy 63-80 (Elsevier, 2021).
48. Kawano, T. et al. Natural killer-like nonspecific tumor cell lysis mediated by specific ligand-activated Vα14 NKT cells. *Proceedings of the National Academy of Sciences* **95**, 5690-5693 (1998).
49. Wingender, G., Krebs, P., Beutler, B. & Kronenberg, M. Antigen-specific cytotoxicity by invariant NKT cells in vivo is CD95/CD178-dependent and is correlated with antigenic potency. *The Journal of Immunology* **185**, 2721-2729 (2010).
50. Kuylenstierna, C. et al. NKG2D performs two functions in invariant NKT cells: direct TCR-independent activation of NK-like cytolysis and co-stimulation of activation by CD1d. *European journal of immunology* **41**, 1913-1923 (2011).
51. Kitamura, H. et al. The natural killer T (NKT) cell ligand α-galactosylceramide demonstrates its immunopotentiating effect by inducing interleukin (IL)-12 production by dendritic cells and IL-12 receptor expression on NKT cells. *The Journal of experimental medicine* **189**, 1121-1128 (1999).
52. Fujii, S.I., Shimizu, K., Hemmi, H. & Steinman, R.M. Innate Vα14+ natural killer T cells mature dendritic cells, leading to strong adaptive immunity. *Immunological reviews* **220**, 183-198 (2007).
53. Song, L. et al. Vα24-invariant NKT cells mediate antitumor activity via killing of tumor-associated macrophages. *The Journal of clinical investigation* **119**, 1524-1536 (2009).
54. Motohashi, S. et al. A phase I study of in vitro expanded natural killer T cells in patients with advanced and recurrent non–small cell lung cancer. *Clinical Cancer Research* **12**, 6079-6086 (2006).
55. Kunii, N. et al. Combination therapy of in vitro-expanded natural killer T cells and α-galactosylceramide-pulsed antigen-presenting cells in patients with recurrent head and neck carcinoma. *Cancer science* **100**, 1092-1098 (2009).
56. Exley, M.A. et al. Adoptive transfer of invariant NKT cells as immunotherapy for advanced melanoma: a phase I clinical trial. *Clinical Cancer Research* **23**, 3510-3519 (2017).

57. Yamasaki, K. et al. Induction of NKT cell-specific immune responses in cancer tissues after NKT cell-targeted adoptive immunotherapy. *Clinical immunology* **138**, 255-265 (2011).
58. Smith, D.J. et al. Genetic engineering of hematopoietic stem cells to generate invariant natural killer T cells. *Proceedings of the National Academy of Sciences* **112**, 1523-1528 (2015).
59. Zhu, Y. et al. Development of hematopoietic stem cell-engineered invariant natural killer T cell therapy for cancer. *Cell stem cell* **25**, 542-557. e549 (2019).
60. Lan, F., Zeng, D., Higuchi, M., Higgins, J.P. & Strober, S. Host conditioning with total lymphoid irradiation and antithymocyte globulin prevents graft-versus-host disease: the role of CD1-reactive natural killer T cells. *Biology of Blood and Marrow Transplantation* **9**, 355-363 (2003).
61. Schneidawind, D. et al. CD4+ invariant natural killer T cells protect from murine GVHD lethality through expansion of donor CD4+ CD25+ FoxP3+ regulatory T cells. *Blood, The Journal of the American Society of Hematology* **124**, 3320-3328 (2014).
62. Schneidawind, D. et al. Third-party CD4+ invariant natural killer T cells protect from murine GVHD lethality. *Blood, The Journal of the American Society of Hematology* **125**, 3491-3500 (2015).
63. Lowsky, R. et al. Protective conditioning for acute graft-versus-host disease. *New England Journal of Medicine* **353**, 1321-1331 (2005).
64. Chaidos, A. et al. Graft invariant natural killer T-cell dose predicts risk of acute graft-versus-host disease in allogeneic hematopoietic stem cell transplantation. *Blood, The Journal of the American Society of Hematology* **119**, 5030-5036 (2012).
65. Heczey, A. et al. Invariant NKT cells with chimeric antigen receptor provide a novel platform for safe and effective cancer immunotherapy. *Blood, The Journal of the American Society of Hematology* **124**, 2824-2833 (2014).
66. Rotolo, A. et al. Enhanced anti-lymphoma activity of CAR19-iNKT cells underpinned by dual CD19 and CD1d targeting. *Cancer Cell* **34**, 596-610. e511 (2018).
67. Tian, G. et al. CD62L+ NKT cells have prolonged persistence and antitumor activity in vivo. *The Journal of clinical investigation* **126**, 2341-2355 (2016).
68. Xu, X. et al. NKT cells coexpressing a GD2-specific chimeric antigen receptor and IL15 show enhanced in vivo persistence and antitumor activity against neuroblastoma. *Clinical Cancer Research* **25**, 7126-7138 (2019).
69. Heczey, A. et al. Anti-GD2 CAR-NKT cells in patients with relapsed or refractory neuroblastoma: an interim analysis. *Nature Medicine* **26**, 1686-1690 (2020).
70. Iriguchi, S. & Kaneko, S. Toward the development of true "off-the-shelf" synthetic T-cell immunotherapy. *Cancer science* **110**, 16-22 (2019).
71. Yamada, D. et al. Efficient Regeneration of Human Vα24+ Invariant Natural Killer T Cells and Their Antitumor Activity In Vivo. *Stem Cells* **34**, 2852-2860 (2016).
72. Kitayama, S. et al. Cellular adjuvant properties, direct cytotoxicity of re-differentiated Vα24 invariant NKT-like cells from human induced pluripotent stem cells. *Stem cell reports* **6**, 213-227 (2016).

CHAPTER 2:

Isolation and Characterization of NY-ESO-1–specific T cell receptors restricted on various MHC molecules

Isolation and characterization of NY-ESO-1–specific T cell receptors restricted on various MHC molecules

Michael T. Bethune[a,1], Xiao-Hua Li[b,1], Jiaji Yu[b,c,1], Jami McLaughlin[b], Donghui Cheng[b], Colleen Mathis[b], Blanca Homet Moreno[d], Katherine Woods[e,f,g], Ashley J. Knights[g], Angel Garcia-Diaz[d], Stephanie Wong[a], Siwen Hu-Lieskovan[d], Cristina Puig-Saus[d], Jonathan Cebon[e,f,g], Antoni Ribas[d,h,i,j,k], Lili Yang[b,h,i,j,2], Owen N. Witte[b,h,k,2], and David Baltimore[a,2]

[a]Division of Biology and Biological Engineering, California Institute of Technology, Pasadena, CA 91125; [b]Department of Microbiology, Immunology, and Molecular Genetics, University of California, Los Angeles, CA 90095; [c]Molecular Biology Institute, University of California, Los Angeles, CA 90095; [d]Division of Hematology and Oncology, Department of Medicine, University of California, Los Angeles, CA 90095; [e]Cancer Immunobiology Laboratory, Olivia Newton-John Cancer Research Institute, Austin Hospital, Heidelberg, VIC 3084, Australia; [f]School of Cancer Medicine, La Trobe University, Bundoora, VIC 3086, Australia; [g]Cancer Immunobiology Laboratory, Ludwig Institute for Cancer Research, Heidelberg, VIC 3084, Australia; [h]Eli and Edythe Broad Center of Regenerative Medicine and Stem Cell Research, University of California, Los Angeles, CA 90095; [i]Jonsson Comprehensive Cancer Center, University of California, Los Angeles, CA 90095; [j]Department of Medicine, University of California, Los Angeles, CA 90095; and [k]Parker Institute for Cancer Immunotherapy, University of California, Los Angeles, CA 90095

Contributed by Owen N. Witte, September 26, 2018 (sent for review June 21, 2018; reviewed by Rafi Ahmed and Stephen P. Schoenberger)

Tumor-specific T cell receptor (TCR) gene transfer enables specific and potent immune targeting of tumor antigens. Due to the prevalence of the HLA-A2 MHC class I supertype in most human populations, the majority of TCR gene therapy trials targeting public antigens have employed HLA-A2–restricted TCRs, limiting this approach to those patients expressing this allele. For these patients, TCR gene therapy trials have resulted in both tantalizing successes and lethal adverse events, underscoring the need for careful selection of antigenic targets. Broad and safe application of public antigen-targeted TCR gene therapies will require (*i*) selecting public antigens that are highly tumor-specific and (*ii*) targeting multiple epitopes derived from these antigens by obtaining an assortment of TCRs restricted by multiple common MHC alleles. The canonical cancer-testis antigen, NY-ESO-1, is not expressed in normal tissues but is aberrantly expressed across a broad array of cancer types. It has also been targeted with A2-restricted TCR gene therapy without adverse events or notable side effects. To enable the targeting of NY-ESO-1 in a broader array of HLA haplotypes, we isolated TCRs specific for NY-ESO-1 epitopes presented by four MHC molecules: HLA-A2, -B07, -B18, and -C03. Using these TCRs, we pilot an approach to extend TCR gene therapies targeting NY-ESO-1 to patient populations beyond those expressing HLA-A2.

NY-ESO-1 | immunotherapy | T cell receptor gene therapy | TCR | MHC

The αβ T cell receptor (TCR) determines the unique specificity of each nascent T cell. Upon assembly with CD3 signaling proteins on the T cell surface, the TCR surveils peptide ligands presented by MHC molecules on the surface of nucleated cells. The specificity of the TCR for a peptide–MHC complex is determined by both the presenting MHC molecule and the presented peptide. The MHC locus (also known as the HLA locus in humans) is the most multiallelic locus in the human genome, comprising >18,000 MHC class I and II alleles that vary widely in frequency across ethnic subgroups (1, 2). Ligands presented by MHC class I molecules are derived primarily from proteasomal cleavage of endogenously expressed antigens. Infected and cancerous cells present peptides that are recognized by $CD8^+$ T cells as foreign or aberrant, resulting in T cell-mediated killing of the presenting cell.

T cells can be engineered to kill tumor cells through the transfer of tumor-reactive αβ TCR genes (3). Key to this approach is that the patient expresses the MHC allele on which the therapeutic TCR is restricted and that the targeted peptide is derived from a tumor-associated or tumor-specific antigen. Private (patient-specific) neoantigens resulting from tumor-specific mutations are a potential source of such targets (4). However, implementation of personalized TCR gene therapy is complicated by the need to identify mutations through sequencing, to isolate mutation-reactive, patient-specific TCRs, and to genetically modify patient T cells on demand. This is still more challenging for tumors that cannot be accessed for sequencing and for low-mutational-burden tumors with few or no neoantigens (5). Particularly for these last tumor types, targeting public, tumor-restricted antigens with off-the-shelf TCRs remains an attractive option.

The first public antigen targeted with TCR gene therapy in the clinic was melanocyte antigen MART1/Melan-A, yielding objective responses in 2/15 patients with metastatic melanoma (6). Use of a higher-affinity MART1-reactive TCR (F5) increased the response rate to 30% but also engendered vitiligo, uveitis, and transient hearing loss due to MART1 expression on healthy

Significance

T immune cells can be engineered to express tumor-specific T cell receptor (TCR) genes and thereby kill cancer cells. This approach—termed TCR gene therapy—is effective but can cause serious adverse events if the target is also expressed in healthy, noncancerous tissue. NY-ESO-1 is a tumor-specific antigen that has been targeted successfully and safely through TCR gene therapies for melanoma, synovial sarcoma, and myeloma. However, trials to date have focused exclusively on a single NY-ESO-1–derived epitope presented on HLA-A*02:01, limiting application to patients expressing that allele. In this work, we isolate TCRs that collectively recognize multiple NY-ESO-1–derived epitopes presented by multiple MHC alleles. We thereby outline a general approach for expanding targeted immunotherapies to more diverse MHC haplotypes.

Author contributions: M.T.B., X.-H.L., J.Y., J.M., D.C., C.M., B.H.M., K.W., J.C., A.R., L.Y., O.N.W., and D.B. designed research; M.T.B., X.-H.L., J.Y., J.M., D.C., C.M., B.H.M., K.W., A.J.K., A.G.-D., S.W., S.H.-L., and C.P.-S. performed research; M.T.B., X.-H.L., J.Y., J.M., D.C., C.M., B.H.M., K.W., J.C., A.R., L.Y., O.N.W., and D.B. analyzed data; and M.T.B., X.-H.L., J.Y., L.Y., O.N.W., and D.B. wrote the paper.

Reviewers: R.A., Emory University; and S.P.S., La Jolla Institute for Allergy and Immunology.

Conflict of interest statement: A patent application has been filed (serial no. 62/727,485) entitled "Composition of NY-ESO-1-Specific T Cell Receptors Restricted on Multiple Major Histocompatibility Complex Molecules."

[1]M.T.B., X.-H.L., and J.Y. contributed equally to this work.

[2]To whom correspondence may be addressed. Email: liliyang@ucla.edu, owenwitte@mednet.ucla.edu, or baltimo@caltech.edu.

This article contains supporting information online at www.pnas.org/lookup/suppl/doi:10.1073/pnas.1810653115/-/DCSupplemental.

Published online October 22, 2018.

melanocytes in the skin, eye, and middle ear (7). T cell therapies targeting other public antigens have similarly engendered morbidity or serious adverse events due to on-target/off-tumor reactivity. Targeting carcinoembryonic antigen produces severe colitis in patients with metastatic colorectal cancer due to reactivity with normal colorectal tissue (8). More seriously, T cell therapies targeted at ERBB2 or MAGE-A3 each resulted in deaths due to unappreciated expression of the target antigen (or similar variant) on vital organs (9, 10). Thus, these studies underscore the importance of identifying stringently tumor-specific public antigens (11), particularly when well-expressed, high-affinity targeting receptors necessary for therapeutic success are employed (7, 12).

NY-ESO-1—the product of the *CTAG1B* gene—is an attractive target for off-the-shelf TCR gene therapy. As the prototypical cancer-testis antigen, NY-ESO-1 is not expressed in normal, nongermline tissue, but it is aberrantly expressed in many tumors (13). The frequency of aberrant expression ranges from 10 to 50% among solid tumors, 25–50% of melanomas, and up to 80% of synovial sarcomas (13–18), with increased expression observed in higher-grade metastatic tumor tissue (14, 15, 19). Moreover, NY-ESO-1 is highly immunogenic, precipitating spontaneous and vaccine-induced T cell immune responses against multiple epitopes presented by various MHC alleles (20–23). As a result, the epitope NY-ESO-$1_{157–165}$ (SLLMWITQC) presented by HLA-A*02:01 has been targeted with cognate 1G4 TCR in gene therapy trials, yielding objective responses in 55% and 61% of patients with metastatic melanoma and synovial sarcoma, respectively, and engendering no adverse events related to targeting (24, 25). Targeting this same A2-restricted epitope with lentiviral-mediated TCR gene therapy in patients with multiple myeloma similarly resulted in 70% complete or near-complete responses without significant safety concerns (26). The majority of patients who respond to therapy relapse within months, and loss of heterozygosity at the MHCI locus has been reported as a mechanism by which tumors escape adoptive T cell therapy targeting HLA-A*02:01/NY-ESO-$1_{157–165}$ (27). Thus, NY-ESO-1 is a tumor-specific, immunogenic public antigen that is expressed across an array of tumor types and is safe to target in the clinic but that is susceptible to escape when targeted through a single HLA subtype.

In this work, we had two goals. First, since TCRs of higher strength and affinity are more efficacious, we sought to identify new TCRs that target A2/$NY_{157–165}$ with comparable or better sensitivity than the clinically employed 1G4 TCR. As affinity-enhanced TCRs can be cross-reactive (28–30), we established a protocol for isolating antigen-reactive TCRs directly from patient blood. Two of these TCRs demonstrated comparable or greater sensitivity than 1G4 both in vitro and in vivo in tumor-killing assays. Second, to broaden the clinical utility of NY-ESO-1 as a TCR gene therapy target, we used our isolation protocol to identify TCRs that target NY-ESO-1 epitopes presented by common MHC alleles other than HLA-A*02:01. We propose that targeting multiple NY-ESO-1 epitopes will enable treatment of a larger patient set and may render treatment more robust toward tumor escape.

Results

Expansion and Isolation of NY-ESO-1–Specific T Cell Clones. We previously reported the presence of T cells reactive with various NY-ESO-1–derived epitopes in the blood of patients with metastatic melanoma (22). To enrich for these reactive T cells, we stimulated expansion of patient peripheral blood mononuclear cells (PBMCs) with a panel of 28 overlapping 18-mers collectively constituting the full NY-ESO-1 protein sequence (Fig. 1*A*). We then restimulated the expanded cells with individual peptides, performed intracellular staining for IFN-γ to determine which peptides drove expansion, and analyzed stimulatory peptides with a predictive algorithm to identify minimal epitopes relevant to each patient's MHC haplotype (31) (Fig. 1*B*). Reactive T cells were reexpanded in the presence of individual 9–10-mer peptides corresponding to immunostimulatory epitopes (Fig. 1*C*) and sorted via FACS using cognate peptide–MHC tetramers (Fig. 1*D*). The cell lines grown from these single-cell sorts were clonal and reactive with their cognate epitopes (Fig. 1*E*). In total, four cell lines reactive with HLA-A*02:01/$NY_{157–165}$ and four cell lines reactive with epitopes presented by HLA-B and HLA-C alleles were selected for further study.

Cloning and Screening of NY-ESO-1–Specific TCRs. We cloned paired TCRα and TCRβ genes from sorted single cells using a commercial RT-PCR kit with custom multiplexed primers targeting all human TRAV and TRBV gene segments. The resulting V_α and V_β cDNAs were subcloned into a retroviral vector backbone with either human or murine TCR constant regions (Fig. 2*A*). To verify the specificity of cloned TCRs, we transfected $CD3^+$ HEK 293T cells with each fully human TCR and stained the transfected cells with peptide–MHC dextramer reagents for each of the targeted NY-ESO-1 epitopes (Fig. 2*B*). All four HLA-A2–restricted TCRs exhibited the expected reactivity (Fig. 2*C*). Although analyzed events were gated for similar transfection level, novel TCRs exhibited highly variable dextramer binding. Dextramer binding for the 9D2 TCR was barely discernible from background, whereas the 3A1 TCR exhibited superior dextramer binding compared with the clinically employed 1G4 TCR. Dextramer binding for 4A2 and 5G6 TCRs were intermediate between 9D2 and 1G4.

Additionally, three of four of the TCRs restricted on MHC alleles other than HLA-A2 were verified to bind their targets specifically (Fig. 2*D*). Transfected 293T cells expressing the B7/$NY_{60–72}$-specific 1E4 TCR, the B18/$NY_{88–96}$-specific 2B8 TCR, or the Cw3/$NY_{96–104}$-specific 3C7 TCR each bound their respective dextramers, whereas untransfected cells did not. Cells transfected with the 9G2 TCR—cloned from T cells that were reactive with Cw3/$NY_{92–100}$—did not detectably bind cognate dextramer relative to untransfected cells. A possible reason for this was that HEK 293T cells do not express the CD8 coreceptor. CD8 increases the avidity of the TCR–pMHC interaction by binding to MHCI directly, enabling lower affinity TCRs to engage (32). We therefore included this TCR for further analysis of CD8 dependency in Jurkat T cells.

Functional Characterization of A2-Restricted, NY-ESO-1–Specific TCRs. The sensitivity of a TCR-transduced T cell is a function of the monomeric affinity of the TCR for its cognate peptide–MHC (K_d ~ 0.1–400 μM) (33) as well as the density of the TCR on the cell surface (12). Transduced TCRs express on the T cell surface at widely varying levels due to variation in the efficiency with which they fold, dimerize, and compete with endogenous TCRs for assembly with limiting CD3 chains (a property termed TCR "strength") (34, 35). Therefore, optimal cytotoxic function of TCR-transduced T cells correlates with TCR affinity and surface expression (3, 12), underscoring the importance of selecting high-affinity, efficiently exported TCRs for gene therapy (7).

As higher-affinity TCR–pMHC interactions are less dependent on CD8 participation, we reasoned that high-affinity TCRs can be identified by comparing dextramer binding of TCR-transduced Jurkat T cells with or without coexpression of CD8. Additionally, because the strength of surface expression for human TCRs can be increased through substitution with murine constant domains (36), we expressed each TCR as a fully human or murinized derivative to assess each TCR's strength. Cells transduced with vehicle only or with a mismatched TCR (MART1-specific F5 TCR) did not exhibit any binding to A2/$NY_{157–165}$ dextramer (Fig. 3 *A* and *B*). By contrast, cells transduced with the well-established 1G4 TCR (K_d = 9.3 μM) (37) bound cognate dextramer whether 1G4 was fully human or murinized, and whether or not CD8 was present. Murinization of

MEDICAL SCIENCES

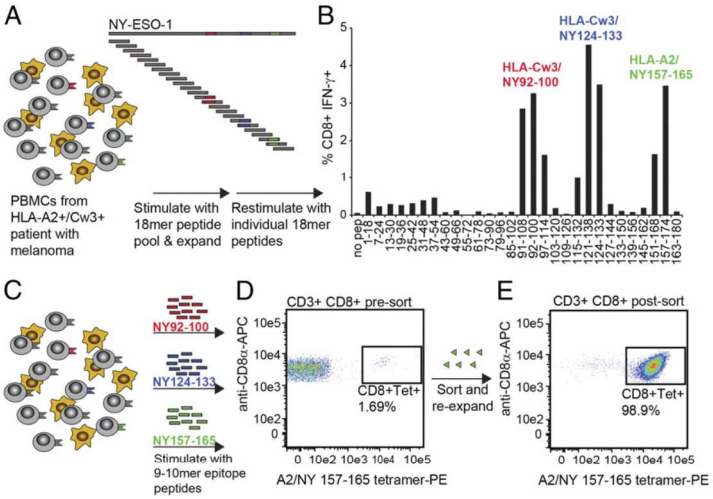

Fig. 1. Expansion and isolation of NY-ESO-1–specific T cell clones. PBMCs were obtained from patients with metastatic melanoma. T cell cloning strategy for a representative HLA-A2$^+$, HLA-Cw3$^+$ donor is shown. (*A*) Schematic outlining the expansion and testing strategy to identify NY-ESO-1–reactive T cell clones. PBMCs were incubated with 28 NY-ESO-1 18-mer peptides (overlapping by 12 aa) and then expanded for 10 d before restimulation with individual peptides in the presence of BFA. Epitopes presented by patient MHC alleles are colored red, blue, and green in those peptides containing the full epitope sequence. (*B*) Representative flow cytometry measurement of intracellular staining for IFN-γ in expanded PBMCs restimulated with individual NY-ESO-1–derived 18-mer peptides. (*C*) Schematic outlining the reexpansion strategy using individual 9–10-mer peptides verified to elicit a T cell response. (*D*) Representative flow cytometry data showing an NY-ESO-1–reactive subpopulation of CD3$^+$CD8$^+$ T cells before sorting. Sorted cells were expanded in the presence of IL-2 and irradiated autologous PBMCs. (*E*) Representative flow cytometry data showing an NY-ESO-1–reactive subpopulation of CD3$^+$CD8$^+$ T cells following sorting.

1G4 increased the intensity of dextramer binding by the muTCR 1.4-fold over the parental huTCR, indicating a modest improvement in strength (Fig. 3 *B* and *C*). The presence of CD8 increased dextramer binding 3.8-fold for 1G4 muTCR. Dextramer binding for TCRs 4A2 and 5G6 was similar in both magnitude and comparative indices to 1G4 (Fig. 3 *A*–*C*). The 3A1 TCR exhibited only a 1.9-fold increase in dextramer binding in the presence of CD8, indicating that this TCR binds A2/NY$_{157–165}$ with higher affinity than 1G4. This is further supported by the reduced dependence of dextramer binding on CD8 level among CD8$^+$ cells transduced with 3A1 muTCR relative to CD8$^+$ cells transduced with 1G4, 4A2, and 5G6 muTCRs (compare slopes of green populations in Fig. 3*A*). Finally, 9D2 exhibited no detectable binding to dextramer on Jurkat cells in the absence of CD8 and only weak binding upon coexpression of CD8. Murinization of 9D2 did not increase its binding to dextramer.

To compare the functional sensitivity of T cells expressing A2/NY-ESO-1–specific TCRs we coincubated TCR-transduced Jurkat T cells with K562 cells expressing either A*02:01/NY$_{157–165}$ or A*02:01/MART1$_{27–35}$ single-chain trimers (38) and measured secreted IL-2. All TCRs exhibited their expected peptide specificity: The control MART1-specific F5 TCR mediated IL-2 release only in response to MART1 presentation and all NY-ESO-1–specific TCRs mediated IL-2 release only in response to NY-ESO-1 presentation (Fig. 3*D*). Murinization improved functional sensitivity for all TCRs except for 1G4. Consistent with dextramer staining

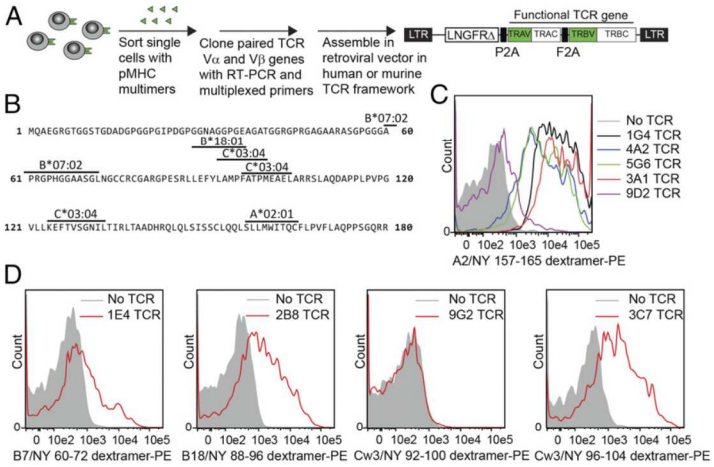

Fig. 2. Cloning and functional screening of NY-ESO-1–specific TCRs. (*A*) Schematic of functional TCR cloning strategy. For each TCR, two constructs were prepared incorporating either human or murine TCR constant domains. (*B*) Protein sequence of NY-ESO-1 with epitopes relevant to this study delineated. (*C*) Flow cytometry histograms comparing HLA-A2/NY$_{157–165}$ dextramer binding by HEK 293T cells transfected with vector backbone only, previously reported 1G4 TCR, and novel A2-restricted, NY-ESO-1–specific TCRs. (*D*) Flow cytometry histograms comparing indicated peptide–MHC dextramer binding by HEK 293T cells transfected with vector backbone only or the indicated novel NY-ESO-1-specificNY-ESO-1–specific TCR restricted on MHC alleles other than HLA-A2. Transfection experiments were performed twice, each in duplicate. Representative histograms are presented.

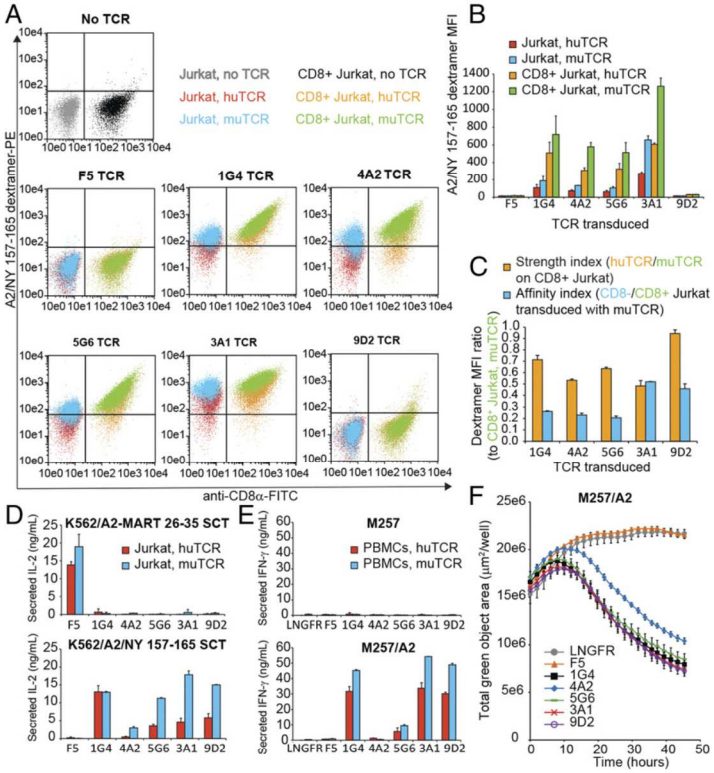

Fig. 3. Function of A2-restricted, NY-ESO-1–specific TCRs. (*A*) Overlay of representative flow cytometry plots comparing A2/NY$_{157–165}$ dextramer binding by Jurkat and CD8$^+$ Jurkat cells expressing A2-restricted TCRs with human or murine constant domains. (*B*) Dextramer binding mean fluorescence intensity measurements from two independent experiments as in *A*. (*C*) Ratio of dextramer binding mean fluorescent intensity measurements from two independent experiments in *B*. (*D*) ELISA measuring secretion of IL-2 from TCR-transduced Jurkat cells following 48-h coincubation with K562 target cells expressing A2/MART$_{26–35}$ or A2/NY$_{157–165}$ single-chain trimer. Experiment was repeated three times, each with two technical replicates. Means ± SD for a representative experiment are shown. (*E*) ELISA measuring secretion of IFN-γ from TCR-transduced PBMCs following 48-h coincubation with the melanoma cell line M257 or an A2$^+$ derivative. Experiment was repeated at least three times, each with two technical replicates. Means ± SD for a representative experiment are shown. (*F*) IncuCyte measurement of total green object area over time as a measurement of TCR-transduced T cell-mediated killing of GFP$^+$ A2$^+$ M257 cells. Means ± SD for four technical replicates are shown.

results, 1G4 and 3A1 muTCRs outperformed 4A2 and 5G6 muTCRs. By contrast, despite its weak binding to dextramer, 9D2 exhibited high functional sensitivity to cognate ligand, comparable to 3A1. To quantify this observation, we pulsed A2$^+$K562 cells with varied concentrations of NY-ESO-1$_{157–165}$ or MART1$_{27–35}$ peptide and then measured IFN-γ secretion from TCR-transduced primary T cells coincubated with peptide-pulsed target cells (*SI Appendix*, Fig. S1 *A* and *B*). As observed with single-chain trimer targets, 3A1, 9D2, and 1G4 exhibited highest sensitivity to NY-ESO-1$_{157–165}$ peptide. The functional sensitivity of 9D2 was 10-fold higher than 4A2, despite 4A2 binding dextramer with 18-fold higher MFI than 9D2 (Fig. 3 *A* and *B*). To evaluate responses to endogenously processed and presented antigen, TCR-transduced primary T cells were coincubated with the human melanoma cell line, A2$^+$M257 (Fig. 3*E*). Again, T cells transduced with 3A1, 9D2, and 1G4 responded comparably to one another, and with higher sensitivity than did those transduced with 5G6 and 4A2. TCR-transduced T cells did not respond to the M257 line lacking HLA-A*02:01. Finally, in vitro cytotoxicity tracked closely with cytokine release: T cells expressing 9D2 or 3A1 killed A2$^+$M257 tumor cells most efficiently, followed by T cells transduced with 1G4, 5G6, and, least efficiently, 4A2 (Fig. 3*F*).

To enable evaluation of TCR function in a tumor xenograft model, we engineered the PC-3 human prostate cancer cell line to express NY-ESO-1 and HLA-A*02:01 and then verified that this line elicited functional responses from TCR-transduced T cells in an antigen-dependent and MHC-restricted manner (*SI Appendix*, Fig. S2*A*). The relative responses to A2$^+$NY$^+$PC-3 from our panel of NY-ESO-1–reactive TCRs were consistent with those elicited by A2$^+$M257 (Fig. 3*E* and *SI Appendix*, Fig. S2*B*). Based on these results, we selected 1G4, 3A1, and 9D2 muTCRs for further functional characterization in vivo. We transduced activated human PBMCs with a vector encoding each murinized TCR and a transduction marker [low-affinity nerve growth factor receptor (LNGFR)] (Fig. 4*A*). We sorted transduced (CD3$^+$LNGFR$^+$) T cells (*SI Appendix*, Fig. S2*C*) and retroorbitally i.v. injected these T cells into irradiated NOD/SCID/γc$^{-/-}$ (NSG) mice preinoculated with PC-3/HLA-A2 (control) and PC-3/HLA-A2/NYESO (target) tumors on opposing flanks (Fig. 4*B*). We then monitored T cell engraftment and tumor size until the conclusion of the experiment 2 wk after T cell injection.

T cells transduced with 1G4 or 9D2 TCRs persisted or minimally expanded in the peripheral blood, while 3A1-transduced T cells expanded significantly (Fig. 4 *C* and *D*). By contrast, T cells transduced only with LNGFR contracted over the course

MEDICAL SCIENCES

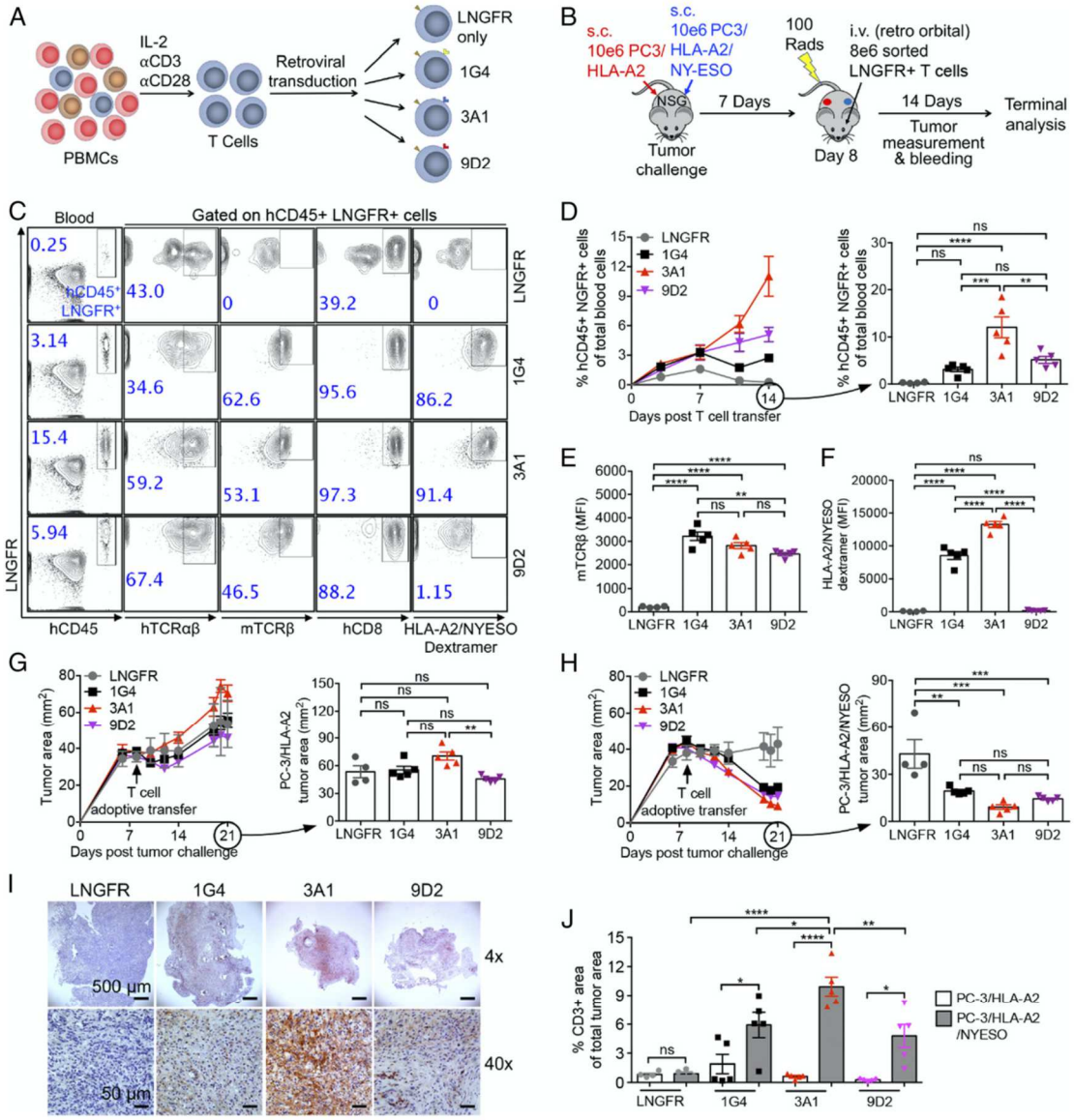

Fig. 4. In vivo antitumor efficacy of NY-ESO-1 TCR–engineered human T cells. (*A* and *B*) Schematics of the experimental designs to (*A*) generate NY-ESO-1 TCR–engineered human T cells and to (*B*) study antitumor efficacy of these engineered T cells in an NSG mouse human prostate tumor xenograft model. NSG, immunodeficient NOD/SCID/$\gamma c^{-/-}$ mice. (*C*) Representative flow cytometry plots characterizing engineered human T cells present in the peripheral blood of experimental mice on day 14 after adoptive T cell transfer. (*D*) Time course showing persistence of engineered human T cells (gated as LNGFR$^+$ hCD45$^+$) in the peripheral blood of experimental mice. (*E* and *F*) Mean fluorescence intensity measurements for (*E*) murine TCR and (*F*) HLA-A2/NYESO dextramer for engineered human T cells in the peripheral blood of experimental mice on day 14 after adoptive T cell transfer. (*G* and *H*) Measurements of cross-sectional area for (*G*) PC-3/HLA-A2 and (*H*) PC-3/HLA-A2/NYESO tumors. (*I*) Immunohistology images showing representative tumor sections. CD3$^+$ cells are stained in red. (Scale bars: *Upper*, 500 μm; *Lower*, 50 μm.) (*J*) Percentage of CD3$^+$ cell area over whole tumor section area. Representative of two experiments. Data are presented as the mean ± SEM (n = 4–5). ns, not significant; *P < 0.05, **P < 0.01, ***P < 0.001, ****P < 0.0001, by one-way ANOVA.

of the experiment, suggesting the expansion of TCR-transduced T cells was antigen-driven. The expression level of murine TCRβ was stable over the experimental time course and comparable between T cells transduced with different murinized TCRs (Fig. 4 *C* and *E*). The respective staining levels of each TCR-transduced T cell cohort with A*02:01/NY$_{157–165}$ dextramer$^+$ were also stable over time, but, as expected from results in vitro, were significantly different between TCRs. Approximately 90% of

human T cells transduced with 1G4 or 3A1 were dextramer$^+$ with high MFI. By contrast, only ~1% of 9D2-transduced T cells were dextramer$^+$ and the MFI of staining was not significantly different from LNGFR-transduced controls (Fig. 4 *C* and *F*). Nonetheless, T cells transduced with 1G4, 3A1, or 9D2 reduced tumor size comparably and in an antigen-specific manner, while LNGFR-transduced T cells failed to control tumor growth (Fig. 4 *G* and *H*).

At the conclusion of the experiment, we killed the mice and analyzed tumors for T cell infiltration by immunohistochemistry. Immunohistochemical staining revealed antigen-specific T cell infiltration only into target tumors in all cohorts receiving TCR-transduced T cells (Fig. 4 *I* and *J*). Infiltration was significantly higher in mice receiving 3A1-transduced T cells relative to mice receiving 1G4- or 9D2-transduced T cells.

Functional Characterization of NY-ESO-1–Specific TCRs Restricted on HLA-B and HLA-C Alleles. The majority of immunotherapies targeting NY-ESO-1 have focused on the A2-restricted $NY_{157–165}$ epitope. To enable broader application of NY-ESO-1–targeted immunotherapies, we cloned TCRs from four non-A2-restricted T cell clones and verified NY-ESO-1 reactivity for three of these in transfected CD3$^+$ 293T (Fig. 2*D*). The fourth TCR—9G2, cloned from Cw3/$NY_{92–100}$-reactive T cells—did not impart specificity for Cw3/$NY_{92–100}$ on transduced Jurkat T cells even with coexpressed CD8 (Fig. 5 *A* and *B*) and was not studied

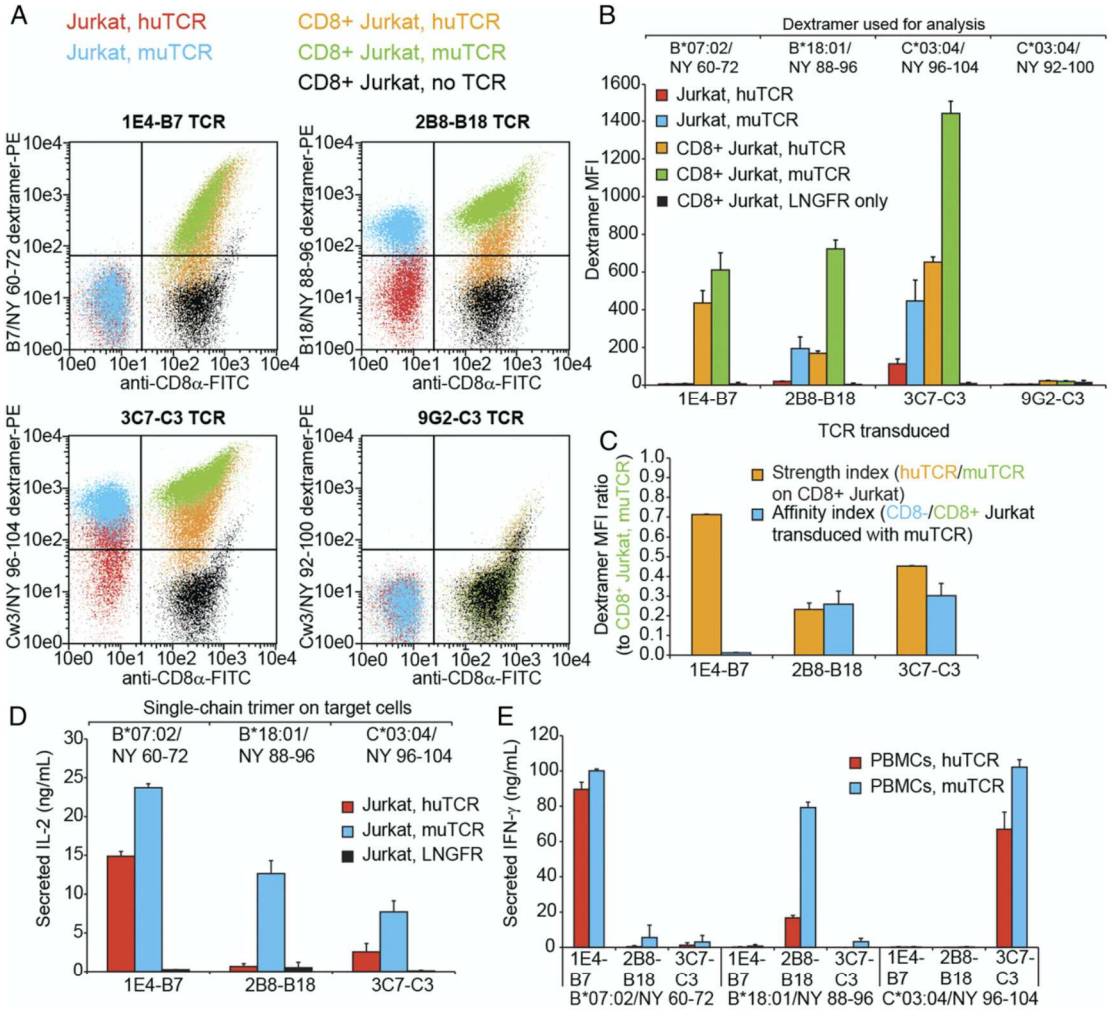

Fig. 5. Function of NY-ESO-1–specific TCRs restricted on MHC alleles other than HLA-A2. (*A*) Overlay of representative flow cytometry plots comparing specified dextramer binding by Jurkat and CD8$^+$ Jurkat cells expressing novel TCRs with human or murine constant domains. (*B*) Indicated dextramer binding mean fluorescence intensity measurements from two independent experiments as in *A*. (*C*) Ratio of respective dextramer binding mean fluorescent intensity measurements from two independent experiments in *B*. (*D* and *E*) ELISA measuring (*D*) secretion of IL-2 from TCR-transduced Jurkat cells or (*E*) secretion of IFN-γ from TCR-transduced PBMCs following 48-h coincubation with K562 target cells expressing indicated single-chain trimer. Experiments were repeated three times, each with two technical replicates. Means ± SD for a representative experiment are shown.

further. Comparisons of dextramer binding by the three validated TCRs expressed in Jurkat or $CD8^+$ Jurkat as human or murine TCRs revealed differences in strength and affinity (Fig. 5 *A*–*C*). The B7/$NY_{60–72}$-specific 1E4 TCR exhibited high strength but low affinity, expressing comparably on the Jurkat cell surface as either a huTCR or a muTCR but binding dextramer only in the presence of $CD8^+$. Dextramer binding to these $CD8^+$, 1E4-transduced cells was steeply dependent on the level of CD8 expressed. By contrast, the B18/$NY_{88–96}$-specific 2B8 TCR bound dextramer in the absence of $CD8^+$, but binding was substantially higher for the murinized TCR. Finally, the Cw3/$NY_{96–104}$-specific 3C7 TCR exhibited intermediate strength of surface expression and an affinity index comparable to 2B8.

These differences in TCR strength and affinity were reflected in functional assays. For all three TCRs, murinization of the TCR constant regions increased production of IL-2 from TCR-transduced Jurkat cells coincubated with cognate target cells. However, this increase was only 1.6- and 3.0-fold over the respective fully human TCRs for 1E4 and 3C7 but was 18.6-fold for 2B8, consistent with the latter's lower strength (Fig. 5*D*). In peptide titration assays, 1E4 TCR imparted lower sensitivity for cognate peptide on transduced $CD8^+$ T cells than did 3C7 or 2B8 (*SI Appendix*, Fig. S1 *C*–*E*), consistent with the presumed lower affinity of 1E4 based on its strictly CD8-dependent dextramer binding.

Primary PBMCs transduced with each TCR responded to the presentation of NY-ESO-1–derived epitopes in a peptide-specific and MHC-restricted manner (Fig. 5*E*). As such, we expect that TCR gene therapies employing NY-ESO-1–specific TCRs restricted on multiple MHCs can be applied more broadly across patient haplotypes and will be more robust toward tumor evasion via loss of heterozygosity at the MHCI locus. To test this, we transduced NY-ESO-1–expressing human cancer cells with HLA-A2 or HLA-B7. We then coincubated one or both of these tumor targets with human T cells transduced with A2-restricted 3A1 TCR, with T cells transduced with B7-restricted 1E4 TCR, or with a mixture of 3A1- and 1E4-transduced T cells (Fig. 6). As expected, combination targeting using a mixture of 3A1- and 1E4-transduced T cells enabled recognition of tumor cell populations expressing both MHC alleles or either MHC allele alone (Fig. 6 *A* and *B*). By contrast, T cells targeting a single NY-ESO-1 epitope did not respond to NY-ESO-1–expressing tumor cells that lacked the cognate MHC allele. Moreover, when tumor targets comprised a mixture of cells expressing different MHC alleles (simulating tumor heterogeneity arising from haploinsufficiency), T cells targeting both NY-ESO-1 epitopes killed tumor cells more completely than did T cells targeting either single epitope (Fig. 6 *C* and *D*).

Discussion

T cell-mediated immunotherapies are making clinical inroads for previously refractory cancers. Two of the most successful immunotherapy modalities are checkpoint blockade and adoptive transfer of cancer-specific T cells. Checkpoint blockade elicits better clinical responses as tumor mutational burden increases (39–41), suggesting that nonsynonymous mutations go undetected by the immune system unless, fortuitously, they generate neoepitopes that are presented by the patient's complement of MHC molecules. This interpretation is bolstered by the recent finding that checkpoint blockade results in higher overall survival for melanoma patients who are heterozygous at the HLA-A, HLA-B, and HLA-C loci and thus present a more diverse array of epitopes than those who are homozygous at one or more of these MHCI loci (42). The importance of a diversely targeted antitumor immune response is likewise supported by results from adoptive T cell therapy, which show that loss of heterozygosity is a mechanism by which tumors can evade monospecific immune recognition while continuing to express an otherwise immunogenic antigen (43). Thus, a prominent narrative emerging from these studies is that diverse targeting of multiple epitopes presented by multiple MHC alleles is desirable for successful immunotherapy. A second takeaway is that targeting multiple epitopes derived from a tumor-specific public antigen may be a promising alternative to targeting neoepitopes in cancers with low mutational burden.

It has proven difficult to identify public tumor-associated antigens that mediate tumor regression without also manifesting serious morbidity or deaths resulting from on-target, off-tumor T cell reactivity. We chose to focus on NY-ESO-1 as a public antigenic target based on the criteria that it (*i*) is expressed exclusively in cancer cells and immunologically privileged germ cells; (*ii*) is expressed in many patients across various tumor types; (*iii*) harbors high-affinity ligands for multiple common MHC alleles; (*iv*) is well-vetted, having yielded objective responses in patients across several tumor types without specificity-related adverse events; and (*v*) is yet underexploited, as the majority of studies have focused on mobilizing T cell responses solely against the A2-restricted NY-ESO-$1_{157–165}$ epitope.

We employed an antigen-specific expansion protocol to isolate NY-ESO-1–reactive T cells from the peripheral blood of patients with metastatic melanoma. Using this approach, we cloned several HLA-A2–restricted TCRs and compared them in terms of their strength of surface expression, affinity (i.e., dependence of target binding on CD8), and function (antigen-induced cytokine release and tumor target killing). From four candidates, we identified two that recognized and killed NY-ESO-1–expressing cancer cells as well or better than the clinically employed 1G4 TCR. This expansion-based approach to TCR candidate identification is ideally suited for targeting public epitopes because the speed of isolation is not a critical parameter; once identified, these TCRs can be used as off-the-shelf targeting receptors for any patient expressing the requisite MHC allele. Antigen-specific expansion of neoantigen-reactive T cells from peripheral blood has also been demonstrated (44, 45). However, on-demand isolation of private neoepitope-targeted TCRs will require more rapid approaches than that used here (e.g., direct capture of antigen-specific T cells from blood or expansion protocols optimized for rapidity). As the release of IFN-γ is strongly correlated with cytotoxicity (46), candidate evaluation can be accelerated by using IFN-γ release as a surrogate for more involved tumor xenograft assays.

One of the HLA-A2/NY-ESO-1–reactive TCRs isolated—9D2—exhibited poor staining with cognate multimer but high functional avidity toward cognate antigen-presenting target cells. This is consistent with the observation that multimer staining underestimates functional T cell subsets (47) and may be explained by the higher-affinity threshold for multimer binding relative to that for T cell activation (48). However, another isolated A2-restricted TCR—4A2—exhibited robust multimer staining but poor function in cell-based assays, seemingly at odds with this affinity threshold explanation. While we do not have an explanation for this latter result, both results caution against relying too much on multimer staining when down-selecting immunotherapy candidates.

The HLA-A*02:01 allele is the most prevalent MHCI allele in Caucasian (45%) and Hispanic (41%) US populations, but it is less common among Asian (15%) and African (16%) US populations (2). These latter populations would be particularly well-served by expanding the targeting of TCR gene therapies beyond HLA-A2 to a more expansive panel of targetable MHC alleles. In addition to HLA-A2–restricted TCRs, we isolated and functionally characterized NY-ESO-1–specific TCRs restricted on various HLA-B and HLA-C alleles. In doing so, we demonstrated in principle that TCR gene therapy can be extended to a greater subset of patients/haplotypes and that, when used in combination, TCRs recognizing multiple epitopes from the same antigen can more robustly kill tumors with heterogeneous MHC expression (e.g., resulting from somatic loss of heterozygosity).

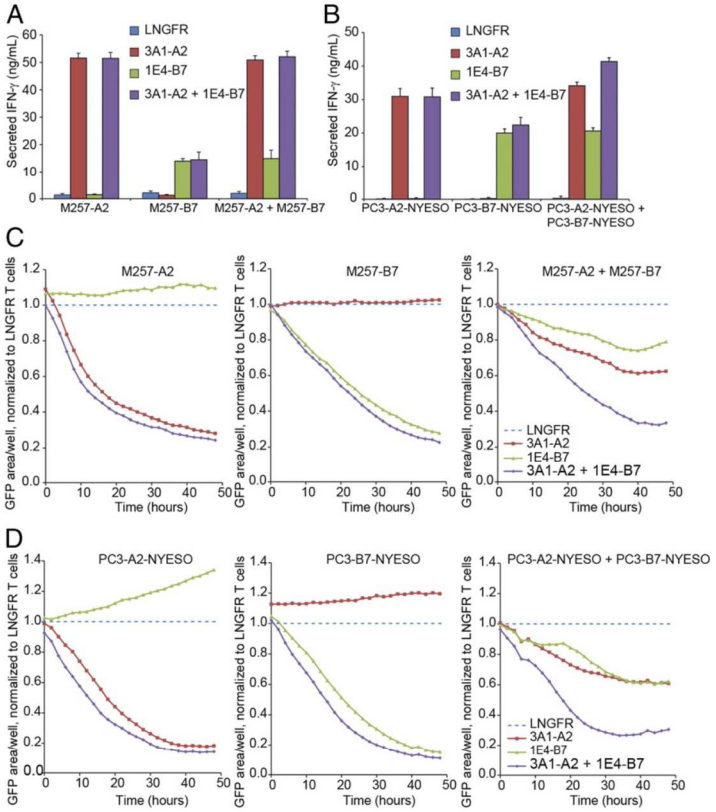

Fig. 6. Targeting NY-ESO-1 epitopes restricted on multiple MHC alleles broadens the application of TCR gene therapy and makes it robust toward loss of heterozygosity at the MHC locus. (*A–D*) T cells transduced with LNGFR only, A2-restricted 3A1 TCR, or B7-restricted 1E4 TCR—or a 1:1 mixture of 3A1-transduced and 1E4-transduced T cells—were coincubated for 48 h with HLA-A2$^+$eGFP$^+$ target cells, HLA-B7$^+$eGFP$^+$ target cells, or a 1:1 target cell mixture. (*A* and *B*) ELISA measuring secretion of IFN-γ from TCR-transduced PBMCs following 48-h coincubation with (*A*) M257 or (*B*) PC-3 tumor cell lines engineered to express eGFP and HLA-A*02:01 or HLA-B*07:02. PC-3 lines were additionally engineered to express NY-ESO-1. M257 lines express endogenous NY-ESO-1. Experiments were repeated three times, each with four or eight replicates. Means ± SD for a representative experiment are shown. (*C* and *D*) T cell-mediated killing of (*C*) M257 and (*D*) PC-3 tumor cell line derivatives measured over time using IncuCyte live-cell analysis. Total green object area (indicative of tumor cell density) at each time point measured over 48 h was normalized for each treatment relative to treatment with LNGFR-transduced T cells. Experiments were repeated three times, each with four or eight replicates. Results from a representative eight-replicate experiment are shown.

Over 80% of people across ethnic groups express at least one allele from three MHCI supertypes (A2, A3, and B7, two of which were represented here) and >99% of people express at least one allele from nine MHCI supertypes (49). Therefore, obtaining a panel of public antigen-specific TCR reagents that enable comprehensive application of TCR gene therapy is a finite and surmountable challenge.

Materials and Methods

Materials. Peptides were purchased from Anaspec, Thermo Fisher Scientific, and Mimotopes. Fluorescent antibodies and 7-AAD used for flow cytometry were purchased from BD Biosciences, BioLegend, or eBioscience. Fluorescent peptide–MHC multimers were purchased from TCMetrix or prepared in-house as described (50) from biotinylated monomers [obtained from NIH Tetramer Core, or expressed heterologously in *Escherichia coli*, refolded, and biotinylated in-house as described (51)]. Primers were purchased from Integrated DNA Technologies. KOD polymerase master mix and polybrene were purchased from EMD Millipore. Sequencing was performed by Retrogen Inc. Anti-CD3 (OKT3) and anti-CD28 (CD28.2) activating antibodies were purchased from eBioscience. Cytokines were purchased from Peprotech, Inc. BioT transfection reagent was purchased from Bioland Scientific. Cell culture media, antibiotics, and FBS were purchased from Corning. Human AB serum was purchased from Omega Scientific. Poly-L-lysine and PHA-L (phytohemagglutinin-L) were purchased from Sigma.

Cells. Cell lines (293T/17, Jurkat E6-1, and K562) were purchased from the American Type Culture Collection. The 293T cells were grown in DMEM supplemented with antibiotics (penicillin/streptomycin) and 10% (vol/vol) FBS. Jurkat and K562 cells were grown in RPMI medium 1640 supplemented with antibiotics, 10% (vol/vol) FBS, 10 mM Hepes, 50 μM β-mercaptoethanol, 1× MEM NEAA, and 1 mM sodium pyruvate. The cells were split every 2–3 d to maintain adherent cells subconfluently or nonadherent cells at a density of $<10^6$ cells/mL Jurkat and K562 cells were transduced with nonreplicative viral vectors, analyzed by flow cytometry, and used directly in cell assays or sorted by FACS to establish derivative cell lines as indicated. Primary human PBMCs used in functional assays were purchased from the CFAR Virology Core Laboratory at the University of California, Los Angeles (UCLA) AIDS Institute, stimulated, transduced, and cultured as previously described (52). T cells were grown from PBMCs in T cell medium (AIM-V medium supplemented with 5% heat-inactivated human AB serum, 55 μM β-mercaptoethanol, and 4 mM L-glutamine) with freshly added cytokines. All cells were grown and assayed at 37 °C with 5% atmospheric CO_2.

Generation and Culture of NY-ESO-1–Specific CD8$^+$ T Lymphocyte Clones. CD8$^+$ T lymphocyte clones specific for epitopes from NY-ESO-1 with various HLA restrictions [157–165/HLA-A*02:01 (53), 60–72/HLA-B*07:02 (21), 88–96/HLA-B*18:01 (23), 92–100/HLA-C*03:04 (54), 96–104/HLA-C*03:04 (22), and 124–133/HLA-C*03:04 (22)] were generated from HLA-typed patients with melanoma. All selected patients had grade III/IV metastatic melanoma and previously documented NY-ESO-1 responses to relevant T lymphocyte epitopes ex vivo (55). Patient PBMCs were stimulated in the presence of 1 μM pooled peptides (Mimotopes), comprising 28 × 18-mers overlapping by 12 aa, collectively spanning the NY-ESO-1 protein sequence and then cultured for 10 d in the presence of 25 IU/mL IL-2 (Peprotech).

On day 10, cells were restimulated with 1 μM of each individual peptide in the presence of brefeldin A and activation of CD8$^+$ T cells in response to each peptide was determined by intracellular cytokine stain. Briefly, cells were labeled with live/dead fixable violet stain (Invitrogen) according to the manufacturer's instructions then incubated with antibodies against CD3 and CD8 for 15 min at 4 °C. Samples were washed and fixed with fix/permeabilization reagent (BD Biosciences) for 20 min at 4 °C. Cells were stained with anti–IFN-γ (eBiosciences) in permeabilization/wash solution (BD Biosciences) for 25 min at 4 °C. The gating strategy was SSC/LD$^-$; CD3$^+$/CD8$^+$; CD8$^+$/IFN-γ$^+$. Data from at least 100,000 stained cells were acquired on a FACSCanto and analyzed with FlowJo software. Data collection and analysis was in accordance with the Minimal Information About T cell Assays guidelines (56).

NY-ESO-1–reactive T cells were expanded in the presence of their identified cognate 9–10-mer epitope and then labeled with a fluorescent tetramer comprising the relevant peptide and HLA molecule (TCMetrix) and single-cell-sorted using a MoFlo cell sorter. Clones were reexpanded with pooled, allogeneic healthy donor PBMC as feeder cells, 1 μg/mL PHA-L, and 600 IU/mL IL-2 (Cetus). After ~20 d, 1–10 × 10^3 clones were restimulated in the presence of allogeneic PBMC as feeder cells, PHA-L, and IL-2, as described above. Clone specificity was confirmed by tetramer staining.

T lymphocyte clones/lines were cultured in RPMI 1640 media supplemented with 2 mM Glutamax, 100 IU/mL penicillin, 100 μg/mL streptomycin, 20 mM Hepes, 1% nonessential amino acids, 1 mM sodium pyruvate, 55 μM β-mercaptoethanol, and 10% human serum (TCRPMI). IL-2 (100 IU/mL) was added and replaced every 3 d.

Cloning TCR Constructs. Single NY-ESO-1–reactive T cells were sorted for antigenic specificity on a FACS Aria II and were lysed by freeze–thaw in the presence of RNase inhibitor. Novel TCR variable genes were cloned from single, sorted T cells using a custom panel of human TCR variable region-specific primers with the Qiagen OneStep RT-PCR kit, followed by a nested PCR amplification step. Amplified variable genes were integrated via assembly PCR and restriction enzyme-mediated cloning into a TCR expression cassette with either human or mouse TCR constant domains and a 2A ribosomal skipping peptide linking the alpha and beta genes. A P2A-linked gene encoding a truncated version of the LNGFR was also included in the cassette as an independent transfection/transduction marker. Antigenic specificity and MHC restriction of cloned TCRs were evaluated in 293T cells cotransfected with TCR and CD3 genes, as previously described (52).

Evaluation of TCR Export and Dextramer Binding on Jurkat T Cells. Jurkat T cells were transduced with MSGV-based retroviruses encoding each novel TCR in the format LNGFRΔ-P2A-TCRα-F2A-TCRβ. Viruses were produced in 293T cells as described (52). For transduction, Jurkat T cells were centrifuged (1,350 × *g* for 90 min at 30 °C) with unconcentrated viral supernatants supplemented with 5 μg/mL polybrene. TCR-transduced Jurkat cells were stained with cognate pMHC dextramer for 15 min at room temperature and then costained with antibodies against LNGFR and CD8α for 15 min at 4 °C. Stained cells were analyzed by flow cytometry using a FACSCanto analyzer. Data shown are gated on LNGFR$^+$ (transduced) cells. Transduction efficiency was >95%.

PBMC Activation and Transduction. Primary human PBMCs were purchased from the CFAR Virology Core Laboratory at the UCLA AIDS Institute. The same PBMC donor was used in all reported experiments. Primary human PBMCs were transduced with retroviruses encoding novel TCRs as described (52). Briefly, 2 d before viral transduction, 1–2 × 10^6 total thawed PBMCs were activated per well in 24-well plates with plate-coated anti-CD3 (clone OKT3), T cell medium containing 1 μg/mL soluble anti-CD28 (clone CD28.2), and 300 U/mL IL-2. After 48 h of activation, the majority of the medium was replaced with unconcentrated retroviral supernatant supplemented with 10 μg/mL polybrene and cells were centrifuged for 90 min at 1,350 × *g* at 30 °C. Following spinfection, the majority of retroviral supernatant was replaced with fresh medium containing 300 U/mL IL-2 and 1 μg/mL anti-CD28. The transduction was repeated 24 h later, after which the cells were washed with 1× PBS and then returned to fresh medium containing final 300 U/mL IL-2 and cultured for an additional 3–4 d before being used in antigenic stimulation assays. One day before or on the day of coculturing, PBMCs were analyzed by FACS for assessment of expression levels for LNGFR, TCR, and/or pMHC multimer binding.

Functional Coculture Assays: Cytokine ELISA. When Jurkat T cells were used as effectors, cocultures were performed in RPMI supplemented with 10% FBS, 100 IU/mL penicillin, 100 μg/mL streptomycin, and 4 mM L-glutamine. Effector cells (50,000 TCR-transduced Jurat T cells) were coincubated with target cells (50,000 K562 cells transduced with cognate or control single-chain trimers) in 96-well flat-bottom plates. Supernatants from duplicate wells were collected 44–48 h postcoculturing and analyzed by ELISA as described below.

When primary PBMCs were used as effectors, cocultures were performed in T cell media containing 300 U/mL IL-2. Effector cells (50,000 TCR-transduced PBMCs) were coincubated with target cells (50,000 M257, PC-3, or K562 cells) in 96-well flat-bottom plates. In some experiments target cells were pulsed with peptide. Supernatants from two eightfold replicate wells for each condition were collected 44–48 h postcoculturing and analyzed by ELISA as described below.

For experiments in which target cells were titrated with pulsed peptide, lyophilized peptides were dissolved to 10 mM in DMSO and then further diluted in water to 2 mM working stocks. At point of use, the 2 mM stock was diluted to 250 μM in cell media and then fivefold serially diluted from 250 μM down to 3.2 nM. Target cells were pulsed by adding 25 μL of each serial dilution per well on a 96-well U-bottom plate, followed by addition of 50,000 target cells in 100 μL media, yielding the final peptide concentration ranging from 50 μM to 0.64 nM. Cells were pulsed with peptides for 2 h at 37 °C, diluted with 100 μL of media per well at the end of incubation, and centrifuged, and the supernatant was removed. The cells were washed with 200 μL of media and then resuspended in 100 μL of media. Fifty thousand PBMCs prepared in 100 μL of media were then added to each well for coculturing.

In general, ELISA results were converted to concentration (nanograms per milliliter) by interpolation relative to a standard curve and concentrations from replicate ELISAs were averaged. Supernatants were diluted 50- to 100-fold for ELISA analysis. Occasionally, higher dilutions were required to place signal within the range of the standard curve. All reagents for ELISA analyses were from BD Biosciences: OptEIA Reagent Set B (550534) was used for diluent and washes and OptEIA human IFN-γ ELISA kit (555142) and OptEIA human IL-2 ELISA kit (555190) were used for measuring IFN-γ and IL-2 release, respectively.

Functional Coculture Assays: IncuCyte Cell Killing Assay. Before coculture for IncuCyte killing assays, a 96-well flat-bottom plate was coated with 100 μL of 0.001% poly-L-lysine in PBS for 1 h at 37 °C, washed two times with 200 μL PBS each, and air-dried briefly. Target cells were added and allowed to settle at room temperature for 3 h before the effector cells were added. Cocultures typically employed 25,000 PBMCs and 25,000 target cells per well of a 96-well plate. In assays where multiple effector populations (bearing different TCRs) or multiple targets (bearing different MHC) were mixed, 25,000 of each cell type was used to yield a total of 75,000 or 100,000 cells per well (for single/mixed or mixed/mixed, respectively). The total volume for all wells was adjusted to 200 μL. Total green object area (square micrometers per well) was quantified and its disappearance interpreted as killing of the GFP$^+$ target cells. Cells were imaged at two positions per well every 2 h and these two images were added together for one data point. Data points obtained from four to eight replicate cocultures for each effector/target combination were used to plot graph curves and to calculate SD.

Animals. NOD.Cg-PrkdcSCIDIL-2rgtm1Wjl/SzJ (NOD/SCID/IL-2Rg$^{-/-}$, NSG) mice were purchased from The Jackson Laboratory and maintained in the animal facilities at UCLA. Adult (16 wk old) male mice were used for in vivo tumor challenge experiments. All animal experiments were approved by the Institutional Animal Care and Use Committee of UCLA.

Human Prostate Tumor Xenograft Mouse Model. For xenograft tumor implantation, 10 × 10^6 PC-3/HLA-A2 cells (PC-3 cell line overexpressing HLA-A2) were s.c. injected on one flank of each mouse and 10 × 10^6 PC-3/HLA-A2/NYESO cells (PC-3 cell line overexpressing HLA-A2 and NYESO) were s.c. injected on the other flank. Mice were allowed to develop solid tumors over the course of 1 wk. On day 8 after tumor injection, mice were irradiated (100 rad) and then retroorbitally i.v. injected with 8 × 10^6 purified T cells that were engineered to express LNGFR only or together with a NY-ESO-1–specific TCR (1G4, 3A1, or 9D2). Mice were bled on days 3, 7, 10, and 14 for flow cytometry analysis. On day 14, mice were killed and tumors were collected for immunohistology analysis.

Immunohistology. Solid tumors dissected out from the experimental mice were fixed in 10% neutral-buffered formalin and embedded in paraffin for sectioning (4-mm thickness), followed by H&E staining or antibody staining (for human CD3ε) by using standard procedures (UCLA Translational Pathology Core Laboratory). The sections were imaged using an Olympus BX51 upright microscope equipped with an Optronics Macrofire CCD camera (AU Optronics) at 4× and 40× magnifications. The images were analyzed by using Optronics PictureFrame software (AU Optronics) and ImageJ software (version 1.51J8). With ImageJ human CD3 antibody-stained slides were quantified by measuring $CD3^+$ area through setting color threshold. Parameters used are as follows: thresholding method: default; threshold color: red; color space: HSB; brightness: 168–215.

Statistical Analysis. Statistical analysis of tumor xenograft experiments was performed with one-way ANOVA followed by Tukey's multiple comparison test. Data are presented as the mean ± SEM. $P < 0.05$ was considered significant. ns, not significant; $*P < 0.05$; $**P < 0.01$; $***P < 0.001$; $****P < 0.0001$. All statistical analyses were performed with GraphPad PRISM software (version 6.0).

Ethics Statement. All samples used were IRB-approved and deidentified for all work reported in our study; the research protocol was approved by Austin Health Human Research Ethics Committee (HREC H2006/02633).

ACKNOWLEDGMENTS. We thank John Lee for help setting up the IncuCyte, Nathanael Joshua Bangayan for help optimizing its operation, Christie Qin and Hoang Vu (Leo) Li for technical assistance with ELISA assays, Drake Smith for guidance with animal experiments, and the staff of the UCLA animal facility for animal husbandry. The MSGV vector was provided by Eugene Barsov and Richard Morgan. This work was supported by NIH Grant 5P01CA132681-5 (to D.B., O.N.W., A.R., and L.Y.) and Prostate Cancer Foundation Challenge Award 15CHAL02 (to D.B., O.N.W., L.Y., and M.T.B.). M.T.B. is the recipient of a Jane Coffin Childs Postdoctoral Fellowship. A.R. was supported by NIH Grant R35 CA197633, the Ressler Family Fund, and the Parker Institute for Cancer Immunotherapy. K.W. was supported by Australian National Health and Medical Research Council (NHMRC) Project Grant 1007381. J.C. was supported by an Australian NHMRC Practitioner Fellowship 487905 and by Operational Infrastructure Support Program funding from the Victorian State Government. Primary human PBMCs were purchased from the CFAR Virology Core Laboratory at the UCLA AIDS Institute (NIH Grant 5P30 A1028697).

1. Robinson J, et al. (2015) The IPD and IMGT/HLA database: Allele variant databases. *Nucleic Acids Res* 43:D423–D431.
2. González-Galarza FF, et al. (2015) Allele frequency net 2015 update: New features for HLA epitopes, KIR and disease and HLA adverse drug reaction associations. *Nucleic Acids Res* 43:D784–D788.
3. Johnson LA, et al. (2006) Gene transfer of tumor-reactive TCR confers both high avidity and tumor reactivity to nonreactive peripheral blood mononuclear cells and tumor-infiltrating lymphocytes. *J Immunol* 177:6548–6559.
4. Schumacher TN, Schreiber RD (2015) Neoantigens in cancer immunotherapy. *Science* 348:69–74.
5. Bethune MT, Joglekar AV (2017) Personalized T cell-mediated cancer immunotherapy: Progress and challenges. *Curr Opin Biotechnol* 48:142–152.
6. Morgan RA, et al. (2006) Cancer regression in patients after transfer of genetically engineered lymphocytes. *Science* 314:126–129.
7. Johnson LA, et al. (2009) Gene therapy with human and mouse T-cell receptors mediates cancer regression and targets normal tissues expressing cognate antigen. *Blood* 114:535–546.
8. Parkhurst MR, et al. (2011) T cells targeting carcinoembryonic antigen can mediate regression of metastatic colorectal cancer but induce severe transient colitis. *Mol Ther* 19:620–626.
9. Morgan RA, et al. (2010) Case report of a serious adverse event following the administration of T cells transduced with a chimeric antigen receptor recognizing ERBB2. *Mol Ther* 18:843–851.
10. Morgan RA, et al. (2013) Cancer regression and neurological toxicity following anti-MAGE-A3 TCR gene therapy. *J Immunother* 36:133–151.
11. Anonymous (2013) Do no harm. *Nat Biotechnol* 31:365.
12. Jorritsma A, et al. (2007) Selecting highly affine and well-expressed TCRs for gene therapy of melanoma. *Blood* 110:3564–3572.
13. Chen YT, et al. (1997) A testicular antigen aberrantly expressed in human cancers detected by autologous antibody screening. *Proc Natl Acad Sci USA* 94:1914–1918.
14. Goydos JS, Patel M, Shih W (2001) NY-ESO-1 and CTp11 expression may correlate with stage of progression in melanoma. *J Surg Res* 98:76–80.
15. Sharma P, et al. (2003) Frequency of NY-ESO-1 and LAGE-1 expression in bladder cancer and evidence of a new NY-ESO-1 T-cell epitope in a patient with bladder cancer. *Cancer Immun* 3:19.
16. Li M, et al. (2005) Expression profile of cancer-testis genes in 121 human colorectal cancer tissue and adjacent normal tissue. *Clin Cancer Res* 11:1809–1814.
17. Gure AO, et al. (2005) Cancer-testis genes are coordinately expressed and are markers of poor outcome in non-small cell lung cancer. *Clinical Cancer Res* 11:8055–8062.
18. Jungbluth AA, et al. (2001) Monophasic and biphasic synovial sarcomas abundantly express cancer/testis antigen NY-ESO-1 but not MAGE-A1 or CT7. *Int J Cancer* 94:252–256.
19. Aung PP, et al. (2014) Expression of New York esophageal squamous cell carcinoma-1 in primary and metastatic melanoma. *Hum Pathol* 45:259–267.
20. Ademuyiwa FO, et al. (2012) NY-ESO-1 cancer testis antigen demonstrates high immunogenicity in triple negative breast cancer. *PLoS One* 7:e38783, and erratum (2012) 7:10.1371/annotation/5cdf6105-2a52-497a-86b3-db8f4a4e439c.
21. Ebert LM, et al. (2009) A long, naturally presented immunodominant epitope from NY-ESO-1 tumor antigen: Implications for cancer vaccine design. *Cancer Res* 69:1046–1054.
22. Jackson H, et al. (2006) Striking immunodominance hierarchy of naturally occurring CD8+ and CD4+ T cell responses to tumor antigen NY-ESO-1. *J Immunol* 176:5908–5917.
23. Zhao RY, et al. (2012) A novel HLA-B18 restricted CD8+ T cell epitope is efficiently cross-presented by dendritic cells from soluble tumor antigen. *PLoS One* 7:e44707.
24. Robbins PF, et al. (2011) Tumor regression in patients with metastatic synovial cell sarcoma and melanoma using genetically engineered lymphocytes reactive with NY-ESO-1. *J Clin Oncol* 29:917–924.
25. Robbins PF, et al. (2015) A pilot trial using lymphocytes genetically engineered with an NY-ESO-1-reactive T-cell receptor: Long-term follow-up and correlates with response. *Clinical Cancer Res* 21:1019–1027.
26. Rapoport AP, et al. (2015) NY-ESO-1-specific TCR-engineered T cells mediate sustained antigen-specific antitumor effects in myeloma. *Nat Med* 21:914–921.
27. Klippel ZK, et al. (2014) Immune escape from NY-ESO-1-specific T-cell therapy via loss of heterozygosity in the MHC. *Gene Ther* 21:337–342.
28. Zhao Y, et al. (2007) High-affinity TCRs generated by phage display provide CD4+ T cells with the ability to recognize and kill tumor cell lines. *J Immunol* 179:5845–5854.
29. Cameron BJ, et al. (2013) Identification of a Titin-derived HLA-A1-presented peptide as a cross-reactive target for engineered MAGE A3-directed T cells. *Sci Transl Med* 5:197ra103.
30. Linette GP, et al. (2013) Cardiovascular toxicity and titin cross-reactivity of affinity-enhanced T cells in myeloma and melanoma. *Blood* 122:863–871.
31. Andreatta M, Nielsen M (2016) Gapped sequence alignment using artificial neural networks: Application to the MHC class I system. *Bioinformatics* 32:511–517.
32. Wooldridge L, et al. (2005) Interaction between the CD8 coreceptor and major histocompatibility complex class I stabilizes T cell receptor-antigen complexes at the cell surface. *J Biol Chem* 280:27491–27501.
33. Aleksic M, et al. (2012) Different affinity windows for virus and cancer-specific T-cell receptors: Implications for therapeutic strategies. *Eur J Immunol* 42:3174–3179.
34. Sommermeyer D, et al. (2006) Designer T cells by T cell receptor replacement. *Eur J Immunol* 36:3052–3059.
35. Klausner RD, Lippincott-Schwartz J, Bonifacino JS (1990) The T cell antigen receptor: Insights into organelle biology. *Annu Rev Cell Biol* 6:403–431.
36. Cohen CJ, Zhao Y, Zheng Z, Rosenberg SA, Morgan RA (2006) Enhanced antitumor activity of murine-human hybrid T-cell receptor (TCR) in human lymphocytes is associated with improved pairing and TCR/CD3 stability. *Cancer Res* 66:8878–8886.
37. Robbins PF, et al. (2008) Single and dual amino acid substitutions in TCR CDRs can enhance antigen-specific T cell functions. *J Immunol* 180:6116–6131.
38. Hansen T, Yu YY, Fremont DH (2009) Preparation of stable single-chain trimers engineered with peptide, beta2 microglobulin, and MHC heavy chain. *Curr Protoc Immunol* Chap 17:Unit17.5.
39. Snyder A, et al. (2014) Genetic basis for clinical response to CTLA-4 blockade in melanoma. *N Engl J Med* 371:2189–2199.
40. Van Allen EM, et al. (2015) Genomic correlates of response to CTLA-4 blockade in metastatic melanoma. *Science* 350:207–211.
41. Rizvi NA, et al. (2015) Cancer immunology. Mutational landscape determines sensitivity to PD-1 blockade in non-small cell lung cancer. *Science* 348:124–128.
42. Chowell D, et al. (2018) Patient HLA class I genotype influences cancer response to checkpoint blockade immunotherapy. *Science* 359:582–587.
43. Tran E, et al. (2016) T-cell transfer therapy targeting mutant KRAS in cancer. *N Engl J Med* 375:2255–2262.
44. Gros A, et al. (2016) Prospective identification of neoantigen-specific lymphocytes in the peripheral blood of melanoma patients. *Nat Med* 22:433–438.
45. Strønen E, et al. (2016) Targeting of cancer neoantigens with donor-derived T cell receptor repertoires. *Science* 352:1337–1341.
46. Ioannidou K, et al. (2017) Heterogeneity assessment of functional T cell avidity. *Sci Rep* 7:44320.
47. Rius C, et al. (2018) Peptide-MHC class I tetramers can fail to detect relevant functional T cell clonotypes and underestimate antigen-reactive T cell populations. *J Immunol* 200:2263–2279.
48. Laugel B, et al. (2007) Different T cell receptor affinity thresholds and CD8 coreceptor dependence govern cytotoxic T lymphocyte activation and tetramer binding properties. *J Biol Chem* 282:23799–23810.
49. Sette A, Sidney J (1999) Nine major HLA class I supertypes account for the vast preponderance of HLA-A and -B polymorphism. *Immunogenetics* 50:201–212.
50. Bethune MT, Comin-Anduix B, Hwang Fu YH, Ribas A, Baltimore D (2017) Preparation of peptide-MHC and T-cell receptor dextramers by biotinylated dextran doping. *Biotechniques* 62:123–130.
51. Toebes M, et al. (2006) Design and use of conditional MHC class I ligands. *Nat Med* 12:246–251.
52. Bethune MT, et al. (2016) Domain-swapped T cell receptors improve the safety of TCR gene therapy. *eLife* 5:e19095.
53. Chen JL, et al. (2000) Identification of NY-ESO-1 peptide analogues capable of improved stimulation of tumor-reactive CTL. *J Immunol* 165:948–955.
54. Gnjatic S, et al. (2000) Strategy for monitoring T cell responses to NY-ESO-1 in patients with any HLA class I allele. *Proc Natl Acad Sci USA* 97:10917–10922.
55. Davis ID, et al. (2004) Recombinant NY-ESO-1 protein with ISCOMATRIX adjuvant induces broad integrated antibody and CD4(+) and CD8(+) T cell responses in humans. *Proc Natl Acad Sci USA* 101:10697–10702.
56. Britten CM, et al. (2012) T cell assays and MIATA: The essential minimum for maximum impact. *Immunity* 37:1–2.

Supplemental Figures

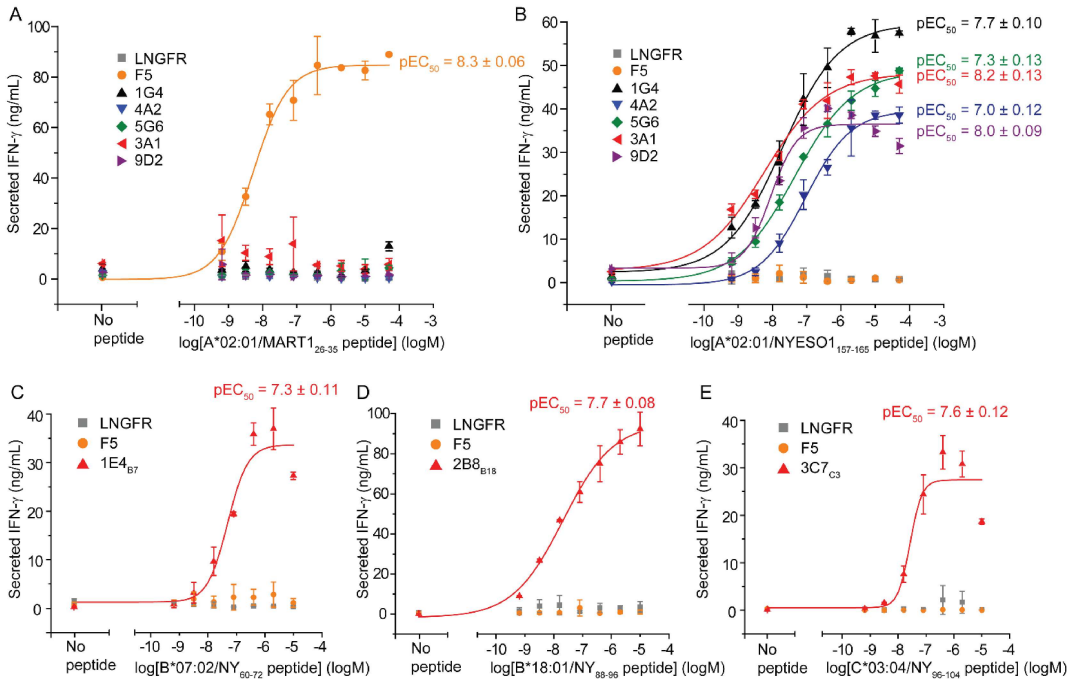

Supplemental Figure S1.
Determination of EC50 for NY-ESO-1-specific TCRs.
(A and B) ELISA measuring secretion of IFN-γ from TCR-transduced PBMCs following 48 hours coincubation with K562 engineered to express HLA-A*02:01 and pulsed with varied concentrations of **(A)** $MART_{26-35}$ or **(B)** $NY_{157-165}$ peptide. **(C-E)** ELISA measuring secretion of IFN-γ from TCR-transduced PBMCs following 48 hours coincubation with K562 engineered to express **(C)** HLA-B*07:02, **(D)** HLA-B*18:01, or **(E)** HLA-C*03:04 and pulsed with varied concentrations of indicated peptides. Means ± SD for two technical replicates are shown. EC_{50} values and associated errors determined by non-linear curve fitting are indicated.

www.pnas.org/cgi/doi/10.1073/pnas.1810653115

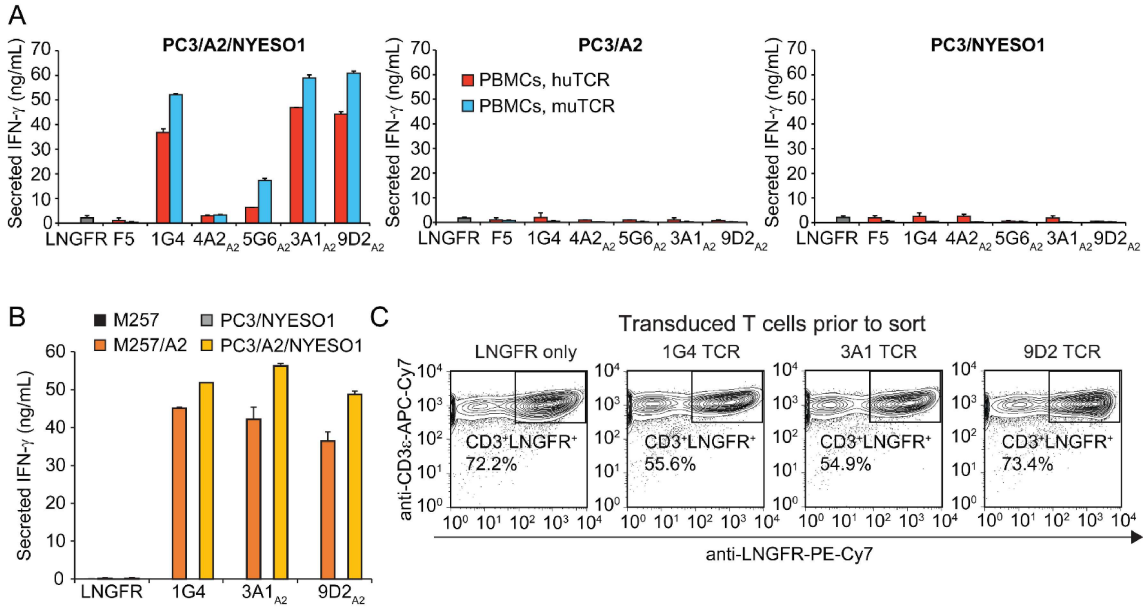

Supplemental Figure S2.
Establishment of xenograft tumor line and function of input T cells for *in vivo* experiment.
(A) ELISA measuring secretion of IFN-γ from TCR-transduced PBMCs following 48 hours coincubation with derivatives of the PC-3 prostate cancer cell line engineered to express (left) HLA-A*02:01 and NY-ESO-1 full protein, (middle) HLA-A*02:01 alone, or (right) NY-ESO-1 full protein alone. Means ± SD for two technical replicates are shown. **(B)** ELISA comparing secretion of IFN-γ from TCR-transduced PBMCs following 48 hours coincubation with indicated M257 or PC-3 target cells. On the 4th day post-transduction, TCR-transduced PBMCs were sorted for $CD3^+$/$LNGFR^+$ and then expanded for 13 additional days prior to the co-culture/ELISA assay and the *in vivo* experiment. Means ± SD for a representative experiment with two technical replicates is shown. **(C)** Flow cytometry contour plots comparing the transduction ($LNGFR^+$) levels of TCR-transduced PBMCs used for the *in vivo* experiment.

CHAPTER 3:

Allogeneic HSC-engineered NY-ESO-1-specific T cells for off-the-shelf solid tumor immunotherapy

TITLE PAGE

Allogeneic HSC-engineered NY-ESO-1-specific T cells for off-the-shelf solid tumor immunotherapy

Jiaji Yu[1,2,3,*], Yu Jeong Kim[1,*], Yan-ruide Li[1,2], Yang Zhou[1,2], Zhe Li[1], Yu-Chen Wang[1], Feiyang Ma[2,4], Derek Lee[1,2], Zoe Hanh[1], Yuchong Zhang[5], Yvonne Y. Chen[1,6], Matteo Pellegrini[2,7] and Lili Yang[1,2,3,8]

Author Affiliation

1. Department of Microbiology, Immunology & Molecular Genetics, University of California, Los Angeles, Los Angeles, CA 90095, USA
2. Molecular Biology Institute, University of California, Los Angeles, Los Angeles, CA 90095, USA
3. Eli and Edythe Broad Center of Regenerative Medicine and Stem Cell Research, University of California, Los Angeles, Los Angeles, CA 90095, USA
4. Department of Molecular, Cell, and Developmental Biology, University of California, Los Angeles, Los Angeles, CA 90095, USA
5. Department of Integrative Biology & Physiology, University of California, Los Angeles, Los Angeles, CA 90095, USA
6. Department of Chemical and Biomolecular Engineering, University of California, Los Angeles, Los Angeles, CA 90095, USA
7. Institute of Genomics and Proteomics, University of California, Los Angeles, CA 90095, USA
8. Jonsson Comprehensive Cancer Center, David Geffen School of Medicine, University of California, Los Angeles, Los Angeles, CA 90095, USA

* Contributed equally

Address Correspondence to

Lili Yang, Ph.D. liliyang@ucla.edu

Introduction

The clinical efficacy of αβ T cell receptor (TCR) and chimeric antigen receptor (CAR)-engineered T-cell immunotherapy has demonstrated that the adoptive transfer of engineered T cells could be a powerful treatment for various diseases, especially for cancer. The CAR T cells have been a great success at treating blood cancers and approved by FDA[1-3]. While the adoptive transfer of TCR-engineered T cells has shown great promise, especially in treating solid tumors to which CAR T cells were less effective[4-6]. Nevertheless, most of the current T cell therapies were constrained by their autologous nature. It means T cells collected from a patient are manufactured and used to treat that particular patient. There are many apparent issues with autologous approaches, such as time-consuming for manufacturing and hence the need for interim therapies, wide variabilities for the quality and quantity of T cells, and quite costly and logistically challenging[3, 7, 8]. One approach to broaden the use of T-cell immunotherapy is developing allogeneic cell products as the source of "off-the-shelf" therapeutic T cells. Such allogeneic T cell sources that are scalable, compatible with various TCR and CAR engineering, and readily distributable are in great demand.

The unique specificity of each TCR for a peptide-MHC complex is determined by both the peptide antigen and the presenting MHC (also known as HLA in humans). Key to the TCR-engineered adoptive T cell (TCR-T) therapy for cancer is that the target peptide is tumor-associated or tumor-specific and that the patient expresses the MHC that the therapeutic TCR is restricted to. One attractive source of such peptide targets is cancer-testis antigens (CTA) for their immunogenicity, stable expression in tumors, and, more importantly, restricted expression in immune-privileged organs[9]. NY-ESO-1 (encoded by the gene *CTAG1B*) is the prototypical CTA

and is particularly promising as a target for cancer immunotherapy. The aberrant expression of NY-ESO-1 was reported in a wide range of tumor types. The aberrant expression frequency ranges from 10-50% among solid tumors, 26% of prostate cancer, 46% of melanoma, 43% of ovarian cancer, and up to 80% in synovial sarcoma neuroblastoma[10-12], with increased expression higher-grade metastatic tumor tissue[13-15]. More importantly, NY-ESO-1 is highly immunogenic and can elicit a potent cellular immune response against multiple epitopes presented by various MHC alleles, including both $CD4^+$ and $CD8^+$ T cell responses[16-18]. Retroviral-mediated clinical trials on adoptive cell transfer (ACT) of NY-ESO-1-specific TCR (esoTCR) engineered T cells have been performed successfully to treat melanoma and synovial sarcoma with response rates of 45% and 67%, respectively[19]. Another lentiviral-mediated esoTCR engineered T cell therapy in patients with multiple myeloma resulted in 70% complete or near-complete responses without significant safety concerns[20]. The majority of these ACT clinical trials focused on esoTCRs specific to the NY-ESO-$1_{157-165}$ (SLLMWITQC) presented by HLA-A*02:01 (HLA-A2) and again falls into the category of autologous therapies[11]. To broaden the clinical utility of NY-ESO-1 as a TCR target, we previously have successfully isolated and characterized multiple esoTCRs targeting NY-ESO-1 epitopes presented by other common MHC alleles different than HLA-A2[10]. With many "off-the-shelf" esoTCRs in the toolbox for T cell therapy, a robust source of "off-the-shelf" T cells is in great need. Artificial thymic organoid (ATO) is one potential source that has been proven to provide functional esoTCR expression T cells[21]. However, this approach is limited by its dependence on murine feeder cells. It could be challenging and costly to work with feeder cell lines for safety and manufacturing measures. Therefore, a feeder-free, scalable and robust allogeneic T cell source is wanted to develop the next-generation "off-the-shelf" NY-ESO-1-specific T (esoT) cell therapy.

This study sought to develop an *in vitro* T cell generation platform based on hematopoietic stem cells (HSCs) for producing allogeneic esoT cells. We established such a system that does not reply on feeder cells for the development of T cells from HSCs, and it was robust to generate allogeneic esoT cells in great quantity with high purity. We tested these allogeneic esoT cells in-depth for their efficacy and safety as candidates for the "off-the-shelf" T cell therapy against solid tumors. A step forward, we further tested the possible additional engineering on these allogeneic esoT cells, including HLA-I/HLA-II KO, for better universality and incorporation of CARs enabling multiple targeting towards a more robust treatment again tumor escape through antigen loss.

Results

Generation of allogeneic HSC-engineered NY-ESO-1-specific T (^{Allo}esoT) cells

Human cord blood-derived $CD34^+$ HSCs were transduced with a tricistronic lentiviral vector that encodes esoTCR α chain, β chain, and a suicide gene sr39 thymidine kinase (Lenti/esoTCR-TK) and then cultured in a 4-stage *ex vivo* feeder-free/serum-free T cell generation system, where they differentiate into ^{Allo}esoT cells over 6 weeks with an expansion of ~10^6 folds (tested from 8 cord blood donors) (Fig. 1a, b, and supplementary Fig. 1a). TCR genes to be loaded onto the lentivector can be versatile. Two esoTCRs with different MHC restrictions were tested in this study, one specific to NY-ESO-$1_{(157-165)}$/HLA-A2 (clone 1G4) and the other specific to NY-ESO-$1_{(60-72)}$/HLA-B7 (clone 1E4) (Supplementary Fig. 1a) (Data presented developed from clone 1G4 transduced cells unless other specified). TCR sequences used were derived from the previous study[10]. In HSCs, we routinely achieved over 50% lentivector transduction rate (Fig. 1c).

For T cell development from HSCs, we established an *ex vivo* feeder-free/serum-free T cell generation system based on plate-bound delta-like 4 (DLL4) to enable lymphoid differentiation as previously described[22-25] (Fig. 1a). Notch signaling through DLL1 or DLL4 is pivotal to thymocyte commitment and was employed in multiple HSC or iPSC-based T cell generation systems[22, 23, 26, 27]. The change of culture medium components determined the stages of the culture and the replacement of fresh DLL-4 coated plates (Fig. 1a). In the culture system, the development of ^{Allo}esoT cells followed a typical T cell developmental path defined by the CD4/CD8 coreceptor expression[28, 29]. One week into the culture system, esoTCR started presented on the cell surface (Fig. 1 d). Over 6 weeks, ^{Allo}esoT cells transited from $CD4^-CD8^-$ (DN) to $CD4^+CD8^+$ (DP), then toward $CD4^-CD8^{+/-}$(Fig. 1d). Later on, we found the culture can be further shortened to 5 weeks (one week less for stage 2) without compromising the yield and cell qualities. By the end of the culture, most ^{Allo}esoT cells (>98%) were $esoTCR^+$ $CD3^+$ DP without any detectable endogenously rearranged TCR, suggesting the induction of allelic exclusion through the introduction of transgenic TCR as previously reported[30, 31]. The *ex vivo* generated ^{Allo}esoT presented a $CD8^+$ single-positive (SP) or $CD4^-$ $CD8^-$ double-negative (DN) phenotype (Fig. 1d). Flow cytometry analysis of the ^{Allo}esoT cell product showed high purity of clonal esoTCR expression (Fig. 1d). Single-cell TCR sequencing analysis confirmed that these ^{Allo}esoT cells uniformly expressed the transgenic esoTCR with nearly undetectable randomly rearranged endogenous αβ TCR pairs (Fig. 1e). In contrast, healthy donor periphery blood mononuclear cells (PBMCs) derived conventional αβ T (PBMC T) cells expressed highly diverse endogenously rearranged αβ TCRs (Fig. 1e). The resulting ^{Allo}esoT cells contained pure transgenic esoTCR expressing T cells with nearly

undetectable bystander T cells, which greatly reduces the risk of graft versus host disease (GvHD) under the context of allogeneic "off-the-shelf" therapies.

The same developmental path and cell product phenotypes were observed for HLA-B7 restricted esoTCR transduced HSCs (Supplementary Fig. 1c). The development of the T cells in this culture system did not require matching the MHC type of the HSC donor with the one transgenic TCR restricted to. HLA-A2^{-} HSC donor supported the development of ^{Allo}esoT cells, and the same independence of HSC donor MHC went for the generation of HLA-B7 restricted ^{Allo}esoT(B7) cells (Fig. 1b, 1f, and supplementary Fig. 1d). All these corroborated the compatibility of this system with all kinds of transgenic TCRs broadening its potential allogeneic applications.

Phenotype and transcriptome profiling of ^{Allo}esoT cells

We characterized the phenotype and functionality of ^{Allo}esoT cells compared to the clinically employed PBMC derived esoT (PBMC-esoT) cells. Cognate dextramer staining confirmed the correct expression of 1G4 clone esoTCR (Fig. 2a). ^{Allo}esoT cells expressed a minimum amount of HLA-II with lower expression of HLA-I when compared to PBMC-esoT cells (Fig. 2a), which may well benefit its allogeneic application. ^{Allo}esoT cells presented many typical T cell functions while showing some NK cell phenotypes. ^{Allo}esoT cells showed a memory phenotype with high expression of CD45RO while negative for CD45RA (Fig. 2a). They express high levels of T cell activation marker (i.e., CD69, CD25), NK markers (i.e., NKG2D, CD56, and DNAM-1), and peripheral tissue and inflammatory site homing markers (i.e., CCR5, CCR4, CXCR3, and CXCR4) (Fig. 2a, supplementary Fig. 2a, and 2c). In addition, ^{Allo}esoT cells produced potent amounts of proinflammatory cytokines (i.e., IFN-γ, IL-2, and TNF-α) and cytotoxic

molecules (i.e., granzyme B and perforin) (Fig. 2a, and supplementary Fig. 2b). Interestingly, ^{Allo}esoT cells expressed a lower level of checkpoint inhibitors than PBMC-esoT cells (Supplementary Fig. 2c). ^{Allo}esoT(B7) cells also displayed the same NKT type of surface markers and functionality profiles (Supplementary Fig. 2d and e). To test the functionality of the esoTCR, we stimulated ^{Allo}esoT cells with the cognate NY-ESO-1 peptide (ESOp) and observed vigorous proliferation (Fig. 2c). ^{Allo}esoT cells secreted high levels of proinflammatory cytokines (i.e., IFN-γ, TNF-α, and IL-2) (Fig. 2d-f).

RNA sequencing was performed to characterize the transcriptome profile of ^{Allo}esoT in comparison with PBMC derived conventional αβ T (PBMC-Tαβ), γδ T (PBMC-Tγδ) and NK (PBMC-NK) cells. $CD8^+$ PBMC-Tαβ cells were used for this experiment to be consistent with the CD8 SP/DN phenotype of ^{Allo}esoT cells (Fig. 2g-l). Principal component analysis (PCA) of the global gene expression profiles showed that ^{Allo}esoT grouped closely together while locating right adjacent to PBMC-Tαβ cells, away from PBMC-Tγδ cells, and the furthest from PBMC-NK cells (Fig. 1g). This PCA result indicated these ^{Allo}esoT cells are unique as their own, yet closely resembled the transcriptome profile of PBMC-Tαβ cells (Fig. 1g). Heatmaps of gene expression analysis further demonstrated the profile signatures of ^{Allo}esoT. Generally, ^{Allo}esoT cells displayed T cell transcriptome while preserving many NK-like phenotypes (Fig. 2h-l). They presented high expression of *NFKB1,* which is essential for TCR signaling; they expressed a high level of *ZBTB16* that encodes PLZF, a signature transcription factor of NKT and NK cells[32]; they showed enrichment on *TBX21* and *GATA3* that regulate Th1 and Th2 responses[33]; they also showed low expression *RORC* that determines Th17 polarization (Fig. 2h)[33, 34]. Of note, compared to all PBMC derived T and NK cells tested, ^{Allo}esoT cells expressed minimal level of HLA-II related genes

across all the donors. They engineered cell product types and generally low levels of HLA-I related genes, which potentially would benefit their use in "off-the-shelf" therapy reducing the risk of GvHD (Fig. 2i)[35]. For immune responses in the tumor, tissue inflammatory homing markers on effector immune cells are essential for enabling the entry to inflammatory tumor site[36]. ^{Allo}esoT cells expressed high levels of multiple tissue inflammatory homing marker genes (e.g., CCR1, CCR5, CCR6, CXCR3, and CXCR6), comparable to those of innate PBMC-Tγδ cells, and significantly higher than PBMC-Tαβ and PBMC-NK cells (Fig. 2j). Furthermore, compared to PBMC-iNKT and even PBMC-NK cells, ^{Allo}esoT cells expressed exceedingly high levels of NK activating receptor genes and low levels of NK inhibitory receptor genes suggesting their NK phenotype and related functionalities (Fig. 2k and l)[37]. Many corresponding protein expressions of the transcriptome results were confirmed by flow cytometry results (Fig. 2a, b, and supplementary Fig. 2a-c).

Solid tumor targeting by ^{Allo}esoT cells

We used two tumor models, A375 human melanoma and PC3 human prostate cancer, to study the tumor-targeting efficacy of ^{Allo}esoT cells. Engineering was made on the parent cell lines as previously described to express esoTCR target HLA-A2 and NY-ESO-1 (denoted as A2-ESO)[10]. Firefly luciferase and enhanced green fluorescence protein dual-reporters (denoted as FG) were also transduced to these cell lines as reporters[31]. Scanning electronic microscopy showed the morphology of ^{Allo}esoT cells attacking an A375-A2-ESO cell (Fig. 3a). As indicated by gene profiling and flow cytometry staining, we proposed a TCR/NK dual killing mechanism for ^{Allo}esoT cells targeting tumors with NY-ESO-1 and cognate MHC (Fig. 3b). When cocultured with A375-FG and PC3-FG cells, ^{Allo}esoT cells presented A2-ESO independent tumor killing while PBMC-

Tc and PBMC-esoT showed no killing effect (Fig. 3c and e). In *in vitro* killing assays with A375-A2-ESO-FG and PC3-A2ESO-FG, ^{Allo}esoT cells showed robust tumor-killing that was better than PBMC-esoT (Fig. 3d and f). By comparing the killing of A2-ESO positive and negative lines, the strong esoTCR-mediated tumor targeting was corroborated (Fig. 3c-f). To further study the NK killing of ^{Allo}esoT cells, PBMC derived NK cells were included to control the killing of three non-A2-ESO cell lines, including the NK sensitive cell line K562-FG. Across all three A2-ESO negative cell lines, ^{Allo}esoT cells performed better than endogenous NK cells in the *in vitro* killing assays measured by luciferase activity (Fig. 3g, supplementary Fig. 3a, and c). To dissect the killing mechanism, we set up *in vitro* killing assays with NKG2D and DNAM-1 blocking antibodies which significantly reduced the tumor-killing (Fig. 3h and supplementary Fig. 3b). This confirmed the NK activating-receptor-mediated tumor-targeting function of ^{Allo}esoT cells. Interestingly, NKG2D and DNAM-1 blocking did not reduce the A2-ESO independent killing of PC3-FG by ^{Allo}esoT cells, implying additional NK killing pathways (Supplementary Fig. 3d).

Using a human A375-A2-ESO solid tumor xenograft NSG (NOD/SCID/$\gamma c^{-/-}$) mouse model, we studied the *in vivo* efficacy of ^{Allo}esoT cells compared to the current clinically employed PBMC-esoT cells (Fig. 3i). With weekly administration, both ^{Allo}esoT and PBMC-esoT cells effectively killed and suppressed the growth of A375-A2-ESO tumor cells (Fig. 3j, k, and supplementary Fig. 4a). However, mice receiving conventional PBMC-esoT cells, despite the minimal tumor load after the treatment, quickly developed severe GvHD due to xenoreactivity and died. In contrast, AlloesoT cells treated mice survived much more prolonged (Fig. 3l). In terminal analysis, we analyzed effectors in liver and tumor sites to observe that ^{Allo}esoT cells retained their proinflammatory and cytotoxic function *in vivo* while maintained still a minimal level of PD-1

expression (Supplementary Fig. 4b-g). To challenge ^{Allo}esoT cells with a heavy tumor load, we established another PC3-A2-ESO xenograft mouse model (Fig. 3m). With weekly administration of effector cells, both ^{Allo}esoT and PBMC-esoT cells suppressed the tumor growth at a comparable level within the time frame test (Fig. 3n and o). In this *in vivo* experiment, we sacrifice the mice and performed biodistribution analysis through flow cytometry. ^{Allo}esoT cells are distributed primarily to the tumor site while enriched in the liver at a lesser magnitude (Fig. 3p). In contrast, PBMC-esoT cells heavily infiltrate to the liver and peripheral blood owing to GvHD of xenoreactivity (Supplementary Fig. 4h).

Safety and immunogenicity of ^{Allo}esoT cells

GvHD is a major safety concern for "off-the-shelf" allogeneic immune cell therapies[7, 38, 39]. The safety aspects of esoTCR, especially for the clone 1G4, have been tested in clinical trials with no on-target off-tumor toxicities[19, 20]. The allogeneic safety concerns of PBMC derived T cells mainly lie in the endogenous bystander TCRs, which may alloreact with the host cells[7, 38, 39]. Due to the TCR clonality of ^{Allo}esoT cells, such GvHD risk was significantly reduced. An *in vitro* mixed lymphocyte reaction (MLR) was used to evaluate the GvHD risk of ^{Allo}esoT cells (Fig. 4a). ^{Allo}esoT cells did not react to donor-mismatched PBMCs, in contrast to PBMC-esoT cells, which produced a significant amount of IFN-γ for alloreactivity (Fig. 3b). In the A375-A2-ESO NSG model (Fig. 3i), 35 days post effector cell transfer, *in vivo* tissue histology analysis showed severe mononuclear cell infiltration in kidney, liver, and lung for PBMC-esoT treated mice (Fig. 4c-f). As for ^{Allo}esoT treated mice, minimal mononuclear cell infiltration was observed (Fig. 4c-f). In allogeneic therapies, host T cells could deplete allogeneic therapeutic cells through the recognition of mismatched HLA-I&II molecules, which is a significant contributor of the host-versus-graft

(HvG) concerns[38] Interestingly for ^{Allo}esoT cells, both HLA-I and HLA-II molecules were naturally expressed at a lower level compared to conventional PBMC-esoT cells, particularly for HLA-II (Fig. 2a and i), which significantly reduced the immunogenicity. We further examined HLA-I&II expression on ^{Allo}esoT cells in an *in vitro* IFN-γ response experiment and confirmed a much lower expression of both HLA-I&II molecules when compared to PBMC-esoT cells (Fig. 4g and h). We then set up another *in vitro* MLR assay to evaluate the immunogenicity and HvG risk of ^{Allo}esoT cells (Fig. 4i). ^{Allo}esoT cells triggered significantly reduced IFN-γ production from mismatched PBMCs of 3 donors when compared to PBMC-esoT cells (Fig. 3g). Allogeneic host NK cell-mediated rejection could be an additional HvG concern. An MLR assay with the coculture of mismatched PBMC-NK cells was performed to study this concern (Fig. 4k), in which ^{Allo}esoT cells persisted well against PBMC-NK destruction compared to conventional PBMC-esoT cells (Fig. 4l). The low expression of stress molecules such as ULBP, an NKG2D ligand, on ^{Allo}esoT may contribute to the resistance to NK cell killing (Fig. 4m and n). In the design of ^{llo}esoT cells, we especially included a TK suicide gene as a safety net of any unforeseen safety risks during allogeneic application (Supplementary Fig. 1a). TK gene enables the elimination of TK expression cells with prodrug in the event of severe adverse responses, and it would also allow *in vivo* monitoring with positron emission tomography (PET) imaging[31]. In an *in vitro* prodrug ganciclovir (GCV) coculture assay (Fig. 4o), GCV induced effective depletion of ^{Allo}esoT cells (Fig. 4p). Overall, these studies demonstrated the high safety and low immunogenicity profile of ^{Allo}esoT cells supporting their "off-the-shelf" therapeutic applications.

Development of HLA-ablated universal ^{Allo}esoT (^{U}esoT) cells

Although ^{Allo}esoT cells presented a stable phenotype of low HLA-I&II expression, especially for HLA-II (Fig. 2a, i, 4g and h), the residue HLA-I expression could still make them targets of host T-cell mediated allorejection at certain levels. The residue expression of HLA could be further reduced and even ablated with direct gene disruption. It can be achieved with just two genes: 1) the *B2M* gene that encodes beta 2-microglobulin (B2M), which is an essential component for all HLA-I molecules[40]; 2) the *CIITA* gene that encodes the class II transactivator (CIITA) that is pivotal for the transcription of all HLA-II molecules[41]. The gene disruption can be achieved by CRISPR-Cas9/gRNA system[40, 42]. Yet, with the successful ablation of HLA-I&II, cell products would become susceptible to host NK killing due to the lack of self-signal (HLA expression)[43]. This can be circumvented by introducing HLA-E, which is conserved across human populations and proven to suppress host NK allorejection[44]. For the successful generation of HLA-ablated universal ^{Allo}esoT (^{U}eso-T) cells, we have three hypotheses: 1) CRISPR-mediated gene disruption and lentiviral vector transduction would not interfere with each other; 2) the disruption of *B2M* and *CIITA* genes would not affect the development of ^{Allo}esoT cells; 3) Host NK-mediated allorejection due to the lack of HLA expression could be avoided by introducing HLA-E expression. Thereby we designed a new workflow to generate HLA- ^{U}eso-T cells, wherein HLA-E was included in the lentiviral vector, and an additional CRISPR/Cas9 gene-editing step through electroporation was implemented at day 3 (Fig. 5a and supplementary Fig. 5a). For the new design of the vector, TK was replaced by HLA-E, and more than 30% of the transduction rate of both esoTCR and HLA-E can be achieved in HSCs (Supplementary Fig. 5b and c). Confirming our hypothesis, we found that the CRISPR/Cas9 gene-editing did not interfere with the T cell differentiation from engineered HSCs (Fig. 5b). We were able to obtain a high yield and purity of ^{U}eso-T cells resembling that of ^{Allo}esoT cells. The CRISPR/Cas9 gene editing was robust, and ~50%

of HLA-I knockdown and near total ablation of HLA-II could be stably kept in the final ^{U}eso-T cell product with HLA-E well expressed (Fig. 5c).

In PCA analysis of global gene expression profile, ^{U}eso-T cells clustered closely with ^{Allo}esoT and PBMC-Tαβ cells, away from PBMC-Tγδ cells, and furthest from PBMC-NK cells (Supplementary figure 5d). This further corroborated our hypothesis that CRISPR/Cas-9 engineering is compatible with the culture system while B2M/CIITA disruption will not affect the development of engineered T cells. Apart from HLA-I&II ablation, ^{U}eso-T cells showed a typical effector memory NKT cell phenotypes resembling those of ^{Allo}esoT cells in flow cytometry analyses (Fig. 5d and supplementary 5e). More importantly, these ^{U}eso-T cells are functional in producing a potent amount of proinflammatory cytokines and cytotoxic molecules (Fig. 5d and supplementary Fig. 5f). In an *in vitro* tumor killing assay, ^{U}eso-T cells performed as well as ^{Allo}esoT cells exceeding the performance of PBCM-esoT cells (Fig. 5e). ^{U}eso-T cells presented a minimal expression of both HLA-I&II molecules much lower than that of ^{Allo}eso-T and PBMC-esoT cells, which essentially brought down the immunogenicity concerns of GvH risk (Fig. 5f and g).

As expected, ^{U}eso-T cells induced nearly undetectable T cell-mediated alloreactivity when mixed with mismatched healthy donor PBMCs (Fig. 5h, I and supplementary Fig. 5g). ^{U}eso-T cells preserved the resistance to NK cell-mediated allorejection, which was especially evident through the comparison with HLA-I&II disrupted ^{Allo}eso-T cells without HLA-E overexpression (Fig. 5j and k). Jointly, these studies support the generation of HLA-ablated HLA-E overexpressed ^{U}eso-T cells that are fully resistant to both host T and NK cell-mediated allorejection and indicated the potentially improved safety profile in therapeutical applications.

The generation of CAR-armed esoT (^{Allo}CAR-esoT) cells

In the T cell targeting of solid tumors, the heterogeneous expression of tumor antigen and MHC molecules leads to poor targeting, thus hamper the therapeutic responses[45, 46]. In addition, during the adoptive T cell therapy, tumors can also escape from targeting through the loss of cognate MHC expression for TCR-T therapies and the loss of antigen for both TCR-T and CAR-T therapies[45, 47]. The loss of MHC heterozygosity could be overcome by multi-targeting with esoTCRs restricted to various MHCs[10], which could also be achieved through ^{Allo}esoT cells with various MHC restrictions (Fig. 1d, 3b-f, supplementary Fig. 1c, and 3e-h). Nevertheless, the loss of NY-ESO-1 expression would be detrimental to NY-ESO-1 single targeted therapies. To overcome tumor escape through antigen loss, we propose to target the solid tumor with both TCR targeting and CAR targeting through incorporating CAR into our constructs for the generation of ^{Allo}CAR-esoT cells (Fig. 6a). We designed two vectors with two different CAR, prostate-specific membrane antigen (PSMA) CAR (PCAR) and mesothelin CAR (MCAR), to demonstrate the feasibility of this approach (Supplementary Fig. 6a). Both esoTCR and CAR were transduced to HCSs at the beginning of the culture through a single lentivector (Fig. 6a and supplementary Fig. 6a). Of note, CAR engineering did not interfere with the development of transgenic T cells, and both ^{Allo}PCAR-esoT and ^{Allo}MCAR-esoT cells followed the same developmental path and shared phenotypic profiles (Fig. 6b, supplementary Fig. 6b, and c). Moreover, CAR expression was stable, resulting in esoTCR^{+} CAR^{+} DP cell product with high purity (Fig. 6c). This approach saved the additional CAR transducing process upon mature T or NK cells required for all current allogeneic products, including many with the iPSC approach[23, 25, 48]. With the addition of CAR construct, the TCR/CAR/NK triple targeting of solid tumor become possible for ^{Allo}CAR-esoT cells (Fig. 6d). The *in vitro* tumor killing of the parental solid tumor cell lines demonstrated the NK type of killing

(Supplementary Fig. 6e); the killing of A2-ESO positive cell line showed the esoTCR-mediated killing (Supplementary Fig. 6f); the killing of PSMA positive cell line confirmed the CAR-mediated killing (Supplementary Fig. 6f). Under the clinical scenario, cancer cells often present a very heterogeneous population of tumor antigen expression. To simulate that, we employed a mixed tumor population of PC3-FG, PC3-PSMA-FG, PC3-A2-ESO-FG, and PC3-PSMA-A2-ESO-FG in the ratio of 1:1:1:1 to test the tumor-killing capacity of ^{Allo}PCAR-esoT cells (Fig. 6e). In this *in vitro* mixed tumor-killing assay, ^{Allo}PCAR-esoT performed significantly better than conventional PBMC-PCART and PBMC-esoT cells in all effector-to-tumor ratios (Fig. 6e). In short, CAR engineering was compatible with the ^{Allo}esoT culture platform, and the resulting ^{Allo}CAR-esoT cells could lead to a complete tumor-targeting, especially for the heterogeneous tumor population. Multitargeting through TCR, CAR, and NK pathways of ^{Allo}CAR-esoT cells may lead to more successful cell therapy for cancer, minimizing the possibility of tumor escape through antigen loss.

Discussion

This study reported the generation and characterization of allogeneic HSC-engineered NY-ESO-1-specific T (^{Allo}esoT) cells and their variations (i.e., ^{U}esoT and ^{Allo}CAR-esoT). Establishing an *ex vivo* HSC-based transgenic TCR engineered T cell differentiation culture, we showed the generation of ^{Allo}esoT cells of high yield and purity, high antitumor efficacy with multi-targeting capacity, and low GvH and HvG risks. In addition, this platform was versatile and compatible with additional engineerings like CRISPR/Cas9 gene editing and CAR engineering. Collectively, our studies have generated ^{Allo}esoT cells and demonstrated the potential of such transgenic T cells as promising cell carriers for developing allogeneic cancer immunotherapy.

It has been the frontier of immunotherapy in the development of robust allogeneic "off-the-shelf" cell sources. Currently, two major categories of such cell sources were under extensive study. One source comes from healthy donor PBMC-derived conventional T or NK cells[40, 49, 50], and the other is pluripotent stem cell (PSC)-based cell sources[23, 25, 48]. For PBMC-derived conventional αβ T cells, they risk inducing GvHD in allogeneic therapies due to HLA incompatibility. Thus these T cells need to be gene-edited to ablate endogenous TCR expression, usually achieved through the disruption of the *TRCA* or/and *TRBC* gene loci[51-54]. As for PBMC-NK-based allogeneic cell products, they are regarded of low GvHD risk so that additional gene editing is unnecessary; however, compared with conventional αβ T cells, their clonal expansion and antitumor performance *in vivo* may have limitations[49]. The advancement in the generation and differentiation of induced PSCs (iPSCs) provided another allogeneic cell source for T-cell immunotherapy[23, 25, 55, 56]. For all these iPSC-based approaches, additional differentiation steps into hematopoietic progenitor stem (HPC) cells were required, while the following T-cell differentiation relied on murine OP9 feeder cells for many of them; furthermore, additional transduction steps were necessary if CAR was invovled[23, 25, 55, 56]. The sophistication of iPSC generation and differentiation (~4 months of induction from a T cell clone to iPSC), the dependence on feeder cells, and the prolonged time of culture due to additional steps all could be unfavorable for allogeneic clinical applications[23, 25, 55, 56]. Our work here provided a novel allogeneic cells source with the *ex vivo* HSC-based transgenic TCR engineered T cell generation platform. There are abundant sources of HSCs available, including cord blood and G-CSF-mobilized human periphery blood stem cells (PBSCs). With our approach, there is no generation of endogenously rearranged TCR pair (Fig. 1e), no feeder cells involve for the T cell differentiation

(Fig. 1a), no additional CAR engineered needed at the end (Fig. 6a), and the culture time can be as short as 5 weeks with ~10^6 fold of cell expansion (Fig. 1b).

With the *ex vivo* ^{Allo}esoT cell generation culture, it was estimated that from one cord blood donor (~5 x 10^6 HSCs), ~5 x 10^{12} ^{Allo}esoT cells could be generated that can potentially be formulated into ~5,000-50,000 doses (~10^8-10^9 cells per dose)[2]. In this culture, transgenic TCR-guided T cell differentiation was a key to induce allelic exclusion[30, 31, 57], resulting in high purity of final ^{Allo}esoT cell product and nearly free of bystander conventional αβ T cells (Fig. 1d and e). Another key is DLL1/DLL4, which is pivotal for T-cell lineage commitment and essential for all available *in vitro* T cell differentiation methods[21, 22, 26]. Missing the MHC signals of the natural thymic environment, the mere provision of DLL1/DLL4 *in vitro* is insufficient to forward the T cell development through the positive selection from $CD4^+CD8^+$ DP stage to $CD8^+$ SP stage[22, 25, 26]. This resulted in the dependence on the employment of anti-CD3 antibodies to mimic the MHC engagement of natural positive selection[23, 25], which was also incorporated in our culture method reported here (Fig. 1a). Interestingly, the dependence on anti-CD3 antibodies also makes our system independent of the cognate MHC of the transgenic TCR (Fig. 1f and supplementary Fig. 1d), so that theoretically, any transgenic TCR with various MHC restrictions could be adopted to the same system. Here we demonstrated the generation of HLA-A2 restricted ^{Allo}esoT and HLA-B7 restricted ^{Allo}esoT(B7) cells. For public antigens like NY-ESO-1, with the approach reported here, we would be able to generate a library of "off-the-shelf" ^{Allo}esoT cells targeting multiple epitopes and MHC. In the US population, the HLA-A2 allele is the most common MHC-I allele in Caucasians (45%) and Hispanics (41%), but it is less common among Asians (15%) and African (16%)[58]. Moreover, the expression of at least one allele from three MHC-I supertypes (A2, A3,

and B7) presents over 80% of the population across ethnic groups, and >99% of people express at least one allele from nine MHC-I supertypes[59]. With the ability to generate a library of allogeneic transgenic T cells targeting a particular tumor antigen, we would have the freedom to extend the allogeneic TCR-T therapy to a more significant subset of patients, and when used in combination with a single patient, multi-targeting of epitopes from the same antigen can more effectively kill tumors preventing evasion through loss of MHC heterozygosity.

The antitumor efficacy of ^{Allo}esoT cells was promising. They presented both typical effector memory T cell and NK cell phenotypes while producing a potent amount of proinflammatory cytokines and cytotoxic molecules outperforming conventional T cells (Fig. 2). These ^{Allo}esoT cells also expressed exceedingly high levels of NK activating receptors and low levels of NK inhibitory receptors (Fig. 2k and l), which explained their superior NK function in tumor killing (Fig 3 and supplementary Fig. 3). Our study confirmed ^{Allo}esoT cells killed tumors through NKG2D and DNAM-1 (Fig. 3h). However, these two mechanisms were insufficient to explain the tumor-killing of PC3-FG cells (Supplementary Fig. 3d), indicating more NK killing mechanisms exist for ^{Allo}esoT cells. The TCR/NK dual-tumor-targeting mechanism of ^{Allo}esoT cells granted them a more robust antitumor efficacy (Fig. 3). Moreover, the empowerment with CAR rendered ^{Allo}CAR-esoT cells TCR/CAR/NK triple-targeting capacity against solid tumor (Fig. 6), which would enable them to counteract tumor antigen escape which has been observed in many current mono-tumor-antigen targeting T-cell therapies[2, 45, 47, 60]. In two human solid tumor xenograft mouse models (i.e., prostate cancer and melanoma) employed here, ^{Allo}esoT cells demonstrated robust tumor killing with overall enhanced *in vivo* performance than conventional

PBMC-esoT cells, highlighting their potential in cancer therapies (Fig. 3i-p and supplementary Fig 4a-h).

Another two outstanding features of ^{Allo}esoT cells were their safety and low immunogenicity. In our studies, ^{Allo}esoT cells showed no GvH responses both *in vitro* and *in vivo,* owing to their monoclonal expression of esoTCR (Fig. 4a-d). An additional layer of safety was included that a suicide switch (sr39TK/GCV) could ablate all transgenic T cells with high efficacy (Fig. 4p). ^{Allo}esoT cells expressed reduced levels of HLA-I and minimal levels of HLA-II compared to PBMC-derived αβ T, γδ T and NK cells (Fig. 2i). This feature may reduce the risk of allorejection by host T cells, thus mitigate the necessity of additional MHC gene editing or intense precondition treatment to deplete host T cells[51, 52]. Meanwhile, ^{Allo}esoT cells were also resistant to NK-cell-mediated host rejection (Fig. 4 k and l), which may be partly explained by their reduced NK activating ligand expression (Fig. 4m and n). The biological regulation behind the low immunogenicity of ^{Allo}esoT cells remains to be studied, and the *ex vivo* programming nature of these cells will be accountable.

The compatibility with additional engineering approaches like CAR and CRISPR/Cas9 gene-editing makes this ^{Allo}esoT cell generation platform versatile and being able to evolve (Fig. 5 and 6). These additional engineering approaches were easily incorporated at the HSCs stage, and they will not interfere with the generation and antitumor functionality of ^{Allo}esoT cells (Fig. 5 and 6). With such compatibility, additional tumor-targeting modalities (e.g., CARs, TCRs, and CD16), functional enhancement genes (e.g., IL15, IL21), and ablation of immune checkpoint inhibitors like PD-1, all of these could be potential plug into the current platform leading to “off-the-shelf”

T cells of better allogeneic cancer therapeutic potential. In future work with this platform, we will study the developmental regulation of these T cells and evaluate rational combinations of modalities that affect persistence, exhaustion, and tumor targeting under the context of "off-the-shelf" immunotherapy for cancer.

Material and methods

Mice and cell lines.

All animal experiments used NOD.Cg-Prkdc^{SCID}Il2rg^{tm1Wjl}/SzJ (NOD/SCID/IL-2Rγ-/-, NSG) mice purchased from The Jackson Laboratory. All mice were 6- to 10-weeks old and maintained at the animal facilities of the University of California, Los Angeles (UCLA) under pathogen-free conditions. Human melanoma A375 and prostate cancer PC3 were purchased from American Type Culture Collection (ATCC). Human peripheral blood mononuclear cells (PBMCs) and derived human T cells, unless otherwise specified, were cultured using RPMI1640 medium supplemented with 10% (vol/vol) FBS, 1% (vol/vol) penicillin/streptomycin/glutamine, 1% (vol/vol) MEM NEAA, 10mM HEPES, 1mM sodium pyruvate and 50uM β-ME (C10 medium). A375 and PC3 cells were cultured in DMEM supplemented with 10% (vol/vol) FBS and 1% (vol/vol) penicillin/streptomycin/glutamine (D10 medium). Parental cell lines were transduced with lentiviral vectors overexpressing human NY-ESO-1 (ESO), HLA-A2 (A2) or HLA-B7 (B7), and/or firefly luciferase (Fluc) to produce stable tumor cell lines for *in vitro* and *in vivo* analysis. In lab generated cell lines used in this study are listed as follows: A375-Fluc, A375-A2-ESO, A375-A2-ESO-FLuc, A375-B7-ESO-FLuc, PC3-FLuc, PC3-A2-ESO, PC3-A2-ESO-FLuc and PC3-B7-ESO-FLuc.

Animal study approval.

All mouse studies were conducted in accordance with national guidelines for the humane treatment of animals and were approved by the Institutional Animal Care and Use Committee of UCLA.

Human PBMCs, CD34+ HSCs, and Thymus Tissues

Human peripheral blood mononuclear cells (PBMCs) were obtained from the CFAR Gene and Cellular Therapy Core Laboratory at UCLA, without identification information under federal and state regulations. Hematopoietic stem cells (HSCs) isolated from healthy cord blood (CB) donors were purchased from HemaCare. For all CB HSCs aliquots, the purity of CD34+ cells were more than 97% as evaluated by flow cytometry.

Lentiviral vector construction and transduction.

Lentiviral vectors used in this study were constructed from a parental lentivector pMNDW containing the MND retroviral LTR U2 region, an internal promoter, and an additional truncated Woodchuck Responsive Element (WPRE) to stabilize viral mRNA[1, 2]. The pMNDW lentivector mediates high and stable expression of transgene both in humans and in progeny human immune cells[3]. To construct the Lenti/1G4 vector, a synthetic bicistronic gene encoding human TCR specific to HLA-A*02:01–NY-ESO-1157-165 (TCR clone 1G4[4, 5]) (TCRa-F2A-TCRb-P2A-sr39TK) was inserted into pMNDW. To construct the Lenti/1E4 vector, a synthetic bicistronic gene encoding human TCR specific to HLA-B*07:02–NY-ESO-160-72 (derived from 1E4 TCR clone[5]) (TCRa-F2A-TCRb) was inserted into pMNDW. To construct the Lenti/1G4-HLAE-TK vector, a synthetic tetracistronic gene encoding human TCR specific for HLA-A*02:01–NY-ESO-1157-165 (TCR clone 1G4[4, 5], HLA-E, and sr39 thymidine kinase (TK) (TCRa-F2A-TCRb-P2A-HLAE-T2A-sr39TK) was inserted into pMNDW. The Lenti/Fluc vector was constructed by inserting a synthetic bicistronic gene encoding Fluc-P2A-EGFP into pMNDW. The Lenti/HLA-A2-EGFP vector was constructed by inserting a synthetic bicistronic gene encoding human

HLAA2.1-P2A-EGFP into pMNDW. The Lenti/HLA-B7-EGFP vector was constructed by inserting a synthetic bicistronic gene encoding human HLAB7.2-P2A-EGFP into pMNDW. The lentiviral vector pRRL-CMV-NY-ESO-1- mStrawberry was provided by O.W. Lentiviral vectors pHAGE6-CMV-HLAA2.1-IRES-ZsGreen and pHAGE6- CMV-HLAB7.2-IRES-EGFP were cloned and provided by M. T. B.[5]. Synthetic gene fragments were obtained from GenScript and IDT. Lentiviruses were produced using HEK 293T virus packaging cells in accordance with a standard calcium precipitation protocol, an ultracentrifugation concentration protocol, or a tandem tangential flow filtration concentration protocol, which was used as previously described[6, 7]. Lentivector titers were measured by transducing HEK 293T-hCD3 (human CD3 expressing line, cloned in Lili Yang lab) with serial dilutions and performing flow cytometry following established protocols [6, 7].

Flow cytometry.

Fluorochrome-conjugated antibodies specific for human CD45 (Clone H130), TCRαβ (Clone I26), CD3 (Clone HIT3a), CD4 (Clone OKT4), CD8 (Clone SK1), CD45RO (Clone UCHL1), CD45RA (Clone HI100), CD161 (Clone HP-3G10), CD25 (Clone BC96), CD69 (Clone FN50), CD56 (Clone HCD56), CD62L (Clone DREG-56), HLA-A2 (clone BB7.2), HLA-B7 (clone BB7.1), TCR Vβ13.1 (H131), CTLA-4 (Clone BNI3), PD-1 (clone EH12.2H7), CCR4 (Clone L291H4), CCR5 (Clone HEK/1/85a), CCR7 (Clone G043H7), CXCR3 (Clone G025H7), CXCR4 (Clone 12G5), NKG2D (Clone 1D11), DNAM-1 (Clone 11A8), CD158 (KIR2DL1/S1/S3/S5) (Clone HP-MA4), IFN-γ (Clone B27), granzyme B (Clone QA16A02), perforin (Clone dG9), TNF-α (Clone Mab11), IL-2 (Clone MQ1-17H12), HLAE (Clone 3D12), β2-microglobulin (B2M) (Clone 2M2), HLA-DR, DP, DQ (Clone Tü 39) were purchased from

BioLegend. Fluorochrome-conjugated antibodies specific for human CD34 (Clone 581) were purchased from BD Biosciences. Fluorochrome-conjugated antibodies specific for human PLZF (alone 9E12), and T-bet (clone 4B10) were purchased from eBioscience. Human Fc Receptor Blocking Solution (TrueStain FcX) was purchased from Biolegend, and Mouse Fc Block (anti-mouse CD16/32) was purchased from BD Biosciences. Fixable Viability Dye eFluor506 (e506) was purchased from affymetrix eBioscience. HLA-A2-NYESO-1157-165 dextramer was prepared in house following a protocol as previously described #. HLA-B*07:02–NY-ESO-160-72 tetramer was prepared and provided by NIH Tetramer Core Facility at Emory University.

All flow cytometry stains were performed in PBS for 15 min in 4 degrees. Samples were stained with Fixable Viability Dye eFluor506 (e506) mixed with Mouse Fc Block (anti-mouse CD16/32) or Human Fc Receptor Blocking Solution (TrueStain FcX), followed by PBS washing to remove e506 and blocking antibodies. Antibody staining was added to all samples at specified dilutions according to the manufacturer's instructions. Intracellular cytokines were stained using a Cell Fixation/Permeabilization Kit (BD Biosciences), and transcription factors were stained using Foxp3/Transcription Factor Fixation/Permeabilization (Invitrogen). Flow cytometry was performed using a MACSQuant Analyzer 10 flow cytometer (Miltenyi Biotech) and FlowJo software version 9 and 10 was used for data analysis.

Human CD34$^+$ and PBMC cells.

Cord blood CD34$^+$ cells were positively selected from freshly collected cord blood and provided by Hemacare. Cells were cryopreserved in Cryostor CS10 (BioLife Solution, Seattle, WA) using CoolCell (BioCision, San Diego, CA). For experiments and long-term storage, cells

were frozen in liquid nitrogen. Fresh PBMCs were obtained from healthy donors and purchased from UCLA virology core.

***In vitro* off-the-shelf TCR-engineered T cell generation culture.**

Non-tissue culture-treated 24-well plates were coated with StemSpan lymphoid differentiation coating material (LDCM, 500µl/well, StemCell Technologies) for 2 hours at room temperature or alternatively, overnight at 4ºC. Coating supernatants were removed and plates were washed with a D-PBS buffer. Transduced $CD34^+$ human stem cells (HSCs) at 2 x 10^4/well were suspended in 500 µL of StemSpan lymphoid progenitor expansion medium (LPEM, StemCell Technologies) and seeded into coated wells of the 24-well plate on day 0. Cells were cultured for 3 days at 5% CO_2 and 37ºC. On day 4, another 500 µL LPEM was added into each well and cells were cultured for additional 4 days. On days 7 and 11, half of the medium was removed and replenished with 500 µL fresh LPEM. On day 14, cells were harvested, counted, and re-seeded into a LDCM-coated 12-well plate in 1mL of T cell progenitor maturation medium per well (TPMM, StemCell Technologies) (5 x 10^5 - 1 x 10^6 cells/well). On day 18, 1mL of fresh TPMM was added to each well. On days 21 and 24, half of the medium in each well was discarded and replaced with 1mL of TPMM. On day 28, cells were harvested, counted, and re-seeded into a new coated 12-well plate in 1mL of TPMM (1 x 106 cells/mL/well) with 12.5 µL/well CD3/CD28/CD2 T Cell Activator (StemCell Technologies) and 10 ng/mL Human Recombinant IL-15 (PeproTech). On Day 31, 1mL of fresh TPMM containing 10 ng/mL Human Recombinant IL-15 was added into the culture. On day 35, cells were harvested and analyzed by flow cytometry for double-positive (DP) and single-CD8 (SP) cells. Usually, over 50% DP/ SP CD8 cells could be reliably generated after 5 weeks of differentiation.

***In vitro* expansion of ^{Allo}esoT cells.**

Healthy donor PBMCs were loaded with NY-ESO-1157-165 peptide or NY-ESO-160-72 peptide (ESOp) by culturing 1 x 10^8 PBMCs in 5 mL C10 medium containing 5 uM ESOp for 1 hour. PBMCs were then irradiated at 6,000 rads and used to stimulate ^{Allo}esoT cells (denoted as ESOp/PBMCs). Freshly generated ^{Allo}esoT cells were collected from feeder-free serum-free off-the-shelf TCR-engineered T cell generation culture. ^{Allo}esoT cells were mixed with ESOp/PBMCs (at 1:3 or 1:5 ratios) and cultured in C10 medium for 7 days. On day 2, recombinant human IL-7 (10 ng/ml) and IL-15 (10 ng/ml) were added to the cell culture. ^{Allo}esoT cells were allowed to expand for 7-14 days, then were aliquoted and frozen in liquid nitrogen storage tanks. For mechanistic and efficacy studies, esoT cells were thawed from frozen stock before use.

Cell phenotype and function assay.

Cells analyzed for functionality and phenotype included ^{Allo}esoT cells and ^{U}esoT cells, as well as T cells derived from PBMCs and transduced with esoTCR (denoted as PBMC esoT cells). To study cell phenotype, flow cytometry was used to detect cell surface markers including co-receptors (CD4 and CD8), memory T cell markers (CD45RO, CD45RA, CD25, CD69, CD62L), checkpoint inhibitors (PD-1, CTLA-4) and homing markers (CCR4, CCR5, and CXCR3). Cytokines (IFN-γ, TNF-α and IL-2) and cytotoxic factors (perforin and granzyme B) produced by studied cells were quantified using a Cell Fixation/Permeabilization Kit (BD Biosciences).

To study ^{Allo}esoT cell response to antigen stimulation, cells were cultured *in vitro* in C10 medium for 7 days. On day 0, ESOp (5uM/well) was added to half of the cells, and the other half served as a non-ESOp control. Regular cell counting and flow cytometry were used to assess

proliferation of ^{Allo}esoT cells. Cell culture supernatants were collected on day 1 to record and evaluate cytokine production via ELISA analysis (human IFN-γ, TNF-α, IL-2, IL-4, IL-10 and IL-17a).

Enzyme-Linked Immunosorbent Cytokine Assays (ELISA).

ELISAs for detecting human cytokines were performed following the standard protocol from BD Biosciences. Capture and biotinylated antibody pairs for detecting human IFN-g, IL-4, and IL-17 were purchased from BD Biosciences. Human IFN-g, IL-4 and IL-17 standards were purchased from eBioscience. The streptavidin-HRP conjugate used was purchased from Invitrogen. The tetramethylbenzidine (TMB) substrate was purchased from KPL. Co-culture assay supernatants were collected and assayed to measure the presence of IFN-γ, TNF-α, IL-2, IL-4, IL-10 and IL-17a cytokines. Samples were analyzed for absorbance at 450 nm using an Infinite M1000 microplate reader (Tecan).

***In vitro* tumor killing assay.**

A375-Fluc, PC3-Fluc, A375-A2-ESO-FLuc, PC3-A2-ESO-FLuc, A375-B7-ESO-FLuc, PC3-B7-ESO-FLuc (5x 10^3 cells per well) were co-cultured with effector cells at certain ratios (generally 1:1 unless indicated otherwise) in Corning 96-well clear bottom black plates. Cells were cultured in C10 medium for 24-72 hours. After culturing, D-luciferin (150 µg/ml) (Caliper Life Science) was added to cell cultures to detect live tumor cells and an Infinite M1000 microplate reader (Tecan) was used to measure luciferase activity in accordance to the manufacturer's instructions. In tumor cell assays involving blocking, 10 ug/ml of LEAF^{TM} purified anti-human NKG2D (Clone 1D11, Biolegend), anti-human DNAM-1 antibody (Clone 11A8, Biolegend), or

LEAF™ purified mouse lgG1bk isotype control antibody (Clone MG2B-57, Biolegend) was added to the effector/tumor cell coculture.

***In vitro* Mixed Lymphocyte Reaction (MLR) assay.**

To test GvH response, PBMCs from different donors were irradiated with 2500 rads, seeded in 96-well plates (5 x 10^5 cells/well) in C10 medium, and co-cultured with ^{Allo}esoT, ^{U}esoT (2 x 10^4 cells/well) cells. To test HvG response, PBMCs from different donors were seeded in 96-well plates (2 x 10^4 cells/well) in C10 medium, and co-cultured with irradiated ^{Allo}esoT and ^{U}esoT cells (2500 rads, 5 x 10^5 cells/well). Four days after seeding, cell culture supernatants were collected and IFN-γ was measured via ELISA. To test NK killing resistance, PBMC-NK were seeded into 96-well plates (2 x 10^4 cells/well) in C10 medium, and co-cultured with ^{Allo}esoT or ^{U}esoT (2 x 10^4 cells/well) cells. Cells were counted on indicated days using flow cytometry.

***In vivo* anti-tumor efficacy assay.**

Human melanoma xenograft NSG mice (6-10 weeks of age) were inoculated with 1 x 10^6 A375-A2-ESO-Fluc cells subcutaneously on day 0 and allowed to grow solid tumors over the course of 5-6 weeks. Three days post-tumor inoculation, experimental mice received 100 rads of total body irradiation followed by i.v. injection of vehicle (PBS), 1 x 10^7 ^{Allo}esoT cells, or 1 x 10^7 PBMC-esoT cells (isolated from health donor PBMCs using NK isolation beads). Tumor loads in experimental animals were monitored twice a week starting from day 2 by measuring total body luminescence using BLI (shown as TBL p/s), and by measuring tumor size using a Fisherbrand™ Traceable™ digital caliper (Thermo Fisher Scientific). Tumor size was calculated using W x L mm^2. At approximately week 6, mice were terminated for analysis. Solid tumors were retrieved

and weighed using a PA84 precision balance (Ohaus) and processed for flow cytometry analysis to determine the presence of tumor-infiltrating esoT cells (identified as hCD45+hCD3+V□13.1+ cells). Blood, spleen, and liver tissues were also collected and processed to detect tissue-residing esoT cells (identified as hCD45+V□13.1+ cells), following established flow cytometry protocols[7]. Cell surface expression of checkpoint inhibitor PD-1 and intracellular expression of TNFa, IL-2, IFNg, perforin, and granzyme B were measured using flow cytometry to quantify status of ^{Allo}esoT and PBMC-esoT cells.

Ganciclovir (GCV) *in vitro* and *in vivo* killing assay.

Expanded ^{Allo}esoT cells were cultured in C10 media with 10ng/ml IL-7 and 10ng/ml IL-15. On day 0, titrated amounts of GCV (0-50 mM) were added into the cell culture. On day 3, the suvival percentage of suicide gene sr39TK expressing ^{Allo}esoT was analyzed using microscopical cell counting and flow cytometry.

Electroporation.

$CD34^+$ cells were spun at 90 × g for 10 minutes, then resuspended in a 20 µl P3 solution (Lonza, Basel, Switzerland). 1ul gRNA (100 uM) and 4 ul Cas9 (6.5 mg/ml) were added to each sample per reaction. Cells were placed in a cuvette and electroporated using the Amaxa 4D Nucleofector X Unit (Lonza, Basel, Switzerland) following the ER-100 program. After electroporation, cells were kept at room temperature for 10 minutes before being transferred to a 24-well tissue culture treated plate. Cells were kept in the tissue culture plate overnight before the T cell differentiation culture.

Histopathologic analysis.

Liver, kidney, lung and spleen tissues were taken from all experimental mice. Tissue samples were fixed in 10% Neutral Buffered Formalin for up to 36 hours and embedded in paraffin for sectioning (3 μm thickness). After sectioning, tissues were stained either with Hematoxylin and Eosin or anti-human CD3 primary antibodies following standard procedures (UCLA Translational Pathology Core Laboratory, Los Angeles, CA). Stained sections were imaged using an Olympus BX51 upright microscope equipped with an Optronics Macrofire CCD camera (AU Optronics) at 20 x and 40 x magnifications. All images were analyzed using Optronics PictureFrame software (AU Optronics).

TCR repertoire single cell sequencing.

^{Allo}esoT cells ($CD45^+CD3^+V\square13.1^+$) and conventional PBMC-T cells ($CD45^+CD3^+$) were FACS-sorted. Single cell suspensions were sent to UCLA TCGB (Technology Center for Genomics and Bioinformatics) to perform single cell cDNA library and sequencing. TCR α and β CDR3 regions were analyzed by using 10X Genomics Chromium™ Controller Single Cell Sequencing System (10X Genomics) on the 2 x 150 cycle setting with 5,000 reads/cell.

RNA sequencing (RNA-seq) and data analysis.

MiRNeasy Mini Kit (QIAGEN) was used to isolate total RNA from ^{Allo}esoT, PBMC-Tαβ ($CD8^+$), PBMC-NK, and PBMC-Tγδ cells. All samples were chosen from 2-8 independent experiments from different donors. Nanodrop 2000 spectrophotometer (Thermal Scientific) was used to assess total RNA concentration. UCLA TCGB (Technology Center for Genomics and Bioinformatics) provided cDNA library construction and deep sequencing. Single-Read 50bp

sequencing was performed on Illumina Hiseq 3000. A total of 32 libraries were multiplexed and sequenced in 3 lanes. Raw sequence files were quality checked using Illumina's proprietary software.

Cell imaging by scanning electron microscope (SEM).

The SEM buffer with pH 7.4 was made by 0.1 M Na-phosphate buffer containing 0.1M Sucrose. The cells were rinsed with warm HBSS. Then they were fixed with warm 3% glutaraldehyde in the SEM buffer, moved to 4 degrees, and stored overnight. The next day the cells were washed with SEM buffer 2 times with 5 minutes each time. Next, they were fixed with 2% osmium tetroxide in SEM buffer on ice for 1 hour and then washed with SEM buffer 2 times with 5 minutes each time. The cells were dehydrated with 50%, 70%, 95%, 100%, 100% ethanol successively, 15 minutes each time: The final 100% ethanol was replaced with hexamethyldisilazane and then evaporated in the hood. The processed cells were then ready for Low-vacuum Scanning Electron Microscopy (LV-SEM) which was conducted on a FEI Nova Nano 230 SEM.

Statistics.

Statistical analysis used Graphpad Prism 8 software (Graphpad). Pairwise comparisons were made using a 2-tailed Student's T test. Multiple comparisons were performed using an ordinary 1-way ANOVA, followed by Tukey's multiple comparisons test. Kaplan- Meier survival curves were analyzed by log rank (Mantel-Cox) test adjusted for multiple comparisons. Data are presented as the mean ± SEM, unless otherwise indicated. In all figures and figure legends, ''n'' represents the number of samples or animals utilized in the indicated experiments. *P* values less

than 0.05 were considered significant. “ns” denotes not significant; * denotes $P < 0.05$; ** denotes $P < 0.01$; *** denotes $P < 0.001$; **** denotes $P < 0.0001$.

Data availability.

Data is available upon reasonable request from the corresponding author. RNA sequencing data collected for this study will be publicly available in the NCBI Gene Expression Omnibus upon the publication of this manuscript.

References for materials and methods

1. Giannoni, F. et al. Allelic exclusion and peripheral reconstitution by TCR transgenic T cells arising from transduced human hematopoietic stem/progenitor cells. *Molecular Therapy* **21**, 1044-1054 (2013).
2. Zakrzewski, J.L. et al. Tumor immunotherapy across MHC barriers using allogeneic T-cell precursors. *Nature biotechnology* **26**, 453-461 (2008).
3. Cartier, N. et al. Hematopoietic stem cell gene therapy with a lentiviral vector in X-linked adrenoleukodystrophy. *science* **326**, 818-823 (2009).
4. Robbins, P.F. et al. Single and dual amino acid substitutions in TCR CDRs can enhance antigen-specific T cell functions. *The Journal of Immunology* **180**, 6116-6131 (2008).
5. Bethune, M.T. et al. Isolation and characterization of NY-ESO-1–specific T cell receptors restricted on various MHC molecules. *Proceedings of the National Academy of Sciences* **115**, E10702-E10711 (2018).
6. Cooper, A.R. et al. Highly efficient large-scale lentiviral vector concentration by tandem tangential flow filtration. *Journal of virological methods* **177**, 1-9 (2011).
7. Smith, D.J. et al. Propagating humanized BLT mice for the study of human immunology and immunotherapy. *Stem cells and development* **25**, 1863-1873 (2016).

References for the main text

1. June, C.H. & Sadelain, M. Chimeric antigen receptor therapy. *New England Journal of Medicine* **379**, 64-73 (2018).
2. Labanieh, L., Majzner, R.G. & Mackall, C.L. Programming CAR-T cells to kill cancer. *Nature biomedical engineering* **2**, 377-391 (2018).
3. Mikkilineni, L. & Kochenderfer, J.N. Chimeric antigen receptor T-cell therapies for multiple myeloma. *Blood* **130**, 2594-2602 (2017).
4. Zhang, J. & Wang, L. The emerging world of TCR-T cell trials against cancer: a systematic review. *Technology in cancer research & treatment* **18**, 1533033819831068 (2019).
5. Liu, Y. et al. Chimeric STAR receptors using TCR machinery mediate robust responses against solid tumors. *Science Translational Medicine* **13** (2021).
6. Leko, V. & Rosenberg, S.A. Identifying and targeting human tumor antigens for T cell-based immunotherapy of solid tumors. *Cancer Cell* (2020).
7. Aftab, B.T. et al. Toward "off-the-shelf" allogeneic CAR T cells. *Advances in Cell and Gene Therapy* **3**, e86 (2020).
8. Lim, W.A. & June, C.H. The principles of engineering immune cells to treat cancer. *Cell* **168**, 724-740 (2017).
9. Gjerstorff, M.F., Andersen, M.H. & Ditzel, H.J. Oncogenic cancer/testis antigens: prime candidates for immunotherapy. *Oncotarget* **6**, 15772 (2015).
10. Bethune, M.T. et al. Isolation and characterization of NY-ESO-1–specific T cell receptors restricted on various MHC molecules. *Proceedings of the National Academy of Sciences* **115**, E10702-E10711 (2018).
11. Thomas, R. et al. NY-ESO-1 based immunotherapy of cancer: current perspectives. *Frontiers in immunology* **9**, 947 (2018).

12. Jain, R.K. et al. (American Society of Clinical Oncology, 2017).
13. Goydos, J.S., Patel, M. & Shih, W. NY-ESO-1 and CTp11 expression may correlate with the stage of progression in melanoma. *Journal of Surgical Research* **98**, 76-80 (2001).
14. Sharma, P. et al. Frequency of NY-ESO-1 and LAGE-1 expression in bladder cancer and evidence of a new NY-ESO-1 T-cell epitope in a patient with bladder cancer. *Cancer Immunity Archive* **3** (2003).
15. Aung, P.P. et al. Expression of New York esophageal squamous cell carcinoma-1 in primary and metastatic melanoma. *Human pathology* **45**, 259-267 (2014).
16. Raza, A. et al. Unleashing the immune response to NY-ESO-1 cancer testis antigen as a potential target for cancer immunotherapy. *Journal of translational medicine* **18**, 1-11 (2020).
17. Ademuyiwa, F.O. et al. NY-ESO-1 cancer testis antigen demonstrates high immunogenicity in triple negative breast cancer. *PloS one* **7**, e38783 (2012).
18. Zhao, R.Y. et al. A novel HLA-B18 restricted CD8+ T cell epitope is efficiently cross-presented by dendritic cells from soluble tumor antigen. (2012).
19. Robbins, P.F. et al. Tumor regression in patients with metastatic synovial cell sarcoma and melanoma using genetically engineered lymphocytes reactive with NY-ESO-1. *Journal of Clinical Oncology* **29**, 917 (2011).
20. Rapoport, A.P. et al. NY-ESO-1–specific TCR–engineered T cells mediate sustained antigen-specific antitumor effects in myeloma. *Nature medicine* **21**, 914-921 (2015).
21. Seet, C.S. et al. Generation of mature T cells from human hematopoietic stem and progenitor cells in artificial thymic organoids. *Nature methods* **14**, 521-530 (2017).
22. Shukla, S. et al. Progenitor T-cell differentiation from hematopoietic stem cells using Delta-like-4 and VCAM-1. *Nature Methods* **14**, 531-538 (2017).
23. Iriguchi, S. et al. A clinically applicable and scalable method to regenerate T-cells from iPSCs for off-the-shelf T-cell immunotherapy. *Nature Communications* **12**, 1-15 (2021).
24. Huijskens, M.J. et al. Technical Advance: Ascorbic acid induces development of double-positive T cells from human hematopoietic stem cells in the absence of stromal cells. *Journal of leukocyte biology* **96**, 1165-1175 (2014).
25. Themeli, M. et al. Generation of tumor-targeted human T lymphocytes from induced pluripotent stem cells for cancer therapy. *Nature biotechnology* **31**, 928-933 (2013).
26. La Motte-Mohs, R.N., Herer, E. & Zúñiga-Pflücker, J.C. Induction of T-cell development from human cord blood hematopoietic stem cells by Delta-like 1 in vitro. *Blood* **105**, 1431-1439 (2005).
27. Reimann, C. et al. Human T-Lymphoid Progenitors Generated in a Feeder-Cell-Free Delta-Like-4 Culture System Promote T-Cell Reconstitution in NOD/SCID/γc−/− Mice. *Stem Cells* **30**, 1771-1780 (2012).
28. Ellmeier, W., Sawada, S. & Littman, D.R. The regulation of CD4 and CD8 coreceptor gene expression during T cell development. *Annual review of immunology* **17**, 523-554 (1999).
29. Koch, U. & Radtke, F. Mechanisms of T cell development and transformation. *Annual review of cell and developmental biology* **27**, 539-562 (2011).
30. Giannoni, F. et al. Allelic exclusion and peripheral reconstitution by TCR transgenic T cells arising from transduced human hematopoietic stem/progenitor cells. *Molecular Therapy* **21**, 1044-1054 (2013).

31. Zhu, Y. et al. Development of hematopoietic stem cell-engineered invariant natural killer T cell therapy for cancer. *Cell stem cell* **25**, 542-557. e549 (2019).
32. Alonzo, E.S. & Sant'Angelo, D.B. Development of PLZF-expressing innate T cells. *Current opinion in immunology* **23**, 220-227 (2011).
33. Zhang, Y., Zhang, Y., Gu, W. & Sun, B. TH1/TH2 cell differentiation and molecular signals. *T Helper Cell Differentiation and Their Function*, 15-44 (2014).
34. Gagliani, N. & Huber, S. Basic aspects of T helper cell differentiation. *T-Cell Differentiation*, 19-30 (2017).
35. Ozdemir, Z.N. & Bozdağ, S.C. Graft failure after allogeneic hematopoietic stem cell transplantation. *Transfusion and Apheresis Science* **57**, 163-167 (2018).
36. Franciszkiewicz, K., Boissonnas, A., Boutet, M., Combadière, C. & Mami-Chouaib, F. Role of chemokines and chemokine receptors in shaping the effector phase of the antitumor immune response. *Cancer research* **72**, 6325-6332 (2012).
37. Fujii, S.-i. et al. NKT cells as an ideal antitumor immunotherapeutic. *Frontiers in immunology* **4**, 409 (2013).
38. Perez, C., Gruber, I. & Arber, C. Off-the-Shelf Allogeneic T Cell Therapies for Cancer: Opportunities and Challenges Using Naturally Occurring "Universal" Donor T Cells. *Frontiers in Immunology* **11** (2020).
39. Depil, S., Duchateau, P., Grupp, S., Mufti, G. & Poirot, L. 'Off-the-shelf'allogeneic CAR T cells: development and challenges. *Nature Reviews Drug Discovery* **19**, 185-199 (2020).
40. Ren, J. et al. Multiplex genome editing to generate universal CAR T cells resistant to PD1 inhibition. *Clinical cancer research* **23**, 2255-2266 (2017).
41. Steimle, V., Siegrist, C.-A., Mottet, A., Lisowska-Grospierre, B. & Mach, B. Regulation of MHC class II expression by interferon-gamma mediated by the transactivator gene CIITA. *Science* **265**, 106-109 (1994).
42. Abrahimi, P. et al. Efficient gene disruption in cultured primary human endothelial cells by CRISPR/Cas9. *Circulation research* **117**, 121-128 (2015).
43. Lanier, L.L. NK cell recognition. *Annu. Rev. Immunol.* **23**, 225-274 (2005).
44. Gornalusse, G.G. et al. HLA-E-expressing pluripotent stem cells escape allogeneic responses and lysis by NK cells. *Nature biotechnology* **35**, 765 (2017).
45. Majzner, R.G. & Mackall, C.L. Tumor antigen escape from CAR T-cell therapy. *Cancer discovery* **8**, 1219-1226 (2018).
46. Gnjatic, S. et al. NY-ESO-1: review of an immunogenic tumor antigen. *Advances in cancer research* **95**, 1-30 (2006).
47. Klippel, Z.K. et al. Immune escape from NY-ESO-1-specific T-cell therapy via loss of heterozygosity in the MHC. *Gene therapy* **21**, 337-342 (2014).
48. Li, Y., Hermanson, D.L., Moriarity, B.S. & Kaufman, D.S. Human iPSC-derived natural killer cells engineered with chimeric antigen receptors enhance antitumor activity. *Cell stem cell* **23**, 181-192. e185 (2018).
49. Basar, R., Daher, M. & Rezvani, K. Next-generation cell therapies: The emerging role of CAR-NK cells. *Hematology 2014, the American Society of Hematology Education Program Book* **2020**, 570-578 (2020).
50. Lanza, R., Russell, D.W. & Nagy, A. Engineering universal cells that evade immune detection. *Nature Reviews Immunology* **19**, 723-733 (2019).
51. Benjamin, R. et al. Preliminary data on safety, cellular kinetics and anti-leukemic activity of UCART19, an allogeneic anti-CD19 CAR T-cell product, in a pool of adult and pediatric

patients with high-risk CD19+ relapsed/refractory B-cell acute lymphoblastic leukemia. *Blood* **132**, 896-896 (2018).
52. Benjamin, R. et al. Genome-edited, donor-derived allogeneic anti-CD19 chimeric antigen receptor T cells in paediatric and adult B-cell acute lymphoblastic leukaemia: results of two phase 1 studies. *The Lancet* **396**, 1885-1894 (2020).
53. Qasim, W. et al. Molecular remission of infant B-ALL after infusion of universal TALEN gene-edited CAR T cells. *Science translational medicine* **9** (2017).
54. Stadtmauer, E.A. et al. CRISPR-engineered T cells in patients with refractory cancer. *Science* **367** (2020).
55. Vizcardo, R. et al. Regeneration of human tumor antigen-specific T cells from iPSCs derived from mature CD8+ T cells. *Cell stem cell* **12**, 31-36 (2013).
56. Nishimura, T. et al. Generation of rejuvenated antigen-specific T cells by reprogramming to pluripotency and redifferentiation. *Cell stem cell* **12**, 114-126 (2013).
57. Smith, D.J. et al. Genetic engineering of hematopoietic stem cells to generate invariant natural killer T cells. *Proceedings of the National Academy of Sciences* **112**, 1523-1528 (2015).
58. González-Galarza, F.F. et al. Allele frequency net 2015 update: new features for HLA epitopes, KIR and disease and HLA adverse drug reaction associations. *Nucleic acids research* **43**, D784-D788 (2015).
59. Sette, A. & Sidney, J. Nine major HLA class I supertypes account for the vast preponderance of HLA-A and-B polymorphism. *Immunogenetics* **50**, 201-212 (1999).
60. Brudno, J.N. et al. T cells genetically modified to express an anti–B-cell maturation antigen chimeric antigen receptor cause remissions of poor-prognosis relapsed multiple myeloma. *Journal of Clinical Oncology* **36**, 2267 (2018).

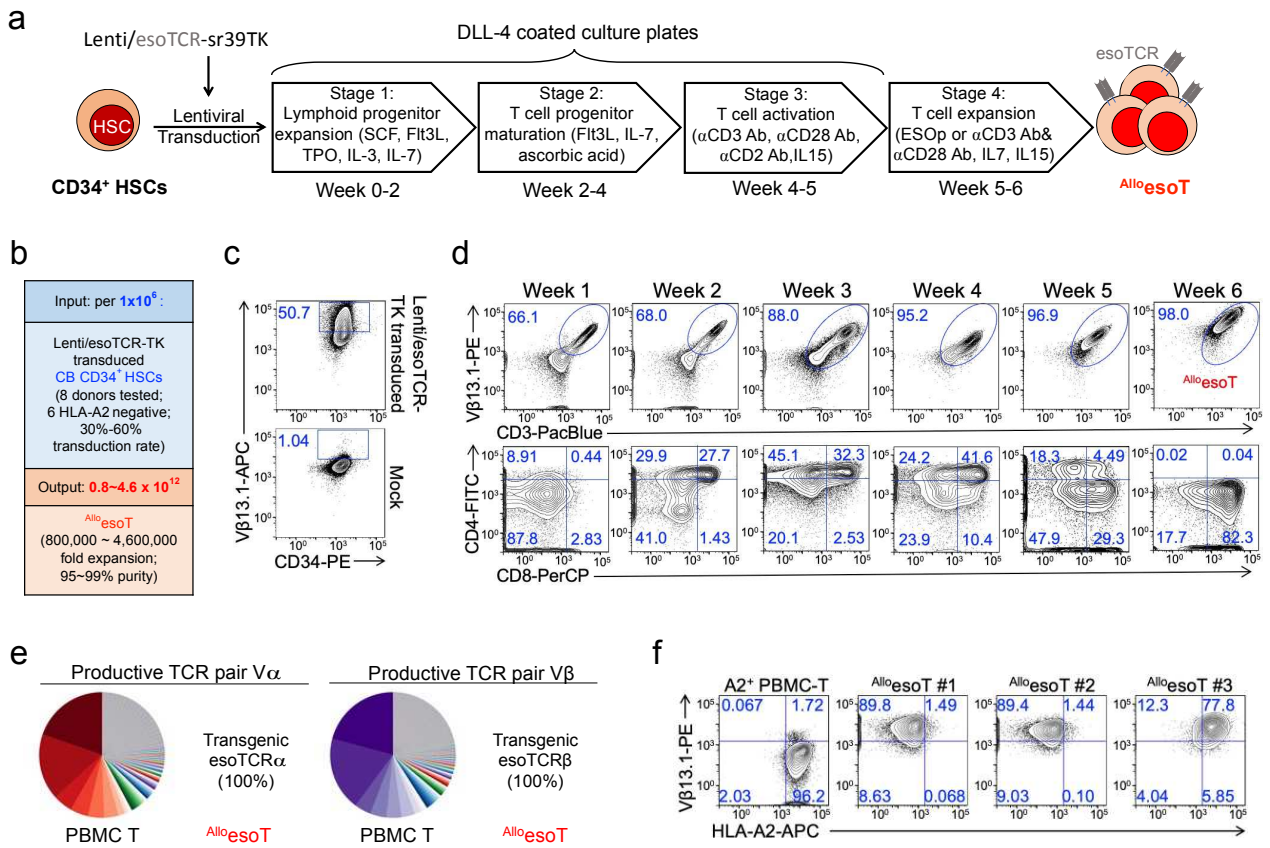

Figure 1. *In vitro* generation and gene profiling of off-the-shelf allogenic HSC-engineered NY-ESO-1-specifc T (^{Allo}esoT) cells.

(a) Schematic design to generate ^{Allo}esoT cells in *in vitro* off-the-shelf HSC-based TCR-engineered T cell generation system.

(b) FACS detection of intracellular expression of HLA-A*02:01–NY-ESO-$1_{157–165}$-specific TCR (identified as Vβ13.1$^+$) in CD34$^+$ HSC cells 72h post lentivector transduction.

(c) Representative kinetics of ^{Allo}esoT cell development and differentiation from CD34$^+$ HSCs at the indicated weeks. ^{Allo}esoT cells were gated as Vβ13.1$^+$CD3$^+$.

(d) Yield of ^{Allo}esoT cells from 8 different CB donors.

(e) Single cell RNA sequencing Analysis of TCR Vα and Vβ CDR3 VDJ sequences of ^{Allo}esoT, and conventional αβ T (PBMC-T) cells. The relative abundance of each unique T cell receptor sequence among the total unique sequences identified for the sample is represented by a pie slice.

(f) TCR-engineered T cell generation in the off-the-shelf HSC-based system is independent of matching MHC expression for positive selection. Generation of ^{Allo}esoT cells with HLA-A2$^-$ CB HSC donors.

Representative of 5 (b), 10 (c), 3 (f) experiments. See also supplementary figure 1.

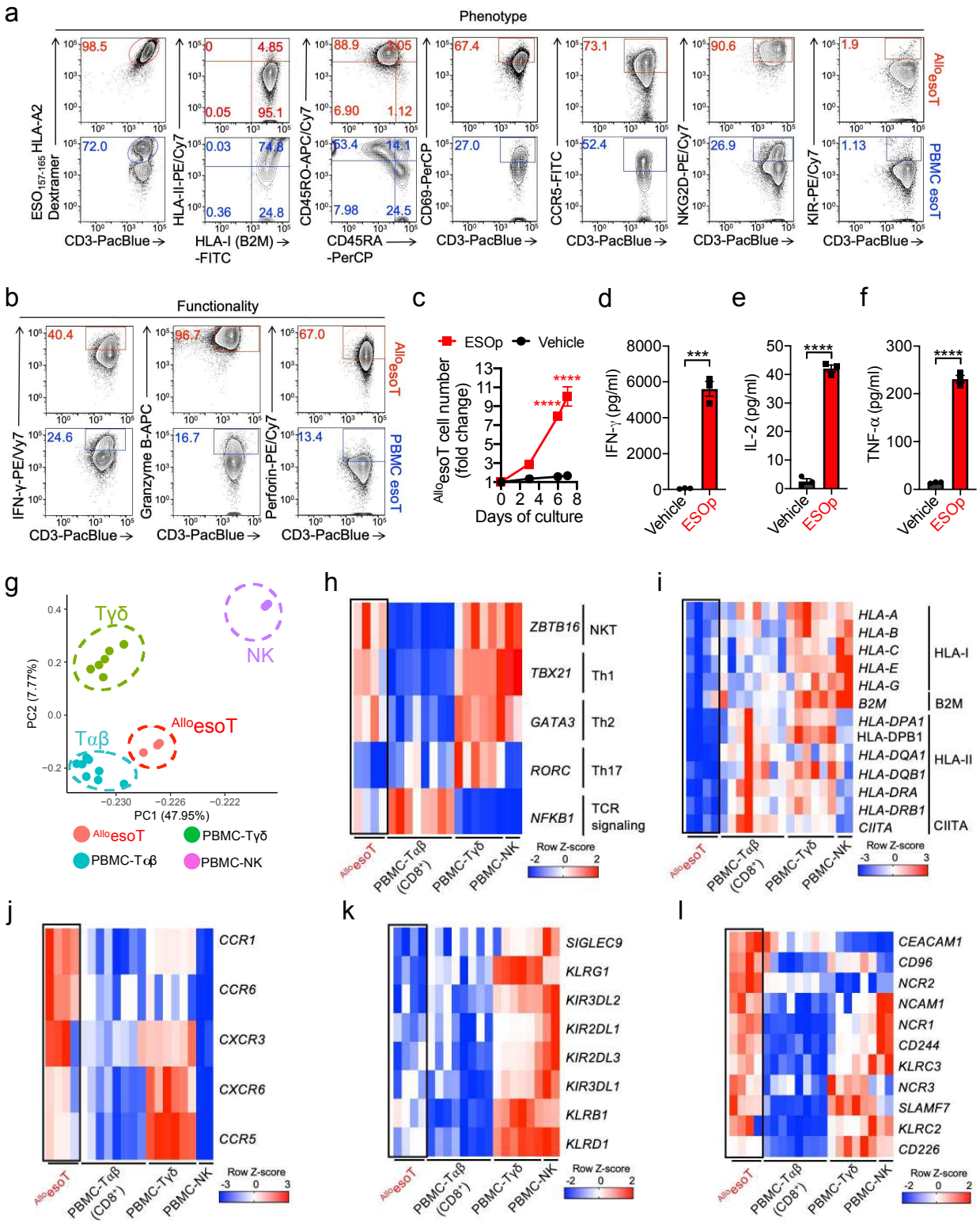

Figure 2. Phenotype and gene profiling of AlloesoT cells.

Figure 2. Phenotype and gene profiling of ^{Allo}esoT cells.

(a) Characterization of ^{Allo}esoT. FACS plots showing the expression of surface markers on ^{Allo}esoT cells (identified as Vβ13.1^{+} CD3^{+}) compared to PBMC-esoT cells (identified as Vβ13.1^{+} CD3^{+}).

(b) Functionality of ^{Allo}esoT. FACS plots showing the intracellular staining of cytokines and cytotoxic molecules from ^{Allo}esoT cells (identified as Vβ13.1^{+} CD3^{+}) compared to PBMC-esoT cells (identified as Vβ13.1^{+} CD3^{+}).

(c-f) Antigen responses of ^{Allo}esoT cells. ^{Allo}esoT cells were expanded in the presence or absence of NY-ESO-1$_{157-165}$ peptide (ESOp) for 7 days. (c) Growth curve of ^{Allo}esoT expansion over time (n=3). (d-f) Cytokine production of ^{Allo}esoT cells measure through ELISA responding to αGC stimulation.

(g-l) Gene profiling of ^{Allo}esoT cells. (g) Principal component analysis of gene expression for five cell types. Each symbol shape represents an individual biological replicate for the corresponding cell type. Shown is the ordination using the first two principal components PC1 and PC2. (h-l) Hierarchical clustering of selected gene expression profiles related to transcription factors (h), HLA (i), chemokines (j), NK activating receptors (k), and NK inhibitory receptors (l). Levels of mRNA expression were determined using RNA sequencing. Heatmaps show the differential expression of genes across samples. Red and blue indicate increased and decreased expressions, respectively.

Representative of 4 (a-b), 3 (c-f) experiments. See also supplementary figure 2.

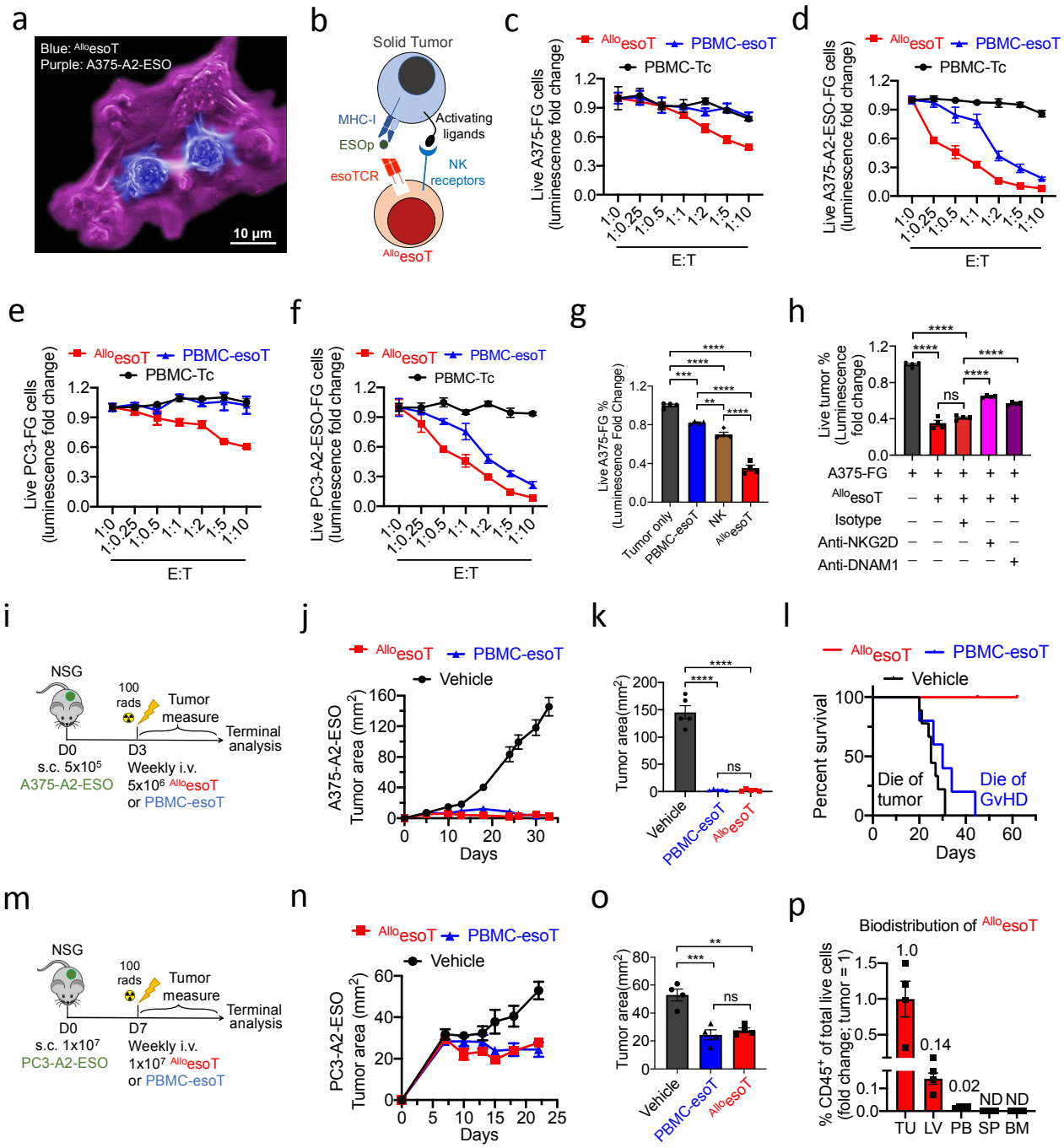

Figure 3. Anti-tumor capacity of AlloesoT

Figure 3. Anti-tumor capacity of ^{Allo}esoT

(a) Scanning electron microscope (SEM) image of ^{Allo}esoT attacking A375-A2-ESO cells *in vitro*.

(b-h) Studying the tumor killing of ^{Allo}esoT cells against multiple solid tumor cell lines compared to PBMC-esoT cells. (b) Schematic showing the TCR/NK-mediated tumor killing mechanisms of ^{Allo}esoT cells against HLA-A2 and NYESO-1 positive solid tumors. (c-d) Luciferase activity analysis of *in vitro* tumor killing of A375-FG and A375-A2-ESO-FG (n=4). E:T, effector/target ratio. (e-f) ^{Allo}esoT tumor killing against PC3-FG and PC3-A2-ESO-FG (n=4). E:T, effector/target ratio. (g-h) A2/ESO independent tumor killing of ^{Allo}esoT cells tumor killing (g) Tumor killing of A375-FG by ^{Allo}esoT cells (h) Tumor killing mechanisms of ^{Allo}esoT cells. NKG2D and DNAM-1 mediated NK pathways were studied. Tumor cell killing was analyzed at 24-hours post co-culture.

(i-l) Studying *in vivo* anti-tumor efficacy of ^{Allo}esoT cells against solid tumor in a human melanoma (A375-A2-ESO) xenograft mouse model. (i) Experimental design. (j) Measurement of tumor size over time (n=4). (k) Tumor measurement comparison at day 33 (n=4). (l) Kaplan-Meier analysis of mouse survival rate (n=7 or 8).

(m-p) Studying *in vivo* anti-tumor efficacy of ^{Allo}esoT cells with solid tumor with large tumor burden. A human prostate cancer cell line (PC3-A2-ESO) xenograft mouse model was adopted. (m) Experimental design. (n) Measurement of tumor size over time (n=4). (o) Tumor measurement comparison at day 27 (n=4). (p) Biodistribution of ^{Allo}esoT quantified by terminal FACS analysis. TU=tumor, LV=liver, PB=peripheral blood, SP=spleen, BM=bone marrow.

Representative of 3 experiments. See also supplementary figure 3 and 4. Data are presented as the mean ± SEM. ns, not significant, *P<0.05, **P<0.01, **P<0.001, ****P<0.0001, by by One-way ANOVA (g, h, k and o), or by log rank (Mantel-Cox) test adjusted for multiple comparisons (l).

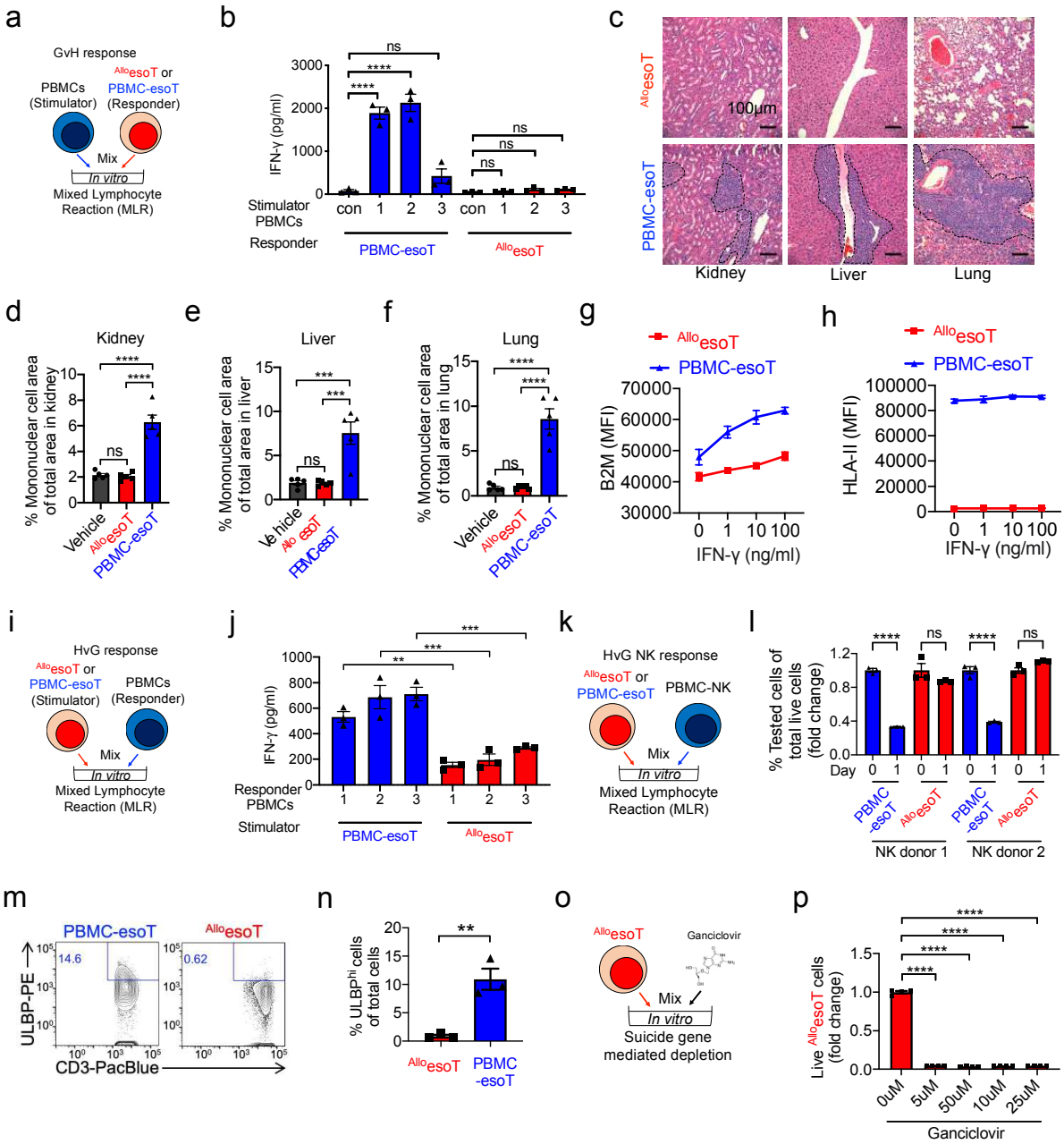

Figure 4. Safety and immunogenicity study of AlloesoT cells.

Figure 4. Safety and immunogenicity study of ^{Allo}esoT cells.
(a-b) An *in vitro* mixed lymphocyte reaction (MLR) assay for the study of GvH responses of ^{Allo}esoT cells in comparison of conventional PBMC-esoT cells. (a) Experimental design. (b) ELISA analysis of IFN-γ in the supernatants of MLR assay (n=3), showing no GvH response induced by ^{Allo}esoT cells. PBMCs from 3 different healthy donors were included as stimulators.
(c-f) An *in vivo* GvH response study with a human A375-A2-ESO xenograft mouse model treated with ^{Allo}esoT or PBMC-esoT cells. (c-f) Histology analysis of tissue sections from experimental mice post corresponding effector cell treatment. (c) Representative H&E staining images from various tissues. The area with heavy mononuclear cell infiltration was highlighted with black dash line. (d-f) Quantification of (c).
(g-h) *In vitro* HLA-I (B2M) and HLA-II expression on indicated cells in response to IFN-γ coculture.
(i-j) An *in vitro* mixed lymphocyte reaction (MLR) assay for host-versus-graft (HvG) responses of ^{Allo}esoT cells compared to PBMC-esoT cells. (i) Experimental design. (j) ELISA analysis of IFN-γ in the supernatants of MLR assay (n=3), showing less HvG response induced by ^{Allo}esoT cells. PBMCs from 3 different healthy donors were included as responders.
(k-n) Studying allogenic NK cell response against ^{Allo}esoT cells using an in vitro MLR assay. ^{Allo}esoT cells were co-cultured with donor-mismatched PBMC-NK cells. PBMC-esoT cells were included as controls. (k) Experimental design. (l) Quantification of FACS analyses of the indicated cells at day 0 and 1 (n=3). (m) Representative FACS plots of ULBP expression on the indicated cells. (n) quantification of (m). (o-p) Functional test of suicide gene sr39TK as an additional safety mechanism. (o) Experimental design of the *in vitro* ganciclovir killing assay. ^{Allo}esoT cells were cultured in vitro in the presence of gradient concentrations of GCV for 3 days. (p) Quantification of live cells via FACS analysis at day 3 (n=4).

Representative of 2 (c-f), 3 (a-b, g-p) experiments. Data are presented as the mean ± SEM. ns, not significant, *p<0.05, **p<0.01, **p<0.001, ****p<0.0001, by 1-way ANOVA (b, d-f, j, l and p), by Student's *t* test (n).

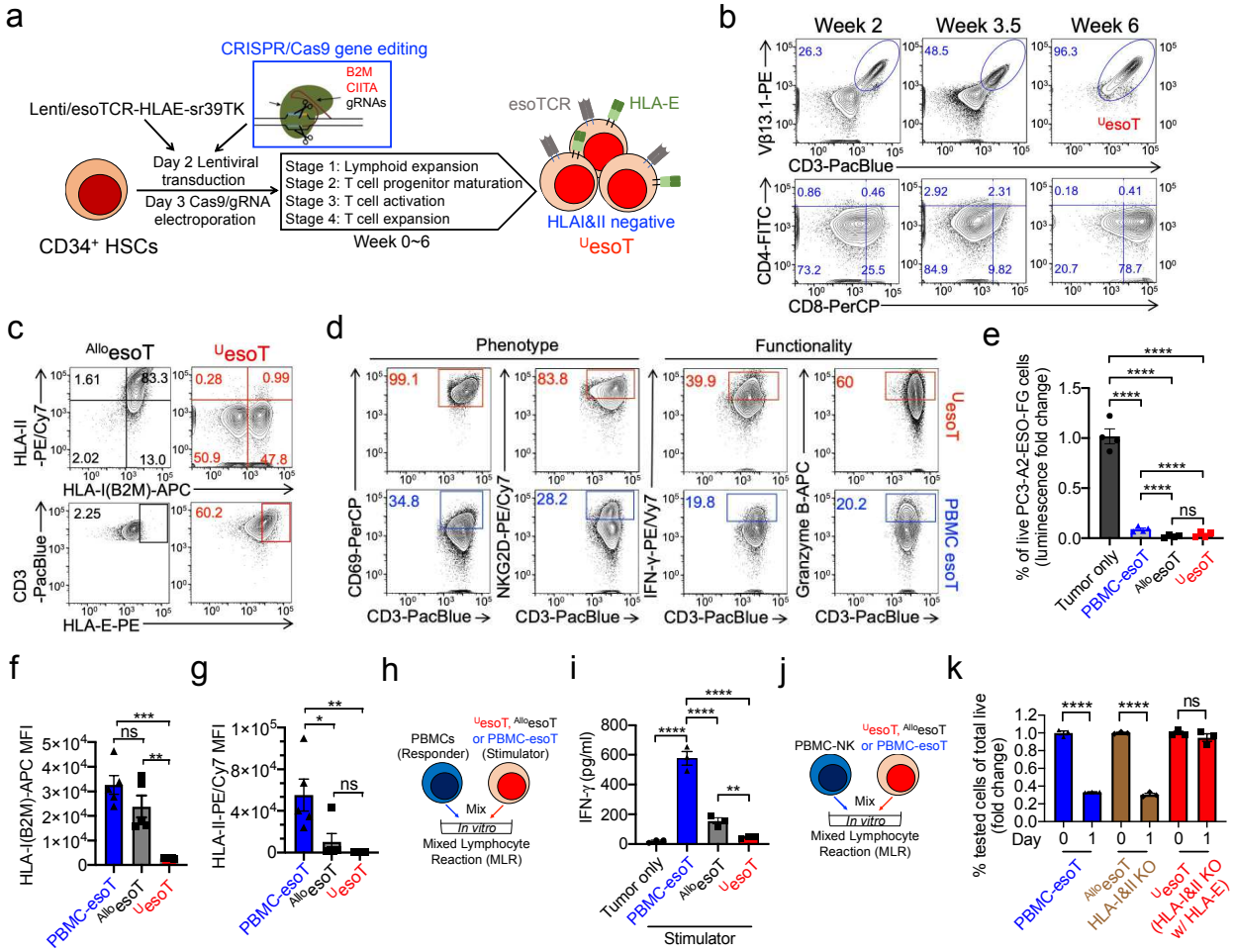

Figure 5. The generation of HLA-ablated universal esoT (ᵁesoT) cells

(a) Schematic design to generate HLA-I/II-reduced universal HSC-engineered NY-ESO-1-specific T (ᵁesoT) cells in off-the-shelf HSC-based TCR-engineered T cell generation system.

(b) Kinetics of ᵁesoT cells development and differentiation from CD34⁺ HSCs at the indicated week. ᵁesoT cells were gated as Vβ13.1⁺CD3⁺.

(c) FACS plots showing the HLA-I&II expression of ᵁesoT in comparison with ᴬˡˡᵒesoT.

(d) Characterization of ᵁesoT. FACS plots showing the expression of surface markers, intracellular cytokines, and cytotoxic molecules from ᵁesoT cells (identified as Vβ13.1⁺ CD3⁺) compared to PBMC-esoT cells (identified as Vβ13.1⁺ CD3⁺).

(e) Studying the NY-ESO-1-specific killing of PC3-A2-ESO-Fluc by ᵁesoT cells compared to ᴬˡˡᵒesoT cells and PBMC-esoT cells (n=4).

(f-g) Quantification of reduced HLA-I (f) and HLA-II (g) expression on ᵁesoT cells compared to ᴬˡˡᵒesoT and PBMC-esoT (n=5).

(h-i) HvG response study of ᵁesoT cells. (h) Experimental design. (i) ELISA analysis of IFN-γ in the supernatants of MLR assay (n=3), showing reduced HvG response induced by ᵁesoT cells. PBMCs from 2 different healthy donors were included as stimulators, data with the 2nd PBMC donor shown in the supplementary figure 5.

(j-k) Studying *in vitro* allogenic NK cell response against ᵁesoT (HLA-E overexpressing), ᴬˡˡᵒesoT DKO cells without HLA-E overexpression and PBMC-esoT cells. (j) Experimental design. (k) Quantification of FACS analyses of the indicated cells at day 0 and 1 (n=3).

Representative of 3 experiments. See also supplementary figure 5. Data are presented as the mean ± SEM. ns, not significant, *P<0.05, **P<0.01, **P<0.001, ****P<0.0001, by 1-way ANOVA (e, f-g, I, and k).

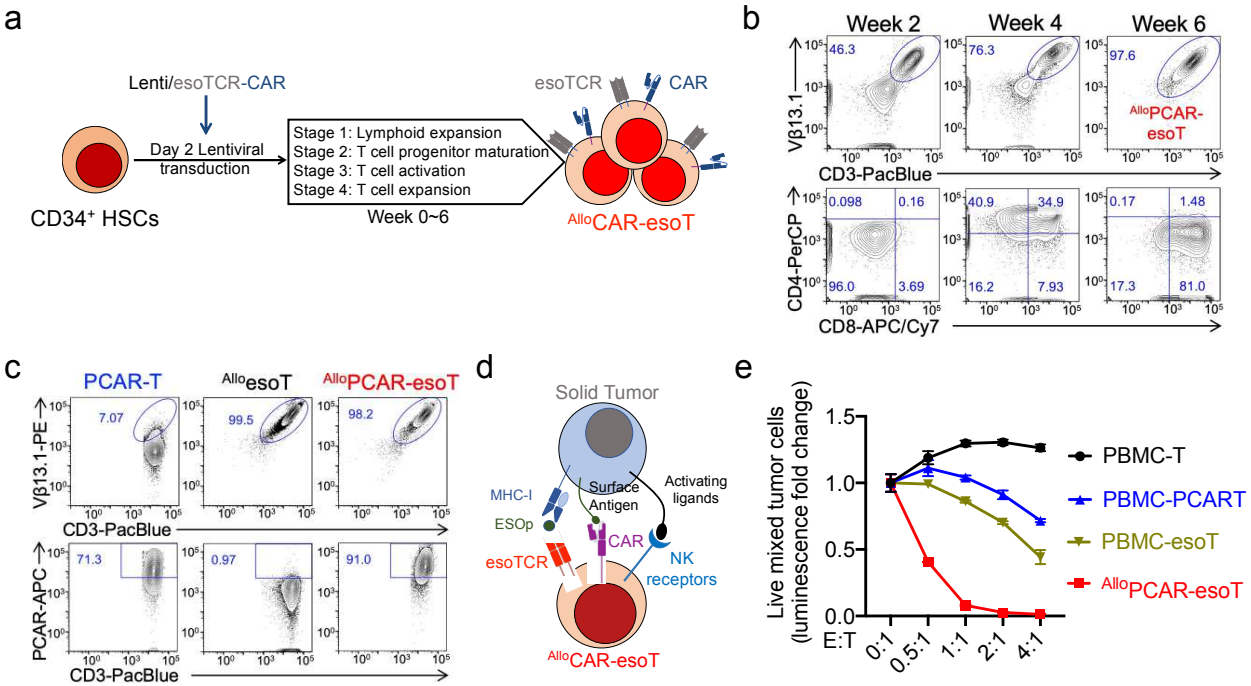

Figure 6. The generation of CAR-armed esoT (^{Allo}CAR-esoT) cells

(a) Schematic design to generate CAR-armed HSC-engineered NY-ESO-1-specific T (^{Allo}CAR-esoT) cells in off-the-shelf HSC-based TCR-engineered T cell generation system.

(b) Kinetics of ^{Allo}PCAR-esoT cells development and differentiation from CD34^{+} HSCs at the indicated week. ^{U}esoT cells were gated as Vβ13.1^{+}CD3^{+}.

(c) Flow plots showing the CAR and esoTCR expression of ^{Allo}esoT and ^{Allo}PCAR-esoT in comparison to PBMC derived conventional PCAR T (PBMC-PCART) cells.

(d-e) Studying the solid tumor killing by ^{Allo}PCAR-esoT cells. (d) Schematic showing the TCR/CAR/NK-mediated triple tumor killing mechanisms performed by ^{Allo}PCAR-esoT cells. (e) Tumor killing titration of various effector cells against a mixed tumor population of PC3-FG, PC3-PSMA-FG, PC3-A2-ESO-FG, and PC3-A2-ESO-PSMA-FG with a ratio of 1:1:1:1 (n=4) (E:T = effector : tumor).

Representative of 3 experiments. See also supplementary figure 6. Data are presented as the mean ± SEM.

a

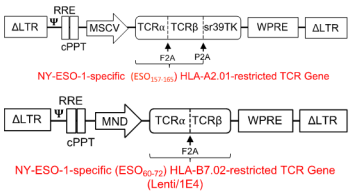

b

Viral titer on HEK-293T-hCD3 cells	
Vector \ Titer	Titer (IFU/mL)
Lenti/1G4-TK	1.256×10^8
Lenti/1E4	1.482×10^8

c

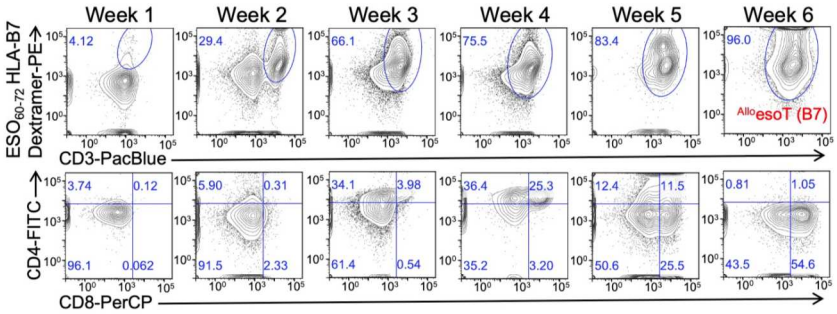

d

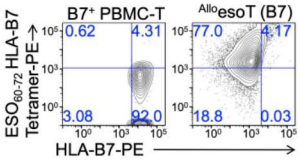

Supplementary figure 1. The generation of off-the-shelf allogenic HSC-engineered NY-ESO-1-specifc T (^{Allo}esoT) cells; related to figure 1.

(a) Design of the Lentiviral vector carrying two version of NY-ESO-1-specifc TCR. HLA-A2*01-NY-ESO-$1_{157-165}$-specific clone is denoted as 1G4, HLA-B7*02-NY-ESO-1_{60-72}-specific clone is denoted as 1E4.

(b) Representative titer of lentivirus packaged with indicated vectors.

(c) Representative kinetics of ^{Allo}esoT(B7) cell development and differentiation from $CD34^+$ HSCs at the indicated weeks. ^{Allo}esoT(B7) cells were gated as ESO_{60-72}HLA-B7 $Tetramer^+$ $CD3^+$.

(d) Generation of ^{Allo}esoT(B7) cells with HLA-$B7^-$ CB HSC donor.

Representative of 3 experiments.

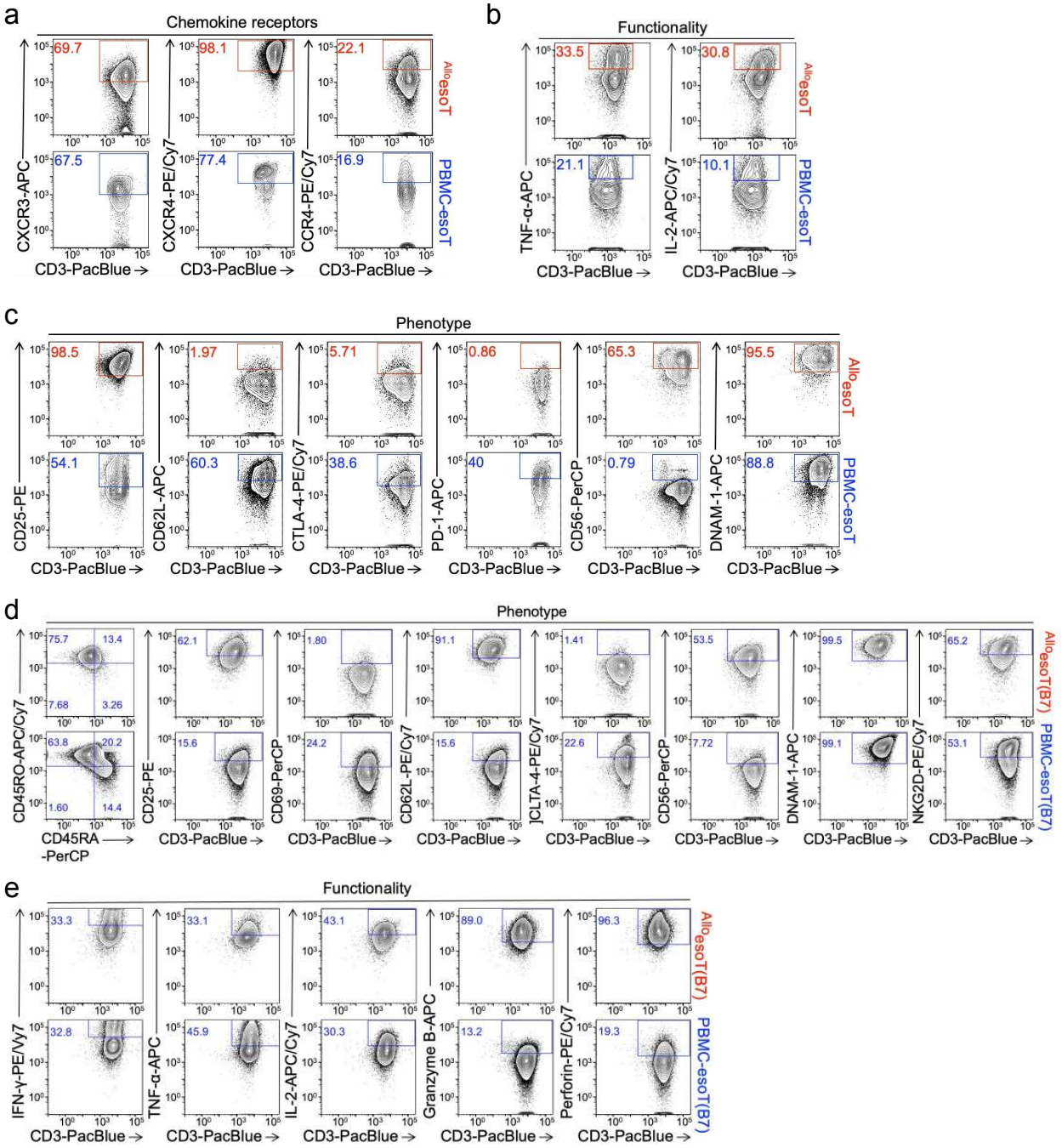

Supplementary figure 2. Characterization of ^{Allo}esoT and ^{Allo}esoT(B7); related to figure 2.
(a-c) Characterization of ^{Allo}esoT. FACS plots showing the expression of chemokine receptors (a), intracellular cytokines (b), and surface markers (c) from ^{Allo}esoT cells (identified as Vβ13.1$^+$ CD3$^+$) compared to PBMC-esoT cells (identified as Vβ13.1$^+$ CD3$^+$).
(d-e) Characterization of ^{Allo}esoT(B7). FACS plots showing the expression of surface markers (D), intracellular cytokines, and cytotoxic molecules (e) from ^{Allo}esoT(B7) cells (identified as ESO_{60-72}HLA-B7 Tetramer$^+$ CD3$^+$) compared to PBMC esoT(B7) cells (identified as ESO_{60-72}HLA-B7 Tetramer$^+$ CD3$^+$).

Representative of 3 experiments.

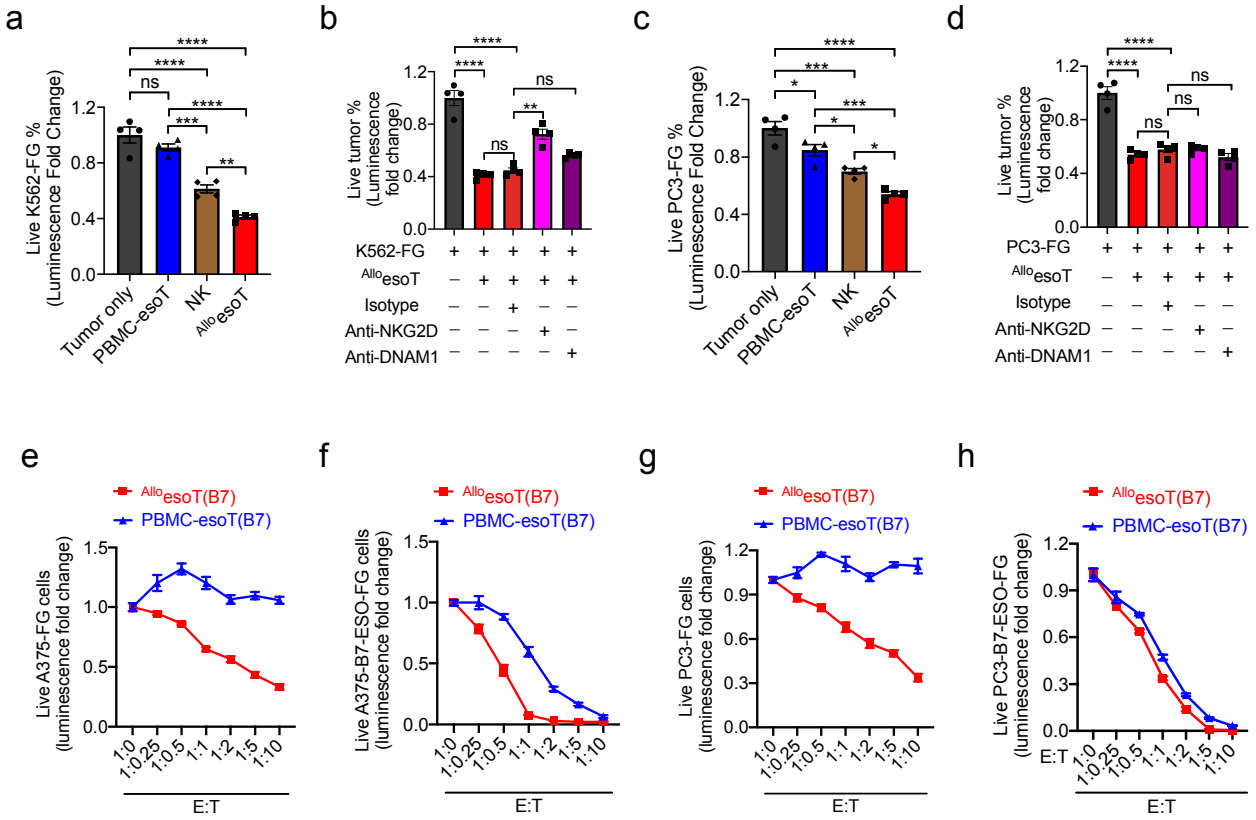

Supplementary figure 3. *In vitro* tumor killing capacity of ^{Allo}esoT and ^{Allo}esoT(B7) cells; related to figure 3.

(a-d) A2/ESO independent tumor killing by ^{Allo}esoT cells. (a) Tumor killing of K562-FG by ^{Allo}esoT cells (n=4). (h) K562-FG killing mechanisms of ^{Allo}esoT cells. NKG2D and DNAM-1 mediated NK pathways were studied. Tumor cell killing was analyzed at 24-hours post co-culture (n=3). (c) ^{Allo}esoT tumor killing against PC3-FG through A2/ESO independent pathway. (d) PC3-FG killing mechanisms of ^{Allo}esoT cells. NKG2D and DNAM-1 mediated NK pathways were studied. Tumor cell killing was analyzed at 24-hours post co-culture (n=3).

(e-h) Studying the tumor killing of ^{Allo}esoT(B7) cells against multiple solid tumor cell lines compared to PBMC-esoT(B7) cells. (e-f) Luciferase activity analysis of *in vitro* tumor killing of A375-FG and A375-By-ESO-FG (n=4). E:T, effector/target ratio. (g-h) ^{Allo}esoT(B7) tumor killing against PC3-FG and PC3-B7-ESO-FG (n=4). E:T, effector/target ratio.

Representative of 3 experiments. Data are presented as the mean ± SEM. ns, not significant, *P<0.05, **P<0.01, **P<0.001, ****P<0.0001, by 1-way ANOVA (a-d).

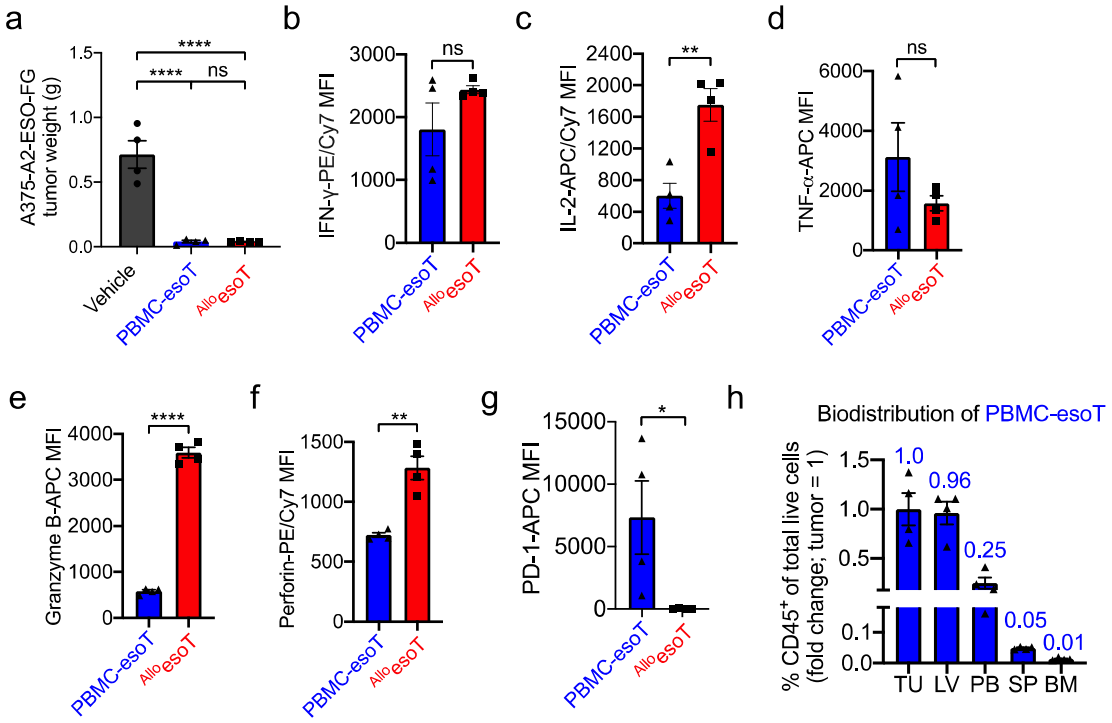

Supplementary figure 4. *In vivo* anti-tumor capacity of ^{Allo}esoT, related to figure 3.
(a-g) Studying *in vivo* anti-tumor efficacy of ^{Allo}esoT cells against solid tumor in a human melanoma (A375-A2-ESO-FG) xenograft mouse model. (a) Quantification of tumor weight at the terminal analysis (n=4). (b-d) Intracellular cytokines expression of *in vivo* persistent ^{Allo}esoT cells and PBMC-esoT cells in liver (n=4). (e-g) Intracellular cytotoxic molecules expression of *in vivo* persistent ^{Allo}esoT cells and PBMC-esoT cells in liver (n=4). (h) PD-1 expression of *in vivo* persistent ^{Allo}esoT cells and PBMC-esoT cells in bone marrow (n=4). (h) *In vivo* biodistribution of PBMC-esoT cells in a human melanoma (PC3-A2-ESO-FG) xenograft mouse model. TU=tumor, LV=liver, PB=peripheral blood, SP=spleen, BM=bone marrow.
Representative of 3 experiments. Data are presented as the mean ± SEM. ns, not significant, *P<0.05, **P<0.01, **P<0.001, ****P<0.0001, by 1-way ANOVA (a), student's t-test (b-g).

a

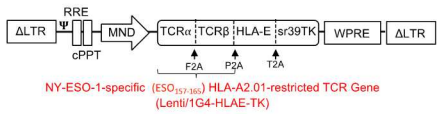

b

Viral titer on HEK-293T-CD3 cells	
Vector \ Titer	Titer (IFU/mL)
Lenti/1G4-TK	1.256×10^8
Lenti/1G4-HLAE-TK	6.36×10^7

c

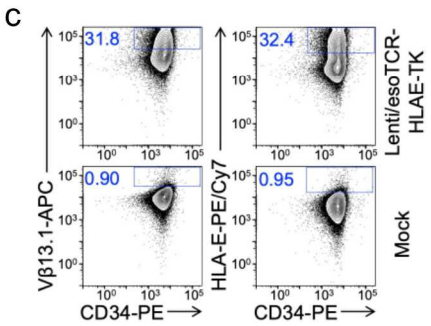

d

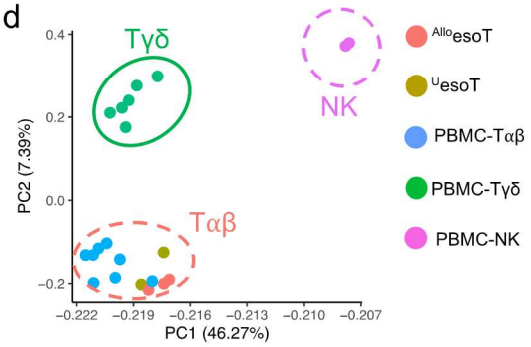

e

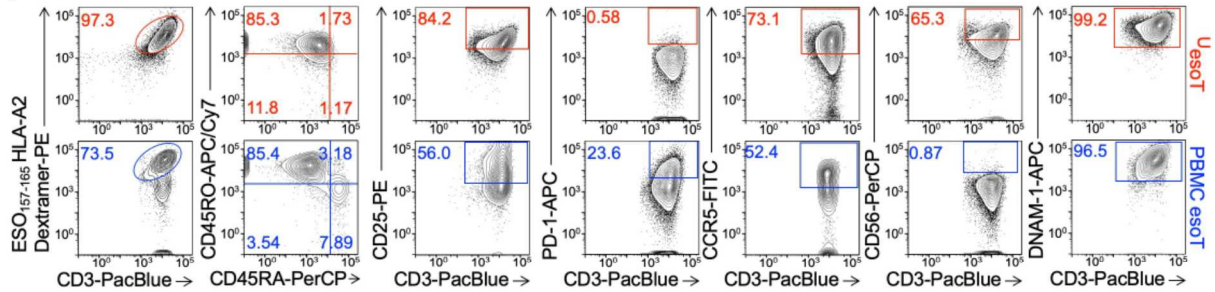

f

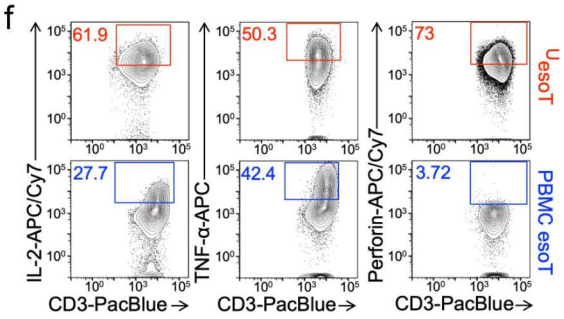

g

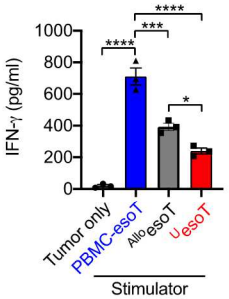

Supplementary figure 5. The generation and characterization of ᵁesoT; related to figure 5.
(a) Design of the lentiviral vector encoding esoTCR (clone 1G4), HLA-E and sr39TK.
(b) Representative titer of virus packaged with indicated lentivectors.
(c) FACS detection of intracellular expression of esoTCR (identified as Vβ13.1⁺) and HLA-E in CD34⁺ HSC cells 72h post lentivector transduction.
(d) Gene profiling of ᵁesoT cells clustered closely with ᴬˡˡᵒesoT cells . Principal component analysis of gene expression for six cell types. Each symbol shape represents an individual biological replicate for the corresponding cell type. The ordination using the first two principal components PC1 and PC2.
(e-f) Characterization of ᵁesoT. (e) FACS plots showing the expression of surface markers from ᵁesoT cells (identified as Vβ13.1⁺ CD3⁺) compared to PBMC-esoT cells (identified as Vβ13.1⁺ CD3⁺). (f) FACS plots showing intracellular cytokines from ᵁesoT cells compared to PBMC-esoT cells.
(g) ELISA analysis of IFN-γ in the supernatants of an MLR assay (n=3), showing reduced HvG response induced by ᵁesoT cells.

Representative of 3 experiments. Data are presented as the mean ± SEM. ns, not significant, *P<0.05, **P<0.01, **P<0.001, ****P<0.0001, by 1-way ANOVA (g).

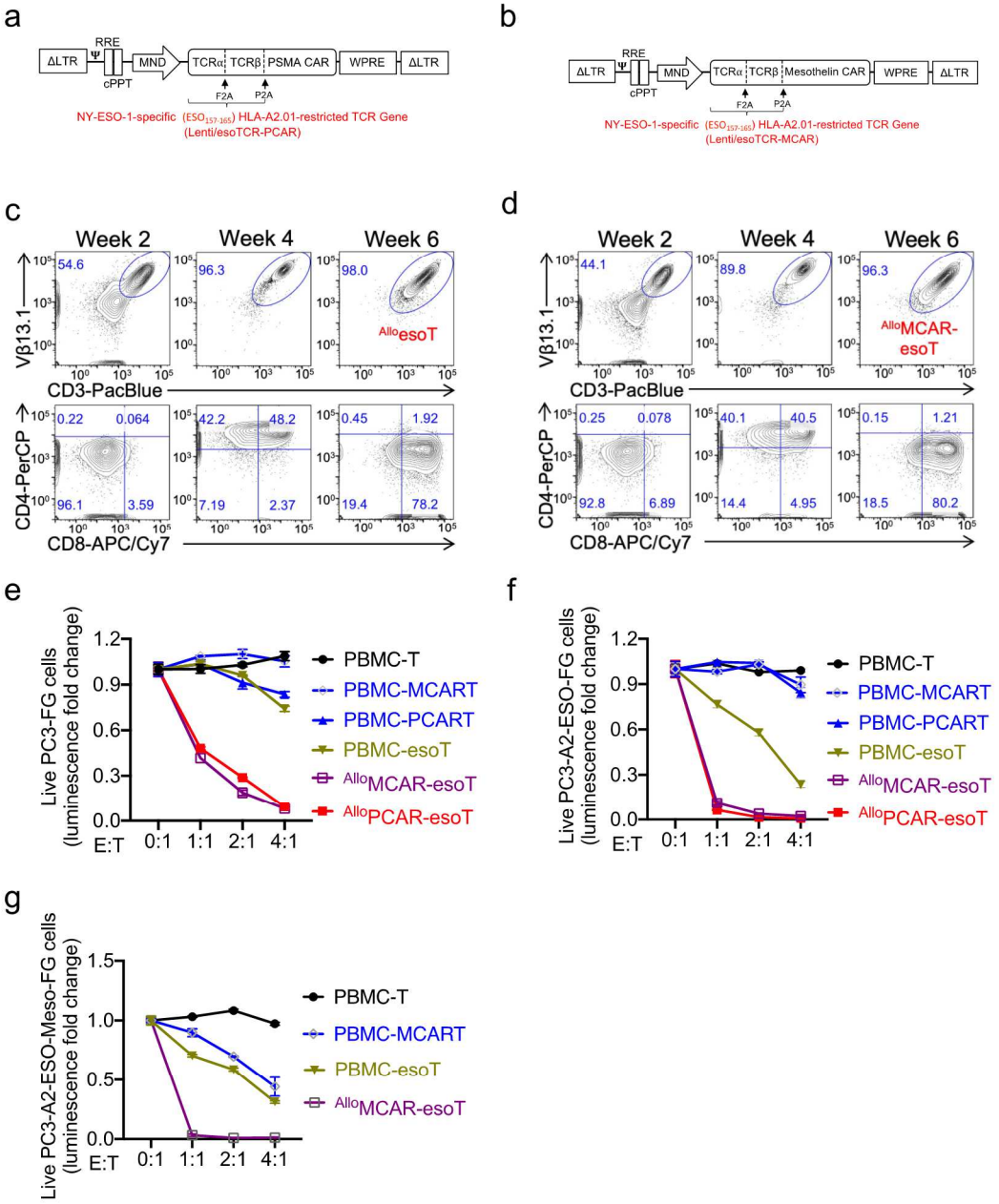

Supplementary figure 6. The generation of CAR-armed esoT (^{Allo}CAR-esoT) cells; relate to figure 6.
(a) Design of the lentiviral vector encoding esoTCR (clone 1G4) and PSMA CAR (PCAR).
(b) Design of the lentiviral vector encoding esoTCR (clone 1G4) and mesothelin CAR (MCAR).
(c) Representative kinetics of ^{Allo}esoT cell development and differentiation from CD34$^+$ HSCs (donor 009) at the indicated weeks. ^{Allo}esoT cells were gated as Vβ13.1$^+$ CD3$^+$.
(d) Representative kinetics of ^{Allo}MCAR-esoT cell development and differentiation from CD34$^+$ HSCs (donor 009) at the indicated weeks. ^{Allo}MCAR-esoT cells were gated as Vβ13.1$^+$ CD3$^+$.
(e-f) Studying the tumor killing of ^{Allo}CAR-esoT cells against PC3 prostate cancer line and its derivative cell lines. (e-f) Luciferase activity analysis of *in vitro* tumor killing of PC3-FG and PC3-A2-ESO-FG (n=4).
(g) Tumor killing of ^{Allo}MCAR-esoT cells against PC3-A2-ESO-Meso-FG cell line (n=4). E:T, effector/tumor ratio.

Representative of 3 experiments. Data are presented as the mean ± SEM.

CHAPTER 4:

Allogeneic HSC-engineered CAR-armed NKT cells for off-the-shelf cancer immunotherapy

TITLE PAGE

Allogeneic HSC-engineered CAR-armed NKT cells for off-the-shelf cancer immunotherapy

Jiaji Yu[1,2,3,*], Yu Jeong Kim[1,*], Yang Zhou[1,2], Yan-ruide Li[1,2], Zhe Li[1], Yu-Chen Wang[1], Feiyang Ma[2,4], Derek Lee[1,2], Yuchong Zhang[5], Zoe Hanh[1], Matteo Pellegrini[2,6] and Lili Yang[1,2,3,7]

Author Affiliation

1. Department of Microbiology, Immunology & Molecular Genetics, University of California, Los Angeles, Los Angeles, CA 90095, USA
2. Molecular Biology Institute, University of California, Los Angeles, Los Angeles, CA 90095, USA
3. Eli and Edythe Broad Center of Regenerative Medicine and Stem Cell Research, University of California, Los Angeles, Los Angeles, CA 90095, USA
4. Department of Molecular, Cell, and Developmental Biology, University of California, Los Angeles, Los Angeles, CA 90095, USA
5. Department of Integrative Biology & Physiology, University of California, Los Angeles, Los Angeles, CA 90095, USA
6. Institute of Genomics and Proteomics, University of California, Los Angeles, CA 90095, USA
7. Jonsson Comprehensive Cancer Center, David Geffen School of Medicine, University of California, Los Angeles, Los Angeles, CA 90095, USA

* Contributed equally

Address Correspondence to

Lili Yang, Ph.D. liliyang@ucla.edu

Autologous transfer of engineered T cells has shown excellent efficacy in cancer immunotherapy, especially in treating blood cancer with chimeric antigen receptor (CAR) T cells[1-4]. Nevertheless, the autologous nature renders current T-cell therapies patient selective, time-consuming in manufacturing, and costly[2, 5-7]. Thus, to broaden the use of T-cell therapies, allogeneic sources of T cells are in great need for developing the "off-the-shelf" cell products that are scalable in the manufacture and readily administrable for patients at various cancer stages[6].

As an allogeneic cell source, invariant natural killer T (iNKT) cells are a small population of unconventional αβ T cells[8]. Compared to conventional CAR-T cells, CAR-engineered iNKT cells can attack tumor cells using multiple mechanisms and at higher efficacy; can more effectively traffic to and infiltrate tumor sites; and most importantly, do not induce graft-versus-host disease (GvHD). However, the use of iNKT cells is constrained by their low percentages in human blood (0.001-1%)[8-12]. Here, we report a novel *ex vivo* HSC-derived CAR engineered NKT cell (^{Allo}CAR-eNKT) culture method that can produce pure, potent, and safe allogeneic cell products. This method is robust, of high-yield, and can be feeder-free/serum-free, potentially fitting for clinical translation.

This study collected human cord blood CD34+ hematopoietic stem and progenitor cells (referred to as HSCs) through CliniMACS selection and cryopreserved. Thawed HSCs were transduced with iNKT TCR encoded lentivector and then differentiate and expand in the *ex vivo* ^{Allo}CAR-eNKT cell culture over 6 weeks with ~10^6 folds of expansion (tested from 10 cord blood donors) (Fig. 1a). Cargo genes loaded on the lentivector can be versatile and polycistronic, while two examples (Lenti/iNKT-sr39TK and Lenti/iNKT-BCMA CAR (BCAR)) were demonstrated

here (Supplementary Fig. 1)[13]. Over 50% of the transduction rate was routinely achieved with lentivectors described (Supplementary Fig. 1c-d). We adopted an *in vitro* system of plate-bound delta-like 4 (DLL4) to enable lymphoid differentiation as previously described[14-17]. Notch signaling through DLL1 or DLL4 is pivotal to thymocyte commitment[14, 18, 19]. One week into the culture, HSCs gave rise to $CD7^+CD5^+$ T-cell progenitors (Supplementary Fig.1e, f) with iNKT TCR presented on the cell surface (Fig. 1 b, c). At week 4, more mature $CD4^+CD8^+$ double-positive (DP) population emerges. By the end of culture at week 6, the final cell product can reach a purity of more than 99% iNKT TCR^+ $CD3^+$ DP without any detectable endogenously rearranged TCR, suggesting the induction of allelic exclusion through the transgenic iNKT TCR as previously reported. The *ex vivo* generated ^{Allo}HSC-eNKT and ^{Allo}BCAR-eNKT cells presented a $CD8^+$ single-positive (SP) or $CD4^-$ $CD8^-$ double-negative (DN) phenotype (Fig. 1 b, c). The introduction of CAR at the HSCs stage did not interfere with the *ex vivo* development of ^{Allo}BCAR-eNKT cells compared to ^{Allo}HSC-eNKT (Fig. 1 b, c), and the product coexpresses BCAR and iNKT TCR (Fig. 1d). Our approach saves the additional CAR transducing process upon mature T or NK cells required for all current allogeneic products, including many with the iPSC approach[15, 17, 20]. The *ex vivo* ^{Allo}CAR-eNKT cell culture was robust and compatible with various CAR designs, the generation and development of ^{Allo}CAR19-eNKT cells (CD19-specific CD28 co-stimulation CAR) followed the same pattern and shared phenotypic results with ^{Allo}BCAR-eNKT cells (BCMA-specific 41BB co-stimulation CAR) (Supplementary Fig. 2a-f). Single-cell TCR sequencing analysis confirmed that these ^{Allo}HSC-eNKT and ^{Allo}CAR-eNKT (refers to ^{Allo}BCAR-eNKT and ^{Allo}CAR19-eNKT in this study) cells uniformly expressed the transgenic iNKT TCRs with nearly undetectable randomly rearranged endogenous αβ TCR pairs (Fig. 1e). In contrast, healthy donor periphery blood mononuclear cells (PBMCs) derived conventional αβ T (PBMC- αβTc) cells

expressed highly diverse endogenously rearranged αβ TCRs. In contrast, PBMC derived iNKT (PBMC-iNKT) cells expressed a conserved invariant TCR α chain (Vα24-Jα18) and limited diverse TCR β chains (dominantly Vβ11) (Fig. 1e).

We performed deep RNA sequencing to characterize the transcriptome profile of ^{Allo}HSC-eNKT, and ^{Allo}BCAR-eNKT cells in comparison with PBMC derived conventional αβ T (PBMC-αβTc), iNKT (PBMC-iNKT), γδ T (PBMC-γδT) and NK (PBMC-NK) cells. In consistence with the CD8 SP/DN phenotype of ^{Allo}HSC-eNKT and ^{Allo}CAR-eNKT cells, CD4^{-} population of PBMC-iNKT (CD8 SP/DN) and PBMC-αβTc (CD8^{+}) were used for this sequencing experiment (Fig. 1f, g). Principal component analysis (PCA) of the global gene expression profiles showed that ^{Allo}HSC-eNKT and ^{Allo}CAR-eNKT grouped closely together while locating next to PBMC-iNKT and PBMC-αβTc cells, away from PBMC-γδT cells, and the furthest from PBMC-NK cells (Fig. 1f). This PCA result indicated these ^{Allo}HSC-eNKT and ^{Allo}CAR-eNKT cells are unique as their own, yet closely resembled the transcriptome profile of PBMC-iNKT and PBMC-αβTc (Fig. 1f). Gene expression analysis further revealed the distinctive profile signatures of ^{Allo}HSC-eNKT and ^{Allo}CAR-eNKT cells in several aspects. Overall, ^{Allo}HSC-eNKT and ^{Allo}CAR-eNKT cells presented an NKT-like Th1 phenotype on their transcription factor expression profile. They presented high expression of *NFKB1,* which is essential for TCR signaling; they expressed a high level of *ZBTB16* that encodes PLZF, a signature transcription factor of NKT and NK cells[21]; they showed enrichment on *TBX21* that encodes T-bet, which directs Th1 commitment[22]; they also showed low expression on *GATA3* and *RORC* that regulate Th2 and Th17 polarization (Fig. 1g)[22, 23]. Interestingly, compared to all PBMC derived T and NK cells tested, ^{Allo}HSC-eNKT and ^{Allo}CAR-eNKT cells expressed minimal level of HLA-II related genes across all the donors and

engineered cell product types, and generally low level of HLA-I related genes, which potentially would benefit their use in "off-the-shelf" therapy against the allorejection (Fig. 1g)[24]. Furthermore, compared to PBMC-iNKT and even PBMC-NK cells, ^{Allo}HSC-eNKT and ^{Allo}CAR-eNKT cells expressed exceedingly high NK activating receptor genes while low levels of NK inhibitory receptor genes suggesting their NK phenotype and related functionalities (Fig. 1g)[25].

Next, we characterized the phenotype and functionality of ^{Allo}BCAR-eNKT cells compared to the clinically employed PBMC derived BCAR-T cells. ^{Allo}BCAR-eNKT cells conserved many typical T cell functions while displaying a distinct NKT cell phenotype. ^{Allo}BCAR-eNKT cells express high levels of T cell memory marker (i.e., CD45RO), T cell activation marker (i.e., CD69), NK markers (i.e., CD161, NKG2D, CD56, and NKp44), and peripheral tissue and inflammatory site homing markers (i.e., CCR4, CCR5 and CXCR3) (Fig. 2a, and Supplementary Fig. 3a). In addition, ^{Allo}BCAR-eNKT cells were able to produce potent amounts of proinflammatory cytokines (i.e., IFN-γ, IL-2, and TNF-α) and cytotoxic molecules (i.e., granzyme B and perforin) (Fig. 2a, and supplementary Fig. 3a). The same surface markers of the NKT type and functionality profiles were confirmed in ^{Allo}HSC-eNKT and ^{Allo}CAR19-eNKT cells (Supplementary Fig. 4a-d and supplementary Fig. 7a). Corroborating the low MHC expression in the RNAseq results (Fig.1g), ^{Allo}BCAR-eNKT cells expressed a minimum amount of HLA-II with lower expression of HLA-I when compared to BCAR-T cells (Supplementary Fig. 2a). To test the functionality of the iNKT TCR, we stimulated ^{Allo}BCAR-eNKT cells with the iNKT antigen α-galactosylceramide (αGC) and observed vigorous proliferation (Fig. 2b). ^{Allo}BCAR-eNKT secreted high levels of Th0/Th1 cytokines (i.e., IFN-γ, TNF-α, and IL-2) while a minimal amount of Th2 (i.e., IL-4) and Th17 (i.e., IL-17) cytokines were secreted (Fig. 2c-f and supplementary Fig. 3b).

To study the tumor-targeting efficacy of ^{Allo}BCAR-eNKT cells, we used a BCMA^{+} human multiple myeloma (MM) cell line, MM.1s, engineered to express human CD1d, firefly luciferase, and enhanced green fluorescence protein dual-reporters (denoted as MM.1s-CD1d-FG) (Supplementary Fig. 3c). With the NKT nature and the CAR empowerment, we proposed a CAR/TCR/NK triple-targeting mechanism of ^{Allo}BCAR-eNKT attacking MM (Fig. 2g). Scanning electronic microscopy showed the morphology of ^{Allo}BCAR-eNKT cells attacking an MM.1s-CD1d-FG cell (Fig. 2h). When cocultured with MM.1s-CD1d-FG cells, ^{Allo}BCAR-eNKT cells were activated and responded with IFN-γ production (Fig. 2i). In an *in vitro* tumor killing assay, ^{Allo}BCAR-eNKT cells effectively killed MM.1s-CD1d-FG tumor cells, at an efficacy comparable to conventional BCAR-T cells and superior to ^{Allo}HSC-eNKT cells (Fig. 2j). When pulse with the iNKT TCR cognate lipid antigen αGC, both ^{Allo}BCAR-eNKT and ^{Allo}HSC-eNKT cells, but not BCAR-T cells, demonstrated enhanced tumor killing (Supplementary Fig. 3d). To further confirm the killing mechanism, we blocked CD1d and NK activating receptors (i.e., NKG2D and DNAM-1), which reduced the killing efficacy of ^{Allo}BCAR-eNKT cells (Fig. 2k), confirming the CD1d and NK activating receptor-mediated tumor-targeting function. In MM patients, CD1d expression level may vary regarding the disease stages (Fig. 2l). Considering the possible absence of CD1d, we examined the tumor-killing against MM.1s-FG (Fig. 2m). Without CD1d interaction, ^{Allo}BCAR-eNKT cells showed effective tumor-killing efficacy, and ^{Allo}HSC-eNKT was still capable of tumor-killing, indicating embedded NK killing mechanisms (Fig. 2m). Beyond the MM cell line, tumor-killing of ^{Allo}HSC-eNKT pertained to NK mechanism were further demonstrated with human melanoma (i.e., A375) and myelogenous leukemia (i.e., K562) (Supplementary Fig. 5) ^{Allo}CAR19-eNKT cells phenotypically perform in consistence with ^{Allo}BCAR-eNKT and

^{Allo}HSC-eNKT cells (Supplementary Fig. 7a-e), they killed CD19^{+} NLAM-6-FG leukemia line effectively *in vitro* and responded to additional αGC stimulation (Supplementary Fig. 7d-f).

Using an MM.1s-CD1d-FG xenograft NSG (NOD/SCID/γc$^{-/-}$) mouse model, we studied the *in vivo* efficacy of ^{Allo}BCAR-eNKT cells in comparison with BCAR-T cells (Fig. 2n). With single administration of effector cells, both ^{Allo}BCAR-eNKT and BCAR-T cells effectively killed and suppressed the development of MM tumor cells (Fig. 2o). Nevertheless, both ^{Allo}BCAR-eNKT and BCAR-T cells could not eradicate MM.1s-CD1d-FG with this regimen (Supplementary Fig. 6a-b). With weekly administration of effector cells (Fig. 2p), both ^{Allo}BCAR-eNKT and BCAR-T cells effectively eradicated MM tumor cells (Fig. 2q and supplementary Fig. 6d). Under this condition, mice receiving the conventional BCAR-T cells, despite being tumor-free, eventually die of GvHD due to xenoreactivity (Fig. 2r). On the contrary, mice receiving ^{Allo}BCAR-eNKT cells remained tumor-free and survived long-term without GvHD (Fig. 2r). In the MM.1s-FG xenograft mouse model, which does not express CD1d, a single injection of ^{Allo}BCAR-eNKT cells can suppress the tumor progression as well as BCAR-T cells (Supplementary Fig. 6e-g). When transferred into mice with heavy tumor load (Fig. 2s), ^{Allo}BCAR-eNKT cells mounted an impressive *in vivo* expansion at an even higher magnitude than that of BCAR-T cells (Fig. 2t). Biodistribution analysis showed that ^{Allo}BCAR-eNKT cells distribute across tissues similarly to the BCAR-T cells (Fig. 2 u, v). Although with the significant expansion, the proinflammatory cytokine IFN-γ produced by ^{Allo}BCAR-eNKT cells in the peripheral blood of experimental mice does not differ from that of BCAR-T (Fig. 2w). The CD19 targeting ^{Allo}CAR19-eNKT cells, with a single injection regimen, could suppress the tumor progression as effectively as conventional CAR19-T cells (Supplementary Fig. 7g-j).

For allogeneic immune cell therapy, GvHD is a major safety concern[5, 6, 26]. Due to the glycolipid recognizing and invariant nature of iNKT TCR, NKT cells are not expected to mount GvH responses[10, 25]. We implemented an *in vitro* mixed lymphocyte reaction (MLR) assay to evaluate the GvHD risk of ^{Allo}BCAR-eNKT cells (Fig. 3a), which clonally express iNKT TCR. ^{Allo}BCAR-eNKT cells did not react to donor-mismatched PBMCs, whereas BCAR-T cells produced a significant amount of IFN-γ for alloreactivity (Fig. 3b). In an *in vivo* tumor-bearing NSG model (Fig. 2p), 45 days post effector cell transfer, *in vivo* tissue histology analysis showed severe mononuclear cell infiltration in multiple vital organs for BCAR-T treated mice. At the same time, a minimum amount of that could be observed in ^{Allo}BCAR-eNKT treated mice (Fig. 3c, d, and supplementary Fig. 8f). In the same experiment, BCAR-T treated mice die of GvHD despite being tumor-free (Fig. 2r). For allogeneic therapies, a significant concern is the host-versus-graft (HvG) risk that may lead to the depletion of allogeneic therapeutic cells by the host immune cells, particularly by the host T cells through their recognition of mismatched HLAI/II molecules on allogeneic therapeutic cells[26]. We performed *an in vitro* MLR assay to evaluate the HvG risk of ^{Allo}BCAR-eNKT cells (Fig. 3f). Compared to BCAR-T cells, ^{Allo}BCAR-eNKT cells triggered significantly reduced IFN-γ production from PBMCs of multiple mismatched donors (Fig. 3g). This result may attribute to the naturally low expression of HLA molecules of ^{Allo}BCAR-eNKT cells, which were confirmed by RNAseq (Fig. 1g), *in vitro* FACS analyses post cell production (Supplementary Fig. 8 a-b), and *in vitro* IFN-γ response experiment (Fig. 3g, h), and an *in vitro* tumor response experiment (Supplementary Fig. 8c, d). In the *in vivo* biodistribution experiment (Fig. 2s), bone marrow samples of tumor-bearing mice were analyzed, in which persisted ^{Allo}BCAR-eNKT cells presented much low expression of both HLA-I (B2M) and HLA-II (HLA-

DR, DP, DQ) molecules compared to BCAR-T cells (Fig. 3i, j). Allogeneic host NK cell-mediated destruction could be another HvG concern; we designed another MLR assay to study this aspect (Fig. 3k). In the coculture with allogeneic PBMC derived NK cells, ^{Allo}BCAR-eNKT cells persisted well compared to conventional BCAR-T cells (Fig. 3l, m). The resistance to the NK rejection of ^{Allo}BCAR-eNKT cells may attribute to their low expression of "stress molecules" like the NKG2D ligand ULBP (Fig. 3n and supplementary Fig. 8e). We can also validate the same safety and immunogenicity properties on ^{Allo}CAR19-eNKT cells (Supplementary Fig.9), demonstrating the robustness of the allogeneic cell product produced from the ^{Allo}CAR-eNKT cell culture platform. To further enhance the safety profile of the ^{Allo}CAR-eNKT cell products, we have demonstrated the feasibility of engineering an sr39TK suicide gene into our product with ^{Allo}HSC-eNKT cells as an example (Fig. 1a). The incorporated sr39TK gene would allow *in vivo* monitoring with positron emission tomography (PET) imaging and, most importantly, eliminating sr39TK expression cells in case of a severe adverse event[13]. The prodrug ganciclovir (GCV) induced effective depletion of ^{Allo}HSC-eNKT cells *in vitro* (Fig. 3o). Overall, these studies suggested ^{Allo}CAR-eNKT cell products be of low GvHD risk and largely HvG-resistant, supporting their "off-the-shelf" therapeutic applications.

IL-15 plays a critical role in NKT cell survival and homeostasis[27]. IL15 was reported to enhance cell number during production, promote *in vivo* persistence, and improve tumor control in NKT-based cell therapies[28]. An IL15 expressing NKT CAR therapy was also showed to be safe in a recent phase-I clinical trial[29]. To demonstrate the versatility of the ^{Allo}CAR-eNKT cell culture platform in incorporating various add-on enhancement genes (Fig. 1a), we designed a lentivector encoding iNKT TCR, BCAR, and IL-15, enabling the production of IL-15 coexpressing

^{IL15}BCAR-eNKT cells (Fig. 3p and supplementary Fig. 10a). IL-15 production did not interfere with the generation and development of ^{IL15}BCAR-eNKT cells (Fig. 3q and supplementary Fig. 10b). We confirmed the IL-15 production from ^{IL15}BCAR-eNKT cells with ELISA (Fig. 3r). During a feeder-free activation and expansion test, ^{IL15}BCAR-eNKT cells proliferated more significantly than the cognate ^{Allo}BCAR-eNKT cells (Fig. 3s and supplementary Fig. 10c). Consistent with ^{Allo}BCAR-eNKT cells, ^{IL15}BCAR-eNKT cells showed NKT-like phenotypes and functionalities (Supplementary Fig. 10d). Putting ^{IL15}BCAR-eNKT cells to the *in vivo* examination (Fig. 3t) with a single injection regimen, ^{IL15}BCAR-eNKT cells showed better tumor control when compared to conventional BCAR-T cells (Fig. 3u). Within a month after the transfer of effector cells, ^{IL15}BCAR-eNKT and BCAR-T cells showed equally great tumor control compared to the vehicle group (Fig. 3v, w). Nevertheless, MM relapsed first in the BCAR-T cells treated group (Fig. 3u). Mice in BCAR-T group manifested cytokine release syndrome showing exceedingly high levels of IFNγ in the peripheral blood (Fig. 3x). Two mice of the BCAR-T group succumbed to GvHD before the tumor load overwhelmed them at day 85 and 87 (Fig. 3u). Overall, the ^{IL15}BCAR-eNKT cells treated group showed better survival (Fig. 3y).

There is a strong interest in finding a robust and scalable allogeneic cell source for "off-the-shelf" therapy with the advancement in cancer immunotherapy. Safety and tumor targeting capacity are two keys to successful cell therapy for cancer. In the ^{Allo}CAR-eNKT cell culture platform that we developed, iNKT TCR directed the *ex vivo* development of NKT cells from HSCs giving the clonal expression of iNKT TCR, which significantly reduces the GvHD risks while bringing in the unique tumor-targeting capacity of iNKT TCR. This eNKT cell culture platform was scalable, high yield and purity, and highly editable with compatibility with CARs, suicide

genes, and other enhancement genes like IL-15. ^{Allo}CAR-eNKT cells generated from the platform targeted tumor through an effective CAR/TCR/NK triple-targeting mechanism. In addition, they are of low immunogenicity resistant to T and NK cell-mediated allorejection. The IL-15 producing derivative ^{IL15}CAR-eNKT cells presented even superior tumor control evidencing the possibility of further improvement of these cell products. Have established an eNKT generation platform, in future work, we will study the development of NKT cells and evaluate ration combinations with genes and agents that affect persistence, exhaustion, and tumor targeting under the context of "off-the-shelf" cancer immunotherapy.

Materials and methods

Human CD34+ Hematopoietic Stem Cells (HSCs) and Periphery Blood Mononuclear Cells (PBMCs). Human CD34+ HSCs from cord blood (CB) sources were purchased from HemaCare. For all CB HSCs aliquots, the purity of CD34+ cells was more than 97%, as evaluated by flow cytometry. CB HSCs were cultured in X-VIVO 15 Serum-free Hematopoietic Cell Medium (Lonza). Healthy donor human PBMCs were obtained from the UCLA/CFAR Virology Core Laboratory without identification information under federal and state regulations. PBMCs were cultured in a complete lymphocyte culture medium (denoted as C10 medium) unless other specified. C10 was made of RPMI 1640 supplemented with FBS (10% vol/vol), P/S/G 40 (1% vol/vol), MEM NEAA (1% vol/vol), HEPES (10 mM), Sodium Pyruvate (1 mM), β-ME (50 mM), and Normocin (100 mg/ml).

Cell lines. Human multiple myeloma cancer cell line MM.1S, chronic myelogenous leukemia cell line K562 and melanoma cell line A375 were purchased from American Type Culture Collection (ATCC). MM.1S and K562 cells were cultured in R10 medium, made of RPMI 1640 supplemented with FBS (10% vol/vol) and P/S/G (1% vol/vol). A375 cells were cultured in DMEM supplemented with FBS (10% vol/vol) and P/S/G (1% vol/vol). The parental tumor cell lines were transduced with lentiviral vectors encoding the intended gene(s) as needed. Genes of interest include human CD1d and a dual reporter of firefly luciferase and enhanced green fluorescence protein (FG)[1]. 72h post lentivector transduction, cells were subjected to flow cytometry sorting to isolate gene-engineered cells for making stable cell lines. Six stable tumor cell lines were generated for this study, including MM.1S-FG, MM.1S-CD1d-FG, A375-FG, and K562-FG.

Mice. All animal experiments used NOD.Cg-Prkdc^{SCID}Il2rg^{tm1Wjl}/SzJ (NOD/SCID/IL-2Rγ-/-, NSG) mice were purchased from The Jackson Laboratory. All mice were 6- to 10-weeks old and maintained at the animal facilities of the University of California, Los Angeles (UCLA) under pathogen-free conditions. All mouse studies were conducted in accordance with national guidelines for the humane treatment of animals and were approved by the Institutional Animal Care and Use Committee of UCLA.

Lentiviral vector construction and transduction. Lentiviral vectors used in this study were all constructed from a parental lentivector pMNDW as previously described[1]. The Lenti/iNKT-sr39TK vector was constructed by inserting into pMNDW vector a synthetic tricistronic gene encoding human iNKT TCRα-F2A-TCRβ-P2A-sr39TK; The Lenti/iNKT-BCAR vector was constructed by inserting into pMNDW vector a synthetic tricistronic gene encoding human iNKT TCRα-F2A-TCRβ-P2A-BCMA CAR; The Lenti/iNKT-CAR19 vector was constructed by inserting into pMNDW vector a synthetic tricistronic gene encoding human iNKT TCRα-F2A-TCRβ-P2A-CD19 CAR; The Lenti/iNKT-BCAR-IL15 vector was constructed by inserting into pMNDW vector a synthetic tetracistronic gene encoding human iNKT TCRα-F2A-TCRβ-P2A-BCMA CAR-T2A-human IL15; the Lenti/FG vector was constructed by inserting into pMNDW a synthetic bicistronic gene encoding Fluc-P2A-EGFP; the Lenti/CD1d vector was constructed by inserting into pMNDW a synthetic gene encoding human CD1d. The synthetic gene fragments were obtained from GenScript and IDT. Lentiviruses were produced using HEK 293T cells, following a standard lipofection with Trans-IT-Lenti Transfection reagent (Mirus Bio) and centrifugation concentration protocol as previously described[1, 2]. Lentivector titers were measured

by transducing HEK 293T-hCD3 (human CD3 expressing line, cloned in Lili Yang lab) with serial dilutions and performing flow cytometry following established protocols[1, 2].

Antibodies and Flow cytometry. Fluorochrome-conjugated antibodies specific for human CD45 (Clone H130), TCRαβ (Clone I26), CD3 (Clone HIT3a), CD4 (Clone OKT4), CD8 (Clone SK1), CD45RO (Clone UCHL1), CD45RA (Clone HI100), CD161 (Clone HP-3G10), CD25 (Clone BC96), CD69 (Clone FN50), CD56 (Clone HCD56), CD62L (Clone DREG-56), CTLA-4 (Clone BNI3), PD-1 (clone EH12.2H7), CD1d (Clone 51.1), CCR4 (Clone L291H4), CCR5 (Clone HEK/1/85a), CXCR3 (Clone G025H7), CXCR4 (Clone 12G5), NKG2D (Clone 1D11), DNAM-1 (Clone 11A8), CD158 (KIR2DL1/S1/S3/S5) (Clone HP-MA4), IFN-γ (Clone B27), granzyme B (Clone QA16A02), perforin (Clone dG9), TNF-α (Clone Mab11), IL-2 (Clone MQ1-17H12), HLAE (Clone 3D12), β2-microglobulin (B2M) (Clone 2M2), HLA-DR, DP, DQ (Clone Tü 39) were purchased from BioLegend. Biotinylated Human BCMA and Biotinylated Human CD19 (20-291) Protein were purchased from Acrobiosystems. Fluorochrome-conjugated antibodies specific for human CD34 (Clone 581) and human iNKT TCR Vα24-Jβ18 (Clone 6B11) were purchased from BD Biosciences. Fluorochrome-conjugated antibodies specific for human iNKT TCR Vβ11 were purchased from Beckman-Coulter; Fluorochrome conjugated antibodies specific for human ULBP-2,5,6 (Clone 165903) was purchased from R&D Systems. Human Fc Receptor Blocking Solution (TrueStain FcX) was purchased from Biolegend, and Mouse Fc Block (anti-mouse CD16/32) was purchased from BD Biosciences. Fixable Viability Dye eFluor506 (e506) was purchased from Affymetrix eBioscience. All flow cytometry stains for surface markers were performed in PBS at 4°C for 15mins. Samples were stained with Fixable Viability Dye eFluor506 (e506) mixed with Mouse Fc Block (anti-mouse CD16/32) or Human Fc Receptor Blocking

Solution (TrueStain FcX), followed by PBS wash. Antibody staining was then added to all samples at specified dilutions according to the manufacturer's instructions. Intracellular cytokines were stained using a Cell Fixation/Permeabilization Kit (BD Biosciences). Flow cytometry was performed using a MACSQuant Analyzer 10 flow cytometer (Miltenyi Biotech), and FlowJo software version 9 and 10 was used for data analysis.

***Ex vivo* allogeneic HSC-derived CAR-engineered NKT (^{Allo}CAR-eNKT) cell culture.** Non-tissue culture-treated 24-well plates were coated with StemSpan lymphoid differentiation coating material (LDCM, 500µl/well, StemCell Technologies) for 2 hours at room temperature or alternatively, overnight at 4°C. Coating supernatants were removed, and plates were washed with a D-PBS buffer. Transduced CD34^{+} human stem cells (HSCs) at 2 x 10^{4}/well were suspended in 500 µl of StemSpan lymphoid progenitor expansion medium (LPEM, StemCell Technologies) and seeded into coated wells of the 24-well plate on day 0. Cells were cultured for 3 days at 5% CO_2 and 37°C. On day 4, another 500 µL LPEM was added to each well, and cells were cultured for additional 4 days. On days 7 and 11, half of the medium was removed and replenished with 500 µl fresh LPEM. On day 14, cells were harvested, counted, and reseeded into an LDCM-coated 12-well plate in 1mL of T cell progenitor maturation medium per well (TPMM, StemCell Technologies) (5 x 10^{5} - 1 x 10^{6} cells/well). On day 18, 1mL of fresh TPMM was added to each well. On days 21 and 24, half of the medium in each well was discarded and replaced with 1mL of TPMM. On day 28, cells were harvested, counted, and re-seeded into a new coated 12-well plate in 1mL of TPMM (1 x 106 cells/mL/well) with 12.5 µL/well CD3/CD28/CD2 T Cell Activator (StemCell Technologies) and 10 ng/mL Human Recombinant IL-15 (PeproTech). On Day 31, 1mL of fresh TPMM containing 10 ng/mL Human Recombinant IL-15 was added into the

culture. On day 35, cells were harvested and analyzed by flow cytometry for double-positive (DP) and single-CD8 (SP) cells. Usually, over 50% DP/ SP CD8 cells could be reliably generated after 5 weeks of differentiation.

Feeder-free expansion of ^{Allo}CAR-eNKT cells. One day before the expansion, 24-well plates were coated with 1ug/ml anti-human CD3 antibody (OKT3, Biolegend) at 4°C overnight. Freshly collected ^{Allo}CAR-eNKT cells were seeded at 5x10^{5}/ml in OpTmizer™ CTS™ T-Cell Expansion serum-free medium (Gibco, Thermo Fisher Scientific) with IL-7 (10ng/ml), IL-15 (10ng/ml) and IL-21 (30ng/ml) for 3 days. The cultures were then collected, washed, and reseeded into new plates without Ab coating at 1x10^{6}/ml with 10ng/ml IL-7 and 10ng/ml IL-15. Medium change was performed every 2-3 days. ^{Allo}CAR-eNKT cells were allowed to expand for 7-14 days, then were aliquoted and frozen in liquid nitrogen storage tanks for future use.

On-feeder expansion of ^{Allo}CAR-eNKT cells. Healthy donor PBMCs were loaded with α-Galactosylceramide (αGC, Avanti Polar Lipids). Culture 10^{7} - 10^{8} PBMCs with 5 µg/ml αGC in 10ml culture medium for 1 hour. PBMCs were then irradiated at 6,000 rads (denoted as αGC/PBMCs). Freshly generated ^{Allo}CAR-eNKT cells were mixed with αGC /PBMCs (at 1:3 or 1:5 ratios) and cultured in C10 medium with IL-7 (10ng/ml) and IL-15 (10ng/ml). Alternatively, expansion can be achieved with K562-based artificial antigen-presenting cells expression CD80, CD86, and CD137L (K562-aAPC) as previously described[3]. K562-aAPC were engineered to express BCMA or CD19 for the expansion of corresponding ^{Allo}CAR-eNKT cells. Prior to expansion, K562-aAPC was irradiated at 10,000 rads. Freshly generated ^{Allo}CAR-eNKT cells were mixed irradiated K562-aAPC at 4:1 ratio with 10 ng/ml IL-7 and 10 ng/ml IL-15. ^{Allo}CAR-eNKT

cells were allowed to expand for 7-14 days, then were aliquoted and frozen in liquid nitrogen storage tanks for future use. All cultures described here were carried out in OpTmizer™ CTS™ T-Cell Expansion serum-free medium (Gibco, Thermo Fisher Scientific).

Generation of PBMC-Derived Conventional αβT, iNKT, γδT, and NK Cells. Healthy donor PBMCs were obtained from the UCLA/CFAR Virology Core Laboratory and were used to generate the PBMC-Tc, PBMC-iNKT, PBMC-γδT, and PBMC-NK cells. To generate PBMC-Tc cells, PBMCs were stimulated with CD3/CD28 T-activator beads (Thermo Fisher Scientific) and cultured in a C10 medium supplemented with human IL-2 (20 ng/mL) for 2-3 weeks, following the manufacturer's instructions.

To generate PBMC-iNKT cells, PBMCs were MACS-sorted via anti-iNKT microbeads (Miltenyi Biotech) labeling to enrich iNKT cells, which were then stimulated with donor-matched irradiated αGC-PBMCs at the ratio of 1:1 and cultured in C10 medium supplemented with human IL-7 (10 ng/ml) and IL-15 (10 ng/ml) for 2-3 weeks. If needed, the resulting PBMC-iNKT cells could be further purified using Fluorescence-Activated Cell Sorting (FACS) via human iNKT TCR antibody (Clone 6B11; BD Biosciences) staining. To generate PBMC-γδT cells, PBMCs were stimulated with Zoledronate (5 μM; Sigma-Aldrich) and cultured in C10 medium supplemented with human IL-2 (20 ng/ml) for 2 weeks. If needed, the resulting PBMC-γδT cells could be further purified using FACS via human TCR Vδ2 antibody (Clone B6; Biolegend) staining or via MACS using a human TCRγ/δ T Cell Isolation Kit (Miltenyi Biotech). To generate PBMC-NK cells, PBMCs were FACS-sorted via human CD56 antibody (Clone HCD56; Biolegend) labeling or MACS-sorted using a human NK Cell Isolation Kit (Miltenyi Biotech).

Generation of BCMA CAR / CD19 CAR-Engineered PBMC T (BCAR-T/CAR19-T) cells. Healthy donor PBMCs were stimulated with CD3/CD28 T-activator beads (Thermo Fisher Scientific) in the presence of recombinant human IL-2 (30 ng/ml), following the manufacturer's instructions. On day 3, cells were infected with lentivector encoding BCMA CAR or CD19 CAR. The resulting BCAR-T or CAR19-T cells were expanded for another 7-10 days and then were cryopreserved for future use.

Single-Cell TCR Sequencing. ^{Allo}HSC-eNKT (6B11^{+}TCRαβ^{+}), ^{Allo}BCAR-eNKT (6B11^{+}TCRαβ^{+}), ^{Allo}CAR19-eNKT (6B11^{+}TCRαβ^{+}), PBMC-iNKT (6B11^{+}TCRαβ^{+}), and PBMC-αβTc (6B11^{-}TCRαβ^{+}) cells were sorted using a FACSAria II flow cytometer. Sorted cells were immediately delivered to the UCLA TCGB (Technology Center for Genomics and Bioinformatics) Core to perform single cell TCR sequencing using a 10X Genomics ChromiumTM Controller Single Cell Sequencing System (10X Genomics), following the manufacturer's instructions and the TCGB Core's standard protocol. Libraries were constructed using an Illumina TruSeq RNA Sample Prep Kit (Cat#FC- 122-1001) and sequenced with 150 bp paired-end reads (5,000 reads/cell) on an Illumina NovaSeq. The reads were mapped to the human T cell receptor reference genome (hg38) using Cell Ranger VDJ. The frequencies of the α or β chain recombination were plotted.

Deep RNA Sequencing (Deep RNAseq) and Data Analysis. A total of 22 cell samples were analyzed, including 3 ^{Allo}HSC-eNKT (6B11^{+}TCRαβ^{+}), 3 ^{Allo}BCAR-eNKT (6B11^{+}TCRαβ^{+}), 2 ^{Allo}CAR19-eNKT (6B11^{+}TCRαβ^{+}), 3 PBMC-iNKT (6B11^{+}TCRαβ^{+}CD4^{-}), 3 PBMC- αβTc (6B11^{-}TCRαβ^{+}CD4^{-}), 6 PBMC-γδT (TCRγδ+TCRαβ-), and 2 PBMC-NK (CD56^{+} TCRαβ^{-}). Cell samples

were sorted using a FACSAria II flow cytometer. Total RNAs were isolated from each cell sample using a miRNeasy Mini Kit (QIAGEN) and delivered to the UCLA TCGB Core to perform Deep RNA sequencing using an Illumina HiSeq3000, following the manufacturer's instructions and the TCGB Core's standard protocol. cDNAs were synthesized using an iScript cDNA Synthesis Kit (1708890, BioRad). Libraries were constructed using an Illumina TruSeq Stranded Total RNA Sample Prep kit and sequenced with 50 bp single-end reads (20 M reads/sample) on an Illumina HiSeq3000. The reads were mapped with STAR 2.5.3a to the human genome (hg38). The counts for each gene were obtained using –quantMode GeneCounts in STAR commands, and the other parameters during alignment were set to default. Data quality was checked using Illumina's proprietary software. Sequencing depth normalized counts were obtained from the differential expression analysis and were used for principal component analysis.

Cell phenotype and function assay. ^{Allo}HSC-eNKT cells and their derivatives (i.e., ^{Allo}BCAR-eNKT, ^{Allo}CAR19-eNKT and ^{IL15}BCAR-eNKT cells) were analyzed in comparison with PBMC-Tc, PBMC-NK, PBMC-iNKT, or/and BCAR-T/CAR19-T cells. The phenotype of these cells was studied using flow cytometry by analyzing cell surface markers including co-receptors (i.e., CD4 and CD8), NK cell receptors (i.e., CD161, NKG2D, DNAM-1, and KIR), memory T cell markers (i.e., CD45RO), and inflammatory tissue/tumor homing markers (i.e., CCR4, CCR5, and CXCR3). The capacity of these cells to produce cytokines (i.e., IFN-γ, TNF-α, and IL-2) and cytotoxic molecules (i.e., perforin and granzyme B) were studied using flow cytometry via intracellular staining. Response of ^{Allo}HSC-eNKT cells to antigen stimulation was studied by culturing ^{Allo}HSC-eNKT cells in vitro in C10 medium for 7 days, in the presence or absence of αGC (100 ng/ml). The proliferation of AlloHSC-iNKT cells was measured by cell counting and flow cytometry

(identified as 6B11+TCRαβ+) over time. Cytokine production was assessed by ELISA analysis of cell culture supernatants collected on day 3 (for human IFN-γ. TNF-α, IL-2, IL-4, and IL-17).

Cell imaging by scanning electron microscope (SEM). The SEM buffer with pH 7.4 was made by 0.1 M Na-phosphate buffer containing 0.1M Sucrose. The cells were rinsed with warm HBSS. Then they were fixed with warm 3% glutaraldehyde in the SEM buffer, moved to 4 degrees, and stored overnight. The next day the cells were washed with SEM buffer 2 times with 5 minutes each time. Next, they were fixed with 2% osmium tetroxide in SEM buffer on ice for 1 hour and then washed with SEM buffer 2 times with 5 minutes each time. The cells were dehydrated with 50%, 70%, 95%, 100%, 100% ethanol successively, 15 minutes each time: The final 100% ethanol was replaced with hexamethyldisilazane and then evaporated in the hood. The processed cells were then ready for Low-vacuum Scanning Electron Microscopy (LV-SEM) which was conducted on a FEI Nova Nano 230 SEM.

***In vitro* tumor killing assay.** Tumor cells (1 x 10^4 cells per well) were co-cultured with effector cells (at ratios indicated in figure legends) in Corning 96-well clear bottom black plates for 8-24 hours, in C10 medium with or without the addition of αGC (100 ng/ml). At the end of culture, live tumor cells were quantified by adding D-luciferin (150 μg/ml; Caliper Life Science) to cell cultures and reading out luciferase activities using an Infinite M1000 microplate reader (Tecan). In experiments for tumor killing mechanism studies, 10 μg/ml of LEAF^{TM} purified anti-human CD1d (Clone 51.1, Biolegend), anti-human DNAM-1 antibody (Clone 11A8, Biolegend), or LEAFTM purified mouse lgG2bk isotype control antibody (Clone MG2B-57, Biolegend) was added.

***In vitro* Mixed Lymphocyte Reaction (MLR) assay: studying Graft-versus-Host (GvH) Response.** PBMCs of multiple healthy donors were irradiated at 2,500 rads and used as stimulators to study the GvH response of ^{Allo}BCAR-iNKT or ^{Allo}CAR19-iNKT cells as responders. PBMC derived BCAR-T, or CAR19-T cells were included as responder controls. Stimulators (5 x 10^5 cells/well) and responders (2 x 10^4 cells/well) were co-cultured in 96-well round-bottom plates in C10 medium for 4 days; the cell culture supernatants were then collected to measure IFN-γ production using ELISA.

***In Vitro* MLR Assay: Studying Host-Versus-Graft (HvG) Response.** PBMCs of multiple healthy donors were used as responders to study the HvG response of ^{Allo}BCAR-iNKT or ^{Allo}CAR19-iNKT cells as stimulators (irradiated at 2,500 rads). PBMC derived BCAR-T, or CAR19-T cells were included as stimulator controls. Stimulators (5 x 10^5 cells/well) and responders (2 x 10^4 cells/well) were co-cultured in 96-well round-bottom plates in C10 medium for 4 days; the cell culture supernatants were then collected to measure IFN-γ production using ELISA.

***In Vitro* MLR Assay: Studying NK Cell-Mediated Allorejection.** PBMC-NK cells isolated from PBMCs of multiple healthy donors were used to study the NK cell-mediated allorejection of ^{Allo}BCAR-iNKT or ^{Allo}CAR19-iNKT cells. Allogeneic BCAR-T or CAR19-T cells were included as controls. PBMC-NK cells (2 x 10^4 cells/well) and the corresponding allogeneic cells (2 x 10^4 cells/well) were co-cultured in 96-well round-bottom plates in C10 medium for 24 hours; the cell cultures were then collected to quantify live cells using flow cytometry.

***In vivo* antitumor efficacy and biodistribution study of ^{Allo}BCAR-iNKT and ^{IL15}BCAR-iNKT: human MM.1S xenograft NSG mouse model.** NSG mice were intravenously inoculated with 1 x 10^6 MM.1S-CD1d-FG or MM.1S-FG cells as indicated on experimental design figure (day 0). To study antitumor efficacy with a single administration of effector cells, on day 7 or 8, the tumor-bearing experimental mice received i.v. injection of vehicle (PBS), ^{Allo}BCAR-iNKT cells (2 x 10^7 CAR^+ cells), or conventional BCAR-T cells (2 x 10^7 CAR^+ cells). To study antitumor efficacy with multiple administration of effector cells, on day 6, the tumor-bearing experimental mice received i.v. Injection of vehicle (PBS), ^{Allo}BCAR-iNKT cells (1 x 10^7 CAR^+ cells), or conventional BCAR-T cells (1 x 10^7 CAR^+ cells), followed by weekly injection with the same dosage. For the study of biodistribution of effector cells under high tumor load conditions, on day 32, ^{Allo}BCAR-iNKT cells (1 x 10^7 CAR^+ cells) or conventional BCAR-T cells (1 x 10^7 CAR^+ cells) were injected into the tumor-bearing mice. To study the antitumor efficacy under high tumor load conditions, on day 15, the tumor-bearing experimental mice received i.v. injection of vehicle (PBS), ^{IL15}BCAR-iNKT cells (2 x 10^7 CAR^+ cells), or conventional BCAR-T cells (2 x 10^7 CAR^+ cells). Over time, experimental mice were monitored for survival, and their tumor loads were measured using BLI. Bleeding was performed if needed through the retro-orbital route.

***In vivo* antitumor efficacy study of ^{Allo}CAR19-iNKT: human NALM-6 xenograft NSG mouse model.** NSG mice were intravenously inoculated with 1 x 10^6 NALM-6-FG cells (day 0). On days 5, 6, and 7, the tumor-bearing experimental mice received i.v. injection of vehicle (PBS), ^{Allo}CAR19-iNKT cells (1 x 10^7 CAR^+ cells), or conventional CAR19-T cells (1 x 10^7 CAR^+ cells). Over time, experimental mice were monitored for survival, and their tumor loads were measured using BLI. Bleeding was performed if needed through the retro-orbital route.

Ganciclovir (GCV) In Vitro and In Vivo Killing Assay. For GCV in vitro killing assay, ^{Allo}HSC-eNKT cells were cultured in C10 medium in the presence of the titrated amount of GCV (0-50 μM) for 4 days; live ^{Allo}HSC-eNKT cells were then counted using flow cytometry with viability staining.

Histopathologic analysis. Heart, liver, kidney, and lung tissues were taken from all experimental mice. Tissue samples were fixed in 10% Neutral Buffered Formalin for up to 36 hours and embedded in paraffin for sectioning (3 μm thickness). After sectioning, tissues were stained either with Hematoxylin and Eosin or anti-human CD3 primary antibodies following standard procedures (UCLA Translational Pathology Core Laboratory, Los Angeles, CA). Stained sections were imaged using an Olympus BX51 upright microscope equipped with an Optronics Macrofire CCD camera (AU Optronics) at 20 x and 40 x magnifications. All images were analyzed using Optronics PictureFrame software (AU Optronics).

Statistics. Statistical analysis using Graphpad Prism 8 software (Graphpad). Pairwise comparisons were made using a 2-tailed Student's T test. Multiple comparisons were performed using an ordinary 1-way ANOVA, followed by Tukey's multiple comparisons test. Kaplan- Meier survival curves were analyzed by log rank (Mantel-Cox) test adjusted for multiple comparisons. Data are presented as the mean ± SEM unless otherwise indicated. In all figures and figure legends, "n" represents the number of samples or animals utilized in the indicated experiments. *P* values less than 0.05 were considered significant. “ns” denotes not significant; * denotes $P < 0.05$; ** denotes $P < 0.01$; *** denotes $P < 0.001$; **** denotes $P < 0.0001$.

Data availability. All data associated with this study are present in the paper or Supplemental Information. The genomics data generated during this study will be available from the public repository Gene Expression Omnibus Database when the manuscript is published.

References for materials and methods

1. Zhu, Y. et al. Development of hematopoietic stem cell-engineered invariant natural killer T cell therapy for cancer. *Cell stem cell* **25**, 542-557. e549 (2019).
2. Smith, D.J. et al. Genetic engineering of hematopoietic stem cells to generate invariant natural killer T cells. *Proceedings of the National Academy of Sciences* **112**, 1523-1528 (2015).
3. Bethune, M.T. et al. Isolation and characterization of NY-ESO-1–specific T cell receptors restricted on various MHC molecules. *Proceedings of the National Academy of Sciences* **115**, E10702-E10711 (2018).

References for the main text

1. June, C.H. & Sadelain, M. Chimeric antigen receptor therapy. *New England Journal of Medicine* **379**, 64-73 (2018).
2. Mikkilineni, L. & Kochenderfer, J.N. Chimeric antigen receptor T-cell therapies for multiple myeloma. *Blood* **130**, 2594-2602 (2017).
3. Rosenberg, S.A. & Restifo, N.P. Adoptive cell transfer as personalized immunotherapy for human cancer. *Science* **348**, 62-68 (2015).
4. Labanieh, L., Majzner, R.G. & Mackall, C.L. Programming CAR-T cells to kill cancer. *Nature biomedical engineering* **2**, 377-391 (2018).
5. Aftab, B.T. et al. Toward "off-the-shelf" allogeneic CAR T cells. *Advances in Cell and Gene Therapy* **3**, e86 (2020).
6. Depil, S., Duchateau, P., Grupp, S., Mufti, G. & Poirot, L. 'Off-the-shelf'allogeneic CAR T cells: development and challenges. *Nature Reviews Drug Discovery* **19**, 185-199 (2020).
7. Caldwell, K.J., Gottschalk, S. & Talleur, A.C. Allogeneic CAR Cell Therapy—More Than a Pipe Dream. *Frontiers in immunology* **11**, 3466 (2021).
8. Godfrey, D.I., Le Nours, J., Andrews, D.M., Uldrich, A.P. & Rossjohn, J. Unconventional T cell targets for cancer immunotherapy. *Immunity* **48**, 453-473 (2018).
9. Chandra, S. & Kronenberg, M. Activation and function of iNKT and MAIT cells. *Advances in immunology* **127**, 145-201 (2015).
10. Bae, E.-A., Seo, H., Kim, I.-K., Jeon, I. & Kang, C.-Y. Roles of NKT cells in cancer immunotherapy. *Archives of pharmacal research* **42**, 543-548 (2019).
11. Chaidos, A. et al. Graft invariant natural killer T-cell dose predicts risk of acute graft-versus-host disease in allogeneic hematopoietic stem cell transplantation. *Blood, The Journal of the American Society of Hematology* **119**, 5030-5036 (2012).
12. Exley, M.A. et al. Adoptive transfer of invariant NKT cells as immunotherapy for advanced melanoma: a phase I clinical trial. *Clinical Cancer Research* **23**, 3510-3519 (2017).
13. Zhu, Y. et al. Development of hematopoietic stem cell-engineered invariant natural killer T cell therapy for cancer. *Cell stem cell* **25**, 542-557. e549 (2019).
14. Shukla, S. et al. Progenitor T-cell differentiation from hematopoietic stem cells using Delta-like-4 and VCAM-1. *Nature Methods* **14**, 531-538 (2017).
15. Iriguchi, S. et al. A clinically applicable and scalable method to regenerate T-cells from iPSCs for off-the-shelf T-cell immunotherapy. *Nature Communications* **12**, 1-15 (2021).

16. Huijskens, M.J. et al. Technical Advance: Ascorbic acid induces development of double-positive T cells from human hematopoietic stem cells in the absence of stromal cells. *Journal of leukocyte biology* **96**, 1165-1175 (2014).
17. Themeli, M. et al. Generation of tumor-targeted human T lymphocytes from induced pluripotent stem cells for cancer therapy. *Nature biotechnology* **31**, 928-933 (2013).
18. La Motte-Mohs, R.N., Herer, E. & Zúñiga-Pflücker, J.C. Induction of T-cell development from human cord blood hematopoietic stem cells by Delta-like 1 in vitro. *Blood* **105**, 1431-1439 (2005).
19. Reimann, C. et al. Human T-Lymphoid Progenitors Generated in a Feeder-Cell-Free Delta-Like-4 Culture System Promote T-Cell Reconstitution in NOD/SCID/γc−/− Mice. *Stem Cells* **30**, 1771-1780 (2012).
20. Li, Y., Hermanson, D.L., Moriarity, B.S. & Kaufman, D.S. Human iPSC-derived natural killer cells engineered with chimeric antigen receptors enhance anti-tumor activity. *Cell stem cell* **23**, 181-192. e185 (2018).
21. Alonzo, E.S. & Sant'Angelo, D.B. Development of PLZF-expressing innate T cells. *Current opinion in immunology* **23**, 220-227 (2011).
22. Zhang, Y., Zhang, Y., Gu, W. & Sun, B. TH1/TH2 cell differentiation and molecular signals. *T Helper Cell Differentiation and Their Function*, 15-44 (2014).
23. Gagliani, N. & Huber, S. Basic aspects of T helper cell differentiation. *T-Cell Differentiation*, 19-30 (2017).
24. Ozdemir, Z.N. & Bozdağ, S.C. Graft failure after allogeneic hematopoietic stem cell transplantation. *Transfusion and Apheresis Science* **57**, 163-167 (2018).
25. Fujii, S.-i. et al. NKT cells as an ideal anti-tumor immunotherapeutic. *Frontiers in immunology* **4**, 409 (2013).
26. Perez, C., Gruber, I. & Arber, C. Off-the-Shelf Allogeneic T Cell Therapies for Cancer: Opportunities and Challenges Using Naturally Occurring "Universal" Donor T Cells. *Frontiers in Immunology* **11** (2020).
27. Gordy, L.E. et al. IL-15 regulates homeostasis and terminal maturation of NKT cells. *The Journal of Immunology* **187**, 6335-6345 (2011).
28. Xu, X. et al. NKT cells coexpressing a GD2-specific chimeric antigen receptor and IL15 show enhanced in vivo persistence and antitumor activity against neuroblastoma. *Clinical Cancer Research* **25**, 7126-7138 (2019).
29. Heczey, A. et al. Anti-GD2 CAR-NKT cells in patients with relapsed or refractory neuroblastoma: an interim analysis. *Nature Medicine* **26**, 1686-1690 (2020).

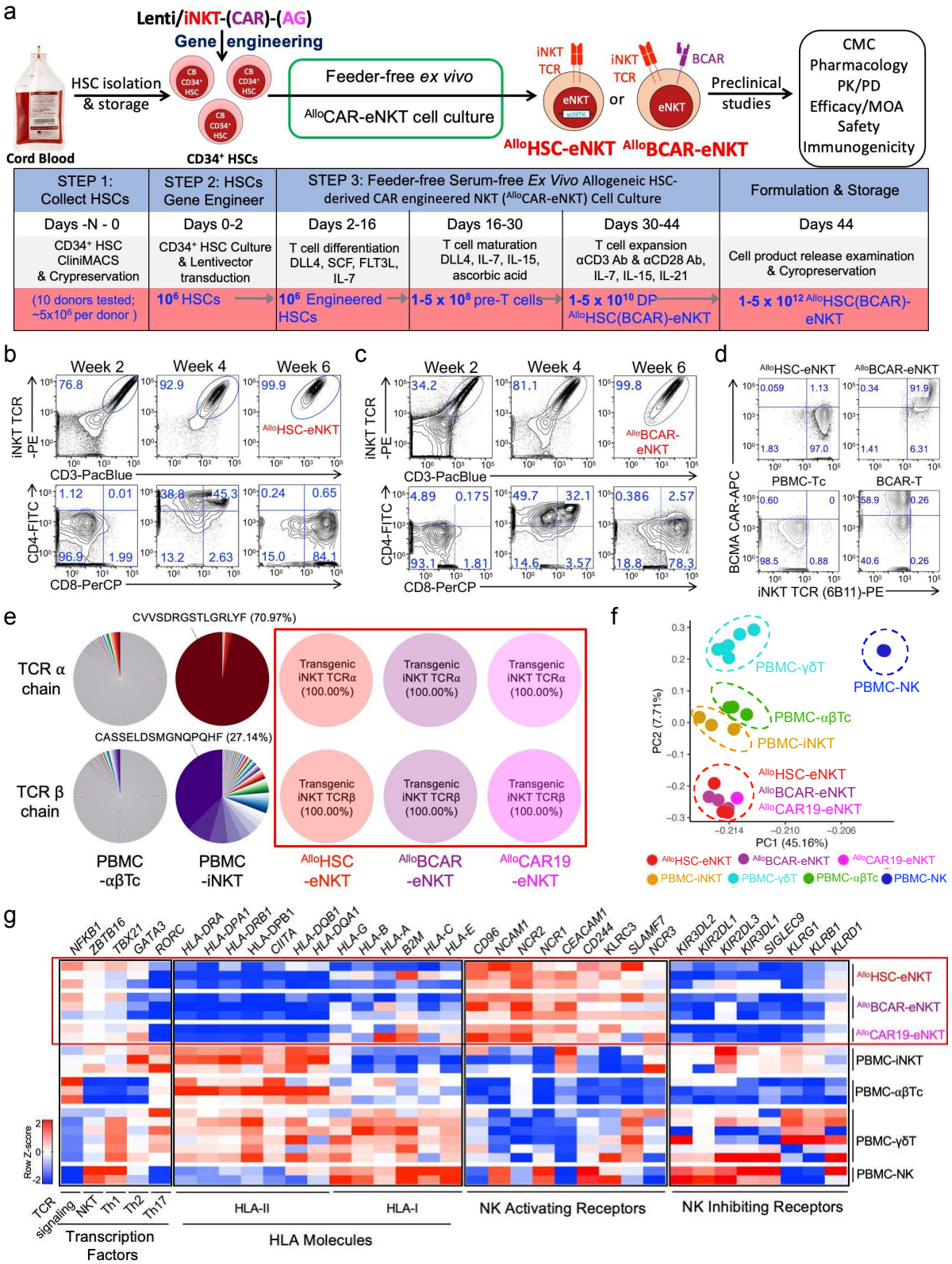

Figure 1. The generation and gene profiling of allogeneic NKT (AlloHSC-eNKT) and allogeneic CAR NKT (AlloCAR) cells (AlloCAR-eNKT).

Figure 1. The generation and gene profiling of allogeneic NKT (^{Allo}HSC-eNKT) and allogeneic CAR NKT (^{Allo}CAR-eNKT) cells.

(A) Schematic design of *ex vivo* allogeneic HSC-derived CAR-engineered NKT (^{Allo}CAR-eNKT) cell culture with cell yield at various stages.

(b) Representative kinetics of ^{Allo}HSC-eNKT cell development from iNKT-sr39TK (Tricistronic) vector modified CB CD34^{+} HSCs and CD4/CD8 co-receptors expression at the indicated weeks and stage of the culture. ^{Allo}HSC-eNKT cells were gated as CD45^{+}6B11^{+}CD3^{+}.

(c) Representative kinetics of ^{Allo}BCAR-eNKT cell development from iNKT-BCAR (Tricistronic) vector modified CB CD34^{+} HSCs and CD4/CD8 co-receptors expression at the indicated weeks and stage. ^{Allo}BCAR-eNKT cells were gated as CD45^{+}6B11^{+}CD3^{+}.

(d) Flow plots showing the CAR and iNKT TCR expression of ^{Allo}HSC-eNKT and ^{Allo}BCAR-eNKT in comparison to PBMC derived conventional t (PBMC-Tc) cells and BCAR-T cells.

(e) Single-cell sequencing analysis of TCR Vα and Vβ CDR3 VDJ sequences of ^{Allo}HSC-eNKT, ^{Allo}BCAR-eNKT, ^{Allo}CAR19-eNKT, PBMC-iNKT, and PBMC-Tc cells. The relative abundance of each unique t cell receptor sequence among the total unique sequences identified for the sample is represented by a pie slice.

(f-g) Gene profiling of ^{Allo}HSC-eNKT, ^{Allo}BCAR-eNKT and ^{Allo}CAR19-eNKT cells. (f) Principal component analysis of gene expression for six cell types. Each symbol shape represents an individual biological replicate for the corresponding cell type. Shown is the ordination using the first two principal components PC1 and PC2. (g) Heat map of selected gene expression profiles related to transcription factors, HLA molecules, NK activating receptors and NK inhibitory receptors for seven cell groups. Each row represents one biological repeat. Levels of mRNA expression were determined using RNA sequencing. Red and blue indicate increased and decreased expressions, respectively.

Representative of over 10 (a-d), 3 (e) and 2(f-g) experiments.

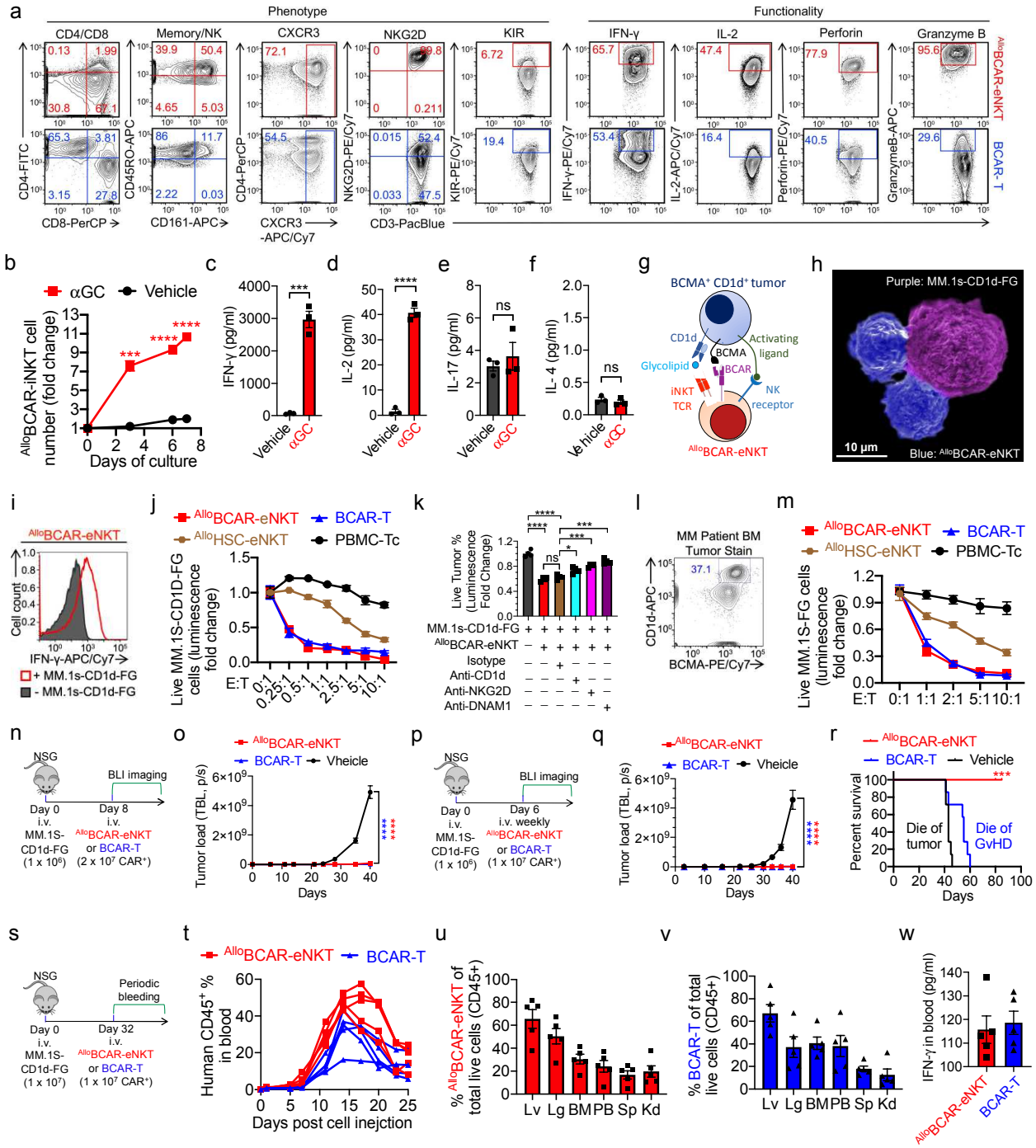

Figure 2. Characterization of AlloBCAR-eNKT cells - phenotype, antitumor efficacy, and mechanism of action (MOA)

Figure 2. Characterization of ^{Allo}BCAR-eNKT cells - phenotype, antitumor efficacy, and mechanism of action (MOA)

(a)FACS analyses showing the expression of surface markers and the production of intracellular cytokines and cytotoxic molecules from ^{Allo}BCAR-eNKT cells compared to conventional BCAR-T cells.
(b-f) Antigen responses of ^{Allo}BAR-eNKT cells. ^{Allo}BCAR-eNKT cells were expanded in the presence or absence of αGC for 7 days. (b) Growth curve of ^{Allo}BCAR-eNKT expansion over time (n=3). (c-f) Cytokine production of ^{Allo}BCAR-eNKT cells measure through ELISA responding to αGC stimulation.
(g) Schematic showing the NK/TCR/CAR-mediated triple tumor killing mechanisms performed by ^{Allo}BCAR-eNKT cells.
(h) Scanning electron microscope (SEM) image of ^{Allo}BCAR-eNKT attacking MM.1s-hCD1d-FG cells *in vitro*.
(i-m) Studying the tumor killing of human multiple myeloma MM.1s-hCD1d-FG cells by ^{Allo}BCAR-eNKT cells. (i) FACS analysis showing the intracellular production of IFNγ with or without MM.1s-hCD1d-FG coculture. (j) Tumor killing titration of indicated effector against MM.1s-hCD1d-FG (n=4) (E:T = effector cell :tumor). (k) Tumor killing mechanisms of ^{Allo}BCAR-eNKT cells. CD1d, NKG2D and DNAM-1 mediated pathways were studied. Tumor cell killing was analyzed at 24-hours post co-culture. (i) FACS plot showing BCMA and CD1d expression of MM patient BM sample. (m) Tumor killing titration of indicated effector cells against MM.1s-FG cells (n=4).
(n-w) Studying *in vivo* anti-tumor efficacy of ^{Allo}BCAR-eNKT cells against hematologic malignancies in MM.1s-CD1d-FG human multiple myeloma xenograft NSG mouse model. (n-o) *In vivo* study with single administration remedy. (n) Experimental design. (o) Tumor loads measured by BLI in experimental mice over time (n=5). (p-r) *In vivo* study with weekly administration remedy. (p) Experimental design. (q) Tumor loads measured by BLI in experimental mice over time (n=5). (r) Kaplan-Meier analysis of mouse survival rate (n=5). (s-w) Biodistribution of ^{Allo}BCAR-eNKT cells in MM.1S-hCD1d-FG human multiple myeloma xenograft NSG mouse model (n=5). (s) Experimental design. (t) Human CD45^{+} cell dynamics in the peripheral blood of ^{Allo}BCAR-eNKT treated mice over time. (u) Quantification showing the percentage of ^{Allo}BCAR-eNKT cells in various tissues of tumor bearing mice (n=5). (v) Quantification showing the percentage of BCAR-T cells in various tissues of tumor bearing mice (n=5). (w) ELISA measurement of IFN-γ in the peripheral blood of indicated cell treated MM bearing mice at day 13 (n=5).
Representative of 5 (a), 3 (b-w) experiments. Data are presented as the mean ± SEM. ns, not significant, *p<0.05, **p<0.01, **p<0.001, ****p<0.0001, by Student's *t* test (C-F), or by 1-way ANOVA (b,l,o,q), or by log rank (Mantel-Cox) test adjusted for multiple comparisons (r).

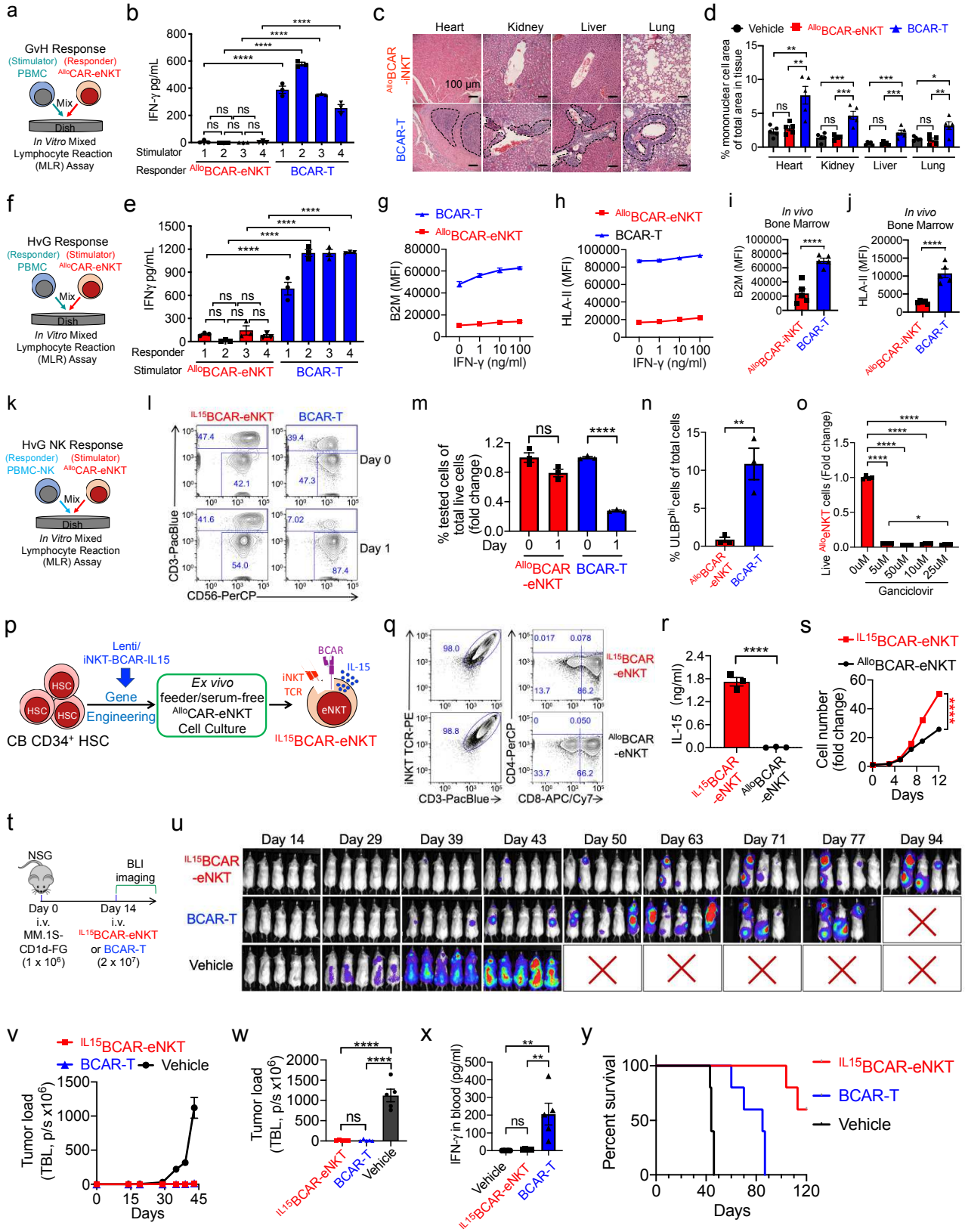

Figure 3. Characterization of alloBCAR-eNKT cells – safety, immunogenicity, and additional modifications

Figue 3. Characterization of ^{Allo}BCAR-eNKT cells – safety, immunogenicity, and additional modifications.

(a-b) An *in vitro* mixed lymphocyte (MLR) assay for the study of graft versus host (GvH) responses of ^{Allo}BCAR-eNKT cells in comparison with conventional BCAR-T cells. (a) Experimental design. (b) ELISA analysis of IFN-γ in the supernatants of MLR assay (n=4). PBMCs from 4 different healthy donors were included as stimulators.

(c-d) Histology analysis of tissue sections from MM.1s-CD1d-FG bearing mice experimental mice post corresponding effector cell treatment. (c) Hematoxylin and eosin (H&E) staining. Heavy mononuclear cell infiltrated area is highlighted with dash line. (d) Quantification of (c).

(f-j) Immunogenicity study of ^{Allo}BCAR-eNKT in comparison with BCAR-T. (f-e) An MLR assay for the study of host versus graft (HvG) response. (f) Experimental design. (e) ELISA analysis of IFN-γ in the supernatants of MLR assay (n=4). PBMCs from 4 different healthy donors were included as responders. (g-h) *In vitro* HLA-I (B2M) and HLA-II expression on indicated cells in response to IFN-γ coculture. (i-j) *In vivo* HLA-I (B2M) and HLA-II expression on indicated cells isolated from bone marrow of MM.1s-CD1d-FG tumor bearing mice (n=5).

(k-n) Studying allogenic NK cell response against ^{Allo}BCAR-eNKT cells using an in vitro MLR assay. ^{Allo}BCAR-eNKT cells were co-cultured with donor-mismatched PBMC-NK cells. BCAR-T cells were included as controls. (k) Experimental design. (l) FACS analyses of the indicated cells at day 0 and 1. (m) Quantification of (l) (n=3). (n) FACS analyses of ULBP
expression on the indicated cells (n=3).

(o) Functional test of suicide gene sr39TK as an additional safety mechanism. *In vitro* ganciclovir killing assay. ^{Allo}HSC-eNKT cells were cultured in vitro in the presence of gradient concentrations of GCV for 3 days, followed by quantification of live cells via FACS analysis(n=4).

(p-y)The generation and characterization of IL15 enhanced BCAR NKT (^{IL15}BCAR-eNKT) cells. (p) Schematic design to generate ^{IL15}BCAR-eNKT cells in an *ex vivo* culture system. (q) FACS characterization of ^{IL15}BCAR-eNKT cells in comparison with ^{Allo}BCAR-eNKT. (r) ELISA analysis of IL-15 production of indicated cells at day 2 post αGC stimulation. (s) Growth curve of ^{IL15}BCAR-eNKT cells in comparison with ^{Allo}BCAR-eNKT in a feeder-free expansion culture. (t-y) Studying *in vivo* anti-tumor efficacy of ^{IL15}BCAR-eNKT cells against hematologic malignancies in MM.1S-hCD1d-FG human multiple myeloma xenograft NSG mouse model. (t) Experimental design. (u) Tumor loads measured by BLI in experimental mice over time (n=5). (v) Quantification of (u) (n=5). (w) BLI measurement comparison of indicated groups at day 43. (x) IFN-γ in the plasma of peripheral blood measured by ELISA at day 35 post therapeutic cell infusion. Severe CRS can be observed in BCAR-T cells treated mice. (y) Kaplan-Meier analysis of mouse survival rate (n=5).

Representative of 3 experiments. Data are presented as the mean ± SEM. ns, not significant, *p<0.05, **p<0.01, **p<0.001, ****p<0.0001, by 1-way ANOVA (B-D,H-I, k,r,t m and k), by Student's *t* test (e,f,n,q), or by log rank (Mantel-Cox) test adjusted for multiple comparisons (u).

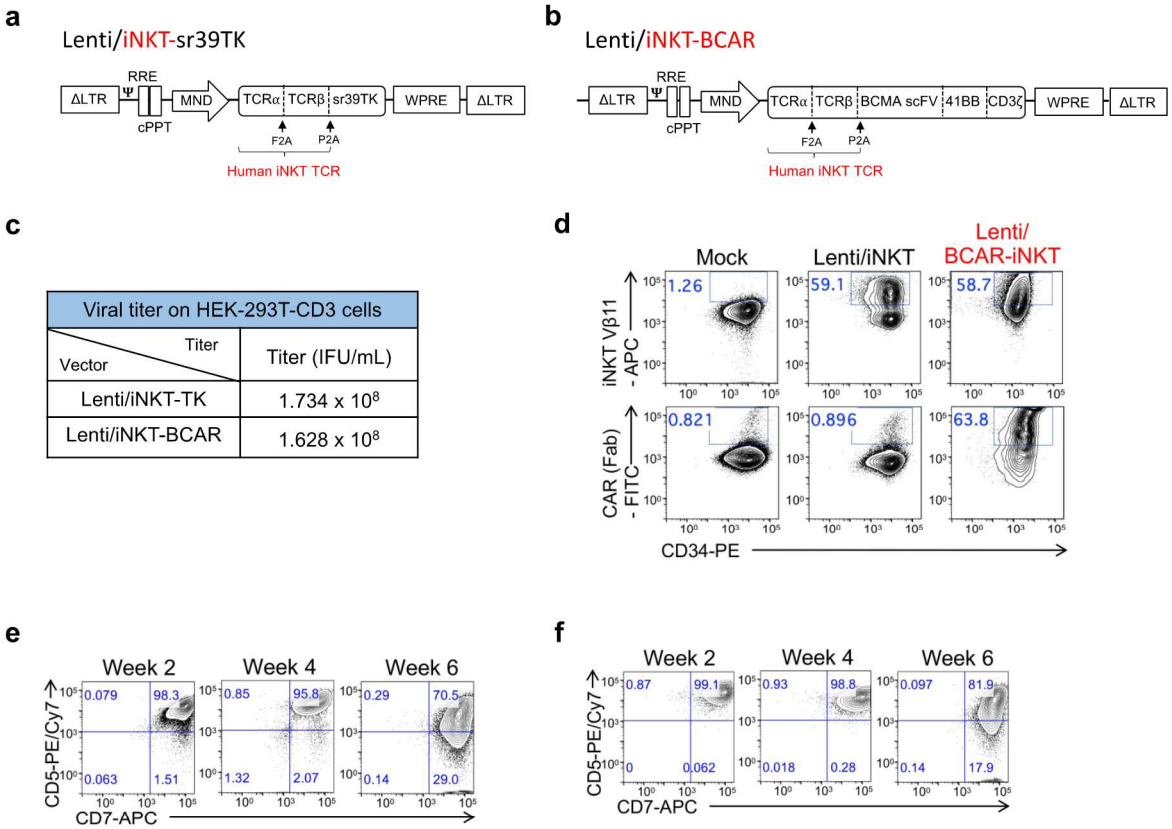

Viral titer on HEK-293T-CD3 cells	
Vector \ Titer	Titer (IFU/mL)
Lenti/iNKT-TK	1.734×10^8
Lenti/iNKT-BCAR	1.628×10^8

Supplementary figure 1. The generation and development of ^{Allo}HSC-eNKT and ^{Allo}BCAR-eNKT cells; related to figure 1.

(a) Schematics of tricistronic iNKT TCR-sr39TK lentivector design

(b) Schematics of tricistronic iNKT-BCAR lentivectors design

(c) Representative titer of lentivirus packaged with indicated vectors

(d) FACS detection of intracellular expression of iNKT-TCR (identified as CD34$^+$vβ11$^+$) and BCAR expression (identified as CD34$^+$ Fab$^+$) in CD34$^+$ CB HSC 72 hours post lentivector transduction with un-transduced CD34$^+$ CB HSC as a mock control.

(e) Representative kinetics of ^{Allo}HSC-eNKT cell development and differentiation from CD34$^+$ HSCs at the indicated weeks. ^{Allo}HSC-eNKT cells were gated as 6B11$^+$CD3$^+$.

(f) Representative kinetics of ^{Allo}BCAR-eNKT cell development from Lenti/iNKT-BCAR vector modified CB CD34$^+$ HSCs. ^{Allo}BCAR-eNKT cells were gated as 6B11$^+$CD3.

Representative of 3 (c-d), over 10 (e-f) experiments.

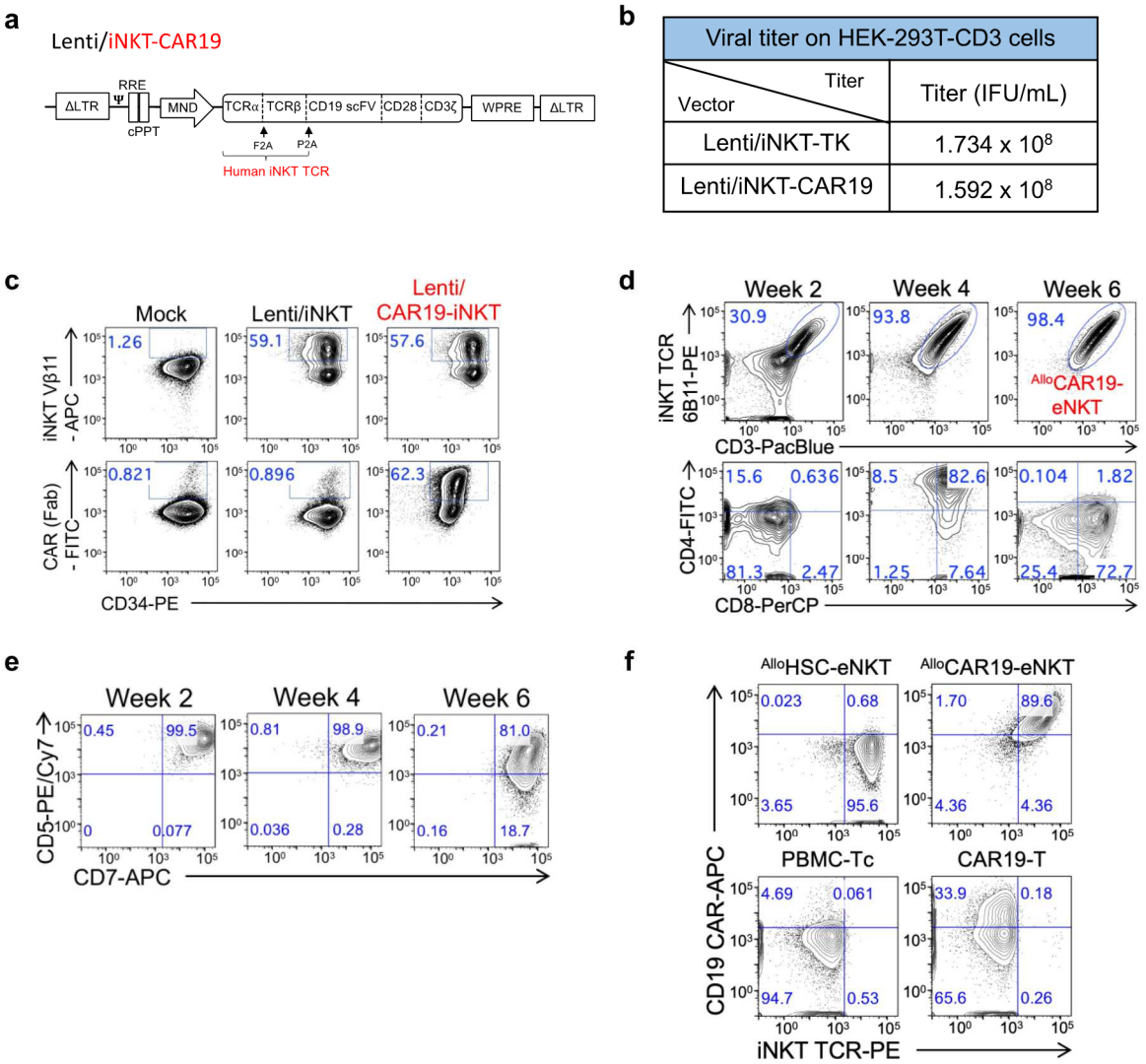

Viral titer on HEK-293T-CD3 cells	
Vector \ Titer	Titer (IFU/mL)
Lenti/iNKT-TK	1.734×10^8
Lenti/iNKT-CAR19	1.592×10^8

Supplementary figure 2. The generation and phenotype of ^{Allo}CAR19-eNKT Cells; related to figure 1.
(a) Schematics of iNKT TCR-CAR19 lentivector design
(b) Representative titer of lentivirus packaged with indicated vectors
(c) FACS detection of intracellular expression of iNKT-TCR (vβ11$^+$) and CAR19 expression (Fab$^+$) of indicated vector transduced cells in CD34$^+$ CB HSC 72 hours post lentivector transduction (Un-transduced CD34$^+$ CB HSC as a mock control).
(d) Representative kinetics of ^{Allo}CAR19-eNKT cell development from iNKT-CAR19 lentivector modified CB CD34$^+$ HSCs and CD4/CD8 co-receptors expression at the indicated weeks and stage of the culture. ^{Allo}CAR19-eNKT cells were gated as 6B11$^+$CD3.
(e) Representative kinetics of ^{Allo}CAR19-eNKT cell development from iNKT-CAR19 (Bicistronic) vector modified CB CD34$^+$ HSCs and CD5/CD7 expression at the indicated weeks and stage of the culture. ^{Allo}CAR19-eNKT cells were gated as 6B11$^+$CD3.
(f) FACS analyses showing the co-expression of iNKT TCR and CD19 CAR on ^{Allo}CAR19-eNKT cells. Representative of 3 (b-c), 4 (d-f) experiments.

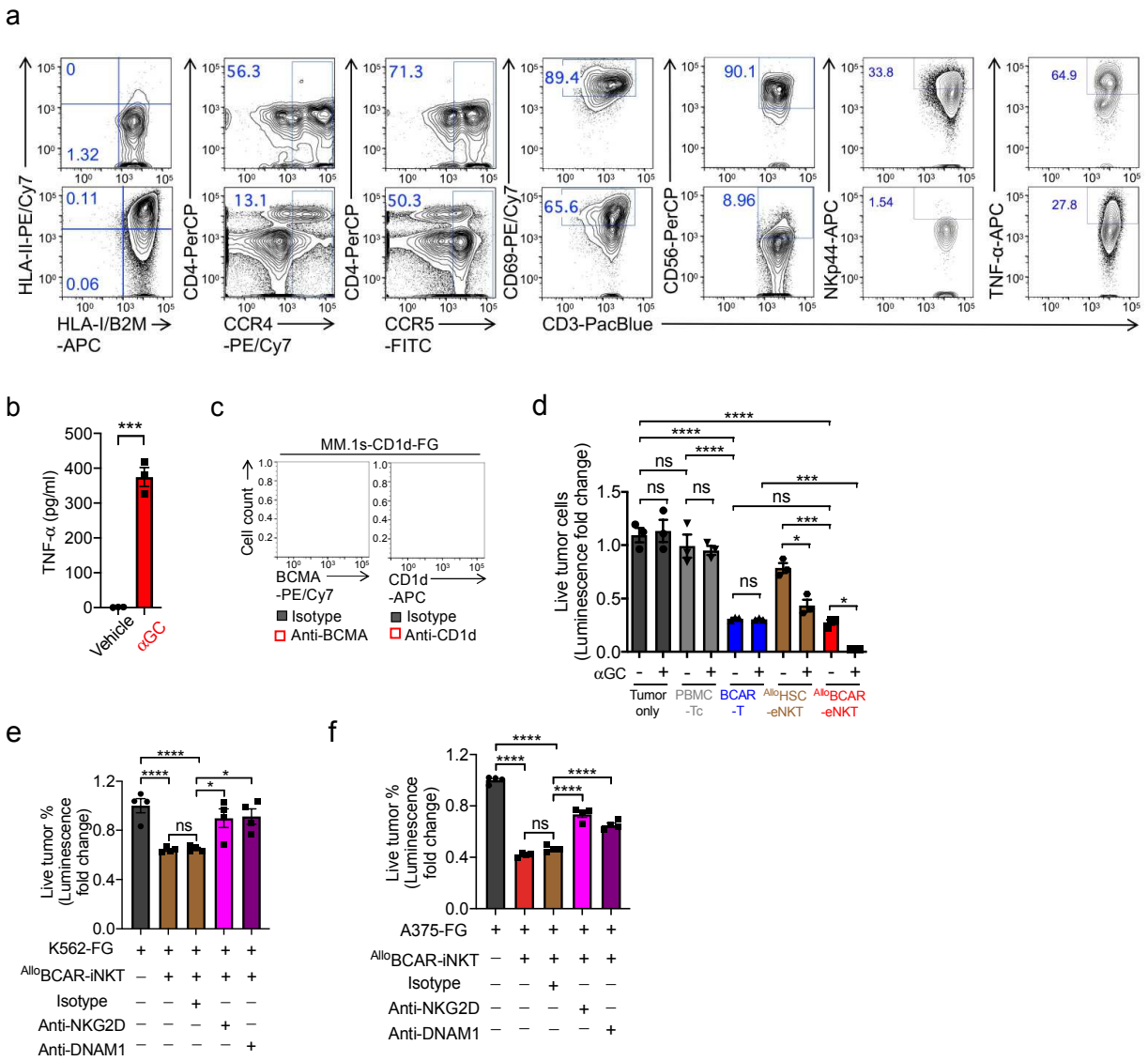

Supplementary figure 3. *In vitro* efficacy and MOA study- ^{Allo}BCAR-eNKT cells; related to figure 2.
(a) FACS plots showing the expression of surface markers from ^{Allo}BCAR-eNKT cells (identified as 6B11^{+}CD3^{+}), compared to BCAR-T cells (identified as 6B11^{-}CD3^{+}Fab^{+}).
(b) Antigen responses of ^{Allo}BCAR-eNKT cells. ELISA analysis of TNF-α production (n=3).
(c) The generation of human multiple melanoma cell line that co-expresses BCMA and CD1d. FACS plots showing the expression of BCMA and CD1d on the engineered MM.1s-CD1d-FG line.
(d) In vitro killing of MM.1S-CD1d-FG human multiple myeloma cells by ^{Allo}BCAR-eNKT cells with titrated e:t ratio compared to that of conventional BCAR-T cells (n = 4).
(e) In vitro killing of K562-FG human leukemia cells by ^{Allo}BCAR-eNKT cells through an antigen independent pathway (n = 4).
(f) In vitro killing of A375-FG human melanoma cells by ^{Allo}BCAR-eNKT cells through an antigen independent pathway (n = 4).
Representative of 3 experiments. Data are presented as the mean ± SEM. ns, not significant, *p < 0.05, **p < 0.01, ***p < 0.001, ****p < 0.0001, by Student's t test (b), or by 1-way ANOVA (D-F) .

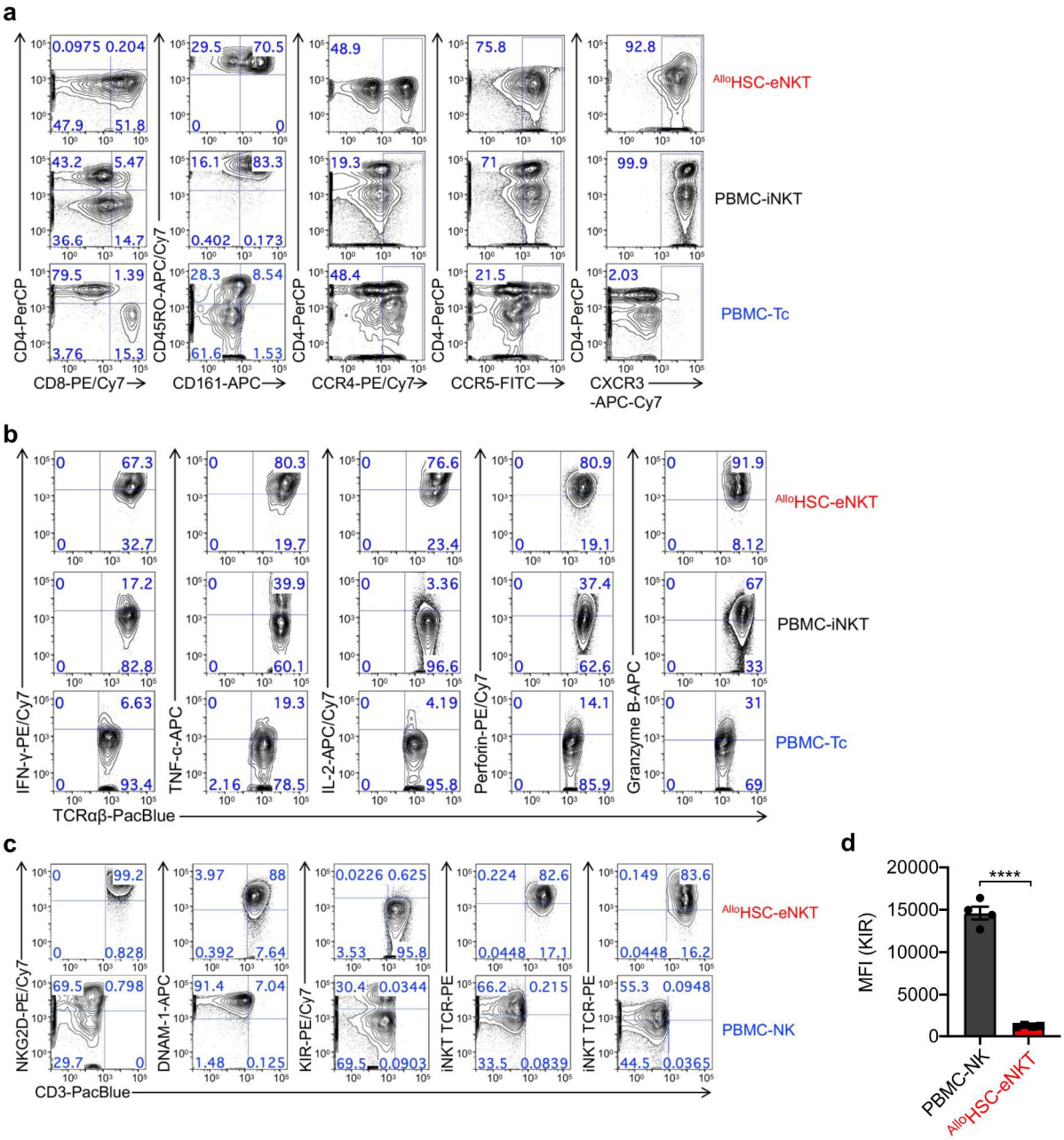

Supplementary figure 4. Phenotype and functionality of AlloHSC-eNKT Cells; related to figure 2.
(a) FACS plots showing the expression of surface markers from HSC-eNKT cells (identified as CD45$^+$6B11$^+$TCRαβ$^+$), compared to PBMC-iNKT cells (identified as CD45$^+$6B11$^+$TCRαβ$^+$) and conventional PBMC -t (identified as CD45$^+$6B11$^-$TCRαβ+).
(b) FACS plots showing the functionality of AlloHSC-eNKT cells (identified as CD45$^+$6B11$^+$TCRαβ$^+$), compared to PBMC-iNKT cells (identified as CD45$^+$6B11$^+$TCRαβ$^+$) and conventional PBMC -t (identified as CD45$^+$6B11$^-$TCRαβ+).
(c) FACS plots showing the expression of NK markers of AlloHSC-eNKT cells (identified as CD45$^+$6B11$^+$TCRαβ$^+$), compared to PBMC-NK cells (identified as CD45$^+$CD56$^+$TCRαβ$^-$). (d)Quantification of NK inhibitor KIR MFI
(d) *In vitro* KIR expression on AlloHSC-eNKT cells in comparison with PBMC-NK cells.
Representative of 3 experiments. Data are presented as the mean ± SEM. ns, not significant, *p < 0.05, **p < 0.01, ***p < 0.001, ****p < 0.0001, by Student's t test (d).

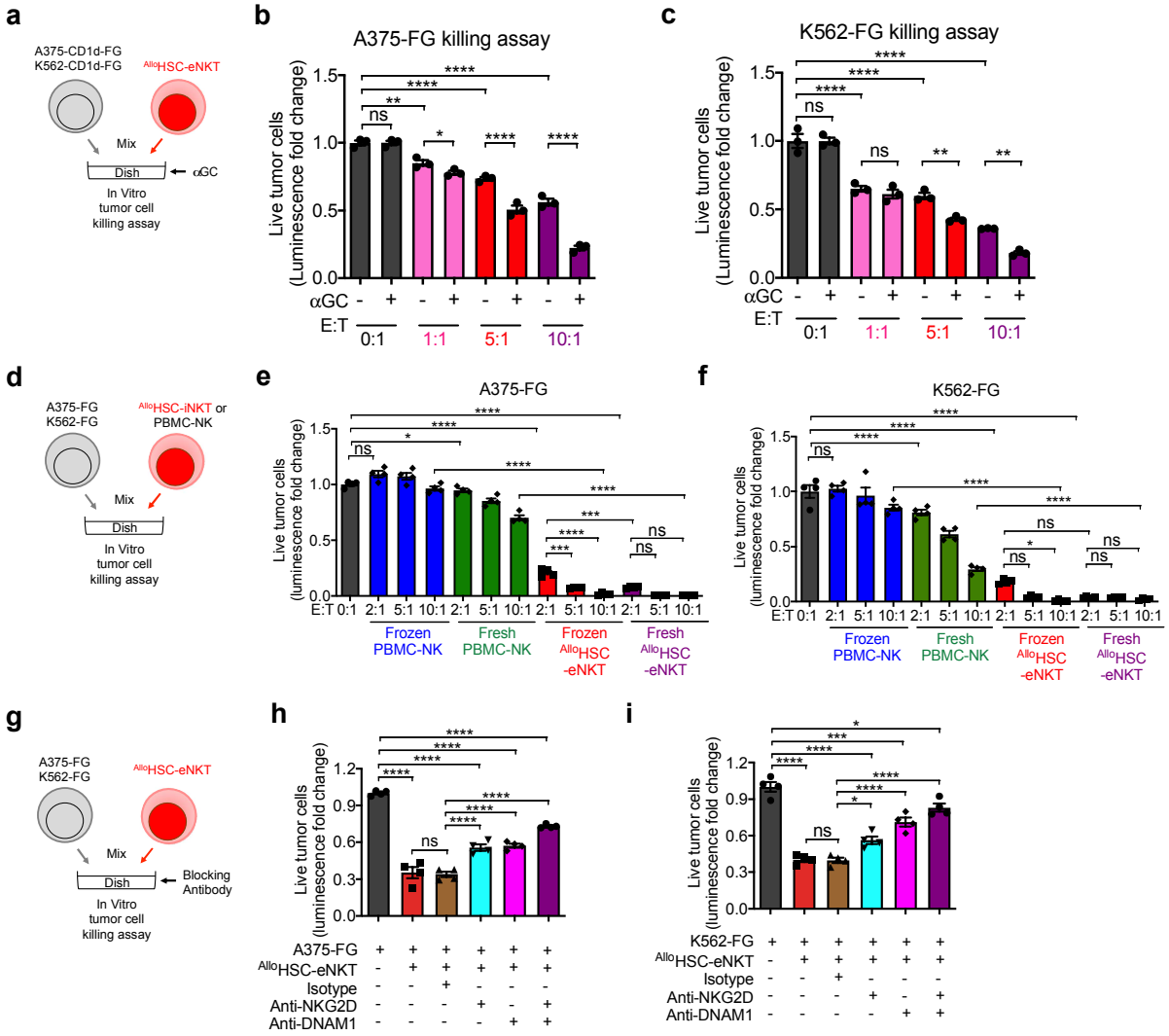

Supplementary figure 5. *In vitro* efficacy and MOA study- AlloHSC-eNKT cells; related to figure 2.
(a-c) CD1d-dependent tumor killing by AlloHSC-eNKT in response to αGC. (a) Experimental design. (b) *In vitro* killing of A375-CD1d-FG human melanoma cells by AlloHSC-eNKT cells (n = 3). (c) *In vitro* killing of K562-CD1d-FG human leukemia cells by AlloHSC-eNKT cells (n = 3).
(d-f) *In vitro* tumor killing by AlloHSC-eNKT cells through an antigen independent pathway in comparison with PBMC-NK. (d) Experimental design. (e) *In vitro* killing of A375-CD1d-FG human melanoma cells by AlloHSC-eNKT cells (n = 4). (f) *In vitro* killing of K562-CD1d-FG human leukemia cells by AlloHSC-eNKT cells (n = 4).
(g-i) Study of NK killing mechanism of AlloHSC-eNKT. NKG2D and DNAM-1 mediated pathways were studied. Tumor cell killing was analyzed at 24-hours post co-culture. (g) Experimental design. (h) *In vitro* killing of A375-CD1d-FG human melanoma cells by AlloHSC-eNKT cells (n = 4). (i) *In vitro* killing of K562-CD1d-FG human leukemia cells by AlloHSC-eNKT cells (n = 4).
Note that AlloHSC-eNKT cells effectively killed multiple types of human cancer cells using both TCR-dependent and TCR-independent (i.e., via NK path) mechanisms.
Representative of 3 experiments. data are presented as the mean ± SEM. ns, not significant, *p < 0.05, **p < 0.01, ***p < 0.001, ****p < 0.0001, by 1-way ANOVA.

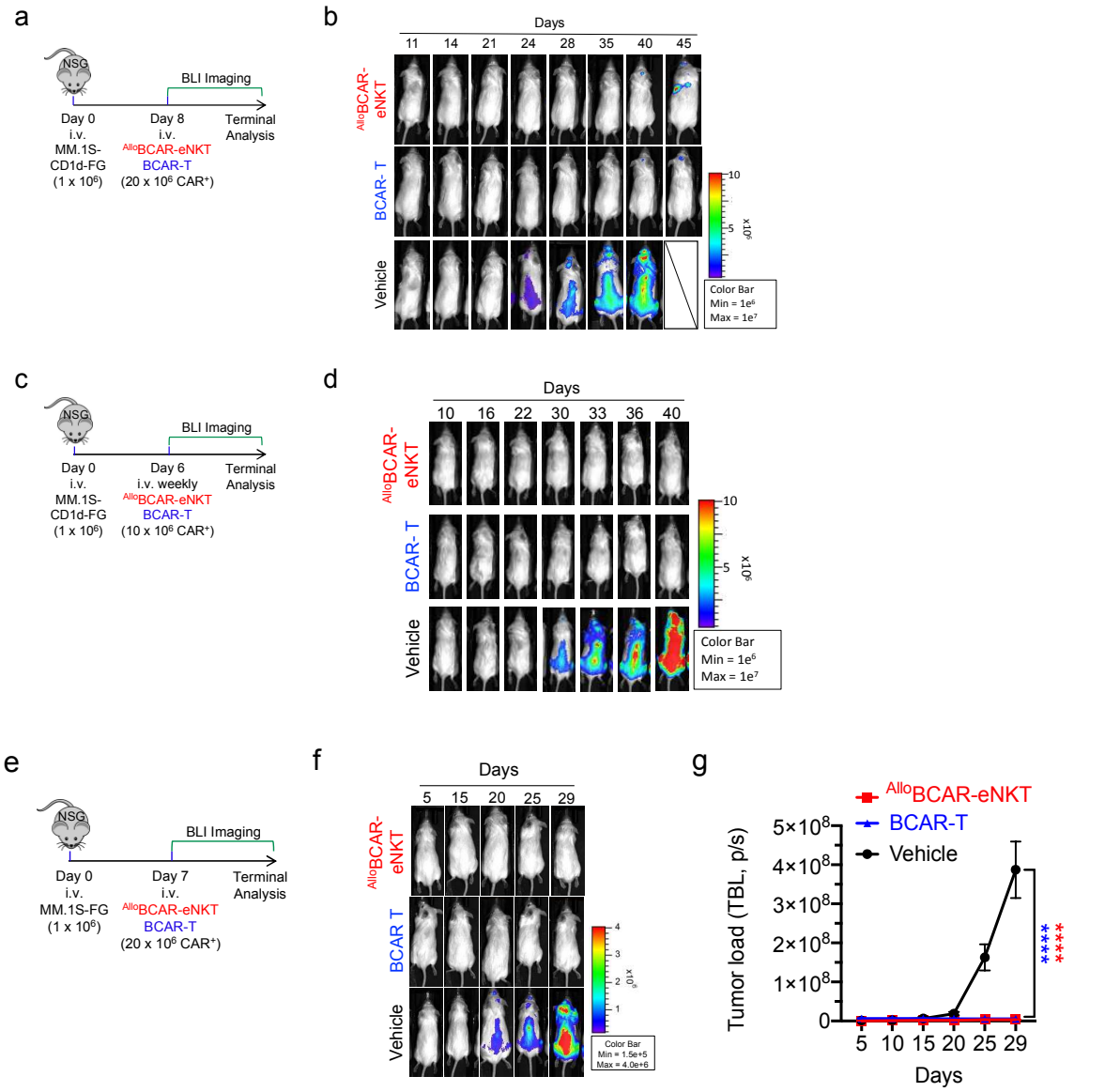

Supplementary figure 6. *In vivo* anti-tumor capacity of AlloBCAR-eNKT, related to figure 2.
(a-b) Studying the *in vivo* antitumor capacity of AlloBCAR-eNKT cells with single administration remedy. (a) Experimental design. (b) Representative BLI images measuring the tumor loads in experimental mice over time.
(c-d) Studying the *in vivo* antitumor capacity of AlloBCAR-eNKT cells with weekly administration remedy. (c) Experimental design. (d) Representative BLI images measuring the tumor loads in experimental mice over time.
(e-g) Studying the *in vivo* antitumor capacity of AlloBCAR-eNKT against MM.1s-FG. (e) Experimental design. (f) Tumor loads measured by BLI in experimental mice over time. (g) Quantification of (f) (n=5). Representative of 3 experiments. Data are presented as the mean ± SEM. ns, not significant, *$p < 0.05$, ***$p < 0.001$, ****$p < 0.0001$, by 1-way ANOVA (j).

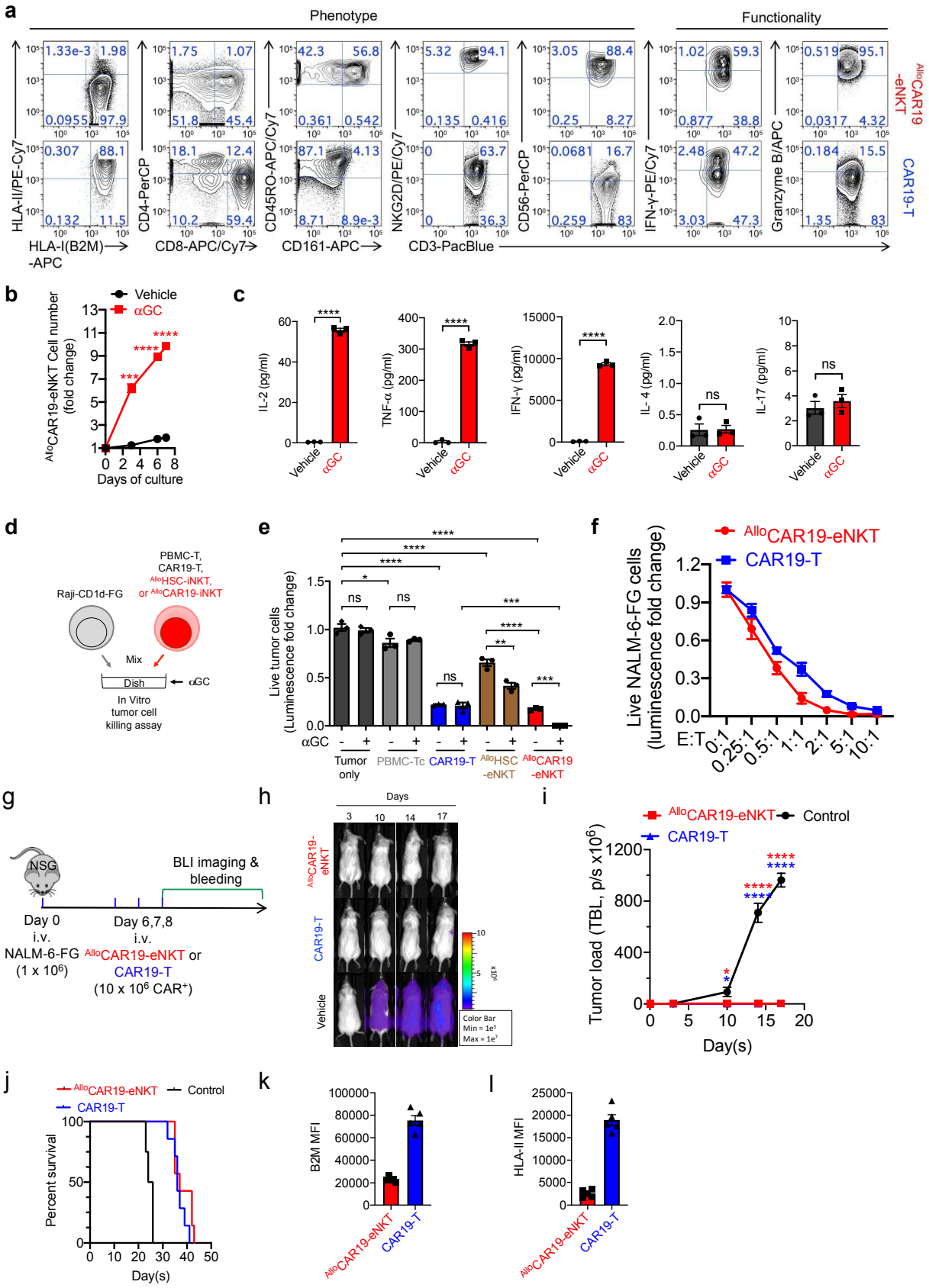
a
Phenotype
Functionality
HLA-II/PE-Cy7
HLA-I(B2M)→ -APC
CD4-PerCP
CD8-APC/Cy7→
CD45RO-APC/Cy7
CD161-APC→
NKG2D/PE/Cy7
CD3-PacBlue
CD56-PerCP
IFN-γ-PE/Cy7
Granzyme B/APC
AlloCAR19 -eNKT
CAR19-T
b
Vehicle
αGC
AlloCAR19-eNKT Cell number (fold change)
Days of culture
c
IL-2 (pg/ml)
TNF-α (pg/ml)
IFN-γ (pg/ml)
IL- 4 (pg/ml)
IL-17 (pg/ml)
ns
d
Raji-CD1d-FG
PBMC-T, CAR19-T, AlloHSC-iNKT, or AlloCAR19-iNKT
Mix
Dish
αGC
In Vitro tumor cell killing assay
e
Live tumor cells (Luminescence fold change)
αGC
Tumor only
PBMC-Tc
CAR19-T
AlloHSC -eNKT
AlloCAR19 -eNKT
f
AlloCAR19-eNKT
CAR19-T
Live NALM-6-FG cells (luminescence fold change)
E:T
0:1
0.25:1
0.5:1
1:1
2:1
5:1
10:1
g
NSG
BLI imaging & bleeding
Day 0
i.v.
NALM-6-FG
(1 x 10^6)
Day 6,7,8
i.v.
AlloCAR19-eNKT or
CAR19-T
(10 x 10^6 CAR+)
h
Days
3
10
14
17
AlloCAR19-eNKT
CAR19-T
Vehicle
Color Bar
Min = 1e5
Max = 1e7
i
AlloCAR19-eNKT
Control
CAR19-T
Tumor load (TBL, p/s x10^6)
Day(s)
j
AlloCAR19-eNKT
Control
CAR19-T
Percent survival
Day(s)
k
B2M MFI
AlloCAR19-eNKT
CAR19-T
l
HLA-II MFI
AlloCAR19-eNKT
CAR19-T

Supplementary figure 7. Characterization and anti-tumor capacity of ^{Allo}CAR19-eNKT; relate to figure 2.

(a) FACS plots showing the expression of surface markers from ^{Allo}CAR19-eNKT cells (identified as 6B11^{+}CD3^{+}), compared to PBMC derived CAR19-T cells (identified as 6B11^{-} CD3^{+}Fab^{+}).

(b) Antigen responses of ^{Allo}CAR19-eNKT cells. ^{Allo}CAR19-eNKT cells were expanded in the presence or absence of αGC for 7 days.

(c) ELISA analysis of cytokines (IFN-γ, TNF-α, IL-2, IL-4 and IL-17) production at day 3 (n=3). (D-F) Studying the tumor killing of human CD19^{+}B-cell Lymphoma NALM6-hCD1d-FG cells by ^{Allo}CAR19-eNKT cells. (d) Experimental design. (e) Tumor killing with/without αGC (n=4) (e:t ratio=5:1, at 24 hours). (f) Tumor killing of ^{Allo}CAR19-eNKT and CAR19 t cells with titrated e:t ratio at 24 hours (n=4).

(g-l) Studying the *in vivo* antitumor capacity of ^{Allo}CAR19-eNKT. (g) Experimental design. a NALM-6-FG human multiple myeloma xenograft NSG mouse model was utilized. The conventional PBMC-derived CAR19-T cells were included as a control. (h) Tumor loads measured by BLI in experimental mice over time. (i) Quantification of (e) (n = 7). (j) Kaplan-Meier analysis of mouse survival rate (n=7). (h) FACS analysis of the surface expression of B2M and HLA-II ^{Allo}CAR19-eNKT and control CAR19-T cells isolated from the peripheral blood of the experimental mice (n=4).

Representative of 3 experiments. Data are presented as the mean ± SEM. ns, not significant, *$p < 0.05$, **$p < 0.01$, ***$p < 0.001$, ****$p < 0.0001$, by 1-way ANOVA (b,e,i) or by Student‘s t test (c,k,l), or by by log rank (Mantel-Cox) test adjusted for multiple comparisons (j).

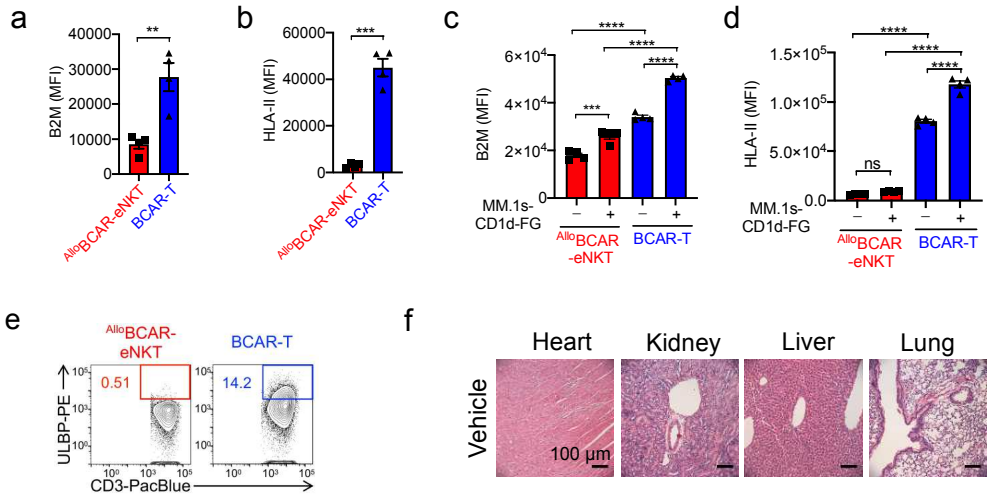

Supplementary figure 8. Safety and immunogenicity study of AlloBCAR-eNKT cells; related figure 3
(a-b) *In vitro* HLA-I (B2M) & HLA-II expression in AlloBCAR-eNKT cells compared to PBMC derived BCAR-T cells.
(c-d) *In vitro* HLA-I (B2M) and HLA-II expression on indicated cells in response to MM.1s-CD1d-FG coculture.
(e) Representative FACS analyses of the ULBP expression in AlloBCAR-eNKT cells compared to BCAR-T cells.
(f) Representative h&e staining of tissue sections from MM.1s-CD1d-FG bearing control mice without any treatment.
(g-h) Immunohistology analysis of tissue sections from MM.1s-CD1d-FG bearing mice experimental mice post corresponding effector cell treatment. (g) Anti-human CD3 staining. CD3 is shown in brown. (h) Quantification of (g).
Representative of 3 (a-e) and 2 (f-h) experiments. Data are presented as the mean ± SEM. ns, not significant, *$p < 0.05$, **$p < 0.01$, ***$p < 0.001$, ****$p < 0.0001$, by Student's t test (A-B) or 1-way ANOVA (c-d, h).

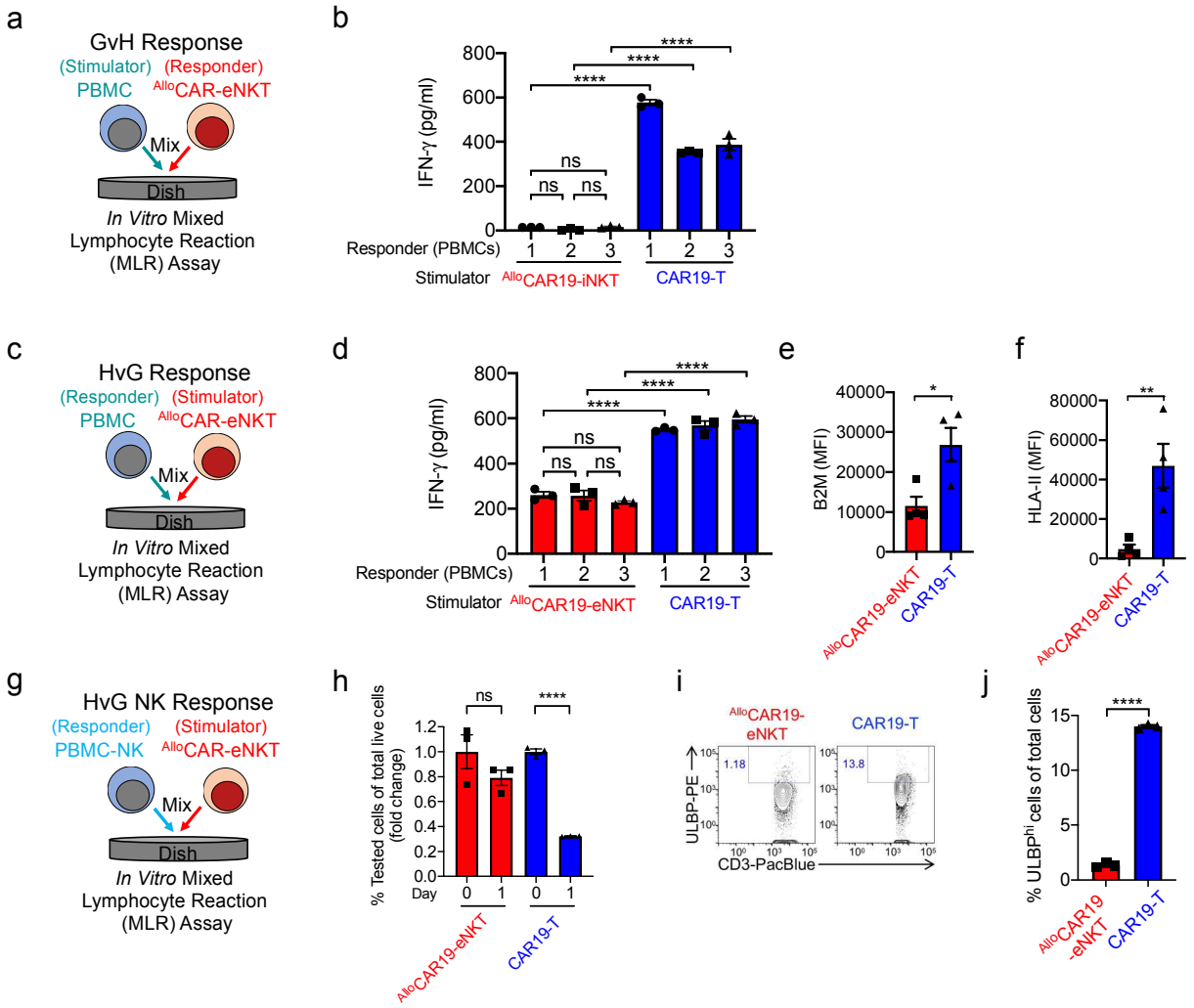

Supplementary figure 9. *In vitro* safety and immunogenicity study of AlloCAR19-eNKT cells; related to figure 3.

(a-b) An MLR assay for the study of GvH response of Allo CAR19-eNKT in comparison with CAR19-T cells. (a) Experimental design. (b) IFN-γ production related to Allo CAR19-eNKT (n = 3). PBMCs from 3 random healthy donors were included as stimulators.

(c-d) An MLR assay for the study of immunogenicity of Allo CAR19-eNKT in comparison with CAR19-T cells. (c) Experimental design of HvG response. (d) IFN-γ production related to AlloCAR19-eNKT (n = 3). PBMCs from 3 random healthy donors were included as responders.

(e-f) *In vitro* HLA-I (B2M) & HLA-II expression in Allo CAR19-eNKT cells compared to CAR19-T cells.

(g-h) The study of allogenic NK cell response against Allo CAR19-eNKT cells using an in vitro MLR assay. Allo CAR19-eNKT cells were co-cultured with donor-mismatched PBMC-NK cells. CAR19T cells were included as control. Quantification of FACS analyses of the indicated cells at day 0 and 1 of coculture (n=3).

(i-j) *In vitro* ULBP expression in Allo CAR19-eNKT cells compared to CAR19-T. (i) Representative FACS analyses. (j) Quantification of (i).

Representative of 3 experiments. Data are presented as the mean ± SEM. ns, not significant, *p < 0.05, **p < 0.01, ***p < 0.001, ****p < 0.0001, by 1-way ANOVA (b,d,h) or by Student's t test (e,f,j).

a

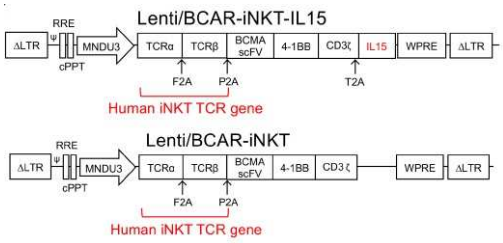

b

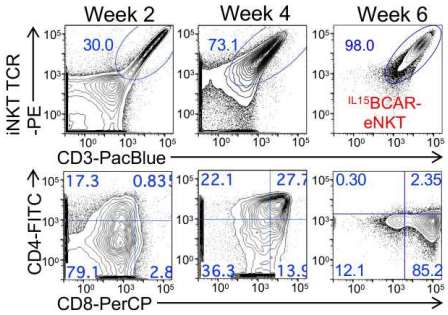

c

Input: per 1x10^6 transduced Cord Blood CD34+ HSCs (paired products from 3 donors)		
Yield of AlloCAR-eNKT cells	Output: AlloBCAR-eNKT cells	Output: IL15BCAR-eNKT cells
	1.3-2.8x10^12	4.7-6.3x10^12

d

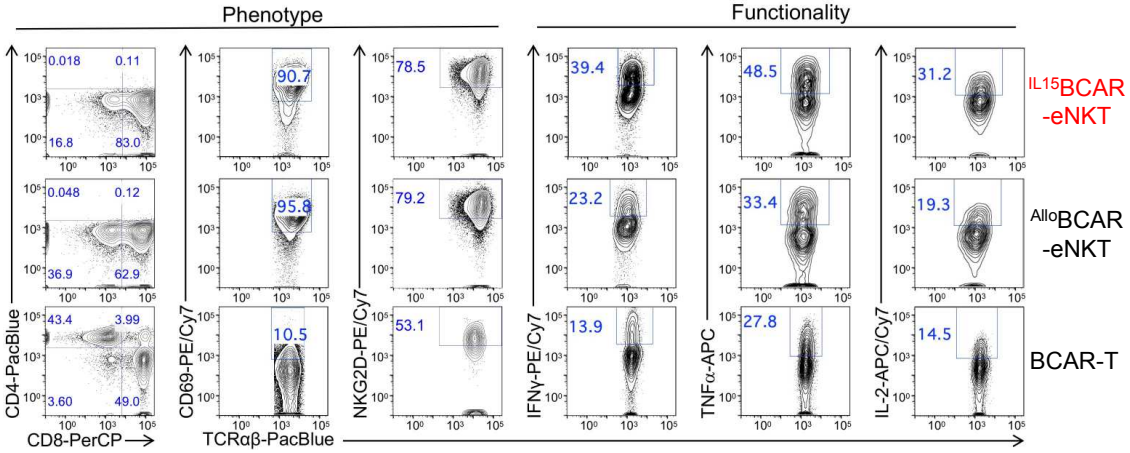

e

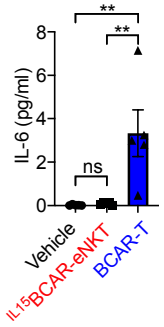

Supplementary figure 10. Generation and characterization of IL-15-enhanced ^{Allo}BCAR-eNKT (^{IL15}BCAR-eNKT) cells; related to figure 3.

(a) Schematic of iNKT TCR/BCAR/IL15 lentivector design in comparison with iNKT TCR/BCAR vector.

(b) Yield table of ^{IL15}BCAR-eNKT cells using the ^{Allo}CAR-eNKT cell culture system in comparison with ^{Allo}BCAR-eNKT.

(c) Representative kinetics of ^{IL15}BCAR-eNKT cell development from Lenti/iNKT-BCAR-IL15 vector modified CB CD34^{+} HSCs and CD4/CD8 co-receptors expression at the indicated weeks and stage of the culture. ^{IL15}BCAR-eNKT cells were gated as 6B11^{+}CD3.

(d) FACS plots showing the expression of surface markers from ^{IL15}BCAR-eNKT cells (identified as 6B11^{+}CD3^{+}), compared to ^{Allo}BCAR-eNKT (identified as 6B11^{+}CD3^{+}) and BCAR-T cells (identified as 6B11^{-} CD3^{+}Fab^{+}).

(f) Cytokine release syndrome study in effector cell-treated MM bearing mice. IL-6 in plasma measured by ELISA at day 35 post therapeutic cell infusion.

Representative of 3 experiments. Data are presented as the mean ± SEM. Data are presented as the mean ± SEM. ns, not significant, *$p < 0.05$, **$p < 0.01$, ***$p < 0.001$, ****$p < 0.0001$, by 1-way ANOVA (e and f).

CHAPTER 5:

Ultrahigh T cell Activation through

Biomimetic Graphene Oxide Antigen Presenting Platform

TITLE PAGE

Ultrahigh T cell Activation through Biomimetic Graphene Oxide Antigen Presenting Platform

Enbo Zhu[1, §], Jiaji Yu[2,3, §], Feiyang Ma[4], Chengzhang Wan[5], Yu Jeong Kim[2], Yang Liu[1] Xucheng Yan[1], Zoe Hanh[2], Yang Zhou[2,3], Yan-Ruide Li[2,3], Yuchong Zhang[2], Matteo Pelegrini[4], Xiangfeng Duan[5,6], Lili Yang[2,3,7,8,*] and Yu Huang[1,6,8*]

Author Affiliation:

1.Department of Materials Science and Engineering, University of California, Los Angeles, CA 90095, USA
2. Department of Microbiology, Immunology & Molecular Genetics, University of California, Los Angeles, Los Angeles, CA 90095, USA
3. Molecular Biology Institute, University of California, Los Angeles, Los Angeles, CA 90095, USA
4. Department of Molecular, Cell, and Developmental Biology, University of California, Los Angeles, Los Angeles, CA 90095, USA
5. Department of Chemistry and Biochemistry, University of California, Los Angeles, CA 90095, USA.
6. California Nanosystems Institute, University of California, Los Angeles, CA 90095, USA.
7. Eli and Edythe Broad Center of Regenerative Medicine and Stem Cell Research, University of California, Los Angeles, Los Angeles, CA 90095, USA
8. Jonsson Comprehensive Cancer Center, David Geffen School of Medicine, University of California, Los Angeles, Los Angeles, CA 90095, USA

[§] Enbo Zhu and Jiaji Yu contributed equally to this work.

Address Correspondence to:

Yu Huang, Ph.D. yhuang@seas.ucla.edu
Lili Yang, Ph.D. liliyang@ucla.edu

Abstract

2-D graphene oxide antigen-presenting platform (GO-APP) was developed with anti-CD3 (αCD3) and anti-CD28 (αCD28) hierarchically anchored on the surface of GO (GO-APP$^{3/28}$). The *in-vitro* interactions between the GO-APP$^{3/28}$s and the T cells delicately mimicked the *in vivo* immunological synapses between the antigen-presenting cells (APCs) and the T cells, featuring large contact areas, high accessibilities of antigen presentations, and consequently strong and sustained activation signals. Compared with the state-of-art commercial αCD3/αCD28-decorated beads (Beads$^{3/28}$), GO-APP$^{3/28}$ can stimulate T cell proliferation and activation without extrinsic interleukin-2 (IL-2) with 70.32 times higher efficiency. Moreover, the antibodies on GO can be programmed in variety, density, hierarchy, *etc.,* and 2-D visualized at the nanometer level; The mimetic immunological synapses can be 3-D visualized at the sub-micron level. Therefore, such 2-D AAPS provided a novel systematic platform complementary to traditional lipid bilayer models to study receptor stimulations.

Adoptive cell transfer had attracted intensive interest due to its promising prospect in cancer treatment[1-3]. In autologous immunotherapy, T cells were extracted from the patient, cultured *in vitro,* and after sufficient stimulation, returned to the same patient, where these cells were expected to elicit potent responses[4, 5]. Therefore, an efficient *in vitro* activation is crucial.

T cells require two distinct activation signals. The first signal was provided through the T-cell receptor (TCR) engaging with antigen peptides associated with major histocompatibility complex (MHC) on the membrane of antigen-presenting cells (APCs). The second signal was provided through the costimulatory receptors, such as B7 family receptors (e.g., CD28), binding to their ligands on the membrane of APCs. Costimulatory signals play essential roles, particularly in the functional differentiation of T cells, such as cytokine production, proliferation, and survival[6, 7]. Cluster of Differentiation 3 (CD3) was part of the TCR complex; The combination of αCD3 and αCD28 are widely adopted to provide the two signals required for T cell activation and proliferation.

Moreover, full activation of T cells required the clustering at the receptors. IL-2, also known as T-cell growth factor (TCGF), was produced by activated T cells and promoted further growth and differentiation of activated T cells. Although *in vivo* it was self-sufficient and even in some situations redundant, externally added IL-2 was critically required in the *in vitro* T cell activation[8-14]. However, IL-2 has a narrow therapeutic window, and external dosing level usually determines the severity of the side effects.

In this work, A novel 2-D graphene oxide antigen-presenting platform (GO-APP) was designed by hierarchically attaching αCD3 and αCD28 on 2-D single-layer GOs (GO-APP$^{3/28}$). The GO-APP$^{3/28}$ can potently stimulate the proliferation and activation of T cells *in vitro* without external IL-2 added. In a single culture with no cell split, the proliferation efficiency was 70.32 times higher than the state-of-art commercial Beads$^{3/28}$, a dramatic qualitative enhancement. It is expected the enhancement would further increase if split operations were adopted frequently to avoid saturation. With external IL-2 added, GO-APP$^{3/28}$ still exhibited 2.39 times higher stimulation than Beads$^{3/28}$. Besides, we proposed the GO-APP as a novel platform to study the interactions of the signal proteins on the cytomembrane, as the parameters such as variety, density, hierarchy, *etc.* were under precise regelation, and the structures involved in the interaction can be visualized in 2-D and 3-D in nanometer and sub-micrometer resolution respectively.

In the *in vivo* activation of T cells, the interaction between a biological APC and a T cell achieved close apposition of membranes over a large surface contact area and resulted in large-scale protein rearrangements and the subsequent formation of the immunological synapse[15-18]. Previous studies indicated that receptor occupancy over a large surface area of contact is a critical determinant for activation[19]. In the *in vitro* activation of T cells, αCD3 and αCD28 were usually bound to a plate substrate to provide the clustered signals. Or commercially, microbeads (Dynabeads) functionalized with αCD3 and αCD28 were adopted as one of the most commonly used substrates (Beads$^{3/28}$) for *in vitro* culture of T cells[20, 21]. However, both the plate and the Dynabeads had rigid structures differing from the highly flexible and mobile cytomembrane of the APCs, which limited the formation of large-area surface contact and therefore led to inferior T cell

activations. On the other hand, GO-APP may provide a superior surface contacting area because of its ultra-high flexibility. (Figure 1A)

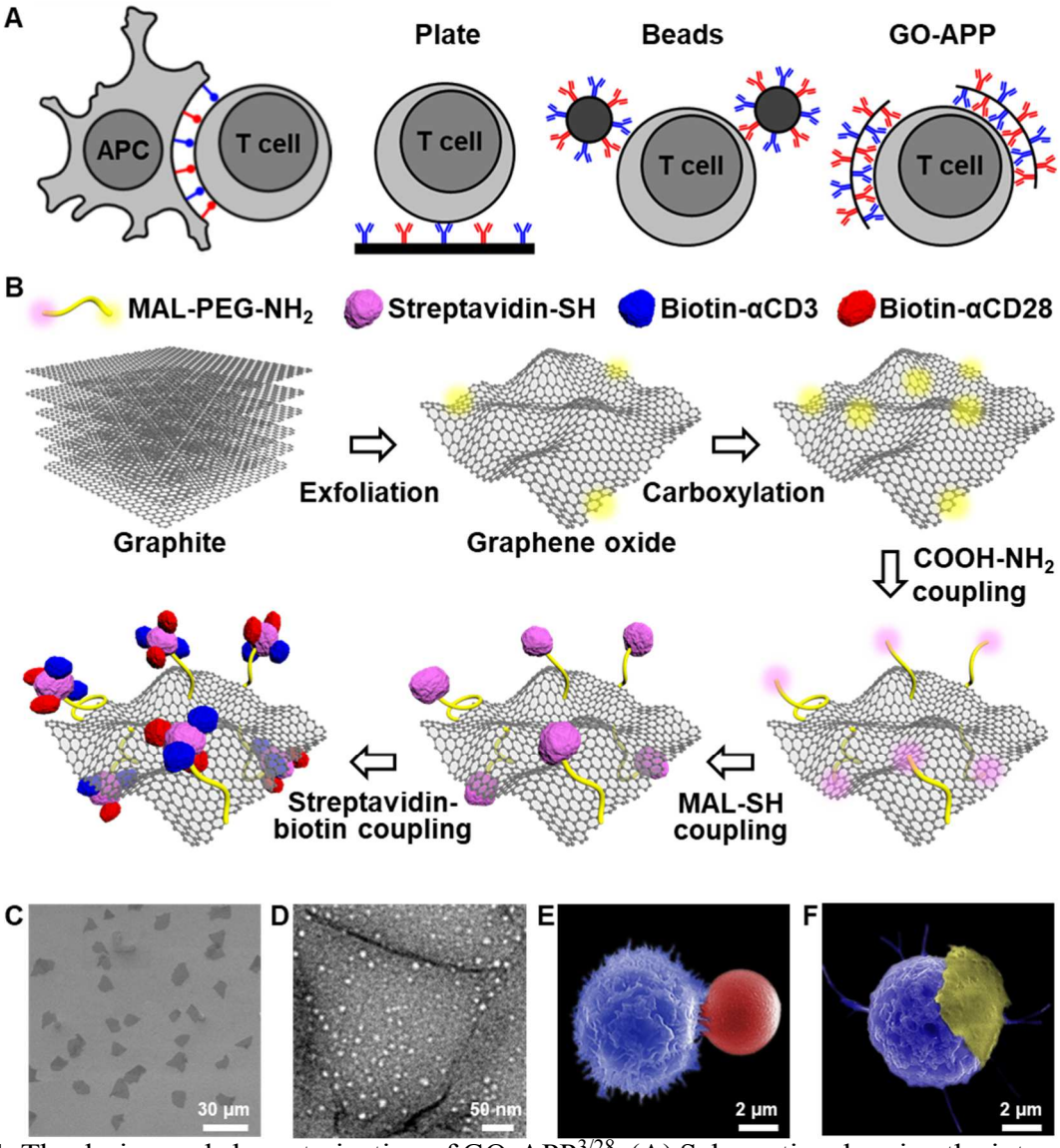

Figure 1. The design and characterization of GO-APP$^{3/28}$. (A) Schematics showing the interactions between a T cell and an antigen-presenting cell, an antibody-coated plate, antibody-coated beads, and GO-APP$^{3/28}$s. (B) Schematics demonstrating the design and the preparation of GO-APP$^{3/28}$. (C) SEM image of the as-prepared GO. (D) Uranyl acetate negative-stain TEM image, where the GO-linked proteins can be observed on the flat region of the GOs. (E-F) Low vacuum SEM image of fixed T cell interacting with (E) Beads$^{3/28}$and (F) a piece of GO-APP$^{3/28}$; The images were falsely colored with T cell in blue, bead in red, and GO-APP$^{3/28}$ in yellow.

The overall schematic of the hierarchical design for the GO-APP$^{3/28}$ was illustrated in Figure 1B. GOs were synthesized with an improved hammer's method [Details see Supporting Information (SI)] and characterized with scanning electron microscopy (SEM) and atomic force microscopy (AFM). Through repeated centrifugation and separation, the size distribution of the GO was narrowed down to ~15±3 μm (the size of a GO was defined as the average of the longest and shortest diagonal length). (Figure 1C) The thickness of the GO was ~1.1 nm, which indicates the single-layer feature. (Figure 2A) The single-layer thickness provides the GO with high flexibility. Virtually 100 % of the 15-μm GO can quickly go through Cyclopore polycarbonate membrane with 3.0 μm true pore size with no visible residual. After the single-layer GO was prepared, the epoxide and hydroxyl groups were activated into carboxyl groups by chloroacetic acid under a basic condition[22]. (Details see SI) The amino end of bifunctional polymer NH_2-PEG-MAL (M_w=2K) was then connected to the carboxyl group of GO through EDC/NHS coupling. (Details see SI) Next, thiol groups were introduced in streptavidin with 2.5 thiols per tetramer through the reaction with 2-iminothiolane (Traut's reagent) and the streptavidin-SH was then linked to the maleimide end of the PEG polymer. (Details see SI) αCD3 and αCD28 were biotinylated with 3-6 biotin molecules per antibody, and then the biotin-αCD3 and biotin-αCD28 were linked to the streptavidin through the strong biotin-streptavidin interaction with a 4-to-1 ratio. After the decoration, GO-APP$^{3/28}$ was thicker than as-prepared GO (Figure 2B), but they still possess high flexibility as they can go through Cyclopore polycarbonate membrane with 8.0 μm true pore size with no noticeable hindrance. Besides, the activation and decoration of GO led to increases in optical absorption in the visible and near-infrared range for the same starting graphitic carbon mass concentration (0.1 mg/mL) (Figure 2C). The opening of epoxide groups and hydrolysis of esters on the GO during the activation led to local changes in the microstructure with

released local strain and increased conjugation in the GO sheets, causing increased optical absorption in the visible and near-infrared range[22].

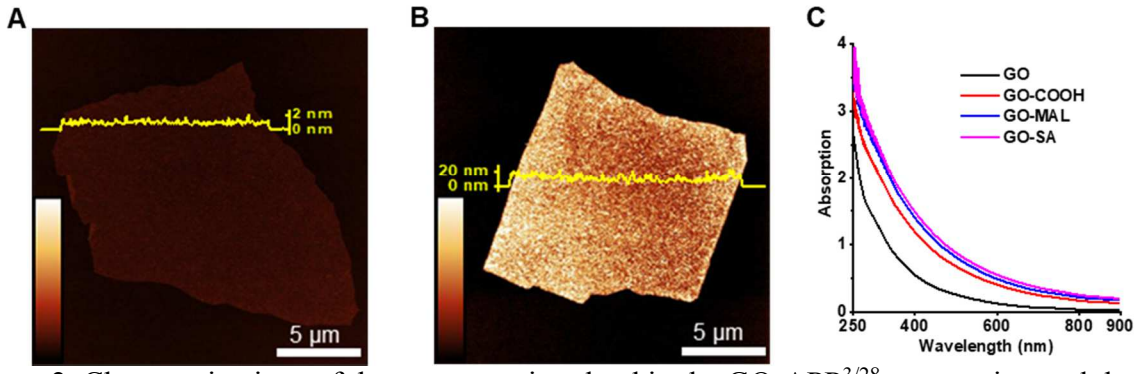

Figure 2. Characterizations of the structures involved in the GO-APP$^{3/28}$ preparation and the dose test of GO-APP$^{3/28}$ in T cell proliferation. AFM images of (A) as-prepared GO and (B) GO-APP$^{3/28}$. (C) UV-vis spectra of the intermediate structures in the GO-APP$^{3/28}$ preparation.

Previous studies also revealed that T cell activation was very sensitive to the density of antigen presented[23]. The density of streptavidin composites containing αCD3 and αCD28 on GO-APP$^{3/28}$ could be observed directly by TEM after deposit GO-APP$^{3/28}$ on the TEM grid followed by negative staining with uranyl acetate (Figure 1D), which is >870 sites/μm^2. Such densities exceed the physiological density of TCR and CD28 on human T cells. Besides, the contact between a T cell and a GO-APP$^{3/28}$ could be directly virtualized by SEM. The ultra-high flexibility of GO provided a much larger contact area (~ 28.5 μm^2 in Figure 1E) compared with commercial beads, which are rigid spheres (~2.5 μm^2, Figure 1F).

The GO-APP$^{3/28}$ was applied to the *in vitro* activation of human T cells from several donors, and the same trend was observed. (Figure 3, Figure 4) GO substrate facilitated the clustering of αCD3 and αCD28 and their exposure to T cells, which is essential in the full activation of T cells. Other conditions for comparison included: (1) the state-of-art commercial Beads$^{3/28}$, (2) αCD3 pre-

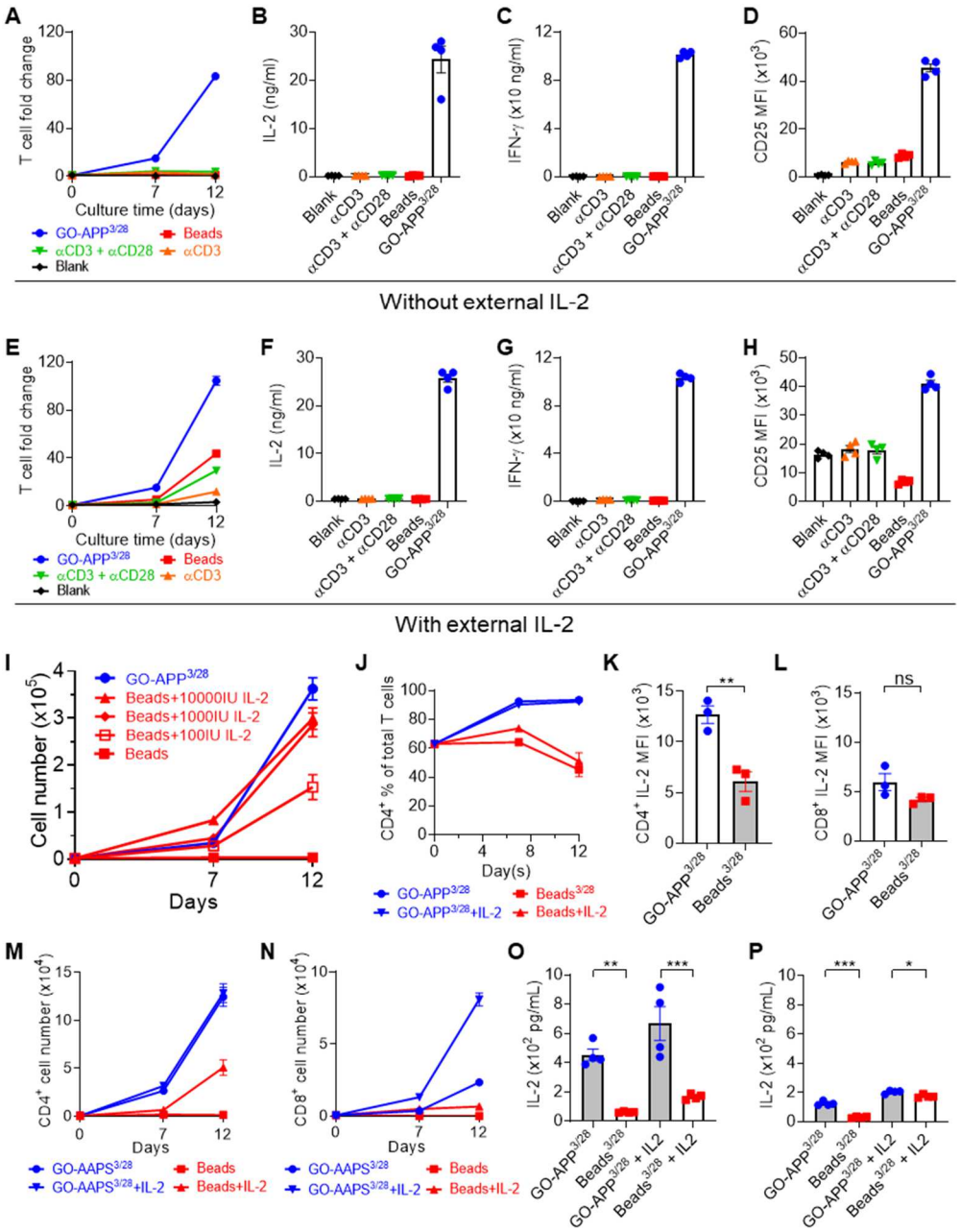

Figure 3. Bioactivities of GO-APP$^{3/28}$. (A) and (E) The live T cell fold change in proliferation. (B) and (F) the Interleukin-2 (IL-2) secretion stimulated by different antigen-presenting structures. (C) and (G) the interferon-gamma (IFN-γ) secretion stimulated by different antigen-presenting structures. (D) and (H) The CD25 surface marker activated by Beads$^{3/28}$ and GO-APP$^{3/28}$. (I) Titration of IL-2 on T cell proliferation. (J) CD4^{+} proportion of the total proliferated T cells. (K) and (L) Intercellular IL-2 in CD4^{+} and CD8^{+} T cells. (M) and (N) The proliferation of pure CD4^{+} T cells and pure CD8^{+} T cells. (O) and (P) IL-2 secretion in (M) and (N).

coated on the culture wells, (3) αCD3 pre-coated on the culture well together with αCD28, (4) control experiments without the presence of αCD3 nor αCD28. During the *in vitro* activation without external IL-2, only GO-APP$^{3/28}$ stimulated a practical proliferation of the T cells, with overwhelming superiority over the rest conditions. (Figure 3A) Quantitatively, after 12-day culture, the proliferated T cells stimulated by GO-APP$^{3/28}$ is 70.32 times higher than those stimulated by Beads$^{3/28}$. From the enzyme-linked immunosorbent assay (ELISA) results, the IL-2 and, the interferon-gamma (IFN-γ), and the high-affinity IL-2 receptor (CD25) stimulated by GO-APP$^{3/28}$ during the activation was all overwhelmingly superior to those under the other conditions (Figure 3B-D).

External IL-2 is usually indispensable for *in vivo* T cell activation. The commercial Beads$^{3/28}$ required 30 IU/mL of IL-2 for *in vivo* T cell activation, according to the manual. In our experiments with external IL-2, 100 IU/mL were added. External IL-2 had little influence on GO-APP$^{3/28}$, but it was clear that T cells under all the other conditions proliferate faster than those with no external IL-2. Even after external IL-2 was applied, dramatic proliferation efficiency between GO-APP$^{3/28}$ and the others still existed. (Figure 3E) With external IL-2, GO-APP$^{3/28}$ stimulated T cell proliferation 2.39 times higher than commercial Beads$^{3/28}$. From the titration of IL-2 (Figure 3I), the promoting effect reached a plateau after the external IL-2 concentration reach as high as ~1000 IU/mL. However, there are still gaps between the plateau and the efficiency of GO-APP$^{3/28}$, indicating the proliferation enhancement of GO-APP$^{3/28}$ cannot be simply compensated by IL-2. Instead, there should be some deeper-level regulations promoting proliferation. The IL-2, IFN-γ, and CD25 stimulated by GO-APP$^{3/28}$ did not rely on the external IL-2 added and were still excessively higher than those in other conditions, even after external IL-2 was compensated.

(Figure 3F-H) The flow cytometry measurement of CD69, an early classical marker, indicated that the stimulation from GO-APP$^{3/28}$ took effect at Day 3 faster than the other conditions, no matter with or without external IL-2. (Figure 4B)

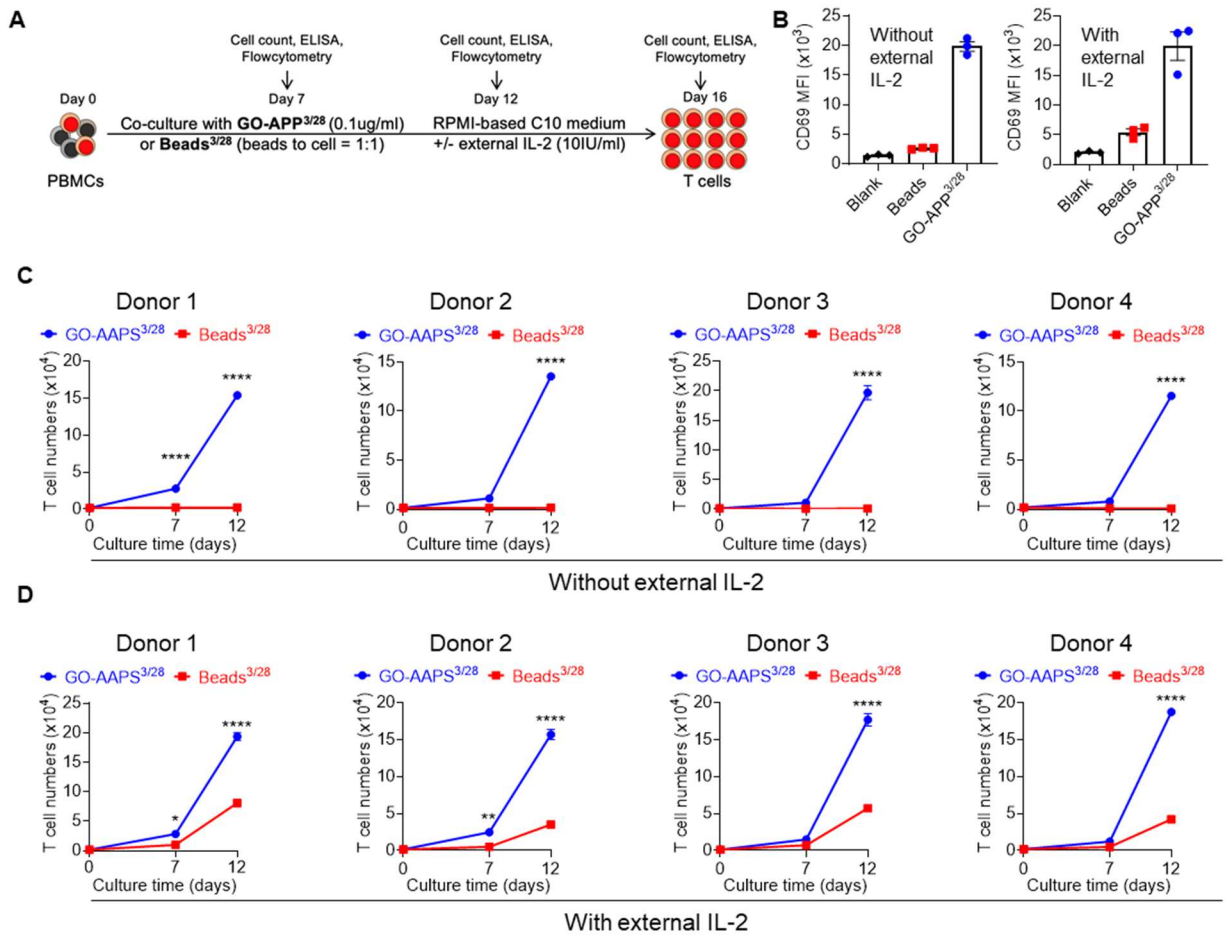

Figure 4. Bioactivities of GO-APP$^{3/28}$ - Experimental design and multi-donor replication (A) Experimental design of the cell count, ELISA, and Flow cytometry. (B) CD69 surface markers activated under different conditions. (C) The proliferation of T cells from different donors in the absence of external IL-2. (D) The proliferation of T cells from different donors in the presence of external IL-2.

Interestingly, the T cells were CD4^{+} rich after 12-day proliferation activated by GO-APP$^{3/28}$. This is different from the T cells after 12-day proliferation activated by Beads$^{3/28}$, which were

$CD8^+$ rich. (Figure 3J) The intracellular IL-2 concentration was determined by flow cytometry. (Figure 3K-L) The IL-2 secretion in $CD4^+$ T cells stimulated by GO-APP$^{3/28}$ was dramatically higher than the secretion in $CD4^+$ T cells stimulated by Beads$^{3/28,}$ as well as the secretion in $CD8^+$ T cells stimulated by GO-APP$^{3/28}$ or Beads$^{3/28}$. The preference of GO-APP$^{3/28}$ to stimulate the proliferation of $CD4^+$ T cells may explain the independence of the GO-APP$^{3/28}$ stimulation on IL-2, as $CD4^+$ T cells are the main producer for IL-2[24]. Besides, typically the *in vivo* T cell proliferation was biased to $CD8^+$ T cells rich. The $CD4^+$ rich stimulation of GO-APP$^{3/28}$ is extraordinary and will bring advantages when $CD4^+$ T cells were preferred to $CD8^+$ T cells. The proliferation of pure $CD4^+$ T cells (Figure 3M) and pure $CD8^+$ T cells (Figure 3N) stimulated by GO-APP$^{3/28}$ and Beads$^{3/28}$ were examined. For both pure $CD4^+$ T cells and pure $CD8^+$ T cells, stimulation from GO-APP$^{3/28}$ led to superior proliferation. But in pure $CD8^+$ cells, the proliferation stimulated by GO-APP$^{3/28}$ was IL-2 dependent, which is in contrast with the case in pure $CD4^+$ T cells, the independent on IL-2. As IL-2 is mainly produced by activated $CD4^+$ T cells[24], the high-level secretion of IL-2 from $CD4^+$ T cells stimulated by GO-APP$^{3/28}$ (Figure 3O) was adequate for the proliferation, while in $CD8^+$ T cells, low-level secretion of IL-2 was stimulated by GO-APP$^{3/28}$ (Figure 3P) and therefore need the supplement of external IL-2 to achieve the maximum proliferation. For both $CD4^+$ and $CD8^+$ T cells, Beads$^{3/28}$ always resulted in low-level secretion of IL-2.

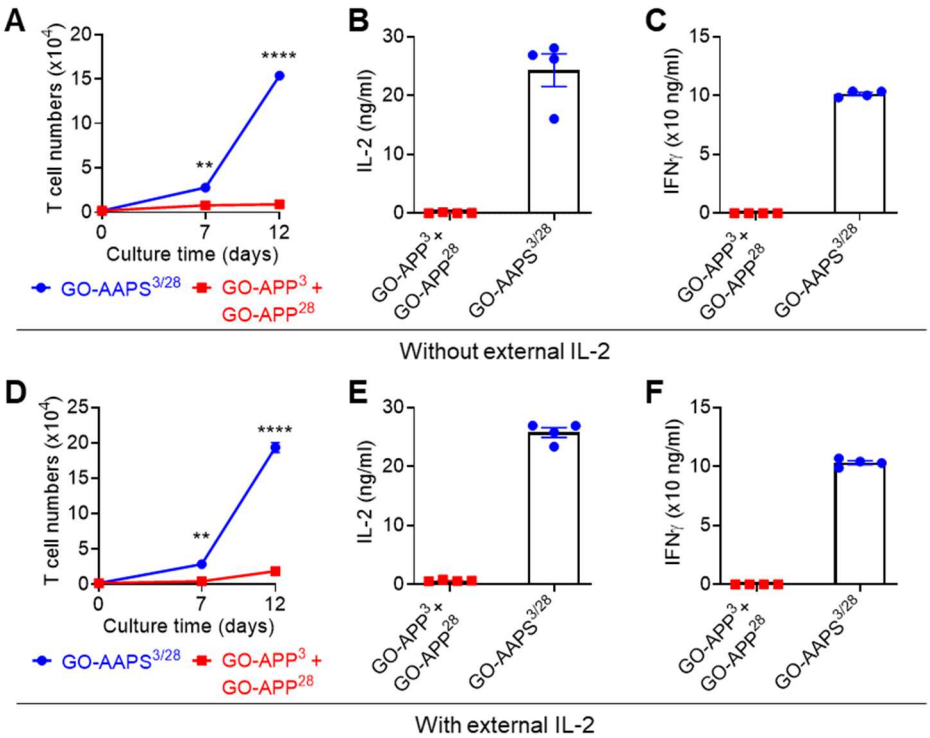

Figure 5. Comparison of T-cell activations using GO-APP$^{3/28}$ and the mixture of GO-APP^{3} and GO-APP^{28}. GO-APP$^{3/28}$ showed superior performance, indicating the significance of the microscopic local coactivation of CD3 and CD28. (A) and (D) Proliferation. (B) and (E) IL-2 secretion. (C) and (F) IFN-γ secretion.

Besides, our results indicated that the αCD3 and αCD28 need to be spatially clustered together for a successful T cell activation and proliferation. (Figure 5) When the GO coated with only αCD3 (GO-APP^{3}) and the GO coated with only αCD28 (GO-APP^{28}) were mixed for T cell activation, the proliferation efficiency was poor no matter with or without external IL-2 added. (Figure 5A and D) Besides, the production of IL-2 and IFN-γ were negligible compared with those produced in GO-APP$^{3/28}$. (Figure 5B,C,E,F) These observations indicated that the T cell activation by αCD3 and αCD28 was curtailed if the engagement of αCD3 and αCD28 was separated by

micrometer-scale distances. This was consistent with the conclusion from the previous study using micropatterned surfaces[25].

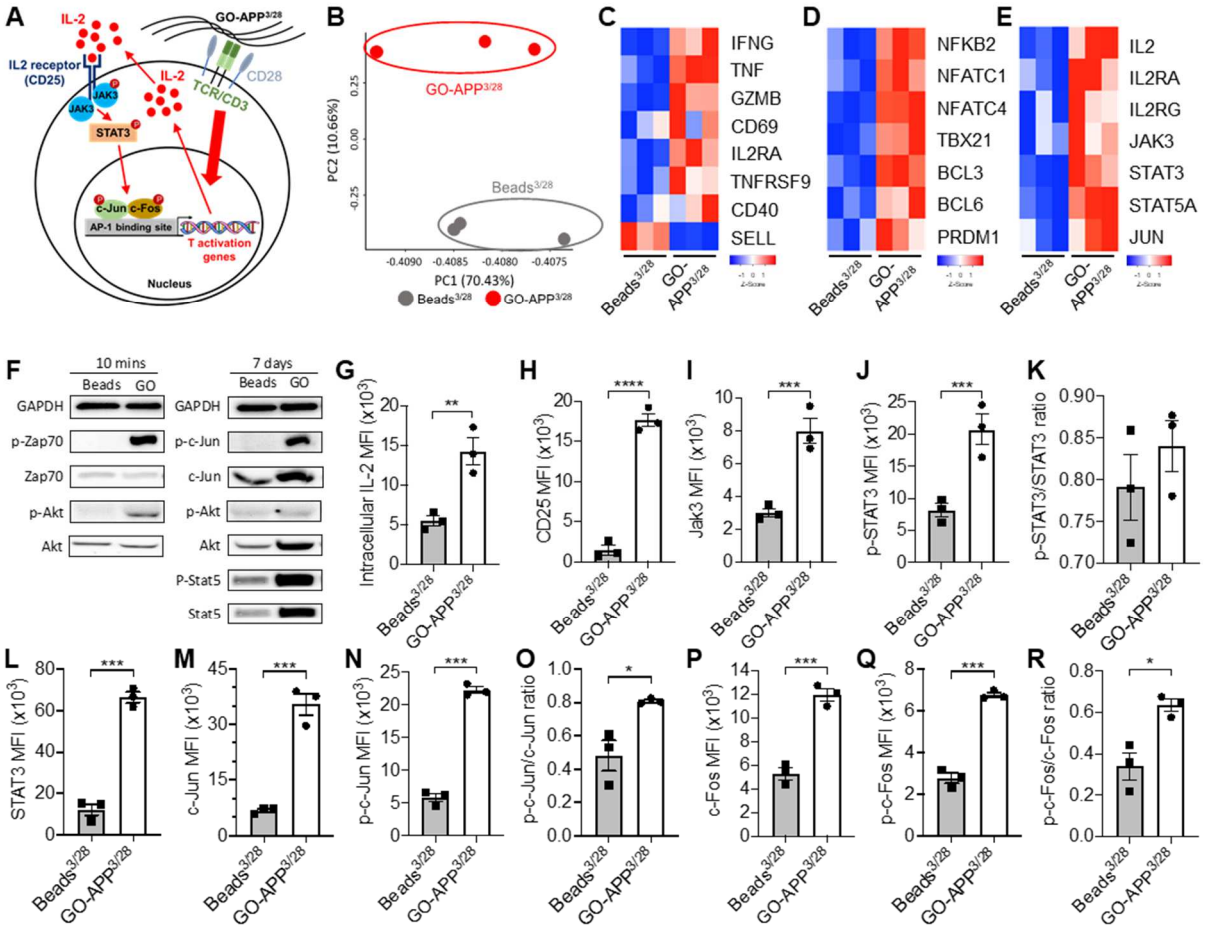

Figure 6. Mechanism study of GO-APP$^{3/28}$ mediated T cell activation. (A) Schematics of GO-APP$^{3/28}$ mediated T cell activation through the IL-2 feedback network. (B) Gene profiling of human T cells activated with GO-APP$^{3/28}$ and Beads$^{3/28}$, 3 different donors were used. (C-E) Heatmap of gene expression profile related to (C) T cell activation, (D) T cell signaling, (E) IL-2 signaling pathway. (F) Western blot showing the enhanced protein expression activated by GO-APP$^{3/28}$ and Beads$^{3/28}$. (G-R) Mean fluorescence intensity (MFI) measurement from flow cytometry on T cells activated by GO-APP$^{3/28}$ and Beads$^{3/28}$ showing the enhanced expression of several pivotal proteins.

Mechanism studies were conducted to investigate how GO-APP$^{3/28}$ mediate T cell activation superior to Beads$^{3/28}$. The schematic of the pathways involved in the T cell stimulation was shown in Figure 6A. Gene profiling of human T cells activated with GO-APP$^{3/28}$ and Beads$^{3/28}$ was conducted. The gene expression induced by GO-APP$^{3/28}$ and Beads$^{3/28}$ had a dramatic difference. (Figure 6B, Figure 7A) From the heatmaps, after the stimulation of GO-APP$^{3/28}$, pathways of T cell activation (Figure 6C), T cell signaling (Figure 6D), and IL-2 signaling (Figure 6E) were all activated. The western blot of several pivotal proteins involved in T cell activations (Figure 6F) demonstrated the superiority of GO-APP$^{3/28}$ over Beads$^{3/28}$ by showing higher expression. Mean fluorescence intensity (MFI) measurement from flow cytometry on Beads$^{3/28}$ and GO-APP$^{3/28}$ activated T cells confirmed the higher expressions of these proteins as well as their higher phosphorylation. (Figure 6G-4R, Figure 7)

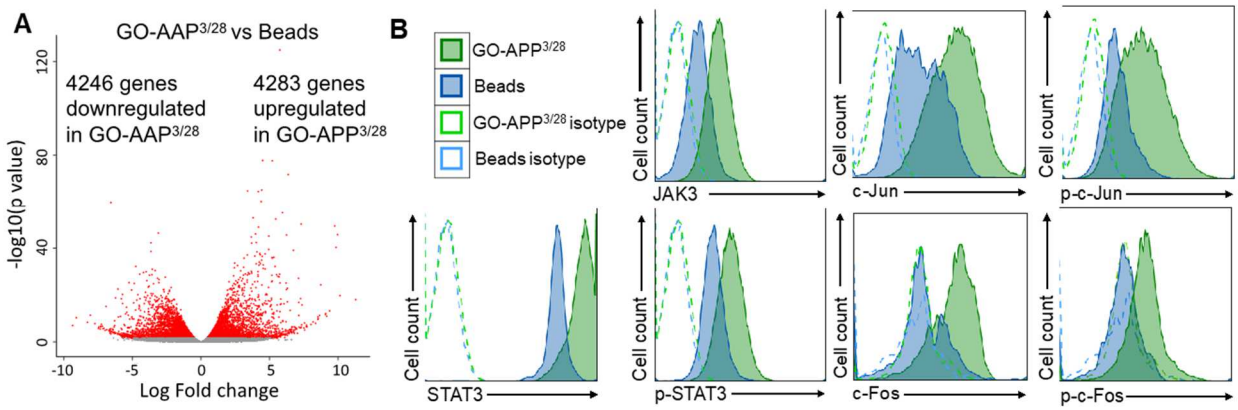

Figure 7. Mechanism study of GO-APP$^{3/28}$-mediated T cell activation – 2. (A) Differential gene expression comparison between GO-APP$^{3/28}$ and Beads$^{3/28}$ activated T cells. Every dot represents per gene. The red color indicates the p-value<0.05. (B) MFI measurement from flowcytometry on GO-APP$^{3/28}$ and Beads$^{3/28}$ activated T cells.

Retro/lentiviral transduction of BCMA CAR was conducted to the T cells activated by GO-APP$^{3/28}$ (no external IL-2) and Beads$^{3/28}$ (with 100 IU/mL external IL-2) for tumor killing assay, respectively. (Figure 8A, Figure 9A and 9B) The efficiency is higher for the T cells activated by GO-APP$^{3/28}$ for both retroviral and lentiviral transduction. (Figure 8B, Figure 9C) In lentiviral transduction, T cells activated by GO-APP$^{3/28}$ have 94.9% transduction efficiency, while T cells activated by Beads$^{3/28}$ only have 66.4%. (Figure 8B) This higher transduction efficiency led to a better *in vitro* killing rate of MM.1S-FG tumor cells. (Figure 8C, Figure 9F) Similar superiority was also demonstrated in retroviral transduction. (Figure 9D-E) *In vivo* experiments were also conducted. (Figure 8D) Cancer developed and dominated in the control group, while both the GO-APP$^{3/28}$ CAR-T cells and Beads$^{3/28}$ CAR-T cells efficiently suppressed and eliminated the cancer development. (Figure 8E and 5F, Figure 9G) Moreover, *in vitro,* high tumor load repetitive challenge assay (Figure 8G) indicated that GO-APP$^{3/28}$ CAR-T cells performed best in suppressing the cancer development (Figure 8H), which may be attributed to the high CD4^{+} component. Previous studies reported that CD4^{+} T cells worked better over CD8^{+} T cells in suppressing the development of severe cancers[26, 27]. Indeed, among the effector cells for *in vitro* repetitive tumor challenge, 86.7% of the GO-APP$^{3/28}$ CAR-T cells were CD4^{+}, while 43.5% of the Beads$^{3/28}$ CAR-T cells were CD4^{+}. (Figure 8I)

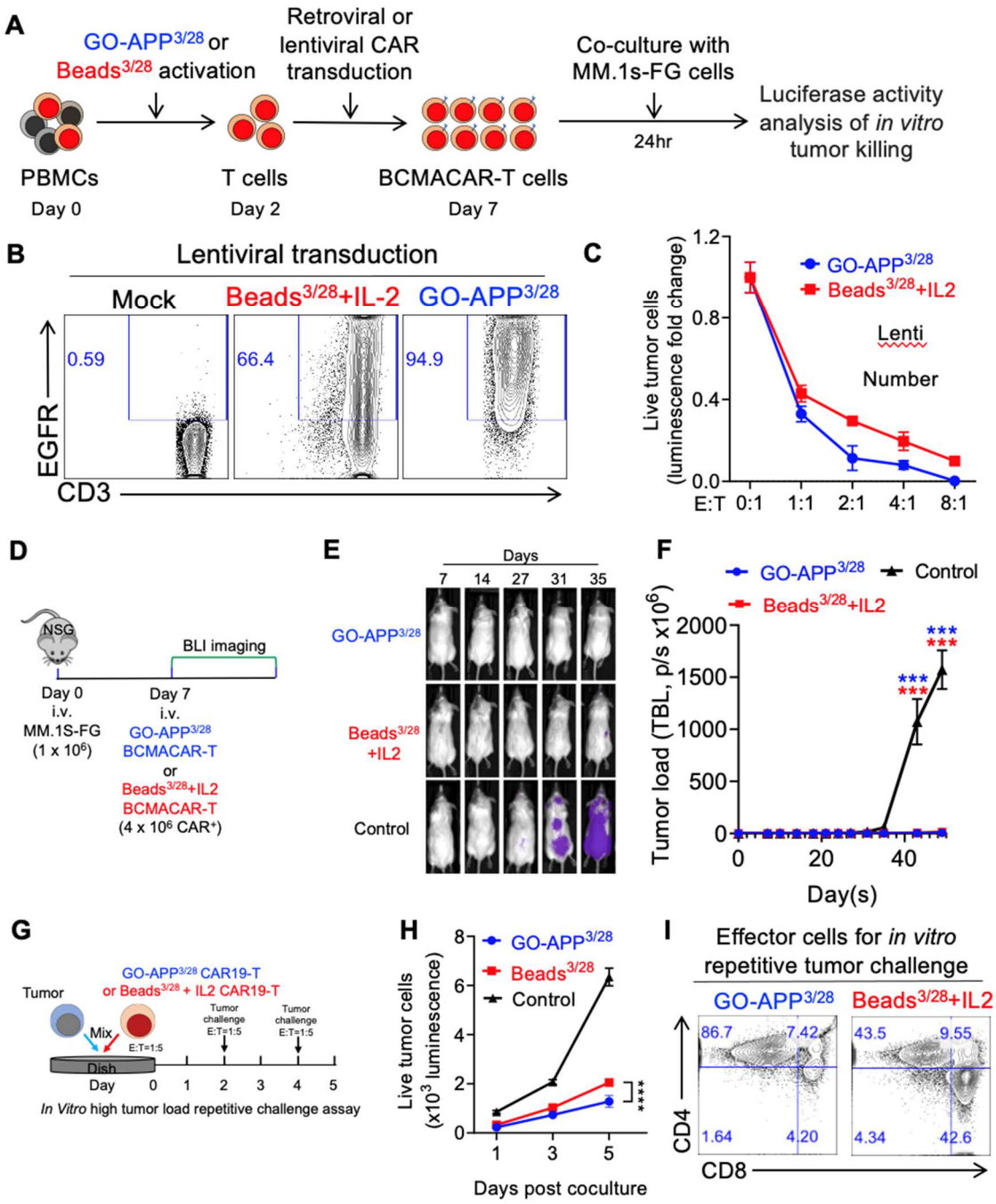

Figure 8. The application of GO-APP$^{3/28}$ in cell therapy for cancer. (A) Experimental design of retro/lentiviral transduction of BCAMCAR to GO-APP$^{3/28}$ or Beads$^{3/28}$ activated T cells for tumor killing assay. (B) Flow cytometry plots showing the CAR transduction (indicated by EGFR expression) with a lentiviral vector. (C) Luciferase activity analysis of *in vitro* tumor killing of MM.1s-FG (n=3). E:T (total cell number matched), effector/target cell number ratio. (D-E) Studying the *in vivo* antitumor efficacy of GO-APP$^{3/28}$ activated BCMACA-T cells in human

multiple myeloma (MM.1s-FG) xenograft mouse model. (D) Experimental design. (E) Representative bioluminescence (BLI) images along the time course. (F) Measurement of tumor load through BLI over time. (G) Design of *in vitro* high tumor repetitive challenge assay. (H) Live tumor cells after the coculture treatment with GO-APP$^{3/28}$ or Beads$^{3/28}$. (I) Effector cells composition for *in vitro* high tumor repetitive challenge.

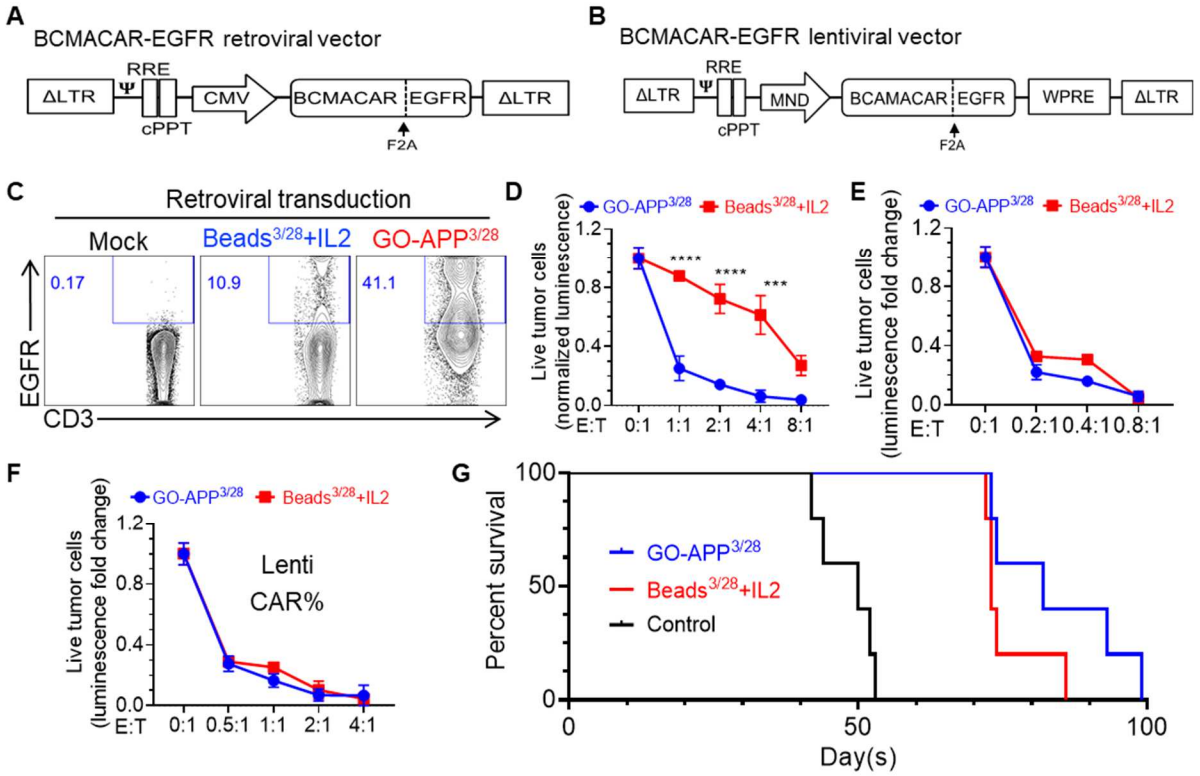

Figure 9. The application of GO-APP$^{3/28}$ in cell therapy for cancer - 2. (A) The vector design of bicistronic retroviral vector encoding BCAMCAR and EGFR. (B) The vector design of bicistronic lentiviral vector encoding BCAMCAR and EGFR. (C) Flow cytometry plots showing the CAR transduction (indicated by EGFR expression) with a retroviral vector. (D) Luciferase activity analysis of *in vitro* tumor killing of MM.1s-FG (n=3). E:T, effector/target. (Retroviral transduction, total cell number matched). (E) Luciferase activity analysis of *in vitro* tumor killing of MM.1s-FG (n=3). E:T, effector/target. (Retroviral transduction, CAR positive cell number matched). (F) Luciferase activity analysis of *in vitro* tumor killing of MM.1s-FG (n=3). E:T, effector/target. (Lentiviral transduction, CAR positive cell number matched). (G) Percentage of the survival mice along time.

In summary, we designed a new antigen-presenting platform based on graphene oxide, GO-APP, which is easy to design and characterize. GO-APP$^{3/28}$ stimulated ultra-high proliferation of T cells, even without the traditionally indispensable IL-2. Compared with the state-of-art commercial Beads$^{3/28}$, GO-APP$^{3/28}$ stimulated the proliferation of T cells with 70.32 times higher efficiency, which could be more pronounced if split operations were adopted. The activation of T cells by GO-APP$^{3/28}$ was biased to CD4^{+} rich, which is distinct from typical *in vitro* T cell proliferation which is usually biased to CD8^{+} rich. The GO-APP$^{3/28}$ stimulated T cells were made into CAR-T cells with much superior transduction efficiency, and these CAR-T cells exhibited great performance in tumor killing both *in vitro* and *in vivo*. Especially the GO-APP$^{3/28}$ CAR-T cells demonstrated great superiority in suppressing severe cancer development because of the dominant of CD4^{+} T cells. The demonstration that one can indeed rational design and hence optimize the antigen presentation on GO-APP opens up vast opportunities for creating new structures in immunological studies.

References

1. Fesnak, A.D., June, C.H. & Levine, B.L. Engineered T cells: the promise and challenges of cancer immunotherapy. *Nature reviews cancer* **16**, 566-581 (2016).
2. Koya, R.C. et al. BRAF inhibitor vemurafenib improves the antitumor activity of adoptive cell immunotherapy. *Cancer research* **72**, 3928-3937 (2012).
3. Rosenberg, S.A. & Restifo, N.P. Adoptive cell transfer as personalized immunotherapy for human cancer. *Science* **348**, 62-68 (2015).
4. Roddie, C., O'Reilly, M., Pinto, J.D.A., Vispute, K. & Lowdell, M. Manufacturing chimeric antigen receptor T cells: issues and challenges. *Cytotherapy* **21**, 327-340 (2019).
5. Kershaw, M.H., Westwood, J.A. & Darcy, P.K. Gene-engineered T cells for cancer therapy. *Nature Reviews Cancer* **13**, 525-541 (2013).
6. Jenkins, M.K. & Schwartz, R.H. Antigen presentation by chemically modified splenocytes induces antigen-specific T cell unresponsiveness in vitro and in vivo. *Journal of Experimental Medicine* **165**, 302-319 (1987).
7. McCormack, J., Callahan, J., Kappler, J. & Marrack, P. Profound deletion of mature T cells in vivo by chronic exposure to exogenous superantigen. *The Journal of Immunology* **150**, 3785-3792 (1993).
8. Bachmann, M.F. & Oxenius, A. Interleukin 2: from immunostimulation to immunoregulation and back again. *EMBO reports* **8**, 1142-1148 (2007).
9. Gillis, S., Baker, P.E., Ruscetti, F.W. & Smith, K. Long-term culture of human antigen-specific cytotoxic T-cell lines. *The Journal of experimental medicine* **148**, 1093-1098 (1978).
10. Gillis, S. & Smith, K.A. Long term culture of tumour-specific cytotoxic T cells. *Nature* **268**, 154-156 (1977).
11. Morgan, D.A., Ruscetti, F.W. & Gallo, R. Selective in vitro growth of T lymphocytes from normal human bone marrows. *Science* **193**, 1007-1008 (1976).
12. Smith, K.A. Interleukin-2: inception, impact, and implications. *Science* **240**, 1169-1176 (1988).
13. Smith, K.A., Gilbride, K.J. & Favata, M.F. Lymphocyte activating factor promotes T-cell growth factor production by cloned marine lymphoma cells. *Nature* **287**, 853-855 (1980).
14. Bamford, R.N. et al. The interleukin (IL) 2 receptor beta chain is shared by IL-2 and a cytokine, provisionally designated IL-T, that stimulates T-cell proliferation and the induction of lymphokine-activated killer cells. *Proceedings of the National Academy of Sciences* **91**, 4940-4944 (1994).
15. Sunshine, J.C. & Green, J.J. Nanoengineering approaches to the design of artificial antigen-presenting cells. *Nanomedicine* **8**, 1173-1189 (2013).
16. Grakoui, A. et al. The immunological synapse: a molecular machine controlling T cell activation. *Science* **285**, 221-227 (1999).
17. Lee, K.-H. et al. T cell receptor signaling precedes immunological synapse formation. *Science* **295**, 1539-1542 (2002).
18. Yokosuka, T. & Saito, T. Dynamic regulation of T□cell costimulation through TCR–CD28 microclusters. *Immunological reviews* **229**, 27-40 (2009).
19. Mescher, M. Surface contact requirements for activation of cytotoxic T lymphocytes. *The Journal of Immunology* **149**, 2402-2405 (1992).

20. Hollyman, D. et al. Manufacturing validation of biologically functional T cells targeted to CD19 antigen for autologous adoptive cell therapy. *Journal of immunotherapy (Hagerstown, Md.: 1997)* **32**, 169 (2009).
21. Cheung, A.S., Zhang, D.K., Koshy, S.T. & Mooney, D.J. Scaffolds that mimic antigen-presenting cells enable ex vivo expansion of primary T cells. *Nature biotechnology* **36**, 160-169 (2018).
22. Li, Y., Gao, W., Ci, L., Wang, C. & Ajayan, P.M. Catalytic performance of Pt nanoparticles on reduced graphene oxide for methanol electro-oxidation. *Carbon* **48**, 1124-1130 (2010).
23. Engelhard, V.H., Strominger, J.L., Mescher, M. & Burakoff, S. Induction of secondary cytotoxic T lymphocytes by purified HLA-A and HLA-B antigens reconstituted into phospholipid vesicles. *Proceedings of the National Academy of Sciences* **75**, 5688-5691 (1978).
24. Keene, J. & Forman, J. Helper activity is required for the in vivo generation of cytotoxic T lymphocytes. *The Journal of experimental medicine* **155**, 768-782 (1982).
25. Bashour, K.T. et al. Cross talk between CD3 and CD28 is spatially modulated by protein lateral mobility. *Molecular and cellular biology* **34**, 955-964 (2014).
26. Perez-Diez, A. et al. CD4 cells can be more efficient at tumor rejection than CD8 cells. *Blood, The Journal of the American Society of Hematology* **109**, 5346-5354 (2007).
27. Agarwal, S. et al. In vivo generation of CAR T cells selectively in human CD4+ lymphocytes. *Molecular Therapy* **28**, 1783-1794 (2020).